MODELLING THE AGULHAS OCEAN CURRENT:

WITH A FOCUS ON THE RELATED SHALLOW WATER HYDRODYNAMICS IN AND AROUND DURBAN BAY, SOUTH AFRICA

Kemira Naidoo

University of KwaZulu Natal

Submitted in fulfilment of the academic requirements for the degree of

Master of Science in Engineering

In the

Civil Engineering programme

College of Agriculture, Engineering and Science, University of KwaZulu Natal

2021

Supervisor: Dr J. J. Pringle

Co-Supervisors: Professor D. Stretch

R. de Graaff

ABSTRACT

The Agulhas Ocean Current is a powerful and persistent western boundary current that flows along the continental shelf edge off the eastern coast of South Africa in a southerly direction. In addition to the tide- and wind-induced currents, the Agulhas Current influences the nearshore currents in Durban Bay, for example, the Durban Eddy. eThekwini Municipality and Deltares proposed that Durban be used as a pilot study to investigate the capabilities of developing a Delft3D Flexible Mesh (D-Flow FM) model that integrates the combined forcing of ocean currents, tide and wind in a coastal model domain, which once successfully achieved, is to be integrated within eThekwini's Forecast Early Warning System.

The aim of this study is to use D-Flow FM to accurately model the Agulhas Current and analyse its effects on the nearshore waters of Durban. Output from global ocean models, such as the NEMO models operated by E.U. Copernicus Marine Service Information (CMEMS) in the Global Reanalysis Multi-Model Ensemble Product (GREP), include the Agulhas Current but are not suitable for coastal applications due to their relatively coarse resolution and absence of tidal forcing. For this reason, model output from the GREP was downscaled to a coastal scale using a D-Flow FM model of KZN with appropriate boundary conditions and evaluating the use of a new Delft3D nudging technique.

The final D-Flow FM model that was developed applied a relatively high-resolution grid on top of the continental shelf. A stable ocean current was simulated by forcing the model with a full set of 3D ocean boundary conditions, including currents, salinity, temperature, sea surface anomalies. In addition, the model was forced with tide and wind. Model tests showed that the nudging technique was not required when applying a suitable model extent. Realistic currents seem to develop along the edge of the shelf in the D-Flow FM model as observed from literature and measurements.

The final coastal model output was compared with Acoustic Doppler Current Profiler (ADCP) data from ACEP (African Coelacanth Ecosystem Program) and data from a SADCO (Southern African Data Centre for Oceanography) database off Durban. The results of the D-Flow FM coastal model correlated better with these measurements when statistically compared to data from the GREP.

The D-Flow FM coastal model was used to reproduce the Durban Eddy and analyse its modelled characteristics. The modelled duration of the eddy was between 8 to 10 days, which included the formation and dissipation of the eddy. A monthly average in agreement with previous observational studies of 1.66 eddies was seen from model outputs, with the reversal of currents along the Durban coast whenever an eddy was present.

DECLARATION

I, Kemira Naidoo, declare that the research reported in this dissertation, except where otherwise indicated, is my original research and has not been submitted for any degree or examination at any other university. This dissertation does not contain other persons' data, pictures, graphs, or other information unless specifically acknowledged as being sourced from other persons. This dissertation does not contain other persons' writing unless specifically acknowledged as being sourced from other researchers. Where other written sources have been quoted, their words have been re-written, but the general information attributed to them has been referenced. Where their exact words have been used, then their writing has been placed in italics and inside quotation marks and referenced. This dissertation does not contain text, graphics or tables copied and pasted from the Internet, unless specifically acknowledged, and the source is detailed in the dissertation and the References sections.

……. …….

Kemira Naidoo Date

As the candidate's Supervisors, I approve the submission of this dissertation.

……. …….

Dr J. J. Pringle Date

……. …….

Prof. D Stretch Date

……. …….

R. de Graaff Date

ACKNOWLEDGEMENTS

This work would not have been possible without the help and support from the following people and organizations:

My main supervisor Dr Justin Pringle, whose academic support and correspondence throughout the duration of this course are extremely appreciated.

Co-supervisor Prof Derek Stretch, whose expertise in fluid dynamics has contributed to this research.

Reimer de Graaff, another co-supervisor, but more importantly an incredible mentor. Thank you for your hospitality during my stay in the Netherlands and the constant support and guidance you have given me throughout the years. I really appreciate all that you have done for me and this research would not have been possible without your efforts.

Tom Bogaard – Thank you also for your incredible kindness during my stay in the Netherlands and your willingness to always assist me throughout this process. I am deeply grateful for all your help and support. Your contributions and hospitality are invaluable.

Ethekwini Municipality for sponsoring this research. In particular, I would like to acknowledge Randeer Kasserchun and Geoff Tooley for their support and approval of my internship. Acknowledgement goes to the Coastal, Stormwater and Catchment Department for providing some of the datasets used in this research.

Deltares, for allowing and offering me an internship at their offices in Delft, Netherlands. I would also like to thank their amazing team who worked on the Durban project. They were instrumental during my internship. I am also grateful to Deltares for the resources and opportunities that they have provided to me.

The South African Environment Observation Network (SAEON) for permission to use data that is still under embargo. This includes the use of the Offshore ADCP and ACEP measurements.

Navy Hydro Office for their bathymetry and tidal measurements.

The journey to completing this master's dissertation has been a long and sometimes enduring one, but my family and friends have been a huge support system. My deepest appreciation goes to my father, Benji Naidoo, for his encouragement and support throughout my entire life. I would also like to thank my mum, Rita Reddy, who is my personal cheerleader. Special thanks also to Sean Naidoo and Kanthen Nair for their assistance.

CONTENTS

Abstract i

Declaration ii

Acknowledgements iii

Contents iv

List of figures viii

List of tables xv

List of symbols xvi

Chapter 1 1

Introduction 1

1.1 Background 1

1.2 Motivation 2

1.3 Research Questions 3

1.4 Aim 4

1.5 Approach 4

1.6 Dissertation Outline 5

Chapter 2 6

Literature Review 6

2.1 Introduction 6

2.2 The Agulhas Ocean Current 7

2.2.1 Agulhas Undercurrent 9

2.2.2 (KZN) Natal Bight and the influence of the Agulhas Current 10

2.2.3 Natal Pulses 12

2.2.4 The Durban Eddy 12

2.3 Modelling Ocean Currents 19

2.3.1. Numerical Schemes 22

2.3.2 Vertical Coordinate System 22

2.3.3 Boundary Conditions 24

2.4 Delft3D 26

2.4.1 Delft3D-FLOW 26
2.4.2 D-Flow FM 29
2.5 Summary 31
Chapter 3 32
Methodology 32
3.1. Model Descriptions and Configurations 32
3.1.1. The Nudging Technique 34
3.2. The Internship Model 36
3.2.1. Extent and Location 36
3.2.2. Refinement 37
3.2.3. Co-ordinate System 37
3.2.4. Bathymetry 38
3.2.5. Forcing Parameters 39
3.3 Model Testing and Developments 42
3.3.1. Initial Boundary Implementation with a coarse, simple grid 42
3.3.2. Testing the Nudging Technique 43
3.3.3. Model Boundary Testing with Nudging 44
3.3.4. Improving the Internship Model 45
3.4. Test08 46
3.5 Measured data 50
3.5.1. Offshore ADCP Data 50
3.5.2 ACEP Data 51
3.5.3 SANHO Tide Gauge 52
Chapter 4 53
Results and comparisons 53
4.1. The Internship Model 53
4.1.1 Initial Model Outputs 53
4.1.2. Comparing the initial model with observed data 56
4.1.3. The Durban Eddy 59

4.2. Test08 65
4.2.1. Offshore ADCP 66
4.2.2. ACEP Data: 74
4.3. Operational Engineering Applications 90
4.3.1. Forecast Early Warning System (FEWS) 90
4.3.2. Coastal Inundation 91
4.3.3 Particle Tracking 93
4.4 Limitations 94
4.4.1 D-Flow FM 94
4.4.2 Bathymetry 95
4.4.3 Current Measurements 95
4.4.4 Durban Eddy 95
Chapter 5 96
Discussions and Conclusions 96
5.1. Discussions 96
5.1.1. Modelling of the Agulhas Current 96
5.1.2. The Durban Eddy 97
5.1.3. The Agulhas Current and the Durban Coastline 97
5.1.4 Summary 98
5.2. Recommendations 100
5.3. Conclusion 101
References 102
Appendix A 112
A.1 Introduction 112
A.2 Initial Boundary Implementation: 112
A.3 Testing the Nudging Technique: 117
A.4 Model Boundary Testing with Nudging: 119
A.5 Larger Model development and testing: 136
A.6 Stable, Refined, Rectangular model: 138

A.7 Summary 140

LIST OF FIGURES

Figure 1: Location map showing the KZN Bight Vs the Durban Bay, adapted from Scharler UM, Ayers MJ (2019) and Corbella S, Stretch D (2012a) 3
Figure 2.1: The Agulhas Current and its features, adapted from figure 20-001 in Lutjeharms (2006) 7
Figure 2.2: Current meter data in the Agulhas Current showing typical undercurrent structure of strong intensity on 14 January 2005. Yellow to red indicates southwest velocities (main Agulhas Current) and northeast velocities are shown in blue (Agulhas Undercurrent). Bathymetry shown in gray. Taken from Beal (2009). 9
Figure 2.3: Bathymetry (m) along the KwaZulu-Natal (KZN) coast, showing the KZN Bight region (from Martin and Flemming 1988). 11
Figure 2.4: The KZN Bight, Durban Eddy and The Agulhas Current, adapted from Scharler et al. (2016) and Pearce et al. (1978). The distance between the coast and the Agulhas Current varies according to formation of Eddy and Natal Pulses. 13
Figure 2.5: Taken from Guastella LA and Roberts MJ. 2016. Dynamics and role of the Durban cyclonic eddy in the KwaZulu-Natal Bight ecosystem. The figure suggests leakage of the Eddy into the Durban Bay. 16
Figure 2.6: Paths of surface satellite-tracked drifters (69 – 75) deployed into the Durban Eddy off Durban during 2010). Taken from Guastella and Roberts (2016). 18
Figure 2.7: Time and Spatial Scales of Various Oceanic and Atmospheric Phenomena taken from Lakshmi et al (2000) 21
Figure 2.8: Typical representation of vertical grid types, adapted from OC2910 - Numerical Ocean Modelling Concepts, 2003) 23
Figure 2.9: Modules within the Delft3D suite taken from dos Santos Gil (2014): With WAQ (Water Quality), PART (Particle Tracking), FLOW (hydrodynamic flow module), WAVE (Short wave propagation), ECO (Ecological Module) and SED (Sediment Transportation). 26
Figure 2.10: Total depth, h, depth corresponding to reference level, d, and variation of reference level, η. 1- Water Surface, 2- Reference Level (M.W.L.) and 3 - σ layers. Adapted from dos Santos Gil (2014). 27
Figure 3.1: Image of D-Flow FM grid with polygon to be used for internal or interior nudging 36
Figure 3.2.1: Location of the model in spherical co-ordinates, with zoomed in snapshot of Durban Bay area and model extents. The grid lies as close as possible to the eastern coastline of South Africa, extended on either ends of the KwaZulu Natal coast. Grid is overlayed on a Google Earth image. 37
Figure 3.3.2: Refinement and Extent of grid 37

Figure 3.2.2:Internship Model showing Vertical Level (m) of sea floor 38
Figure 3.2.3: GREP data for both Salinity (left) and Temperature (right)..... 40
Figure 3.4.1: Large DFM model with Water Level, Salintiy and Temperature boundary conditions, including internal spatial nudging 45
Figure 3.4.1: Variations in model extent and resolution: Coarse resolution (10km) in deep water, high resolution (now 300 m) along the coast and relatively high resolution at upper shelf slope (Deltares, 2019b). Internship model grid configuration shown on the left and new, further developed model grid configuration shown on the right..... 46
Figure 3.4.2: Model Schematisation of Test08 (Deltares, 2019b) 47
Figure 3.4.3: Review and re-interpolate xyz data to ensure best quality and realistic model depth and corresponding to CMEMS in deep part of the model (Deltares, 2019b)..... 48
Figure 3.5.1: Location of Offshore ADCP: 30ºS 31.5ºE (shelf edge) in ±550m deep water..... 50
Figure 3.5.2: ACEP transects along the KZN coastline with locations of various output maps at different periods within the ACEP survey, taken and adapted from Fennessy et al (2016)..... 51
Figure 3.5.3: Locations of UHSLC Datapoint (red) and closest observation point from D-Flow FM Internship model (blue) taken from Google Earth. 52
Figure 4.1.1: Typical Water Level (Tide) initial output from a simulation for May 2010 54
Figure 4.1.2. (a) Typical outputs for water level at SANHO Tide Gauge. Location of SANHO Tide Gauge: 29°52'1.20"S, 31° 3'0.00"E. Blue line reflects tide from the D-Flow FM internship model and red line shows SANHO observed tide. (b) Error Statistics for tidal comparisons in (a) 54
Figure 4.1.3: Typical Temperature output from the internship model simulation including velocity vectors indicating magnitude and direction of flow for 15 July 2010. (a) GREP Temperature Map Output, (b) Internship Model Temperature Map Output and (c) Temperature Profile for location (29°55'34.74"S, 31°27'38.39"E) shown with red dot on (a) and (b) and closest two observation points from the Internship Model..... 55
Figure 4.1.4: Typical Salinity output from the internship model simulation including velocity vectors indicating magnitude and direction of flow for 21 July 2010. (a) GREP Salinity Map Output, (b) Internship Model Salinity Map Output and (c) Salinity Profile for location (29°55'34.74"S, 31°27'38.39"E) shown with red dot on (a) and (b) and closest two observation points from the Internship Model..... 55
Figure 4.1.5: Typical Velocity output from the internship model simulation including velocity vectors indicating magnitude and direction of flow for 21 July 2010. (a) GREP Velocity Map Output, (b) Internship Model Velocity Map Output and (c) Velocity Profile for location (29°55'34.74"S, 31°27'38.39"E) shown with red dot on (a) and (b) and closest two observation points from the Internship Model..... 56

Figure 4.1.6: Time series for the year 2009 showing velocity magnitude of: GREP data (in black), Offshore ADCP (in red) and Internship model data (in green). 57
Figure 4.1.7: Time series for the year 2009 showing velocity direction of: GREP data (in black), Offshore ADCP (in red) and Internship model data (in green). 58
Figure 4.1.8: (a) Location A from ACEP survey, (b) Location B from ACEP survey. 59
(c) Location C from ACEP survey, (d) Location D from ACEP survey. Red vectors show ACEP ADCP velocity magnitude and direction, while black vectors show Internship model velocity magnitude and direction 59
Figure 4.1.9: (a) GREP Surface Map Output extracted from the eThekwini Municipalities FEWS, (b) D-Flow FM Model Surface Map Output extracted from the eThekwini Municipalities FEWS. Both outputs are taken on 6th September 2021at 0m depths (surface). 60
Figure 4.1.10: (a) Map output from the Internship Model indicating simulated size and location of the Durban (red circle), (b) Zoomed in map output showing edge of the Agulhas Current and Durban Eddy from the Internship Model with the Offshore ADCP velocity magnitude and direction shown by the vector in red 60
Figure 4.1.11: Temperature simulations showing the formation of the Durban Eddy from the 8th to the 17th of January 2009. 62
Figure 4.1.12: Velocity magnitude simulations showing the formation of the Durban Eddy from the 1st of July 2009 to the 10th of July 2009 63
Figure 4.1.13: (a) Simulation off the Durban coast showing velocity magnitudes when there is no eddy present and (b) when the eddy is situated off Durban , with the Offshore ADCP velocity vector (red arrow) 65
Figure 4.2.1: Time series comparing velocity magnitudes and directions for the Offshore ADCP measurements, GREP and the D-Flow FM models at similar water depths (approximately 50m) below the surface from April 2010 to July 2010 66
Figure 4.2.2: Time series comparing velocity magnitudes and directions for the Offshore ADCP measurements, GREP and the D-Flow FM models at similar water depths (approximately 300m) below the surface 67
Figure 4.2.3: Error Analysis on Offshore ADCP Daily Data between April and July 2010 for x-velocity component: (a) GREP Error Analysis, (b) Internship Model Error Analysis and (c) Test08 Error Analysis 68
Figure 4.2.4: Error Analysis on Offshore ADCP Daily Data between April and July 2010 for y-velocity component: (a) GREP Error Analysis, (b) Internship Model Error Analysis and (c) Test08 Error Analysis 69
Figure 4.2.5: Error Analysis on Offshore ADCP Hourly Data between April and July 2010 for x-velocity component: (a) Internship Model Error Analysis and (b) Test08 Error Analysis 69

Figure 4.2.6: Error Analysis on Offshore ADCP Hourly Data between April and July 2010 for y-velocity component: (a) Internship Model Error Analysis and (b) Test08 Error Analysis 70
Figure 4.2.7: Current Rose showing frequency distribution of velocity magnitude and direction at depth 60m from surface: (a) Offshore ADCP Current Rose, (b) GREP Current Rose, (c) Internship Model Current Rose and (d) Test08 Current Rose..... 71
Figure 4.2.8: Offshore ADCP Data (white dot on maps) compared to GREP, Test08 and Internship Models. (a) GREP Velocity Magnitude Map, (b) Test08 Velocity Magnitude Map, (c) Internship Velocity Magnitude Map and (d) Vertical Profiles for Magnitude and Direction which include the closest 2 observation points(to the Offshore ADCP) for both the Internship and Test08 models – 20 June 2010..... 73
Figure 4.2.9: (a) Location A from the ACEP survey and (b) vertical average depth velocity magnitude and direction profiles of GREP, ACEP ADCP and both D-Flow FM Models, test08 and internship, for Location A on 24 July 2010..... 74
Figure 4.2.10: Velocity Map outputs for approximately 17m depths on 24 July 2010: (a) GREP Velocity Map Output with Internship (Pink) and Test08 (White) Model Domain Outlines, (b) Internship Model Velocity Map Output, (c) Test08 Model Velocity Map Output and (d) Velocity vectors indicating velocity magnitude and direction at location A: ACEP survey datapoints (light blue), GREP (dark blue), Internship (black) and Test08 (red). Size and direction of vectors correlate to velocity magnitude and direction respectively..... 75
Figure 4.2.11: Velocity Map outputs for approximately 57m depths on 24 July 2010: (a) GREP Velocity Map Output with Internship (Pink) and Test08 (White) Model Domain Outlines, (b) Internship Model Velocity Map Output, (c) Test08 Model Velocity Map Output and (d) Velocity vectors indicating velocity magnitude and direction at location A: ACEP survey datapoints (light blue), GREP (dark blue), Internship (black) and Test08 (red). Size and direction of vectors correlate to velocity magnitude and direction respectively..... 76
Figure 4.2.12: Velocity Map outputs for approximately 161m depths on 24 July 2010: (a) GREP Velocity Map Output with Internship (Pink) and Test08 (White) Model Domain Outlines, (b) Internship Model Velocity Map Output, (c) Test08 Model Velocity Map Output and (d) Velocity vectors indicating velocity magnitude and direction at location A: ACEP survey datapoints (light blue), GREP (dark blue), Internship (black) and Test08 (red). Size and direction of vectors correlate to velocity magnitude and direction respectively..... 77
Figure 4.2.13: (a) Location B from the ACEP survey and (b) vertical average depth velocity magnitude and direction profiles of GREP, ACEP ADCP and both D-Flow FM Models, test08 and internship, for Location A on 26 July 2010..... 78
Figure 4.2.14: Velocity Map outputs for approximately 17m depths on 26 July 2010: (a) GREP Velocity Map Output with Internship (Pink) and Test08 (White) Model Domain Outlines, (b) Internship Model Velocity Map Output, (c) Test08 Model Velocity Map Output and (d) Velocity

vectors indicating velocity magnitude and direction at location B: ACEP survey datapoints (light blue), GREP (dark blue), Internship (black) and Test08 (red). Size and direction of vectors correlate to velocity magnitude and direction respectively..... 79
Figure 4.2.15: Velocity Map outputs for approximately 57m depths on 26 July 2010: (a) GREP Velocity Map Output with Internship (Pink) and Test08 (White) Model Domain Outlines, (b) Internship Model Velocity Map Output, (c) Test08 Model Velocity Map Output and (d) Velocity vectors indicating velocity magnitude and direction at location B: ACEP survey datapoints (light blue), GREP (dark blue), Internship (black) and Test08 (red). Size and direction of vectors correlate to velocity magnitude and direction respectively..... 80
Figure 4.2.16: Velocity Map outputs for approximately 161m depths on 26 July 2010: (a) GREP Velocity Map Output with Internship (Pink) and Test08 (White) Model Domain Outlines, (b) Internship Model Velocity Map Output, (c) Test08 Model Velocity Map Output and (d) Velocity vectors indicating velocity magnitude and direction at location B: ACEP survey datapoints (light blue), GREP (dark blue), Internship (black) and Test08 (red). Size and direction of vectors correlate to velocity magnitude and direction respectively..... 81
Figure 4.2.17: (a) Location C from the ACEP survey and (b) vertical average depth velocity magnitude and direction profiles of GREP, ACEP ADCP and both D-Flow FM Models, test08 and internship, for Location A on 27 July 2010..... 82
Figure 4.2.18: Velocity Map outputs for approximately 17m depths on 27 July 2010: (a) GREP Velocity Map Output with Internship (Pink) and Test08 (White) Model Domain Outlines, (b) Internship Model Velocity Map Output, (c) Test08 Model Velocity Map Output and (d) Velocity vectors indicating velocity magnitude and direction at location C: ACEP survey datapoints (light blue), GREP (dark blue), Internship (black) and Test08 (red). Size and direction of vectors correlate to velocity magnitude and direction respectively..... 83
Figure 4.2.19: Velocity Map outputs for approximately 57m depths on 27 July 2010: (a) GREP Velocity Map Output with Internship (Pink) and Test08 (White) Model Domain Outlines, (b) Internship Model Velocity Map Output, (c) Test08 Model Velocity Map Output and (d) Velocity vectors indicating velocity magnitude and direction at location C: ACEP survey datapoints (light blue), GREP (dark blue), Internship (black) and Test08 (red). Size and direction of vectors correlate to velocity magnitude and direction respectively..... 84
Figure 4.2.20: Velocity Map outputs for approximately 161m depths on 27 July 2010: (a) GREP Velocity Map Output with Internship (Pink) and Test08 (White) Model Domain Outlines, (b) Internship Model Velocity Map Output, (c) Test08 Model Velocity Map Output and (d) Velocity vectors indicating velocity magnitude and direction at location C: ACEP survey datapoints (light blue), GREP (dark blue), Internship (black) and Test08 (red). Size and direction of vectors correlate to velocity magnitude and direction respectively..... 85

Figure 4.2.21: (a) Location D from the ACEP survey and (b) vertical average depth velocity magnitude and direction profiles of GREP, ACEP ADCP and both D-Flow FM Models, test08 and internship, for Location A on 28 July 2010 86
Figure 4.2.22: Velocity Map outputs for approximately 17m depths on 28 July 2010: (a) GREP Velocity Map Output with Internship (Pink) and Test08 (White) Model Domain Outlines, (b) Internship Model Velocity Map Output, (c) Test08 Model Velocity Map Output and (d) Velocity vectors indicating velocity magnitude and direction at location D: ACEP survey datapoints (light blue), GREP (dark blue), Internship (black) and Test08 (red). Size and direction of vectors correlate to velocity magnitude and direction respectively. 87
Figure 4.2.23: Velocity Map outputs for approximately 57m depths on 28 July 2010: (a) GREP Velocity Map Output with Internship (Pink) and Test08 (White) Model Domain Outlines, (b) Internship Model Velocity Map Output, (c) Test08 Model Velocity Map Output and (d) Velocity vectors indicating velocity magnitude and direction at location D: ACEP survey datapoints (light blue), GREP (dark blue), Internship (black) and Test08 (red). Size and direction of vectors correlate to velocity magnitude and direction respectively. 88
Figure 4.2.24: Velocity Map outputs for approximately 161m depths on 28 July 2010: (a) GREP Velocity Map Output with Internship (Pink) and Test08 (White) Model Domain Outlines, (b) Internship Model Velocity Map Output, (c) Test08 Model Velocity Map Output and (d) Internship Model Velocity Map Output with velocity vectors indicating velocity magnitude and direction at location D: ACEP survey datapoints (blue), GREP (green), Internship (black) and Test08 (red). Size and direction of vectors correlate to velocity magnitude and direction respectively and map background is based on Internship model velocity magnitudes. 89
Figure 4.3.1: Screenshot taken from eThekwini Municipalities FEWS, showing CMEMS model (left) and D-Flow FM Flexible Mesh model (right). Deltares (2019b). 90
Figure 4.3.2: Water level output showing hindcast (blue) and forecast (red) data for NSRI tide gauge (black dots) and D-Flow FM model (solid lines). Deltares (2019b). 91
Figure 4.3.3: Typical SWAN output from FEWS for an observation point off the Umhlanga Main Beach, including wave composition (top left), SWAN model grid (top right) and hindcast and forecast data (bottom). Deltares (2019b). 91
Figure 4.3.4: Model outputs for March 2017 Coastal Inundation at Durban Central Beachfront. SWAN model output (left) and SFINCS model output (right). Deltares (2019b). 92
Figure 4.3.5: Typical example of Particle Tracking within FEWS with the D-Flow FM model (left) and corresponding particle migration (right). 93
Figure 4.3.6: CMEMS velocity output (left), D-Flow FM velocity output (middle) and particle tracking simulation (left) 94
Figure A1: BC_ST_IniNudge - Water Level Outputs for surface layer of the model (left) and vertical profile from MSL (right) 119

Figure A2: BC_ST_IniNudge - Temperature Outputs for surface layer of the model (left) and temperature vertical profile (right) 120
Figure A3: BC_ST_IniNudge - Salinity Outputs for surface layer of the model (left) and salinity vertical profile (right) 120
Figure A4: BC_ST_IniNudge - Initial Velocity Outputs for surface layer of the model (left) and initial velocity vertical profile (right) 121
Figure A5: BC_ST_IniNudge - Velocity Outputs for surface layers of the model as the model progresses 121
Figure A6: BC_ST_IniNudge - Velocity Vertical Profiles of the model as the model progresses 121
Figure A7: BC_ST_noIniNudge - Water Level Outputs for surface layer of the model (left) and vertical profile from MSL (right) 122
Figure A8: BC_ST_noIniNudge – Temperature Outputs for surface layer of the model (left) and temperature vertical profile (right) 123
Figure A9: BC_ST_noIniNudge – Salinity Outputs for surface layer of the model (left) and Salinity vertical profile (right) 123
Figure A10: BC_ST_noIniNudge – Velocity Outputs for surface layer of the model (left) and Velocity vertical profile (right) 124
Figure A11: BC_ST_Nudge - Water Level Outputs for surface layer of the model (left) and vertical profile from MSL (right) 124
Figure A12: BC_ST_Nudge – Temperature Outputs for surface layer of the model (left) and temperature vertical profile (right) 125
Figure A13: BC_ST_Nudge – Salinity Outputs for surface layer of the model (left) and salinity vertical profile (right) 125
Figure A14: BC_ST_Nudge – Temperature Outputs for surface layer of the model (left) Salinity Outputs for surface layer of the model (right) 126
Figure A15: BC_ST_Nudge – Velocity Outputs for surface layer of the model (left) and velocity vertical profile (right) 126
Figure A16: BC_STV_IniNudge – Water Level Outputs for surface layer of the model (left) and vertical profile from MSL (right) 127
Figure A17: BC_STV_Nudge – Velocity Outputs for surface layer of the model (left) and velocity vertical profile (right) 128
Figure A18: BC_STV_Nudge – Salinity Outputs for surface layer of the model (left) and salinity vertical profile (right) 128
Figure A19: BC_STV_Nudge – Velocity Outputs for surface layer of the model (left) and velocity vertical profile (right) 129

Figure A20: BC_STV_NoIniNudge – Water Level Outputs for surface layer of the model (left) and vertical profile from MSL (right) 129
Figure A21: BC_STV_NoIniNudge – Temperature Outputs for surface layer of the model (left) and temperature vertical profile (right) 130
Figure A22: BC_STV_NoIniNudge – Salinity Outputs for surface layer of the model (left) and salinity vertical profile (right) 130
Figure A23: BC_STV_NoIniNudge – Velocity Outputs for surface layer of the model (left) and velocity vertical profile (right) 131
Figure A24: BC_STV_Nudge – Water Level Outputs for surface layer of the model (left) and vertical profile from MSL (right) 131
Figure A25: BC_STV_Nudge – Temperature Outputs for surface layer of the model (left) and temperature vertical profile (right) 132
Figure A26: BC_STV_Nudge – Salinity Outputs for surface layer of the model (left) and salinity vertical profile (right) 132
Figure A27: BC_STV_Nudge – Velocity Outputs for surface layer of the model (left) and velocity vertical profile (right) 133
Figure A28: BC_V_Nudge – Water Level Outputs for surface layer of the model (left) and vertical profile from MSL (right) 134
Figure A29: BC_V_Nudge – Temperature Outputs for surface layer of the model (left) and temperature vertical profile (right) 134
Figure A30: BC_V_Nudge – Salinity Outputs for surface layer of the model (left) and salinity vertical profile (right) 135
Figure A31: BC_V_Nudge – Velocity Outputs for surface layer of the model (left) and velocity vertical profile (right) 135
Figure A32: Velocity Magnitude Map Output from large flexible mesh grid 137
Figure A33: Time series showing the comparison between CMEMS data and the Stable, refined, rectangular model with wind, tide, and nudging inputs 139

LIST OF TABLES

Table 1: Summary of Durban Eddy Statistics taken from Guastella and Roberts (2016)..... 17
Table 2: Uniform initial conditions for flow velocity components are zero by default 41
Table 3: Summary of Testing Boundary Conditions and Nudging Results 44

LIST OF SYMBOLS

C	concentration (representing salinity or temperature or both)	(ppt/°C)
c_D	constant to be determined	
d	reference water level/depth	(m)
D_H	horizontal eddy diffusivity coefficient	(m^2 s^{-1})
D_V	vertical eddy diffusivity coefficient	(m^2 s^{-1})
f	represents the Coriolis parameter, $f = 2\Omega \sin(\varphi)$	(s^{-1})
F_u *or* F_x	unbalance of horizontal Reynolds stresses in x-direction	(kg m^2 s^{-1})
F_v *or* F_y	unbalance of horizontal Reynolds stresses in y-direction	(kg m^2 s^{-1})
g	is gravitational acceleration	(m s^{-2})
h	total water depth	(m)
K_z	eddy diffusivity coefficient	(m^2 s^{-1})
k	turbulent kinetic energy	(m^2 s^{-2})
L	mixing length	(m)
M_x	contributions due to external sources or sinks of momentum	
M_y	contributions due to external sources or sinks of momentum	
n	is the prescribed direction	
P_u	pressure gradients in the x-direction	(N m^{-2})
P_v	pressure gradients in the y-direction	(N m^{-2})
Q	effects per unit area due to discharge	
q_{in}	local source of water per unit of volume	(m^3)
q_{out}	local sink of water per unit of volume	(m^3)
S	model salinity	(ppt)
S_{nudge}	target field value	(ppt)

T	Temperature	(°C)
t	time	(s)
T_{nudge}	user-defined nudging timescale	(s)
u	horizontal velocity in the x cartesian direction	(m s^{-1})
$\boldsymbol{u}$	$= (u_x, u_y)^t$, a velocity vector with u_x and u_y components	(m s^{-1})
u_z	vertical velocity component	(m s^{-1})
U	depth-averaged velocities in horizontal direction	(m s^{-1})
V	Velocity	(m s^{-1})
V	depth-averaged velocities in vertical direction	(m s^{-1})
v	is the horizontal velocity in the y cartesian direction	(m s^{-1})
ν_H	horizontal eddy viscosity coefficient	(m^2 s^{-1})
ν_V	vertical eddy viscosity coefficient	(m^2 s^{-1})
w	vertical velocity for the Cartesian coordinate system	(m s^{-1})
z	vertical direction in z-layer models	(m)
Δt	change in time	(s)
Δx	change in horizontal distance in x direction	(m)
Δy	change in horizontal distance in y direction	(m)
η	variation of the reference level	(m)
ω	vertical velocity in the z cartesian direction	(m s^{-1})
σ	vertical coordinate in sigma models	
ρ	density	(kg m^{-3})
∇	$= \left(\frac{\partial}{\partial x}, \frac{\partial}{\partial y}\right)^t$	
👍	Included/ Achieved	

CHAPTER 1

INTRODUCTION

1.1 Background

eThekwini Municipality has developed a Forecast Early Warning System (FEWS) that focuses mainly on predicting inland stormwater-related floods. The next phase of the early warning system for the Municipality is to couple inland and coastal forecasting and modelling. In order to include the dynamics of nearshore processes along the eThekwini coastline, a coastal-scale ocean model needed to be developed that incorporates the combined forcing of the tide, wind, and ocean currents. The Agulhas Current is a strong western boundary current that flows along the east coast of South Africa (Lutjeharms, 2006). There is evidence that this current and its spin off features significantly influence the nearshore coastal dynamics of Durban (Schumann, 1988). This has implications for coastal management and decision making.

eThekwini Municipality and Deltares have shared an ongoing relationship for the past 10 years. Deltares, developer of the coastal modelling software Delft3D, introduced a new package within Delft3D called Delft3D Flexible Mesh or more commonly known as D-Flow FM. This flexible mesh software reduces the need to use nested grids within larger domains and instead, sets up only one grid (structured or unstructured) for any type of model. The established collaboration between Deltares and eThekwini led to a proposal from Deltares for Durban to be used as a pilot study to investigate the capabilities of developing a Delft3D Flexible Mesh model that integrates the combined forcing of ocean currents, tide and wind in one regional model domain. This involved an internship at Deltares, Netherlands, where debugging and additions to the software code were done in conjunction with this research study.

Delft3D uses the shallow-water equations to investigate nearshore conditions in coastal zones but deep ocean waters can also be incorporated within the model if appropriate ocean boundary conditions are prescribed (Deltares, 2019b). Therefore, to incorporate a global ocean current such as the Agulhas within a coastal D-Flow FM model, boundary conditions from Global Ocean Models such as the NEMO (Nucleus for European Modelling of the Ocean) models from CMEMS (Copernicus Marine Environment Monitoring Services) or HYCOM (Hybrid Coordinate Ocean Model) are required. These ocean models provide large-scale analyses of our planet's oceanographic attributes. The coastal D-Flow FM model will be fed into eThekwini Municipalities operational FEWS after validation, with engineering applications such as particle tracking, coastal inundation and water quality modelling emerging from the model's outputs (to be used as boundary conditions).

1.2 Motivation

The Agulhas Current is one of the strongest western boundary currents, and flows close to Durban and neighbouring coastal cities in KZN (Beal et al, 2009, Lutjeharms, 2006). However, the extent of its impacts on nearshore hydrodynamics is not yet fully understood. Although many observations have been recorded, the effect of this ocean current on nearshore coastal currents have led to much debate within the scientific community (Barlow et al., 2013, 2015). A semi-permanent spin-off feature near Durban that originates from the Agulhas Current, called the Durban Eddy, could have significant impacts on the nearshore coastal currents within the Durban Bay and along the KZN coastline.

It is important for the city of Durban to successfully validate and calibrate a 3D ocean model for this region to understand and identify its effects on the Durban coastal circulation. Responsible coastal engineering designs require predicting the impacts that these currents have on eThekwini's coast and to quantify coastal processes. Currently, large-scale global ocean models are useful in predicting mesoscale (10 – 100km) hydrodynamics associated with ocean currents. However, models with higher grid resolution are required to better predict regional-scaled features and are more beneficial for nearshore analytical purposes for role players of coastal cities. Therefore, the need for an ocean model for the KZN coastline stems from the increase in interest in wave and current activity as well as the proposed future purposes of the model for coastal inundation and water quality.

This study aims to downscale output from a global ocean model to a regional scale model using D-Flow FM to replicate the Agulhas Current and its regional-scale features. Data from the GREP was downscaled to a regional scale for the KZN Bight (red arrow in Figure 1 below), with the focus area being the Durban Bay (blue arrow in Figure 1).

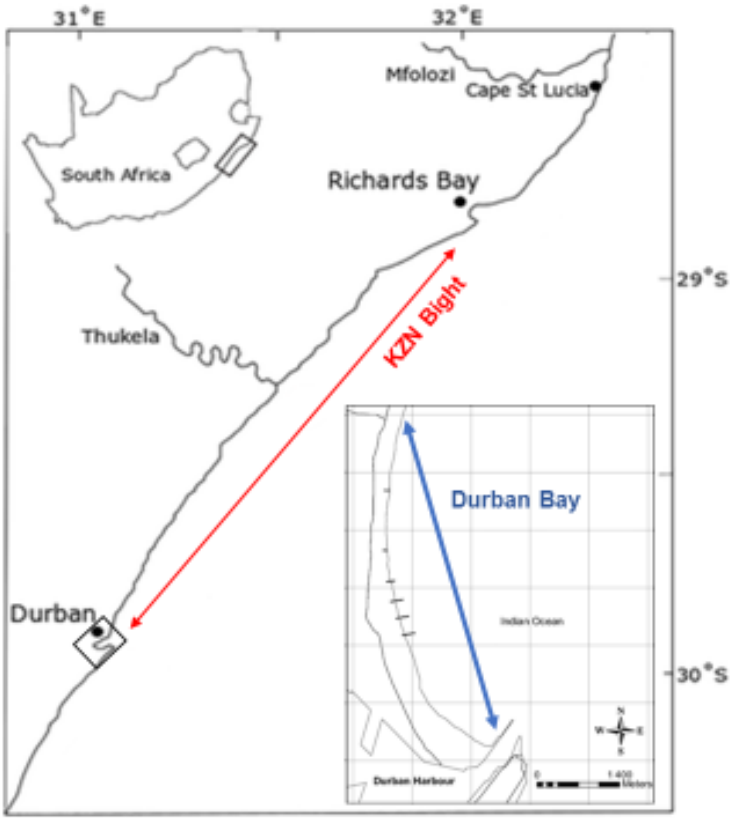

Figure 1: Location map showing the KZN Bight Vs the Durban Bay, adapted from Scharler UM, Ayers MJ (2019) and Corbella S, Stretch D (2012a)

1.3 Research Questions

This research can be divided into three questions. The first question relates to the capability of the D-Flow FM software and depicts the methodology for addressing the second and third questions.

1.1.1 Can a D-Flow FM model be developed that accurately simulates the hydrodynamics in the Durban offshore and nearshore region under the combined forcing of the tide, wind and ocean currents?

1.1.2 Using the model created in 1.1.1, can the physical aspects of the Durban Eddy be verified, i.e., characteristics, duration, frequency, affect from main Agulhas Current and upwelling?

1.1.3 What effect does the Agulhas Current have on the nearshore hydrodynamics of the Durban coastline?

1.4 Aim

This study aims to develop a coastal hydrodynamic model that bridges the gap between global ocean currents and the nearshore coastal environment. This includes a pilot study to investigate the capabilities of developing a D-Flow FM model that integrates the combined forcing of ocean currents, tide and wind, in one coastal model domain.

To analyse the Agulhas Current around the Durban Bight and its surrounding areas and identify how this current and its spin-off features impact the nearshore coastal dynamics of Durban.

To provide recommendations for future development and validation/calibration of the model

1.5 Approach

In order to successfully model the Agulhas Current, the following objectives need to be achieved:

- To understand the processes that drive the current and its features through a literature review
- To develop modelling skills using the D-Flow FM modelling software which includes:
  - curvilinear grid generation, grid refinement and orthogonalization
  - generation and implementation of boundary conditions (Water level, Temperature, Salinity, and UxUy Advection Velocities)
  - inputting metrological forcing and tidal conditions
  - understanding and changing parameters within the MDU (master definition unit) that are required to run the model
- To validate the output of the model from literature and observed measurements
- To develop realistic model simulations of the main Agulhas Current in combination with ocean current, tide and wind forcing, and model its nearshore impacts on the coastal currents off Durban
- To study the characteristics of the Durban Eddy and the spin-off of the ocean current along the Durban shoreline

1.6 Dissertation Outline

This dissertation comprises the following chapters:

Chapter 2 describes the coastal dynamics and global processes that are responsible for shaping the Agulhas Current and its impact on the coastal circulation. A thorough understanding of the currents and their effects on Durban's nearshore is required to accurately model the conditions and examine the results. This chapter starts with a broad analysis of different aspects of this research and narrows down to a more detailed approach for particular attributes that will be further examined and modelled in the chapters to follow.

Chapter 3 describes the modelling methods and techniques used to understand the type of software being utilised to set up a hydrodynamic model. This chapter gives a brief overview of the approaches and procedures. It illustrates the steps taken to configure a D-Flow FM Model for the east coast of South Africa, with a greater focus on the KZN Bights, in particular, off the coast of Durban. This chapter also provides a preliminary setup of steps taken to gather the relevant data and resources to produce a D-Flow FM model for the KZN coastline. It also indicates the numerous testing and trial model runs completed to achieve a stable model that depicts the Agulhas Current well. This includes a thorough testing process that not only allows for a successful establishment of existing modelling methods but also indicates changes of the software done in conjunction with Deltares software developers to improve and stabilize the model.

Chapter 4 presents the model results which are critically analysed and compared to the observed data and existing literature.

Chapter 5 presents the conclusions drawn from the results and recommendations on the further development of the model. Recommendations for further research into the modelling techniques are also included.

CHAPTER 2

LITERATURE REVIEW

2.1 Introduction

Durban is located on the east coast of South Africa in the KwaZulu Natal Province. It is one of the country's biggest cities and has one of the busiest ports in Africa (Guastella, 1994). Durban experiences a semi-diurnal tide with a meso-tidal range of 1-2m (Bosboom and Stive, 2013). The associated tidal currents are small compared to other hydrodynamic processes along the coast and the water column is considered to be generally well mixed in the first 20m (Malange, 2018). Durban has a maximum tidal range of 2m, and storm surges resulting from offshore cyclonic events can increase the water level up to 0.7m (Rautenbach et al, 2019; Mather and Stretch, 2012).

A predominantly north-eastward flow (as evident from the longshore drift of sediment) persists off Durban, with the occurrence of regular current reversals (Schumann EH, 1988). Local wind patterns can occasionally cause flow reversals of near-surface water, but the consistent nature of the flow suggests that the circulation is not entirely wind-driven. Schumann (1988) observed this recirculation in both temperature and current records off Durban's coast. The fact that there was little correlation with wind and air pressure observations from Schumann (1988) suggested that the fluctuations may be caused by the variability in the Agulhas Current and its possible spin-off features off Durban.

Although numerous observations and research has been done on the main Agulhas Current (e.g., Lutjeharms (2006), Boebel et al (2002), Beal (2009)), there have been few studies on the role of the Agulhas Current on nearshore currents and its influence on adjacent coasts. Guastella and Roberts (2016) used ADCP and satellite drifter measurements to describe the influence the Agulhas has on Durban's offshore currents at a local scale (within the KZN Bight shown in Figure 1 focusing on the Durban Eddy), whilst Penven et al (2010) used ROMS to model the current on a coarse, regional scale (highest resolution of 10km at the coast). However, neither study was able to document the influence at a coastal scale, of the Agulhas Current near the Durban coast.

This chapter presents a review of literature explaining the sources, features, spin-off effects and measurements of the main Agulhas Current. Many of the Agulhas Current's associated features will be briefly described in the subsequent sections. However, the key feature for this dissertation which will be explained in more detail is the Durban Eddy. Further on, a review is presented on ocean current modelling which describes the extent of ocean and coastal scales and exhibits the numerical methods and modelling frameworks to be used in this research. The chapter concludes with a detailed analysis on the modelling software to be used; D-Flow FM.

2.2 The Agulhas Ocean Current

The east coast of South Africa is embraced by the warm Agulhas Current ((1) – refer to Figure 2.1) which flows in a south-westerly direction (Schumann et al, 1991) and transports warm and salty equatorial Indian Ocean water (Tedesco et al, 2019) towards the South Pole. The current follows the continental shelf closely in southern African waters until it reaches the south of Port Elizabeth (3 in Figure 2.1), where it becomes unstable and forms frontal eddies (9 in Figure 2.1) (Lutjeharms et al., 1989).

Just south of Africa is the Agulhas bank, a triangular shape region (shallow and wide shelf) by the continental shelf and this is known as the Agulhas Bank. The bank acts as a barrier between the Agulhas and Benguela Current (Hutchings, 1994).

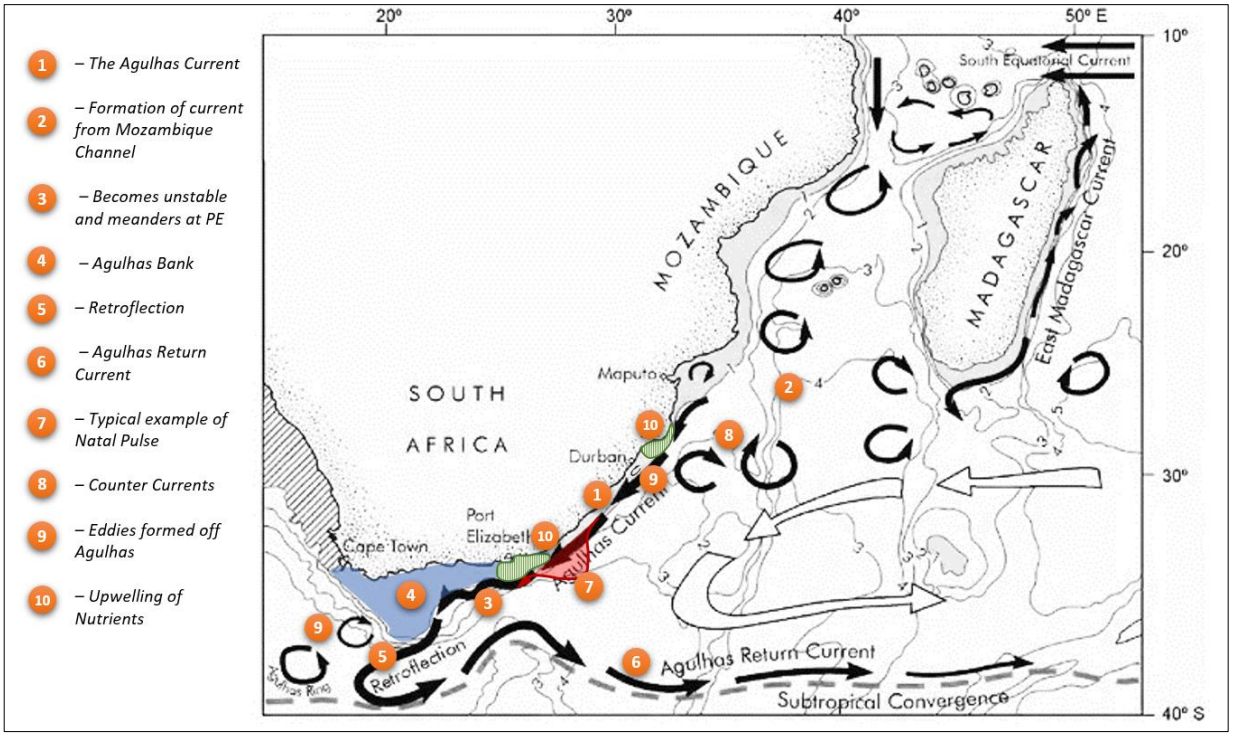

Figure 2.1: The Agulhas Current and its features, adapted from figure 20-001 in Lutjeharms (2006)

At the tip of the Agulhas Bank (4 in Figure 2.1), the current turns back on itself (5 in Figure 2.1), leaving the continental shelf and "retroflects" which is known as Retroflection (Boyd and Oberholster, 1994). The current then flows eastwards into the South Indian Ocean and this is known as the Agulhas Return Current (6 in Figure 2.1) (Lutjeharms and Ansorge, 2001). Early eastward retroflection can be caused by Natal Pulses, if they are large enough to interfere with the Agulhas Return Current (van Leeuwen and de Ruijter, 2000). These pulses can force the core of the Agulhas Current far offshore which induces retroflection further east than usually expected

(Lutjeharms and de Ruijter, 1996). The Agulhas Return Current links in the South Atlantic Current and the South Indian Ocean Current whilst exchanging waters from both regions (Lutjeharms and Ansorge, 2001). The Southern Agulhas Current remains a net source of mesoscale eddy energy due to the strong generation of eddies modulated by the topography (Tedesco et al, 2022).

The Agulhas Current (See Figure 2.1) is one of the largest global ocean currents and is the world's strongest western boundary current (Bryden et al, 2005; Beal et al, 2015; Lutjeharms, 2006). The Agulhas Current forms south of Madagascar and the Mozambique Channel (Source regions of eddies). It is a stable current but there can be alterations to its flow (Kruger, 2014). Beal and Elipot (2016) show in their findings how the greater Agulhas system forms a key component of the global circulation. At its southern extension, leakage of the Agulhas through cyclonic eddies (9 in Figure 2.1) can transport warm and saline Agulhas Current water from the Indian Ocean to the Atlantic. Whilst, on the other hand, the current is fed in by recirculating subtropical gyre waters (as shown in the Mozambique Channel in 2 from Figure 2.1), but also from waters from the Red and Arabian seas, the Indonesian throughflow, and the South Equatorial and East Madagascar Currents (Beal et al, 2006).

Source regions (2 from Figure 2.1) produce both cyclonic and anticyclonic mesoscale eddies that directly influence the variability of the northern Agulhas Current (Braby et al, 2016). These eddies propagate toward the offshore edge of the Agulhas Current, where they dissipate as they approach the current (Braby et al, 2016). Anticyclonic eddies can destabilize the current's trajectory and thus trigger cyclonic meanders (Tsugawa and Hasumi, 2010; Elipot and Beal, 2015). However, Braby et al (2016) suggested that cyclonic eddy interaction with the current results in even larger meanders.

The Agulhas Current which flows between 27°S and 40°S with a core width of 70km (60 to 80km range) (Boebel et al., 2002). Surface temperatures range from 23 to 26°C and surface salinity reaches 35.4 parts per thousand (Gordon et al., 1987). Speeds can exceed 2m/s (Lutjeharms, 2007). Transport range of 41 to 58 Sv$\times 10^6$ occurs in the upper 2000m occurs (McMonigal et al, 2022.

The current follows the continental shelf closely in southern African waters until it reaches the south of Port Elizabeth, where it becomes unstable and forms frontal eddies and meanders (Lutjeharms et al., 1989). The current is responsible for influencing the circulation of water within the shelf (Lutjeharms and van Ballegooyen, 1988) and significantly influences weather and climate over the African continent (Rouault et al., 2002).

Associated features of the Agulhas Current as described by Lutjeharms et al (1989), Boyd and Oberholster (1994), Beal (2009) and Guastella and Roberts (2016) include Natal Pulses, counter-currents, lee and shear eddies, upwelling of nutrients, Agulhas undercurrent and retroflection, which are all shown in Figure 2.1.

2.2.1 Agulhas Undercurrent

Beal and Bryden (1997) first established the existence of the Agulhas Undercurrent which carries water upstream (in the opposite direction) relative to the main Agulhas Current. This undercurrent also hugs the continental slope but at depths of 1200m directly below the core of the Agulhas Current (See figure 2.3).

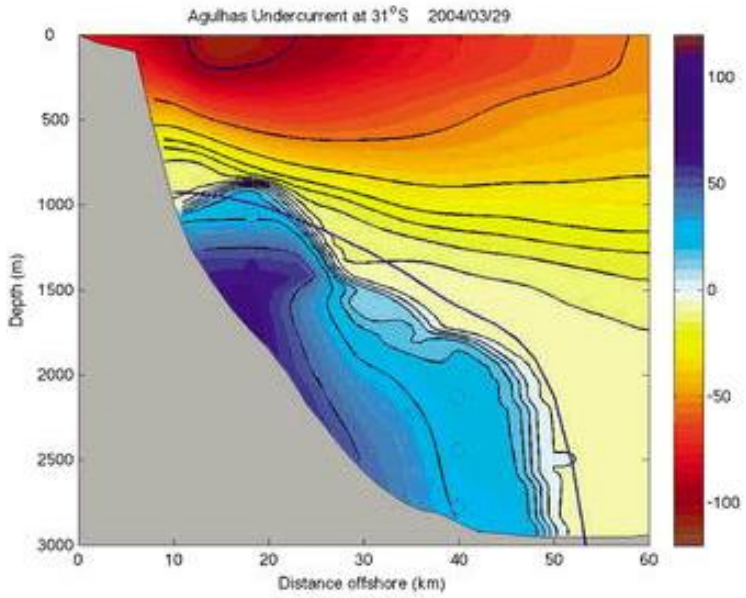

Figure 2.2: Current meter data in the Agulhas Current showing typical undercurrent structure of strong intensity on 14 January 2005. Yellow to red indicates southwest velocities (main Agulhas Current) and northeast velocities are shown in blue (Agulhas Undercurrent). Bathymetry shown in gray. Taken from Beal (2009).

The Agulhas Undercurrent occurs at 2000m deep and is 30km wide with speeds of 0.2m/s (Biastoch et al, 2009). Skogen (1999) stated that the undercurrent is only evident in some models and Maltrud and McClean (2005) suggested that this could be related to proper grid resolution. Undercurrents have also been found in the Mozambique Channel (de Ruijter et al, 2002) and under the East Madagascar Current (Nauw et al, 2008) which are both sources for the Agulhas Current. This suggests that there could be a connection between these undercurrents, and a likelihood of the Agulhas undercurrent being a continuation from the Mozambique channel (de Ruijter, 2002). Beal (2009) reports that north-eastward velocities from the undercurrent can reach

over 0.5m/s. Biastoch et al (2009) proved that the Natal Pulses directly affect the flow of the Agulhas Undercurrent. Their model also suggests little effect from the undercurrent northwards of the Natal Valley and the undercurrent is diffused in the northern Natal Valley. However, McMonigal et al (2022) suggested that the undercurrent (around 32°S) is not visible in the zonal mean across the boundary layer, as its weak northward transport over the continental slope is swamped by the larger southward transport of the Agulhas Current offshore.

2.2.2 (KZN) Natal Bight and the influence of the Agulhas Current

The wind along the KZN coastline originates from two pre-dominant wind directions: south to the southeast from March to November and northeast from December to February (Lamont et al, 2016). Storm winds, extreme swell and heavy rainfall are mostly related to cut-off lows, which are compact, persistent low-pressure weather systems that separate from the main westerly jet stream (Muofhe et al., 2020). These cut-off lows can become isolated and persist for several days southeast of Durban. Wind-induced currents only reach up to 0.2m/s on the adjacent shelf off Durban (DNV-RP-C205, 2010).

The coastline receives its highest rainfall between November and March (Schumann and Martin 1991; Schumann 1992; Kruger 2014) and precipitation is generally high throughout the year (Schumann 1992).

The annual wave climate consists of the south to south-eastern swell (Corbella and Stretch, 2012b), with the significant wave height reaching up to 8m during storm events. Tidal currents are less than 0.1m/s, and wave-induced currents occur only at the breaker zone. The Agulhas Current affects weather patterns, storm events and the diversity of marine life along the KZN coast.

The region between Durban and Cape St Lucia is known as the KZN Bight or historically referred to as the Natal Bight (Roberts et al., 2016). The stepped terrace on the slope off Durban between 300 m and 500 m is important in the formation of the cyclonic spin-off features (See figure 2.6).

Regional ocean circulation is strongly affected by coastline bathymetry (Roberts et al., 2016). The East Coast of South Africa has a steep continental slope that is consistent throughout most of the continental shelf. The Agulhas Current hugs the boundary of this shelf, extending well below 1000 metre depths. (Roberts et al., 2016) As the Agulhas Current travels further south along the eastern coastline, the slope gradually begins to retreat northwards at Cape St Lucia, resulting in a widening of the shelf. Here the continental shelf extends to almost 50km, forcing the Agulhas Current to recede further offshore (Lutjeharms, 2006). This is constant until the shelf edge retracts

at Thukela River towards the Durban coastline. (Roberts et al., 2016) It is evident from the bathymetry that a ridge is formed offshore from the Thukela River Mouth which is depicted as the Thukela Canyon in Figure 2.3 below.

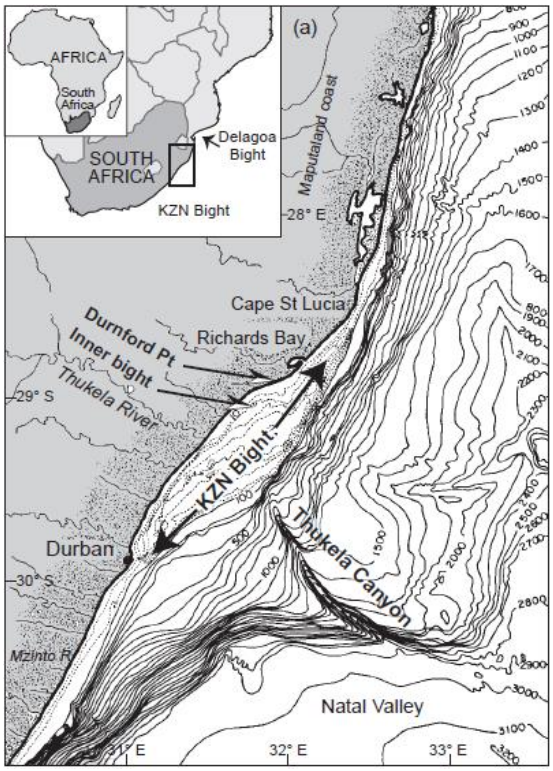

Figure 2.3: Bathymetry (m) along the KwaZulu-Natal (KZN) coast, showing the KZN Bight region (from Martin and Flemming 1988).

Roberts et al (2016) showed ocean circulation characteristics that suggest that both the slope and outer shelf strongly influence the Agulhas Current. This is more evident further north at Richards Bay where the shelf is at its narrowest. Velocities here reach up to 2m/s. As the current travels further south, it widens and travels further from the coast, reducing current speeds (Roberts et al., 2016). The Agulhas Current significantly influences the oceanography of the KZN Bight by driving circulation features into the Bight and in general, influencing the cyclonic circulation across the entire Bight (Lutjeharms, 2006). The northward movement of dune fields suggests dominant north-east trending counter current and persistence of a lee eddy (Kruger, 2014).

2.2.3 Natal Pulses

Large solitary meanders break off from the Agulhas Current and form within the KZN Bight and are known as Natal Pulses (Lutjeharms and Roberts, 1988). This can be seen in Figure 2.5. These pulses occur due to the instabilities of the Agulhas Current and the influence of anticyclonic eddies with the landward side of the current (de Ruijter et al., 1999).

Lutjeharms and Roberts (1988) demonstrated that the Agulhas Current Boundary features transformed into temporary Natal Pulses. These pulses can grow from 30km in size and become large, isolated meanders that have cold water cores (Krug and Penven, 2011). Natal Pulses grow as they move downstream, and sometimes exceed 200 km in size when they come near Port Elizabeth (Tsugawa and Hasumi, 2010). They propagate downstream into the Agulhas Bank at an average rate of 20 km/day (Tsugawa and Hasumi, 2010). Lutjeharms and Roberts (1988) also insinuated that the origination of these Natal Pulses could be from Durban's recessed bathymetry.

Natal pulses can extend to the full depth of the Agulhas Current (Lutjeharms et al., 2001) and can significantly influence the adjacent shelf by causing the upwelling of cooler waters filled with nutrients (Bryden et al., 2005). Lujeharms and Connell (1989) also suggest that these pulses can cause current reversals on the adjoining shelf.

Prolonged periods of light south-westward currents inshore or prolonged periods of light north-eastward currents offshore (which is opposite to the Durban Eddy) can be identified as Natal Pulses. They generally occur 4 to 6 times per year and interrupt the normal flow of the Agulhas Current and the occurrence of the Durban Eddy (Guastella and Roberts, 2016).

2.2.4 The Durban Eddy

A dominant spin-off feature from the Agulhas Current which influences the circulation off Durban is the semi-permanent eddy known as the Durban Eddy. This feature only persists around 50% of the year and has a duration of approximately 8 days during each occurrence.

Globally, western boundary currents are known to be sinks for ocean-eddy energy (Zhai et al., 2010). Instabilities from the mean flow of western boundary currents generate ocean eddies that play a vital role in global ocean energy. A study by Nof [1999] has shown that kinematically driven upwelling cells (such as the Durban Eddy) can interact with a meridional boundaries. The eddy can remain almost stationary until it gradually dissipates until it can no longer be defined as an eddy.

The Agulhas Current is deflected further offshore by the topography of the KZN Bight (as seen in Figure 2.4). Cyclonic eddies form and interact with currents on the shelf that can drive upwelling of cold nutrient-rich water onto the shelf (Lutjeharms, 2006; Roberts et al, 2011). This formation of cyclonic circulation or gyres can ultimately create what is known as an "Eddy". The "Durban Eddy" is a semi-permanent mesoscale cyclonic circulation that occurs in the southern half of the KZN Bight and finds its way into the northward inner and mid-shelf regions (See the orange area in Figure 2.4) (Roberts et al., 2010, 2016).

The Durban Eddy has a length scale of between 60 to 90km in length and 30 to 50km in width (Rossby number of ~ 10^{-1} as explained in Table 1.5.1 in Lakshmi et al, 2000 – See Figure 2.7), deeming the cyclonic eddy as mesoscale (Figure 2.4). The semi-permanent position of the centre of the eddy is located above the 300 to 500m isobath. Moderate Resolution Imaging Spectroradiometer (MODIS) and Medium Resolution Imaging Spectrometer (MERIS) satellite imagery indicate that the northern most boundary of the Durban Eddy reaches Ballito during early formation (Guastella and Roberts, 2016).

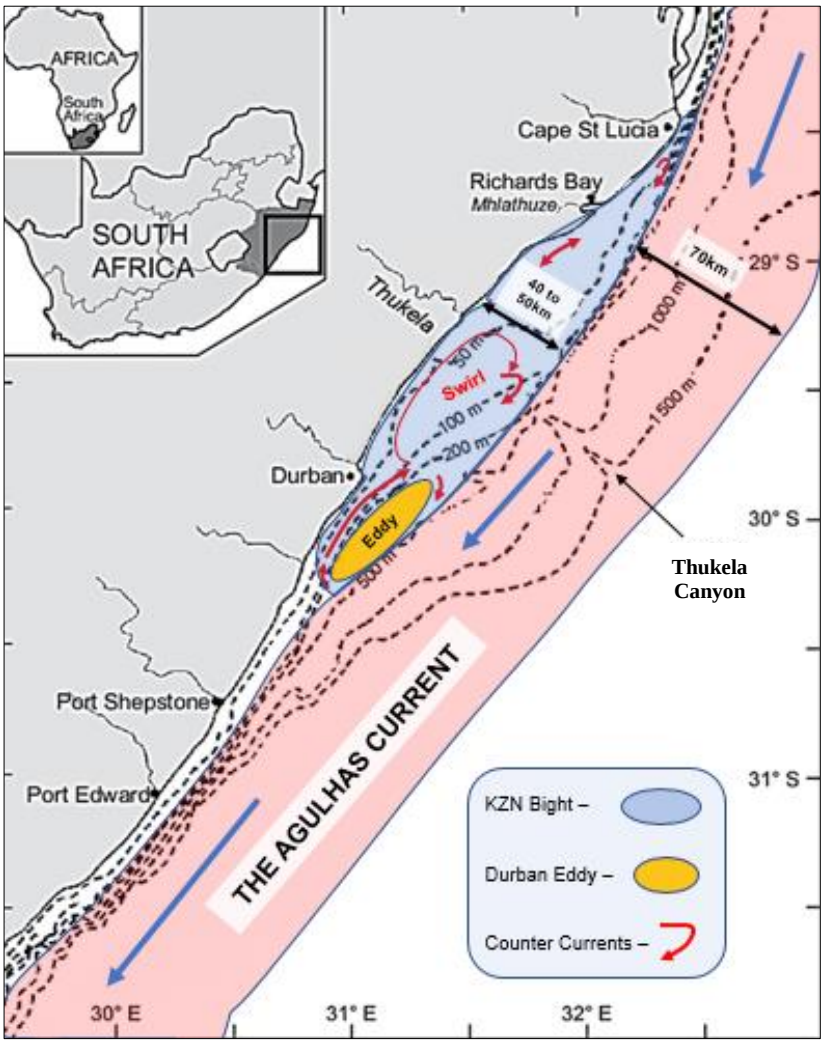

Figure 2.4: The KZN Bight, Durban Eddy and the Agulhas Current, adapted from Scharler et al. (2016) and Pearce et al. (1978). The distance between the coast and the Agulhas Current varies according to formation of Eddy and Natal Pulses.

2.2.4.1 Observations of the Durban Eddy

The first measurements that were conducted in this region were based on ship-drift observations (Tripp, 1967). Tripp (1967) suggested that north-eastward currents existed off Durban only 50% of the time. Oliff (1969) presented the first illustration of the Durban Eddy. He deduced a minimum surface temperature at the core of the Durban Eddy that was linked to the upwelling of colder water. He also identified the rapid growth of Phytoplankton in this vicinity.

Between 1972 and 1974 a 100km orthogonal line off Durban was sampled over five consecutive days. From these cruises, it was evident that the inshore boundary of the Agulhas Current occurred on average at 40km offshore and experienced velocities greater than 1m/s immediately east of this boundary (Pearce 1977a; Schumann 1982). These data sets also revealed the presence of cyclonic eddies that could migrate both northwards and south but only lasted around 1-2 days. However, no direct relationship was found between the Agulhas Current and eddies beside the fact that when an eddy was present, the currents within the Durban Bay flowed northwards. It is important to note that these studies were conducted without satellite imagery as they only became available in the late 1970s (Roberts et al., 2016).

Pearce (1977) proposed that the occurrence of the Durban Eddy was dictated by topography and that cyclonic vorticity was present when the Agulhas Current entered deeper waters off Durban. Gill and Schumann produced a potential vorticity model in 1979 which supported a return flow off Durban due to the vorticity structure of the Agulhas Current over shallower shelf regions. Therefore, a north-eastward flow was apparent for conditions near both Durban and Port Edward.

The analysis of bottom sediment was done by Flemming in 1980 who distinguished a southern extremity by the presence of bedload partings between Umkomaas and Scottburgh (southern tip of the eddy in Figure 2.6). This sediment dispersal on the continental shelf inferred the existence of the Durban Eddy.

Deployment of self-recording current meters off Durban suggested mostly northward movements of currents off Durban (Schumann 1981). Reversal of uniform temperature distribution currents was observed off Durban. A 10-day cycle consisted of current and temperature variations that showed warmer bottom temperatures in a northerly, inshore current and cooler flows in a south-westward direction. Schumann (1982) also observed counter-currents within 20km off the coast of Durban from moorings and ship-board measurements. He devised that these counter-currents formed only 50% of the time, similar to Tripp (1967), and promoted the concept of recirculation flow forming the cyclonic gyre off Durban.

Anderson et al. (1988) postulated that the lee eddy was driven as the passing Agulhas Current enters beyond the shelf offset at Durban. Lutjeharms and Connell derived the phenomenon as the "Natal Pulse Eddy" in 1988 as they witnessed colder waters than the Agulhas Current.

Gründlingh and Pearce (1990) also examined historical Airborne Radiation Thermometer (ART) data collected from 1967 and 1968 that clearly showed clockwise flow off Durban. This re-iterates the regularly occurring cyclonic Durban Eddy as well as the intrusion of warm water into the southern regions of the Natal Bight. Large clockwise loops were also observed to the south of Durban with diameters of 100km. (Gründlingh and Pearce 1990).

In 2002, transportation of nutrients in a northward direction over the Bight region was suggested (Meyer et al., 2002), however, the southern Bight was deemed poor in nutrients and the Durban Eddy was sporadic and variable in intensity. It was then suggested that the lee eddy generates the advection of oligotrophic (poor in nutrients) oceanic water into the southern Bight (Meyer et al., 2002).

Satellite imagery and ship-based ADCP data were used to confirm the existence of a semi-permanent lee-trapped cyclonic eddy off Durban (Roberts et al., 2010). Roberts et al. (2010) identified that the eddy develops between the 100 and 500 metre isobaths (as seen in figure 2.6) and just upstream from Durban, where the shelf narrows, deflection of the Agulhas Current occurs which drives the eddy. They also noticed that every 15 days the Durban Eddy escapes the shelf edge and propagates downstream within the shoreward boundary of the Agulhas Current. These "Durban break-away eddies" flatten against the coast and elongate during their downstream migration. This can be seen in Figure 2.5, where Guastella and Roberts (2016) suggest a leakage of the eddy into the Durban Bight. Eventually, they fade into shallow meanders that travel in the same direction as the current near Port Alfred, in the Eastern Cape (Roberts et al., 2010).

Figure 2.5: Taken from Guastella LA and Roberts MJ. 2016. Dynamics and role of the Durban cyclonic eddy in the KwaZulu-Natal Bight ecosystem. The figure suggests leakage of the Eddy into the Durban Bay.

Kruger (2014) investigated dune fields moving northward which also suggested a dominant north-east trending counter current and the persistence of a lee eddy.

Roberts et al. (2016) explain that inshore currents within the Bight travel in a northerly direction and, combined with the south westerly flow in the outer shelf, form cyclonic circulation within this region. This however is not the Durban Eddy which is situated to the south of Durban as opposed to Anderson et al. (1970) initial assumptions of the Durban Eddy being located within the Durban Bay (Roberts et al., 2016). This circulation was named the "southern Bight swirl" by Roberts et al. (2016) and can be seen in Figure 2.5 as red arrows indicating counter currents.

Guastella and Roberts (2016) used Ship-measurements, satellite-tracked drifters and ADCP moorings from the ACEP initiative to collect data from 2009 to 2010. Details from this research suggest that the inshore counter flow of the Durban Eddy is only half as strong as the main Agulhas Current.

Table 2: Summary of Durban Eddy Statistics taken from Guastella and Roberts (2016)

Parameter	**Value**
Percentage of time eddy present	55%
Number of eddy days per year	200 days
Number of eddies per year	22.5 (almost 2 per month)
Average Durban Eddy lifespan	8.6 days
Average Durban Eddy length (north-east-south/west direction)	60 – 90 km
Average Durban Eddy width (north-west/south-east direction)	40 – 50 km

Guastella and Roberts (2016) showed that a decrease in temperatures and an increase in chlorophyll are indicative of a cyclonic circulation. They also term the formation of the eddy as the "spin-up". With no seasonal trend of the Durban Eddy, it was also identified that Natal Pulses interrupt the Durban Eddy pattern. The average lifespan of a typical eddy is 8.6 days with 7.7 days between events with Natal Pulses, but only 4.3 days without (Guastella and Roberts, 2016). Three phases were categorized for the lifespan of the Durban Eddy by Guastella and Roberts: Spin-up, Maturation and Dissipation (Guastella and Roberts, 2016).

Drifter data shown in Figure 2.8 from Guastella and Roberts (2016) further showed the presence of an eddy off Durban. However, not all the drifters followed the same trajectory which also suggested that the Durban Eddy is not permanent (Guastella and Roberts, 2016).

Drifters 69, 73, 74, and 75 show evidence of a cyclonic gyre (eddy) just South of Durban. Drifter 69 suggests that the Durban Eddy travels further north and influences the Durban Bay region. Guastella and Roberts (2016) also identified that when the Durban Eddy was not present, the Agulhas Current was farther than expected (50 km offshore) as opposed to when it was present (20 to 25 km offshore). We can also note from the data presented by Guastella and Roberts (2016) that salinity differences are evident when the Durban Eddy is present, oxygen levels are much less, and lower temperatures are observed.

Guastella and Roberts (2016) stated that north-eastward currents are experienced in the shallow regions of the Durban bay when the eddy is present, with frequent current reversals due to a returning weaker south-westward flow after the eddy moves away from the area. The north-eastward currents are generally stronger than the south-westward currents. ADCP-measured currents showed that the north-eastward inshore flow from the Durban Eddy reached speeds of up to 0.9m/s (Guastella and Roberts, 2016).

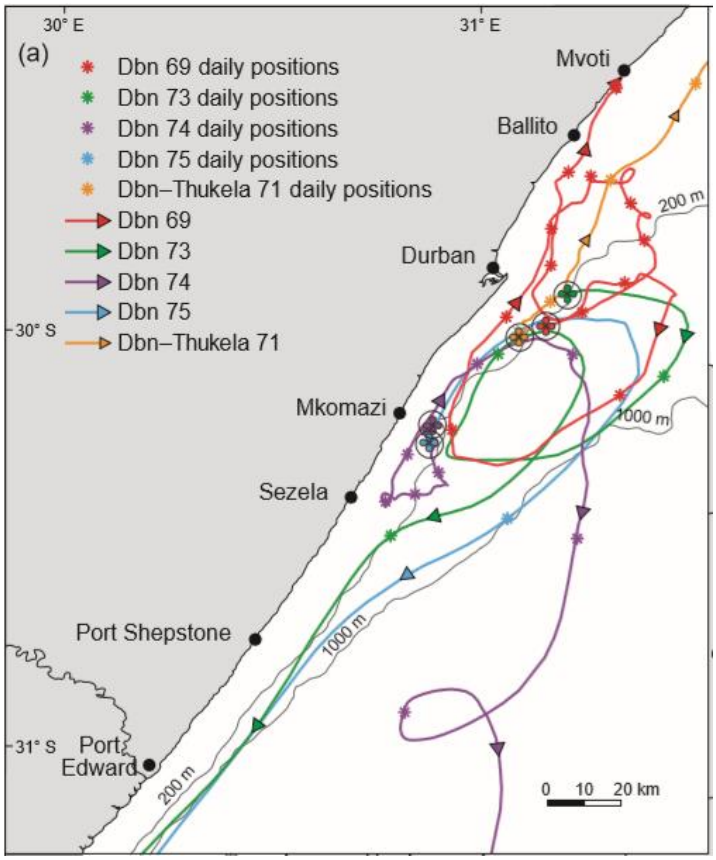

Figure 2.6: Paths of surface satellite-tracked drifters (69 – 75) deployed into the Durban Eddy off Durban during 2010). Taken from Guastella and Roberts (2016).

Pearce (1977), Schumann (1982) and Guastella and Roberts (2016) all agree that the Durban Eddy occurs some 55% of the year between Durban and Sezela (see locations in Figure 2.6). The eddy interacts with the meridional boundary and remains stationary until it eventually dissipates downstream in the inshore edge of the Agulhas, until it can no longer be defined as an eddy (Braby et al, 2016). Frequent current reversals along Durban depend mainly on the presence or absence of the Durban Eddy and less frequently on Natal Pulses that extend further offshore. However, local winds can also cause reversals of near-surface currents (Guastella and Roberts, 2016). The driving force of the Durban Eddy is most likely due to current shear caused by the strong flow from the Agulhas Current moving swiftly past a regressing shelf edge off Durban. The research was done by Guastella and Roberts in 2016 also advocates that there is a direct correlation between the Durban Eddy and biological and physical characteristics within Durban Bay. However, the frequency, intensity, strength and size of the eddy are variable and inconsistent with the records mentioned above.

2.3 Modelling Ocean Currents

Circulation models are created to better understand the impact of ocean mixing and currents on the physical processes within the ocean. These models are used to explain or predict circulation systems. Ocean circulation requires the consideration of many factors when creating such models. Dominant forces that need to be included in ocean models consist of wind, solar radiation, air temperature, cloudiness and relative humidity (National Geographic Society, 2021).

Ocean models are usually classified according to their vertical discretization, numerical schemes and grid generation (Song and Haidvogel, 1994; Bleck, 2002; Chassignet et al., 2006, Fringer et al, 2019). The choice of the vertical coordinate system is one of the most important aspects of the type of model used (Chassignet et al., 2006). Large-scale ocean models use global bathymetry and computational grids at resolutions of 5 to 10 km.

Regional or higher resolution models are nested within large scale or global models. Long spin-up periods (also known as "warming up" of the model) are required to start up the nested models to prevent a "cold start" of the models. A cold start of the model occurs when the model is first initialised with little input data (model is at rest), where the model will then need to be run until the solution converges (spin up time). This requires further computational modelling power and increased spin-up time, where results during this spin-up time could be unstable and should be ignored. The information sharing between the grids can cause numerical errors which allow for unresolved processes within the models that can either underestimate or overestimate the physical dynamics of the ocean (Halo et al., 2014). Errors of uncertainty can also occur due to internal boundary conditions created by the nested grid and a long computational time (Pallares et al, 2016).

Data assimilation is still essential for ocean prediction because many of the ocean's phenomena are due to flow instabilities or non-linear processes and errors can occur in atmospheric forcing. Limitations in numerical algorithms and resolution deem ocean models imperfect (Chassignet et al., 2006). Reanalysis of Ocean Models such as the products described in GREP (Global Reanalysis Multi-Model Ensemble Product) allow for modelling frameworks such as NEMO (Nucleus for European Modelling of the Ocean) to assimilate observed measurements to create a consolidated and more accurate global representation of the oceans dynamics (https://www.nemo-ocean.eu/, https://catalogue.marine.copernicus.eu/documents/PUM/CMEMS-GLO-PUM-001-031.pdf). Global ocean reanalyses are homogeneous 3D gridded descriptions of the physical state of the ocean spanning several decades, produced with a numerical ocean model constrained with data assimilation of satellite and in situ observations (CMEMS, 2019).

The use and development of high-resolution numerical modelling systems promote effective and responsible marine and coastal management (Iglesias et al, 2019). These models can be manipulated to represent impacts of topographic or bathymetric features, coastal structures and changes in boundary conditions. They can also help to overcome the lack of field measurements and provide valuable information on the behaviour of coastal regions. These numeric models are essential to accurately represent the dynamic processes of coastal systems. Ocean processes can be resolved in regional or global ocean modelling. Coastal processes have horizontal scales that are smaller than the internal Rossby deformation scale (Fringer et al, 2019). The coastal model used in this research crosses over between an ocean scale to a coastal scale, with resolutions from 9km to 200m. Coastal-scale models defined in this research can be considered as "shallow water" models that include processes such as tide and wind.

Circulation models can consist of either offshore and/or nearshore currents, which are categorized by their spatial scale. Nearshore currents are located between 1 to 30 km from the coastline and offshore currents occur at 30 to 1000 km (Penven et al, 2006). They are usually modelled and measured with separate methods, with this research being limited to offshore current scales. Coastal models typically have high resolutions and focus on coastal dynamics that directly affect the adjacent coast. These models can include turbulence processes or even eddies and fronts at scales of kilometres extending to hundreds of kilometres. However, nested coastal models still have issues with the development of embedding procedures from ocean boundary conditions (Trotta et al., 2021) .

Figure 2.8 shows various scales of both oceanic and coastal features and their corresponding Rossby number. The coastal model used in this research includes investigating mesoscale eddies, coastal upwelling, and boundary currents which all correlate to a Rossby number of $\sim 10^{-1}$.

Process	Length scale	Timescale	Rossby number
Dissipative scales	1–2 mm	~1 s	$\sim 10^{4}$
Vertical mixing (ocean)	1–100 m	several minutes	$\sim 10^{2}$
Vertical mixing (atm)	1–1000 m	several minutes	$\sim 10^{2}$–10^{3}
Surface waves	1–100	several seconds	~ 10–10^{2}
Internal waves	1–10 km	mins–hrs	$\sim 10^{-1}$–1
Double diffusion	1 cm–10 m	days–weeks	~10
Coastal upwelling	10–20 km	days	$\sim 10^{-1}$–1
Mesoscale eddies	10–400 km	weeks–months	$\sim 10^{-1}$
Atm. weather patterns	100–5000 km	days–weeks	$\sim 10^{-1}$–1
Ocean fronts	5–50 km	weeks	$\sim 10^{-1}$
Boundary currents	50–100 km	months	$\sim 10^{-1}$
Basin gyres	2000–15000 km	years	$\sim 10^{-2}$
Ocean tides	100–1000 km	1/2, 1 day, ...	$\sim 10^{-4}$–10^{-2}
Tornadoes	few km	<1 hr	$\sim 10^{3}$
Hurricanes	500–2000 km	days	~10
Rossby waves	1000 km	months–years	$\sim 10^{-3}$
Tsunamis	100 km	day	$\sim 10^{2}$
Land–sea breeze	10–50 km	1/2 day	~1

Figure 2.7: Time and Spatial Scales of Various Oceanic and Atmospheric Phenomena taken from Lakshmi et al (2000)

Ardhuin et al. (2017) reveal how the presence of eddies, fronts and other features at scales of 10 to 100 km impact wave heights within a local scale. Therefore, the variations in currents at a coastal scale can affect or influence the dynamics offshore of the coast. Surface waves can be directly impacted by mesoscale features that are a result of larger oceanic flows (Ardhuin et al., 2017). Therefore, it is important to resolve these submesoscale processes (small scale and high temporal variability) within a coastal model so that the influences of oceanic features are well represented.

Associated coastal modelling suites that can be used are Delft3D (https://oss.deltares.nl/web/delft3d/), MIKE21 (two-dimensional) and MIKE3 (three-dimensional) (https://www.mikepoweredbydhi.com/). These numerical coastal models can simulate several physical processes and environmental activities (Iglesias et al, 2019). Other coastal processes that can be modelled include morphology and sediment transportation, water quality and coastal inundation. Deltares has a long experience of modelling the coastal ocean and have established a model which can easily integrate different modelling modules suited to modelling the coastal environment, which is why Delft3D was chosen for this research.

2.3.1. Numerical Schemes

Finite Difference Method (FDM), the Finite Element Method (FEM) and the Finite Volume Method (FVM) are three different types of numerical methods that can be used in modelling software that attempt to numerically solve the governing Partial Differential Equations (PDE).

FDM is the oldest method of the three and is derived from a Taylor series expansion. It is based upon the differential form of the PDE which needs to be solved (Sjodin, 2016). FDM is simple and effective on structured grids but cannot resolve complex geometry well. The FEM computational method subdivides the model into very small but finite-sized elements which make up a finite-element mesh. The piecewise representation of the solution in each element is constructed from the specified basis functions (Sjodin, 2016). This method, similar to FDM, also uses a system of equations for nodal values that need to be solved to obtain a solution. Complex analysis of the solution can be made from this method as compared to FDM and FVM, however, this depends heavily on the choice of basis functions, and boundary conditions can be more difficult to express (Fringer et al., 2019).

The FVM is much more common in coastal modelling (Fringer et al., 2019) and is the framework used in D-Flow FM. It is more straightforward to implement and generally less computationally demanding compared to FEM (Sjodin, 2016). It is based on an integral form of the PDE (e.g., conservation of mass, momentum or energy) and is written in a form that can be solved for a finite volume or cell. Finite volumes are discretized within the computational domain and for every volume, the governing equations are solved. This method does not require the use of structured grids as compared to FDM. Although similar to FDM the approximate solution is also discrete, the variables, however, are placed at cell centres instead of the nodal points (Sjodin, 2016). Considering that this scheme can accommodate any type of grid, it is suitable for complex geometries.

2.3.2 Vertical Coordinate System

Fringer et al (2019) suggested that to accurately resolve flow along the bottom of the ocean floor, it is preferable to use terrain-following vertical coordinates such as sigma (See Figure 2.8). In contrast, z-layer vertical coordinates use stair steps to represent bottom topography (See Figure 2.8). Legg et al (2006) suggested that the stair steps in the z-layer method can induce false numerical mixing near the sea-bed floor. Zhang and Baptista (2008) have shown that some models show great promise when using a hybrid vertical coordinate system; sigma coordinates in the upper layers of the water column and z-levels at the depths. Z-layers are beneficial in deeper

regions where slopes can be steeper as they avoid pressure gradient errors that would normally occur in sigma layers. Isopycnal layers change in position or thickness as a function of density stratification and are not fixed in space as opposed to sigma and z-layers (See Figure 2.8). This type of model is suitable for large-scale global ocean climate models. Isopycnal coordinates are not suitable for coastal simulations due to the significant physical mixing within these regions (Fringer et al., 2019) as cross-isopycnal mixing is not allowed. Vertical numerical diffusion of scalars remains difficult to resolve with any type of vertical coordinate system due to the significant physical mixing in coastal simulations.

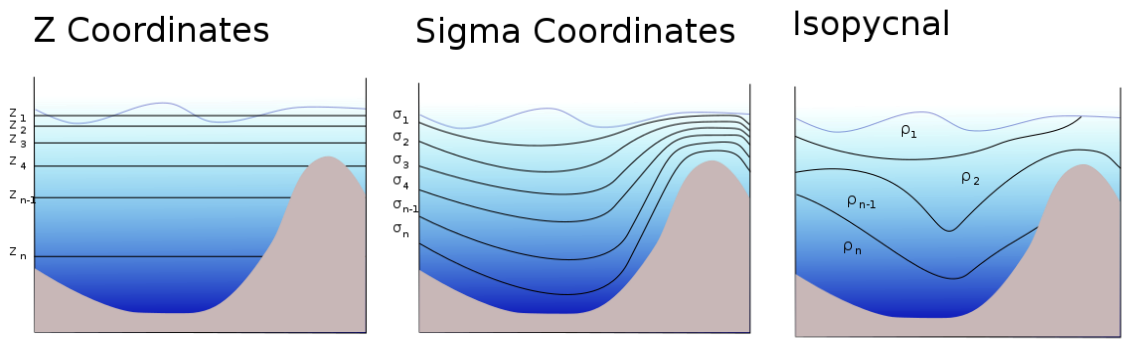

Figure 2.8: Typical representation of vertical grid types, adapted from OC2910 - Numerical Ocean Modelling Concepts, 2003)

In coastal zones, specifically the one being analysed in this research, stratified flow combined with steep topography (like the edge of the continental shelf off the KZN coastline) can occur.

In regions of steep bathymetry where there are large bottom gradients, sigma layers may not resolve stratification well and artificial vertical diffusion or artificial flow may occur due to truncation errors. Therefore, a sigma correction or anti-creep approach can be applied in Delft3D to suppress this phenomenon. This sigma correction, however, can result in numerical diffusion and causes artificial mixing (Deltares, 2020a).

Instead of applying Sigma layers (with/without anti-creep), Z-layers may be applied to resolve stratification in regions with steep bed gradients (Deltares, 2019b).

Compared to the σ-grid, the Z model is not boundary fitted in the vertical. The bottom of this grid can be represented as a staircase. This means that the artificial mixing of salinity and temperature properties can be reduced in the Z-type model and stratification is better represented as compared to sigma models. The thickness of the upper-most layer is determined by the actual water level and the bottom layer is determined by the local topography (Deltares, 2020a). The Z-layer model is recommended for coastal shallow to deep ocean modelling (Deltares, 2019b).

Hybrid models are also possible by using a combination of σ layers and z layers. Generally, z layers are used in the bottom to avoid σ errors in deeper water. Also, σ layers can be used for the top layers to prevent too small layers created by the z-layer type model.

The internship model will only focus on Z-layers, whereas Test08 will consist of a hybrid model using both sigma and Z-layers.

2.3.3 Boundary Conditions

A numerical model's spatial domain needs to be limited in order to achieve higher resolution and feasible calculation time. Such limitations in the size of the model require the information of the area outside of the model domain to be taken into account through boundary conditions (Quinquis, 2011).

The delineation of the model domain consists of land-water barriers such as coastlines or riverbanks. This part of the model contour is called a closed boundary (Deltares, 2020a) and is a natural boundary. The edges of the model that crosses flow fields are called open boundaries. Open boundaries should be situated as far away from the area of interest as possible, as solutions near the boundary are the least accurate.

Open boundary conditions (OBCs) have a significant impact on inner domain solutions in coastal ocean modelling and can be considered one of the most challenging aspects to successfully implement in coastal modelling (Marsaleix, 2006). OBCs serve a dual purpose which includes the following:

- To force the inner solution within the model with external data (either from observations of larger extent/global models) under incoming conditions
- To allow water masses/waves to radiate out and leave the modelling domain under outgoing conditions, without spurious reflections or instabilities

However, both objectives are difficult to satisfy simultaneously, and modellers often choose between the two schemes according to the character of the dynamic field (outgoing or ingoing) (Marsaleix, 2006).

The OBCs for temperature and salinity are often as follows:

$$\frac{\partial \phi}{\partial t} + u\frac{\partial \phi}{\partial n} = 0 \qquad (2.1)$$

where *u* is the current in the direction normal to the boundary and *n* is the prescribed direction.

At an open boundary, the water level, the normal velocity, or a combination should be prescribed to achieve a well-posed initial boundary value. The tangential velocity should also be specified for an inflow boundary. If the incoming waves are not exactly prescribed at the open boundary, the outgoing waves will reflect at the boundary and create disturbances in this area. To reduce the reflections at the open boundary, zero flow can be assumed along the boundary through a zero-order boundary condition. This is obtained using the Riemann invariants as described by Deltares (2020a). However, if there is no information on both water level and velocity to identify the incoming Riemann invariant, another type of boundary can be used. Roelvink and Walstra (2004) suggested letting the model determine the correct solution at the boundaries by imposing the alongshore water level gradient instead of a fixed water level or velocity. This is called a Neumann boundary condition and is interpreted as a gradient type of boundaries for water level. Neumann boundaries can only be applied on cross-shore boundaries, in combination with a water level boundary (Dirichlet type) at the offshore boundary (Deltares, 2020a, dos Santos Gil, 2014). However, for this research, only open boundary conditions were prescribed, with their conditions and physical input parameters described in section 3.2.5.

Although OBC allows the model to avoid some incompatibilities between the difference in model variables and their corresponding forcing counterparts, it does not ensure that the model solutions will be correctly produced by external information. The drift likely to increase between the modelling and forcing fields can be corrected by adding a "nudging" layer in the vicinity of open boundaries. This technique is further described in section 3.1.1.

Every boundary section has specific boundary location points. These are spaced out to represent the same distance between each point similar to that of the incoming data at the boundary location i.e., to exhibit the same resolution at the boundaries as the forcing files. Boundary conditions and Forcing Parameter specifications for this research will be described in 3.2.5.

2.4 Delft3D

Delft3D is a software suite developed by the applied research company Deltares, that incorporates 3D computational modelling for coastal, river and estuarine areas. Delft3D can produce simulations of flow, sediment transport, water quality, waves, morphology, and ecology. It is composed of several modules that can interact with one another (see Figure 2.9 below).

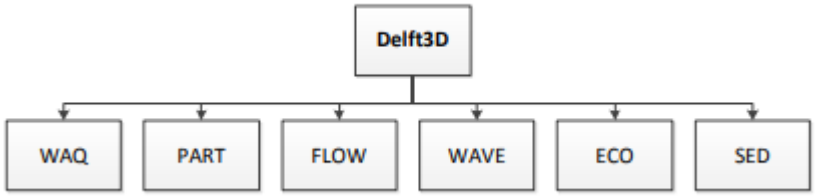

Figure 2.9: Modules within the Delft3D suite taken from dos Santos Gil (2014): With WAQ (Water Quality), PART (Particle Tracking), FLOW (hydrodynamic flow module), WAVE (Short wave propagation), ECO (Ecological Module) and SED (Sediment Transportation).

Delft3D-FLOW and Delft3D-WAVE are hydrodynamic and wave modules respectively, that can produce uncoupled simulations (offline) as well as interact with each other (online). In addition to the six modules shown in Figure 2.9, Delft3D also provides other programs which assist with the processing of raw data. RGFGRID is used for generating orthogonal curvilinear or rectangular grids, and QUICKIN is used to prepare and manipulate data to show parameters such as bathymetry, water levels, salinity, etc, for areas of interest (Deltares, 2020a). QUICKPLOT can also be used to visualise and animate numerical results.

2.4.1 Delft3D-FLOW

Delft3D-FLOW is just one of the modules given in Figure 2.9 and is the module that will be used within this research, so all interactions by waves are neglected. Delft3D-FLOW is a 2D or 3D hydrodynamic simulation program. It computes non-steady flow dynamically from tidal and atmospheric forcing on a specified (rectangular or curvilinear) spatial grid (Deltares, 2020a). Delft3D-FLOW is capable of 3D simulations of ocean basins, coastal seas and even rivers due to the many processes included in the module (Lesser, 2004). Features implemented from Delft3D-FLOW for this research include tidal forcing, the effect of the Earth's rotation, density-driven flows, and wind and atmospheric pressure. Special conditions which will also be applied include the use of a spherical co-ordinate system and incorporating a Z-layer type model which Delft3D-FLOW has made accommodations for and which will be further discussed later on. The software

also allows for the coupling of wave and water quality modules, which the model can be further developed for (Deltares, 2020a).

The two-dimensional approach can be used to solve depth-averaged equations if the fluid properties can be considered vertically homogeneous. However, if there is a significant variation of flow field features along the vertical direction, 3D modelling is preferred.

The Delft3D-FLOW module, under the Boussinesq and shallow water assumptions, simplifies the Reynolds-averaged Navier-Stokes (RANS) equations for an incompressible fluid. After this simplification, cartesian coordinates (*x*,*y*,*z*) are transformed into σ- coordinates ($\tilde{x}, \tilde{y}, \sigma$) (dos Santos Gil, 2014):

$$\begin{cases} \tilde{x} = \mathrm{x} \\ \tilde{y} = y \\ \sigma = \frac{z-\eta}{d+\eta} \end{cases} \qquad (2.1)$$

where η is the variation of the reference level depicted in Figure 2.11.

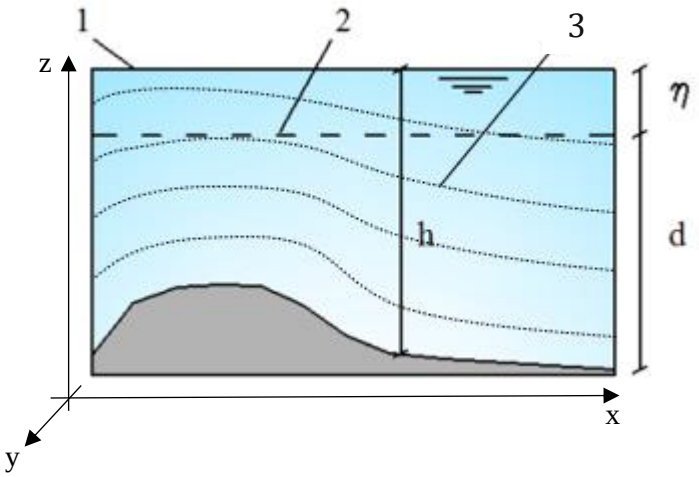

Figure 2.10: Total depth, h, depth corresponding to reference level, d, and variation of reference level, η. 1- Water Surface, 2- Reference Level (M.W.L.) and 3 - σ layers. Adapted from dos Santos Gil (2014).

These derivations and simplifications are well explained in Appendix A in dos Santos Gil (2014).

The continuity equation for an incompressible fluid is:

$$\frac{\partial u}{\partial x} + \frac{\partial v}{\partial y} + \frac{\partial \omega}{\partial \mathrm{z}} = 0 \qquad (2.2)$$

where *u* is the horizontal velocity in the x cartesian direction, *v* is the horizontal velocity in the y cartesian direction and *ω* is the vertical velocity in the z cartesian direction.

This equation, together with the shallow water assumptions, compose the shallow water equations. Large-scale flow processes are well described by the hydrostatic shallow water flow

equations (Kernkamp et al, 2011). De Goede (2020) describes these three-dimensional hydrostatic shallow water equations with the following continuity and momentum equations:

$$\frac{\partial u}{\partial t} + u\frac{\partial u}{\partial x} + v\frac{\partial u}{\partial y} + \frac{\omega}{h}\frac{\partial u}{\partial \sigma} - fv = -\frac{1}{\rho}P_u + F_u + \frac{1}{h^2}\frac{\partial}{\partial \sigma}\left(\nu_V \frac{\partial u}{\partial \sigma}\right) \quad (2.3)$$

$$\frac{\partial v}{\partial t} + u\frac{\partial v}{\partial x} + v\frac{\partial v}{\partial y} + \frac{\omega}{h}\frac{\partial v}{\partial \sigma} + fu = -\frac{1}{\rho}P_v + F_v + \frac{1}{h^2}\frac{\partial}{\partial \sigma}\left(\nu_V \frac{\partial v}{\partial \sigma}\right) \quad (2.4)$$

$$\frac{\partial \omega}{\partial \sigma} = -\frac{\partial \eta}{\partial t} - \frac{\partial [hu]}{\partial x} - \frac{\partial [hv]}{\partial y} + h(q_{in} - q_{out}) + S_{Precip} - S_{Evap} \quad (2.5)$$

where σ is the vertical coordinate, *t* is the time, F_u and F_v represent the unbalance of horizontal Reynolds stresses, P_u and P_v represent the pressure gradients, ρ is the density, *f* represents the Coriolis parameter, $f = 2\Omega \sin(\varphi)$ with **Ω** as the magnitude of earth's rotation vector and φ as the local latitude and ν_V represents the vertical eddy viscosity.

These equations are given in Cartesian rectangular coordinates in the horizontal and σ-coordinate in the vertical for convenience of presentation. The vertical velocities ω in the σ-coordinate system are computed from the following continuity equation:

$$\frac{\partial \eta}{\partial t} + \frac{\partial [hU]}{\partial x} + \frac{\partial [hV]}{\partial y} = hQ \quad (2.6)$$

where ($-1 \leq \sigma \leq 0$), by integrating in the vertical from the bottom to a level σ with the depth-averaged velocities being *U* and *V*. Q is described in equation 2.8.

The vertical velocity *w* for the Cartesian coordinate system with horizontal velocities, water depths, water levels and vertical σ-velocities, can be expressed as:

$$w = \omega + u\left(\sigma\frac{\partial h}{\partial x} + \frac{\partial \eta}{\partial x}\right) + v\left(\sigma\frac{\partial h}{\partial y} + \frac{\partial \eta}{\partial y}\right) + \left(\sigma\frac{\partial h}{\partial t} + \frac{\partial \eta}{\partial t}\right) \quad (2.7)$$

In equation (2.6), Q represents the effects per unit area due to the discharge or withdrawal of water, precipitation, and evaporation:

$$Q = h\int_{-1}^{0}(q_{in} - q_{out})d\sigma + S_{Precip} - S_{Evap} \quad (2.8)$$

where q_{in} is the local source and q_{out} is the local sink of water per unit of volume, S_{Precip} represents the non-local source term of precipitation and S_{Evap} non-local sink term due to evaporation.

These shallow water equations can then be transformed into orthogonal coordinates. These transformed equations are simpler, with some flexibility in determining grid point distribution near coastal boundaries. There are additional terms in non-orthogonal coordinates, which increase the numerical complexity and add computational time (de Goede, 2020).

2.4.2 D-Flow FM

D-Flow FM is the successor of Delft3D FLOW and its main modification from the structured version is that it implements a finite volume solver on a staggered unstructured grid (Deltares, 2021). D-Flow Flexible Mesh (D-Flow FM – unstructured mesh) is a Delft3D package that uses flexible nets/meshes (curvilinear meshes that have triangles, pentagons, etc, all combined in a single mesh) to simulate 1D, 2D or 3D hydrodynamic processes. D-Flow FM is still in development, however, there is already support for Flexible Mesh in RGFGRID's latest version (Deltares, 2020b). Although the same continuity equations are solved as that of Delft3D-FLOW, Flexible mesh changes the numerical solution technique to a volumetric approach.

The use of unstructured grids is the biggest difference between Delft3D-FLOW and D-Flow FM. This feature allows for modelling in large regions, where the same grid can then be refined to suit local scale regions closer to the area of interest along the coast. Including the capabilities already mentioned for Delft3D-FLOW, the other enhanced function within D-Flow FM is that all geometric model input (temperature, salinity, advection velocities, etc.) can now be prescribed in geographical co-ordinates as opposed to grid indices as previously done in Delft3D-FLOW. This advantage caters to changing the grid of the model while keeping the same model inputs as they are now model-independent coordinate inputs (Deltares, 2020b).

Reasons for unstructured grid modelling, as explained by De Goede (2020):

- More modelling flexibility compared to structured grids
- Predictions in both local (coastal) and global (worldwide) scales
- Integrated suite for 1D, 2D and 3D modelling
- Modern software
- Standardization of input and output files

Currently, the Delft3D modelling suite has released its 2D modelling functionality and prototypes are available for the 1D and 3D modelling. Therefore, this research involves exploratory modelling, with new (unstructured) software code, for a new application area. The source code is not fully distributed, and all tests will be done on a trial and error basis.

Using boundary conditions in deep ocean waters for the structured version (Delft3D FLOW), it is easy to obtain unstable results. In waters greater than 2000m depths, small ocean currents can create a huge volume of water entering the model. These local gradients can create and lead to instabilities. In shallow sea models, of less than 200m depths, there is sufficient dampening and friction. Dissipation occurs within the model and prescribing velocities at the boundaries works well with water levels.

However, it is difficult for the shallow water hydrodynamics of Delft3D to adequately simulate a stable ocean current in deep waters. FM is promised to improve vertical discretization, allow for nesting and boundary conditions in a stable way and add tide and direct wind forcing at higher resolutions (Deltares, 2019b).

In ideal hydrodynamic models, grids with high resolution within limited areas are preferred so that the model can resolve small bathymetric details. If the resolution is too coarse, higher details in the model may be stepped over by averaging resolution. Higher resolutions provide schematization of real-world scenarios and prevent missing certain bathymetrical or geometrical details (Deltares, 2019b). Naturally, the water level needs to be prescribed in these detailed models, which has been successfully achieved in the past, but the prescription of velocities has not been as successful. A good velocity reproduction can be achieved by only prescribing water levels for models with domains larger than 30km, as bed friction, pressure gradient and acceleration parameters can balance. However, with smaller model domains, unrealistic velocities can occur at open boundaries with just small water level differences. To alleviate poor model nesting in smaller models, there needs to be an introduction of velocity boundaries at the cross-shore boundaries of the model.

D-Flow FM now has a boundary condition to solve these model nesting problems. A new open boundary condition can now prescribe the incoming momentum advection. This means that along the boundary there can now be an inflow of velocities with a uniform water level. The name “uxuyadvectionvelocitybnd” was prescribed to this boundary condition as both the “x” and “y” velocity components must be stipulated in the time series files. This condition of the boundary, however, is only applicable for inflow. For outflow, the cell centre velocity vector is copied from the virtual boundary cell outside of the model (Deltares, 2019a).

2.5 Summary

A major challenge in coastal models is to integrate the large-scale ocean currents (widths of > 10 km) at their boundary forcing (Chassignet et al., 2006). Tidal currents can be dominant in some shallow coastal areas and along coastlines with a narrow shelf the influence of nearby ocean boundary currents can be significant. The scale of these currents is generally much larger than the scale of the employed coastal models and it is therefore not possible to generate them internally. Moreover, instabilities at these boundary currents may lead to meanders and mesoscale eddies which are difficult to resolve and therefore require assimilation of observations to be accurately simulated. This further complicates the generation of a coastal model that can internally generate ocean currents.

Ocean currents can significantly influence coastal regions. The Agulhas Current's dynamics and variability was reviewed as it is a major driver of the circulation in the KZN bight. The Durban Eddy, which originates from the Agulhas Current, is a semi-permanent feature off Durban which significantly influences current circulation off Durban as described in the literature review.

The type of modelling methods and schematization play a critical role in the parameterization and frameworks in a successful model setup. The proposed modelling instrument for the demonstration is the Delft3D (Deltares, 2020a) open-source software suite which also includes the Flexible Mesh. The Delft3D suite is an integrated modelling system that covers hydrodynamics, waves, sediment transport and water quality.

At the heart of the modelling system is the hydrodynamic simulation, computed by D-FLOW through solving the governing equations for shallow water with the hydrostatic pressure assumption. The system of equations consists of the horizontal momentum equations, the continuity equation, and the transport equation. The model includes robust, accurate and computationally efficient algorithms to simulate drying and flooding processes of intertidal flats (Lesser, et al., 2004). D-Flow FM, which is based on the underlying principles of D-FLOW, will be used to create an unstructured, three-dimensional hydrodynamic model. Further details of the modelling methodology (specifics of Flexible Mesh) are presented in section 3.2.1.

The need for an accurate hydrodynamic model that can reproduce the Agulhas Current and its related on-shelf circulations, in addition to tidal- and wind-induced currents, is essential to predict currents off the Durban and KZN coastline. Output from global ocean models, such as the NEMO models in the GREP operated by CMEMS, include the Agulhas Current, but are not suitable for coastal applications due to their relatively coarse resolution (Storto et al, 2019). For this reason, model output from the NEMO ocean models in the GREP were downscaled to a coastal D-Flow FM Flexible Mesh model of KZN.

CHAPTER 3

METHODOLOGY

This chapter describes the D-Flow FM model, the software required to run/execute Delft3D, as well as new techniques that will be analysed and utilised in the following chapters. The chapter outlines the necessary parameters, quantities, specifications, and data required to construct the D-Flow FM model for the KZN coastline. Specifications for the grid, boundary conditions, bathymetry and various input data are explained and detailed in this chapter.

This chapter also summarises the several simulations conducted in conjunction with the Deltares coastal modellers, and in collaboration with assistance from the Deltares software developers to correct and improve the D-Flow FM software. For a detailed description and progressive stages, the reader is referred to Appendix A.

3.1. Model Descriptions and Configurations

D-Flow FM is a hydrodynamic simulation program designed to calculate non-steady flow and transport phenomena that result from meteorological and tidal forcing on both structured and unstructured boundary-fitted grids (Deltares, 2021). D-Flow FM solves the multidimensional shallow-water equations (Lesser et al, 2004; Kernkamp et al, 2011). In this research, several versions of D-Flow FM were used, ranging from versions 1.2.71.64991 to 1.2.100.66357.

Martyr-Koller et al (2017) first described the 3D numerics and discretization schemes of the flexible mesh model, with the Flexible Mesh manual set to be released for publication in 2022. The three-dimensional incompressible Navier-Stokes equations are the governing equations for FM, with the continuity equation as follows:

$$\frac{\partial \rho}{\partial t} + \nabla \cdot (\rho \boldsymbol{u}) + \frac{\partial \rho u_z}{\partial z} = 0 \qquad (3.1)$$

where ρ is density, z is the vertical direction, $\boldsymbol{u} = (u_x, u_y)^t$ is a velocity vector with u_x and u_y components, and $\nabla = \left(\frac{\partial}{\partial x}, \frac{\partial}{\partial y}\right)^t$ (for consistency with model derivations provided in the supplementary material).

The continuity equation is solved implicitly for all points in a single combined system. The continuity equation can be simplified if the density is assumed to only depend on transported quantities such as salinity and temperature:

$$\nabla \cdot \boldsymbol{u} = 0 \qquad (3.2)$$

Similarly, the transport of matter in three dimensions is simplified in FM by ignoring density variations, including equations 3.1 and 3.2, the hydrostatic pressure assumption, and Eckart's equation of state (Eckart, 1958; Martyr-Koller et al, 2017):

$$\frac{\partial \rho c}{\partial t} + \nabla \cdot (\rho \boldsymbol{u} c) + \frac{\partial \rho c u_z}{\partial z} = \nabla \cdot (\rho K \nabla c) + \frac{\partial}{\partial z}\left(\rho K_z \frac{\partial c}{\partial z}\right) \quad (3.3)$$

With K_z an eddy diffusivity coefficient, c is a concentration (representing salinity or temperature or both), and u_z is the vertical velocity component. Detailed analysis of this derivative can be found in Martyr-Koller et al (2017).

Flexible Mesh uses a finite volume solver on a staggered, unstructured grid. This means that water levels are defined at cell centres and velocity normal components are defined at cell edges.

In section 2.6.2, for ease of reference, the continuity and momentum equations were given in cartesian and sigma (σ) coordinates, as generally used in DFLOW. However, for this research using D-Flow FM, a z-coordinate vertical layer specification was used (see section 3.3.1.5).

Therefore, the corresponding momentum equations are derived as follows:

$$\frac{\partial u}{\partial t} + u \frac{\partial u}{\partial x} + v \frac{\partial u}{\partial y} + \omega \frac{\partial u}{\partial z} - fv = -\frac{1}{\rho_0}\frac{\partial P}{\partial x} + F_x + \frac{\partial}{\partial z}\left(\nu_V \frac{\partial u}{\partial z}\right) + M_x \quad (3.4)$$

$$\frac{\partial v}{\partial t} + u \frac{\partial v}{\partial x} + v \frac{\partial v}{\partial y} + \omega \frac{\partial v}{\partial z} + fu = -\frac{1}{\rho_0}\frac{\partial P}{\partial y} + F_y + \frac{\partial}{\partial z}\left(\nu_V \frac{\partial v}{\partial z}\right) + M_y \quad (3.5)$$

where ν_V is the vertical eddy viscosity coefficient, $\frac{\partial P}{\partial x}$ and $\frac{\partial P}{\partial y}$ represent pressure gradients, forces F_x and F_y represent the unbalance of horizontal Reynolds stresses and M_x and M_y represent the contributions due to external sources or sinks of momentum. Similarly, equations 2.9 and 2.11 can be converted to z-coordinates, as detailed in the Flexible Mesh Manual (Deltares, 2021).

The hydrostatic pressure equation utilized in equation 3.3 is as follows:

$$\frac{\partial P}{\partial z} = -\rho g h \quad (3.6)$$

Under the shallow water assumption, the vertical momentum equation is reduced to the hydrostatic pressure equation (Deltares, 2020). Vertical accelerations due to buoyancy effects and due to sudden variations in the bed topography are not taken into account.

In D-Flow FM, usually, the grid is too coarse, and the time step is too large to resolve turbulent "sub-grid" processes. Therefore, there is a need for appropriate closure assumptions as detailed in Deltares (2021). For 3D shallow water flow, the horizontal eddy viscosity coefficient ν_H and

eddy diffusivity coefficient D_H are much larger than the vertical coefficients ν_V and D_V, i.e., $\nu_H \gg \nu_V$ and $D_H \gg D_V$.

There are two turbulence closure models in D-Flow FM which determine the vertical eddy viscosity (ν_V) and vertical eddy diffusivity (D_V):

- *k*-ε turbulence closure model
- *k*-τ turbulence closure model

Both models solve equations for production, dissipation, and transport of turbulent kinetic energy *k*. In the *k*-ε model, ε is is the dissipation rate of turbulent kinetic energy. Whereas in the *k*-τ model, τ, the dissipation timescale. This research uses the *k*-ε turbulence closure model.

Transport equations must be solved for both the turbulent kinetic energy *k* and energy dissipation rate ε. It is assumed that the production, buoyancy and dissipation terms are the dominating forces, with horizontal scales larger than vertical scales. The mixing length *L* is then determined according to:

$$L = c_D \frac{k\sqrt{k}}{\varepsilon} \tag{3.7}$$

with c_D as a constant to be determined. For a more detailed analyses reference is to be made to the Flexible Mesh Manual (Deltares, 2021).

3.1.1. The Nudging Technique

"Nudging" can be required to better simulate and maintain ocean boundary currents, such as the Agulhas, that are significantly influenced by topography. An interior nudging layer can be used to "relax" or "guide" the model solution towards a prescribed state. Within the nudging layer the model variables are restored towards the 3D boundary forcing values, e.g., Marchesiello et al., 2001. This method is referred to as the "nudging technique". This technique has been implemented in D-Flow FM to input temperature and salinity parameters within a coastal scale model from their respective variables in an ocean/global model. In doing so, data from a large-scale ocean circulation model can be amalgamated within a coastal hydrodynamic model to assist in the simulations of stable ocean boundary currents (Deltares, 2019b).

The following equation depicts the implementation of the Newton relaxation (i.e.: Nudging Technique) in the D-Flow FM code for Salinity, and similarly Temperature:

$$\frac{Ds}{Dt} = \frac{\partial S}{\partial t} + \vec{u}\nabla\vec{S} = \frac{S_{nudge} - S}{T_{nudge}} \tag{3.8}$$

with S the model salinity, S_{nudge} the target field value, u the local velocity and T_{nudge} the user-defined nudging timescale. The model's solution is guided towards the "nudged" value in equation 3.8 for timestep T_{nudge}. Ideally, and for this research, strong nudging (shorter timesteps feeding more data from larger model) should be done in deep-ocean areas to keep the current stable and the model should compute its own solution for hydrodynamic simulations from the shelf area towards the coast (no nudging). The Nudging Technique will be used in various simulations to improve model outputs.

Initial nudging is a new option in D-Flow FM to prescribe initial conditions from global ocean model outputs using a nudging file. This allows for the larger models output to drive the smaller models results by easily transitioning from a global to a coastal scale. Initial nudging is similar to a restart file (files that contain all of the initial condition information necessary to restart from a previous simulation), but instead of values being prescribed from outputs from another model, initial nudging includes 3D scalar data at all grid points and all depth layer values. Nudging is not applied to vector quantities but only scalar. Initial nudging within this research interpolates 3D scalar data (Temperature and Salinity) from the GREP to all grid cells for the first-time step. This mitigates the need to nest within a larger, global model and only initial conditions are taken from the GREP. The benefit of this technique, as compared to a restart file, is that you don't need the exact number of layers or exact grid points for the interpolation of the values.

Complete internal or interior nudging refers to nudging temperature and salinity at every grid point within the model domain. This was done initially to test the nudging technique and to achieve and maintain a stable ocean boundary.

Once this was achieved, a nudging layer was constructed to demarcate an area of the model where nudging would be utilised for temperature and salinity values. As shown in Figure 3.1, the outer edge of the internal nudging polygon was kept away from the boundary of the model to prevent interference with the boundary conditions as this would cause instabilities. The inner edge of the polygon followed the continental shelf edge to keep the strong current along the shelf edge, which before the use of nudging, was difficult to achieve with just boundary conditions. GREP was used to drive the formation of the Agulhas Current with nudging. The area of interest was not included within this polygon to allow the D-Flow FM Model to independently estimate local and coastal flow features within the Durban Bight.

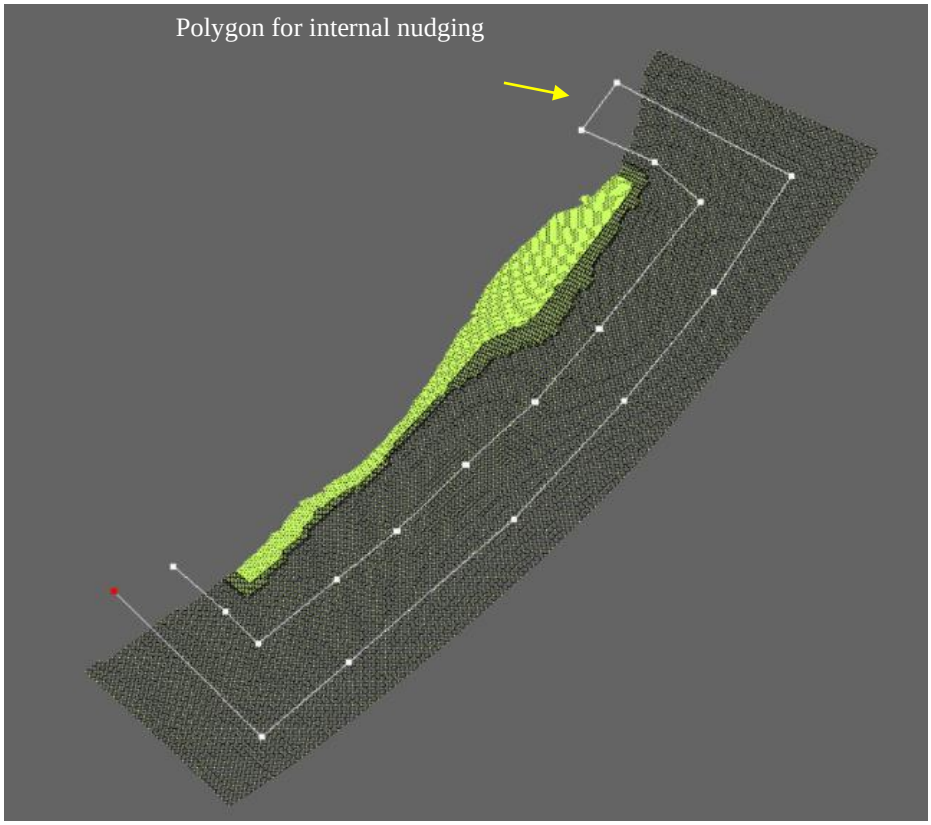

Figure 3.1: Image of D-Flow FM grid with polygon to be used for internal or interior nudging

3.2. The Internship Model

3.2.1. Extent and Location

The land boundary initially covered the KwaZulu-Natal coastline. However, usually, the boundary locations of the grid are less accurate than the inner parts of the model closer to the area of interest (Deltares, 2019b). The model domain must be large enough for any approximate boundary values not to adversely impact the results in the area of interest. Therefore, the extent of the model, and the new land boundary, needed to extend much further than the KwaZulu-Natal coastline. This also ensured that there was enough space for a strong current to form, whilst still restricting the model boundaries to before the Agulhas Current retroflection (as we are not interested in this phenomenon).

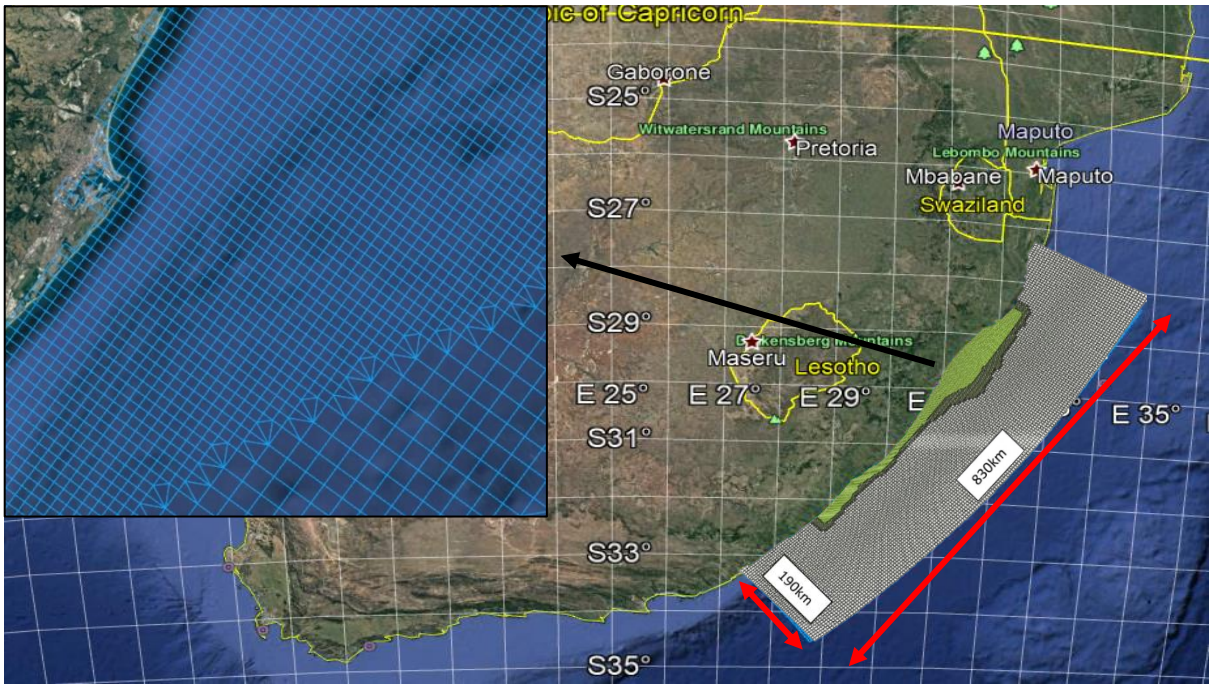

Figure 3.2.1: Location of the model in spherical co-ordinates, with zoomed in snapshot of Durban Bay area and model extents. The grid lies as close as possible to the eastern coastline of South Africa, extended on either ends of the KwaZulu Natal coast. Grid is overlayed on a Google Earth image.

3.2.2. Refinement

The grid was refined at the 1000m and 500m isobath by a factor of two to prevent numerical instability respectively (Deltares, 2019b). These two intervals are where the shelf break is located and where the frontal region of the Agulhas Current lies. As can be seen in Figure 3.2.1, the refinement was done internally (not at the boundaries), narrowing into the area of interest. This means that the smallest cells of the grid can be found closest to the KZN coastline.

3.2.3. Co-ordinate System

The horizontal co-ordinate system that was used for the Internship model was Spherical. Spherical coordinates are stipulated in decimal degrees. The Coriolis force for spherical coordinates is calculated from the latitude coordinates in the grid file, therefore it varies in the latitude direction. A coastal model (for larger domains such as the one used in this research) typically needs spherical co-ordinate specifications (Deltares, 2020a).

Therefore, for this research application, a cartesian grid (to accurately incorporate the cartesian land boundary) will be transformed into spherical coordinates, where the final model configuration will use spherical coordinates.

The land boundary was delineated by tracing the 0m depth contour (edge of the KZN shoreline) from GIS and Google Earth and merged with a coarse outline of South Africa from the World Land Boundary (Deltares, 2019b). This was then imported as a polygon to be used as the eastern land boundary for the model. A suitable curvilinear grid was constructed to fulfil orthogonality criteria as mentioned in (Deltares, 2020a), with the grid having an orthogonality of less than 0.02.

3.2.4. Bathymetry

Three sets of bathymetries were used to interpolate the sea-bed depths for this model:

- General Bathymetric Chart of the Oceans (GEBCO) (GEBCO - The General Bathymetric Chart of the Oceans, 2021) which can be found at https://www.gebco.net/.
- Navy Depth Soundings (South African Navy Bathymetry Data Set, 2005) which can be requested from the Navy Hydro Office.
- Bathymetric Survey Coverage of the Durban Bight (Bathymetric Survey Coverage of the Durban Bight Technical Report, 2016)

These datasets were integrated together using the land boundary and model domain to produce the bathymetry file used in the Internship Model. The Durban Bight bathymetry, having the highest resolution from the three datasets, was prioritise during the interpolation. The GEBCO data was overwritten in areas where there were Navy Depth Soundings and Durban Bight data, as this dataset was coarse, with the lowest resolution. The interpolated bathymetry for the Internship Model can be seen in Figure 3.2.2.

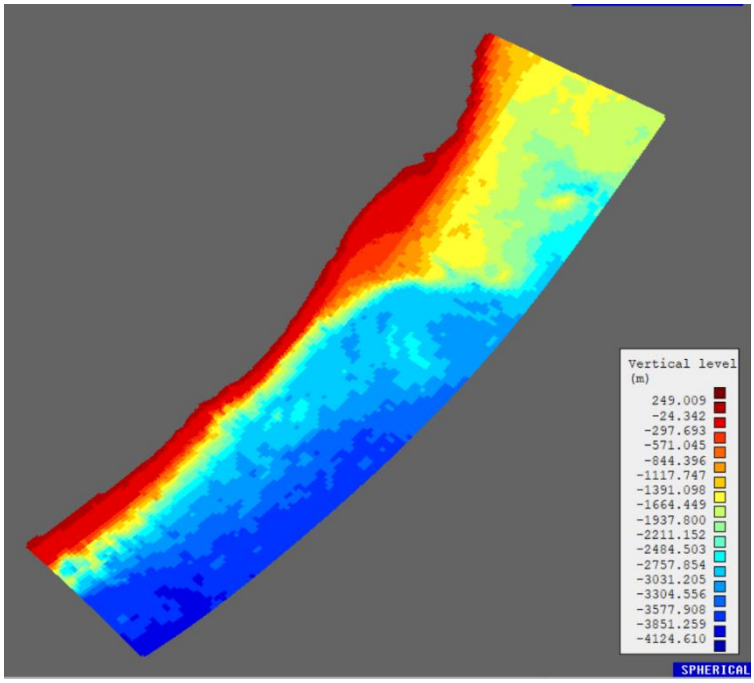

Figure 3.2.3:Internship Model showing Vertical Level (m) of sea floor

3.2.5. Forcing Parameters

Forcing files will be created using the FES 2012, ERA5 and the GREP. Boundary conditions for the Delft3D model will be implemented using the Global Reanalysis Multi-Model Ensemble Product (GREP). The Copernicus Marine Environment Monitoring Services (CMEMS) provides Global Ocean Sea Physical Analysis and Forecasting Products. The product used in this research for the implementation of boundary conditions and creating a file for the nudging technique is the "GLOBAL_REANALYSIS_PHY_001_030-TDS" (https://catalogue.marine.copernicus.eu/documents/PUM/CMEMS-GLO-PUM-001-031.pdf).
The CMEMS GREP has ¼ degree resolution with monthly means of Temperature, Salinity, Currents and Ice variables for 75 vertical levels, starting from 1993 onward. Four reanalyses were post-processed to create the GREP: GLORYS2V4 from Mercator Ocean, ORAS5 from ECMWF, GloSea5 from Met Office, and CGLORS05 from CMCC. They provide four different time series of global ocean simulations of 3D daily estimates and are all assimilated with the NEMO model on the ORCA025 grid. All are forced at the surface by ERA interim and assimilate sea level anomalies. This data will henceforth be referred to as GREP data or outputs (Storto et al, 2019).

3.2.5.1. Tide

This boundary condition was specified in terms of astronomical components. The observed tidal motion includes two main constituents, namely, amplitudes *A* and phases *G* which vary with location. The input data for tidal boundaries were retrieved from the Global Tide FES2012 model. The FES2012 (Finite Element Solution established in 2012) is a global hydrodynamic tide model developed to determine accurate tidal currents. The model consists of 32 tidal constituents which are distributed on $1/16°$ grids (Carrere L, *et al*, 2012). The nodal amplitude and phase factors are updated after each nodal time interval (Deltares, 2020a). The water level boundary (tide) was stipulated for every individual boundary location point at each boundary section (North, South and East).

3.2.5.2. Temperature, Salinity and Advection Velocity

A 3D boundary condition was specified as a time series for every boundary location point in a temperature boundary condition file. The time-series data is arranged similarly to the Z-type model by allocating data for each vertical layer as the vertical position type chosen was the "z-datum". The vertical position specification represented the depth of the vertical layers for each boundary point. Every vertical position specification had a series of temperature values (in Degrees Celsius) over a specified duration, for each time interval. This was done for all three open boundary sections. This procedure was also similarly done for salinity and velocity boundary conditions.

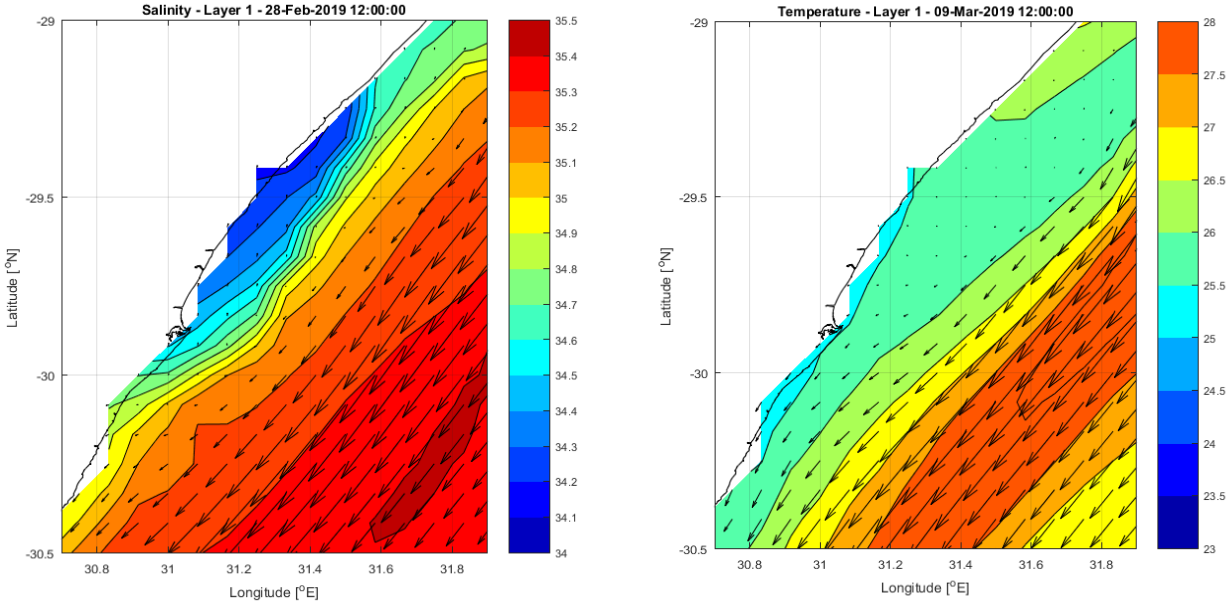

Figure 3.2.3: GREP data for both Salinity (left) and Temperature (right)

GREP output was used to obtain the Temperature, Salinity and Velocity values (GREP for Temperature and Salinity shown in Figure 3.2.3) for their respective boundary conditions. This includes daily average files from the top to the bottom over the global ocean (CMEMS, 2019). Each boundary forcing must indicate the quantity (type of parameter), location file (indicates boundary location points within that section) and the forcing file (the actual data for those boundary location points).

The difference with the velocity files, however, is that the advection velocity consists of two separate parameters namely, ux and uy (both indicating their respective magnitudes and directions, and both measured in m/s). The parameters ux and uy are represented by the "uo" and "vo" variables respectively within the GREP.

The spatial resolution of the GREP data is 0.083 degrees which is approximately 9km (CMEMS, 2019). This is too coarse for a coastal model. In Figure 3.2.3, the gap between the coast and the GREP data is noticeable. Therefore, downscaling of the GREP is necessary to obtain datasets at a finer resolution appropriate to describe coastal zones.

3.2.5.3. Wind and Atmospheric Pressure Gradients (Heat Flux)

The wind and atmospheric pressure parameters were obtained from the ERA5 dataset from the European Centre for Medium-Range Weather Forecasts (ECMWF). ERA5 provides hourly estimates of atmospheric, land and oceanic climate variables that cover the Earth on a 30km scale (ERA5, 2019). Wind fields can be specified as uniform but time-dependent or as space and time-varying wind (and pressure) fields.

Unlike the other forcing parameters, wind and heat flux are not prescribed with boundary parameters such as quantity, location file and forcing file. Instead, they were prescribed by indicating the filename (a NetCDF file), filetype (in this case 11 for ncgrid) and method (3 for interpolation of space and time) which is the older format for initiating boundary conditions.

Heat flux parameterises the effect of cloudiness. The addition of heat flux meant that relative humidity, air temperature and cloudiness are prescribed. This was prescribed by indicating that the model now becomes a composite ocean or composite heat flux model. The effective back radiation and the heat losses due to evaporation and convection were computed by the model (Deltares,2020b).

3.2.5.4. Initial Conditions

Table 4: Uniform initial conditions for flow velocity components are zero by default

Parameter	Lower limit	Upper limit	Default	Unit
Water level	-1,000	1,000	0.0	m
Salinity	0.0	100.0	31.0	ppt
Temperature	0.0	60.0	15.0	°C
Secondary flow	-10.0	10.0	0.0	m/s

Table 2 provides limitations for initial conditions for specific parameters which cannot be changed by users, but only by developers. This could be problematic if the value of the input parameters

from external model outputs lie outside the limits described in Table 2. This could result in the model crashing or rendering it unstable.

The following parameters were given initial conditions for the model:

- Water level (m) – 0m
- Temperature (deg C) - 11 ºC
- Salinity (ppt) – 36 ppt

The initial temperature was changed to 11℃ and the initial salinity was changed to 36 ppt to exhibit more realistic, deeper ocean values throughout all layers of the model.

However, as the model progressed, initial conditions for Temperature and Salinity were prescribed through initial nudging (explained in 3.1.1) throughout the model for the first-time step. This involved using GREP values for Temperature and Salinity for the initial conditions of the model to prevent a "cold" start.

3.3 Model Testing and Developments

3.3.1. Initial Boundary Implementation with a coarse, simple grid

The internship model (before refinement) was run with the forcing parameters detailed in section 3.2.5. Initially the model did not run due to the incorrect setup of boundary condition files. Eventually the files were corrected, however the model crashed shortly after the run was initiated.

Several modelling attempts indicated that the boundary conditions were not being correctly implemented within the model. Further details of these runs can be seen in Annexure A.

After several days of collaboration and testing with Deltares, Water Level, Temperature and Salinity Boundary Conditions were finally successfully applied, and a stable, coarse model was achieved (Refer to Annexure A for further elaboration). The next challenge was to implement the velocity boundaries, but this was done in conjunction with analysing and applying the nudging technique.

3.3.2. Testing the Nudging Technique

Several runs were done to explore the nudging technique, different forms of nudging, boundary conditions with nudging and different input parameters. New data was downloaded for the period between the years 2009 and 2011 for a smaller, more refined grid as compared to the coarse grid used in the previous runs.

The Analysis and Procedures were as follows:

- The model cannot successfully run without a water level boundary
- Two nudging options were available and tested, initial nudging and internal nudging
- Nudging was done for temperature and salinity only
- Nudging velocities internally was attempted but not implemented for initial nudging, and therefore removed
- Complete internal nudging with all boundary conditions caused problems since disturbances would occur near the boundaries due to clashes between the specified values and the GREP values.
- Complete internal nudging was attempted without boundary conditions – GREP values replicated well with model results
- The grid was then refined by a factor of 2, at specified isobaths – 1000 and 500m depths
- The intensity of nudging was varied horizontally – less intense closer to the area of interest. The intensity was determined by the variation in time scale i.e.: values would be nudged by the number of days intervals. The smaller the number of days between the next nudge time step, the higher the intensity of the nudging.
- It was identified that the nudging intensity (prescribed timestep) should correlate with the input data periods – i.e., for GREP values, 3 days nudging intensity is a too high timestep as GREP data was retrieved weekly, 14 days was too low of an intensity (this timestep did not feed enough data to the model from the weekly GREP outputs)
- The implementation of boundary conditions was tested with internal nudging – velocity boundaries were now being read and prescribed within the model

Although the velocity boundary conditions were being implemented, disturbances were identified at the boundary of the model. A step by step approach to investigate each boundary condition and the different nudging techniques was used to determine which attribute was the cause of these disturbances.

3.3.3. Model Boundary Testing with Nudging

Table 3 provides a summary of each run and the type of attributes for that run. These tests were used to determine the contributing factor of instabilities within the model. This was done to analyse each nudging type and boundary condition.

From these runs in Table 3, it is evident that whenever velocity boundaries were being implemented in the model, the model became unstable. A more detailed analysis with several outputs can be closely inspected in Appendix A. Due to the instability of advection velocity inputs within the smaller grid, a larger grid encompassing the entire Agulhas system was then created.

Table 5: Summary of Testing Boundary Conditions and Nudging Results

Test Name	Water Level (Tide)	Test Name	Salinity BC	Velocity BC	Initial Nudging	Complete Nudging	Stable Model
BC_ST_IniNudge	👍	👍	👍		👍		👍
BC_ST_noIniNudge	👍	👍	👍				👍 - long start up
BC_ST_Nudge	👍	👍	👍			👍	👍
BC_STV_IniNudge	👍	👍	👍	👍	👍		
BC_STV_noIniNudge	👍	👍	👍	👍			
BC_STV_Nudge	👍	👍	👍	👍		👍	
BC_V_Nudge	👍			👍		👍	

Key Words for table 3:

BC – Boundary Condition
S – Salinity
T – Temperature
V – Velocity
IniNudge – Initial nudging only
Nudge – Spatial, internal nudging
👍 - Included/ Achieved

3.3.4. Improving the Internship Model

A new version of DFM was then created by the software developers at Deltares to try and alleviate some of the issues experienced in the previous runs. New settings and parameters were introduced into the model. Advection velocity boundary conditions were successfully implemented within the model, with a stable model achieved. Wind and heat flux were also included.

The Agulhas Current has an undercurrent where in deeper layers the current reverses and flows in the opposite direction to the main current on the surface (as explained in 2.2.1). Upon further inspections of the model, it was noticed that the model became a "closed model" where currents were not flowing outwards and rather circulating within the model boundaries. Looking closer into the dynamics of the inputs, only the inflow of velocities was being prescribed by the velocity boundary conditions. This meant that if the velocity had a negative value within the input file, these values were being ignored. The repercussions of this meant that at the south boundary, the outflow values of the main current were not flowing out of the model and only the inflow values of the undercurrent were being prescribed.

The original default for D-Flow FM components is zero (refer to table 2). This issue was resolved by changing the default of the lower limit for flow velocity to allow for negative values.

Heat flux was implemented for the first time within the model. This meant that temperatures would be calculated by the model and temperature would not just be transported or prescribed but also modelled. It was advised by the developers that this would help prevent mixing of temperature in the upper layers and keep stratification.

Although tremendous improvements in both the grid, software code and input parameters were made during the internship period, minor disturbances still occurred at some of the boundaries which could result in inaccurate model results. A dampening mechanism was therefore applied by inducing a high viscosity layer alongside the open boundaries. This did not affect the internal computation of the model but allowed for boundary conditions to be implemented without clashing with the nudging or interpolated values inside the model.

This initial internship model was then used to compare model results with GREP values as well as observed results between a period of 2009 to 2011. My initial identification of the problems in Delft at the boundaries prompted further developments by Deltares and a new model version. These developments were done by Deltares experts and will be compared to my initial model outputs. These results can be found in the next chapter.

This pilot study was the first case for testing boundary conditions in an unreleased version of Flexible Mesh (D-Flow FM). Deltares modellers also attempted these simulations for a coastal

model offshore Massachusetts, USA, where a similar model setup was constructed. Simultaneously working on both this and the Internship Model allowed for improvements in the FM versions.

These improvements (as described in Appendix A) allow for larger domain extents where boundary conditions can now include and incorporate ocean boundary currents. Previously in the structured version of D-FLOW, this was only achieved with nested grids (Deltares, 2019a; Deltares, 2019b). Including these ocean currents can provide a better understanding on the coastal dynamics in regions where these ocean currents may significantly influence their adjacent coastlines. This pilot study also implemented 3D boundary conditions, including advection velocity boundary conditions, whereas previous studies in Delft3D mainly used water level and depth-averaged velocity boundary conditions (Ming, 2014; dos Santos Gil, 2014). Usually in coastal models, salinity and temperature are assumed to be constant as it is complicated to define the time dependent values for these parameters at the model boundaries (Ming, 2014).

3.4. Test08

Deltares Modelling experts further developed the internship model. The grid was transformed into a more curvilinear shape, and refinement was improved towards the coast (for improved accuracy and to allow for smaller scale features to develop). Detailed analysis into the grid

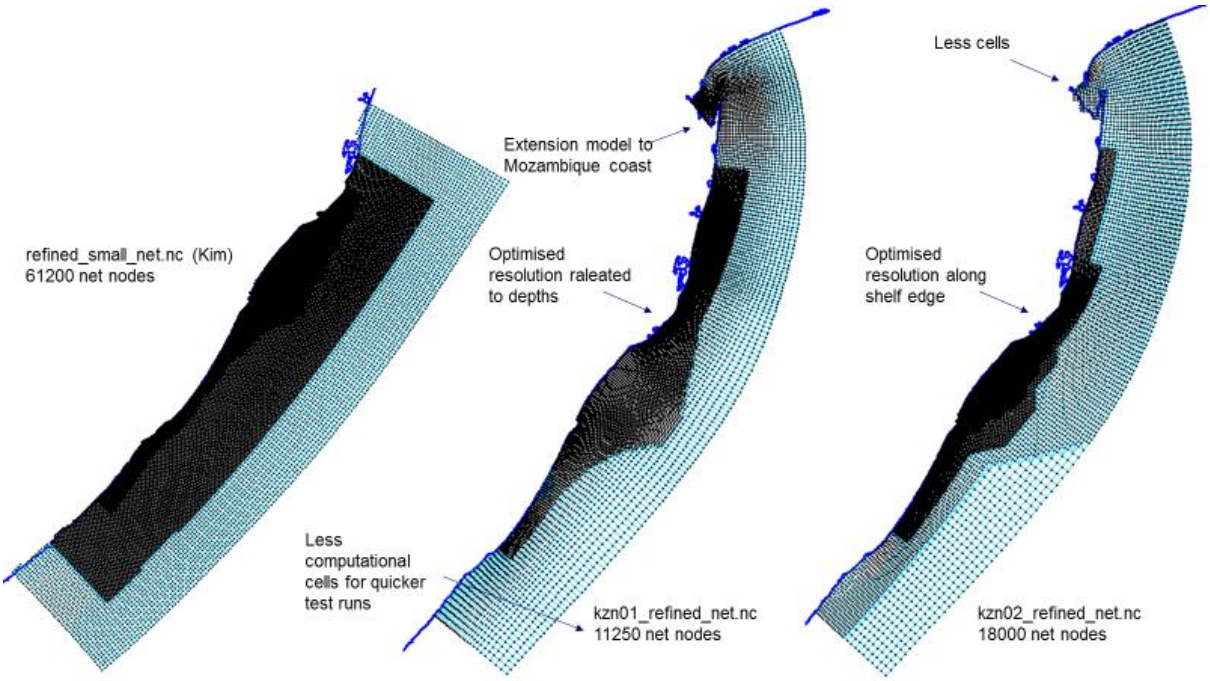

Figure 3.4.1: Variations in model extent and resolution: Coarse resolution (10km) in deep water, high resolution (now 300 m) along the coast and relatively high resolution at upper shelf slope (Deltares, 2019b). Internship model grid configuration shown on the left and new, further developed model grid configuration shown on the right.

formation, refinement and bathymetry was done to improve model results. These steps are exhibited in the next three figures.

The Test08 grid was also extended further north from the original northern boundary in the Internship model. The curvilinear structure was constructed to form a more perpendicular eastern boundary to the land boundary. Less computational time was also required with the new refined resolutions and positions.

The continental shelf was scrutinized further to improve resolution for higher accuracy in Test08. The Agulhas starts to meander within this region, which makes the accuracy of the model here crucial.

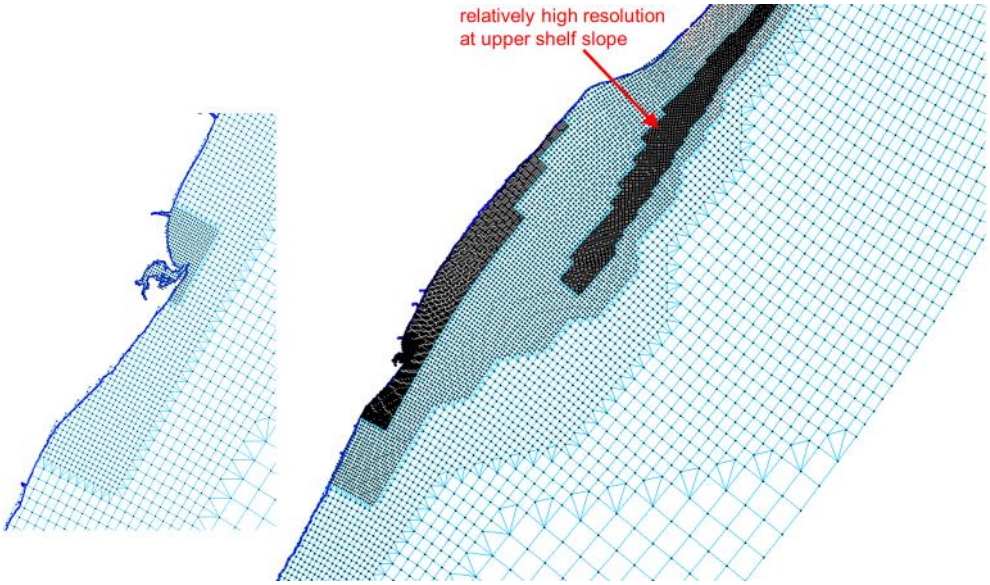

Figure 3.4.2: Model Schematisation of Test08 (Deltares, 2019b)

The bathymetry on the continental shelf was also examined and data cleansing was done within the region shown in the figure below.

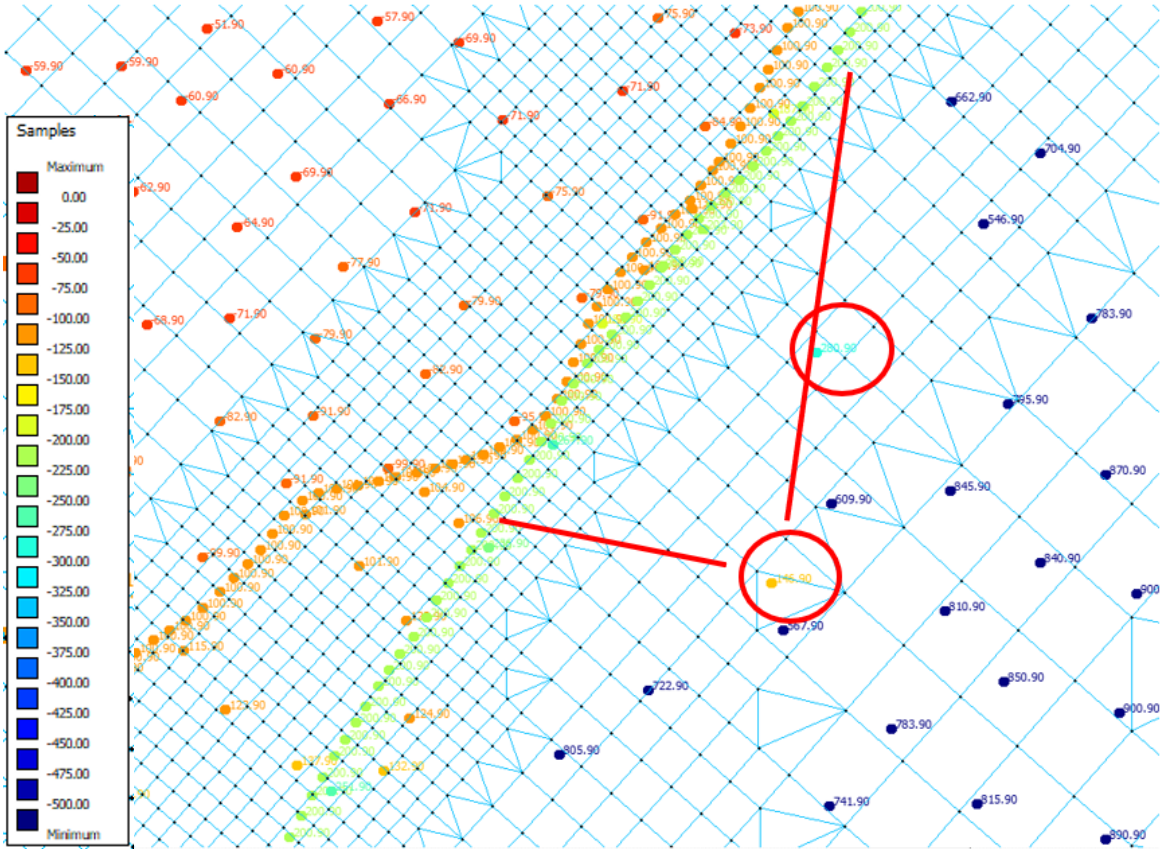

Figure 3.4.3: Review and re-interpolate xyz data to ensure best quality and realistic model depth and corresponding to CMEMS in deep part of the model (Deltares, 2019b)

Further developments that were done:

- A new executable was compiled for a new Operating System at Deltares – this executable is said to better solve for the Coriolis force within the model
- A hybrid vertical coordinate configuration where both sigma and z-layers were used (explained in 2.3.2) – the top half of the layers were prescribed as sigma layers and the rest were configured into z-layers – this was done to better represent the lower layers and avoid sigma errors in deeper waters.
- Extension of the northern domain to allow for northern boundary condition to better include Mozambique channel effects
- Refined grid cells in strategic areas as explained above, with a curvilinear grid more perpendicular or better aligned with the coastline
- Review and interpolation of bathymetry sets

- Nudging was no longer required as suitable boundary conditions and the right model domain was achieved
- No dampening mechanism (high viscosity boundary) was required due to no longer nudging

This model was labelled Test08, and model results will be compared with the Internship model in Chapter 4. Comparisons between the two models with observed measurements should show how the improvements mentioned above assist in achieving more accurate model results.

Both models, Internship and Test08, were run over the available data period (between 2009 to 2010) with hourly timeseries and map outputs. Smaller runs were also made to compare with the Offshore ADCP and ACEP data to save computational time and for ease of comparisons (Between March 2010 to July 2010).

3.5 Measured data

3.5.1. Offshore ADCP Data

The Southern African Data Centre for Oceanography (SADCO) database included ADCP (Acoustic Doppler Current Profiler) measurements retrieved by DEA (Department of Environmental Affairs) at a specific point off the Durban coast (Hereafter referred to as the Offshore ADCP). The Offshore ADCP recorded hourly current magnitude and direction profiles from 60m to 524m water depths (16m bin height). The period covers from 31 March 2009 until 5 September 2010. The location can be seen in the figure below:

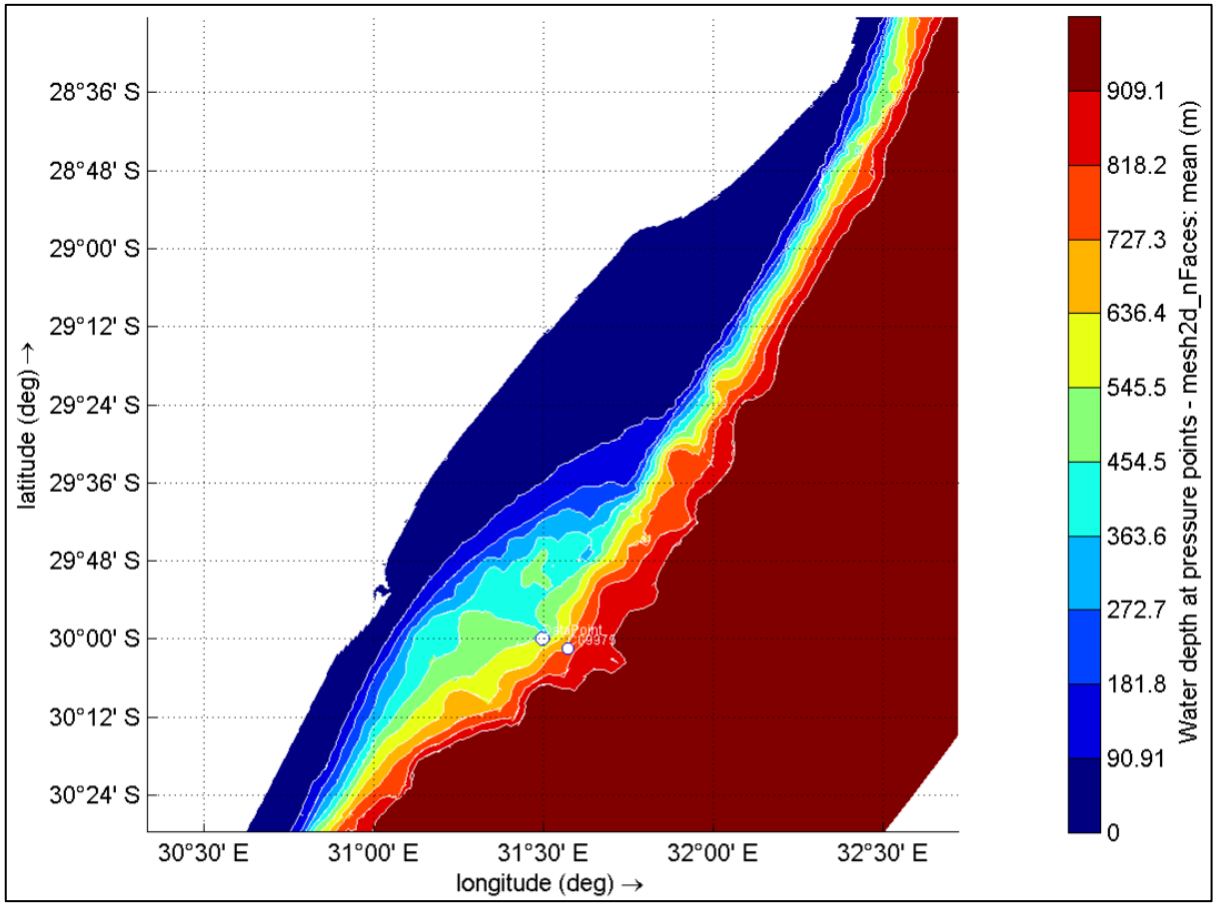

Figure 3.5.1: Location of Offshore ADCP: 30ºS 31.5ºE (shelf edge) in ±550m deep water

It is important to note that the location of the Offshore ADCP is in the middle of the region where we can expect the Durban Eddy to persist (as explained in chapter 2). This could result in stochastic recordings of observations in this vicinity, which should be kept in mind when analysing comparative results.

3.5.2 ACEP Data

Using data collected during the African Coelacanth Ecosystem Programme (ACEP), comparisons were made with the Flexible Mesh model outputs, the GREP global model output and the ADCP measurements from ACEP (see Chapter 4). This dataset is comprised of several ADCP ship-based transects recorded by an oceanographic vessel in 2010 over 18 months. The dataset was taken from Processed CTD (Conductivity, Temperature and Depth) data from Leg 1 of the African Coelacanth Ecosystem Programme (ACEP) II on the Algoa Voyage 176 (22 January to 22 February 2010) and 177 (16 July 2010 to 1 August 2010). Velocity direction and magnitude was extracted from this dataset.

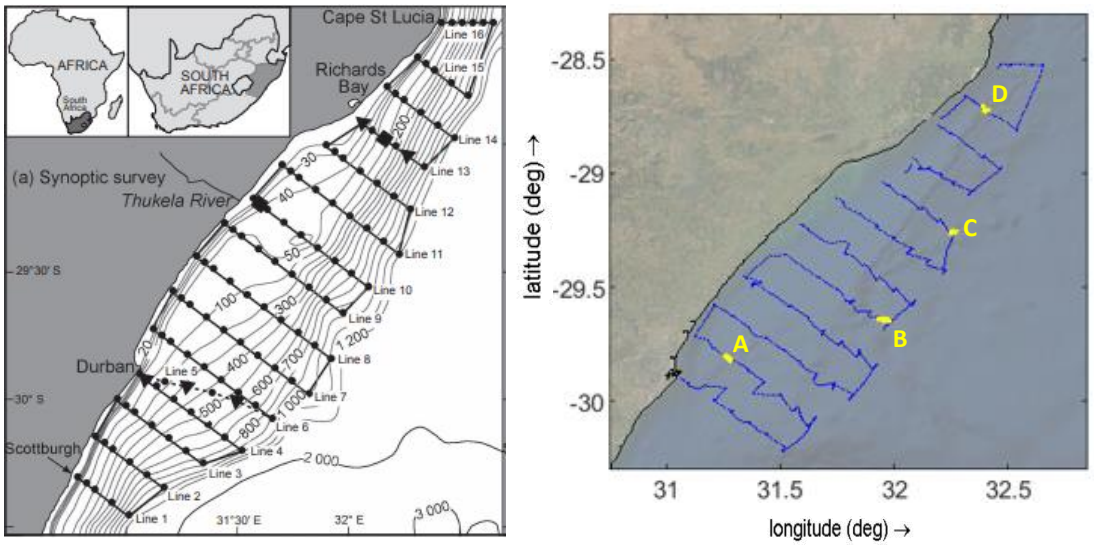

Figure 3.5.2: ACEP transects along the KZN coastline with locations of various output maps at different periods within the ACEP survey, taken and adapted from Fennessy et al (2016)

The surveys described in the above figure were done over several days, and thus essentially represent individual observations at particular locations across the Bight on different days. The data is more representative of the shelf conditions (20m-1000m isobaths) and thus does not capture the Agulhas Current proper (at best, the sampling extending only to the edge of the Agulhas Current or captured plumes of this water extending across the shelf). Also, nearshore (<20m depth) conditions are not represented in this data.

The programme was initiated by the Department of Science and Technology. This dataset was provided by the South African Environmental Observation Network (SAEON).

3.5.3 SANHO Tide Gauge

The University of Hawaii Sea Level Centre is one of the largest global networks of tide gauges. Over 300 tide gauge stations form a sea-level network designed to provide evenly distributed sampling of global coastal sea level variation at different time scales. A tide gauge located near the port of Durban was identified within this network and observed data from this gauge will be used for water level comparisons.

The South African Navy Hydrographic Office (SANHO) is the owner and copyright holder of the sea level data downloaded from the Durban site and their permission was granted for use of the data.

Figure 3.5.3: Locations of UHSLC Datapoint (red) and closest observation point from D-Flow FM Internship model (blue) taken from Google Earth.

It is important to note that the data points are not in the same locations but are both around the Durban port area. Location of SANHO Tide Gauge: 29°52'1.20"S, 31° 3'0.00"E. Location of Delft3D Observation Point (For both Internship and Test08): 29°53'45.72"S, 31° 3'35.04"E.

CHAPTER 4

RESULTS AND COMPARISONS

This chapter presents the results obtained from several model simulation outputs. This section shows the progression of the model, comparisons with GREP data, as well as comparisons with observed data. Observed data includes ocean current data from an Offshore ADCP and ACEP survey transects (as described in section 3.5).

4.1. The Internship Model

4.1.1 Initial Model Outputs

The following qualitative features were used to indicate an initial stabilized model:

- A strong offshore current (Agulhas) hugging the KZN coastline
- The direction of flow indicating the path of the current (north boundary to south boundary)
- Unrealistic sinks in water level conditions were resolved (water not flowing into/out of the model)
- Minimal disturbances/instabilities at boundaries
- No artificial circulation within the model, i.e.: currents are flowing in and out of the model
- Expected temperature conditions (as discussed in the literature review)
- Expected salinity values (as discussed in the literature review)
- Expected velocity magnitudes (as discussed in the literature review)

4.1.1.1. Water Level for Internship model

Figure 4.1.1 shows a typical water level output for the internship model. Some disturbances can be seen at the land boundary due to slightly inaccurate/coarse boundary delineations. Water level conditions seem to be simulated well (around the mean sea level range). The simulated values fall within the expected mesoscale tidal range of 1-2m (as described in section 2.1).

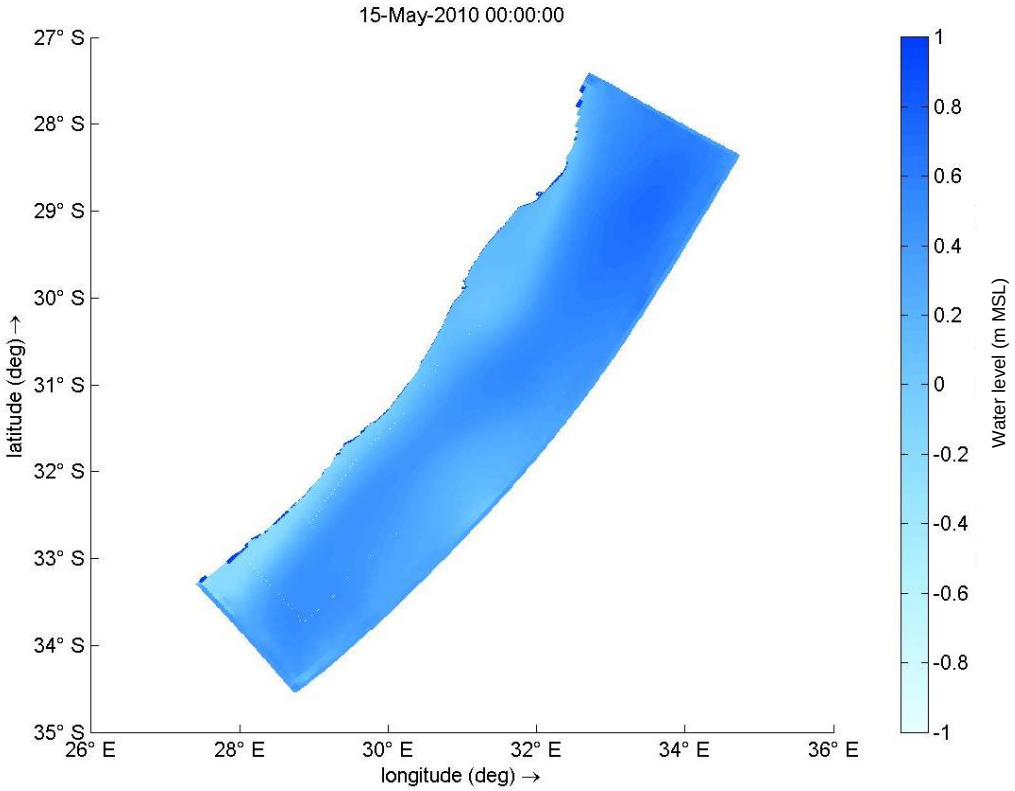

Figure 4.1.1: Typical Water Level (Tide) initial output from a simulation for May 2010

A typical water level time series output can be seen in Figure 4.1.2. Model results are similar to the observed tidal signal. With a RMSE (Root Mean Square Error) of 0.05 and a Bias of 0.03, the Internship model correlates well with the observed tide from the SANHO observation tide gauge. It is important to note the observation point within the Internship model is not in the exact location as the SANHO gauge. However, a strong correlation coefficient of 0.9973 (ρ~1) occurs for the period shown in Figure 4.1.2.

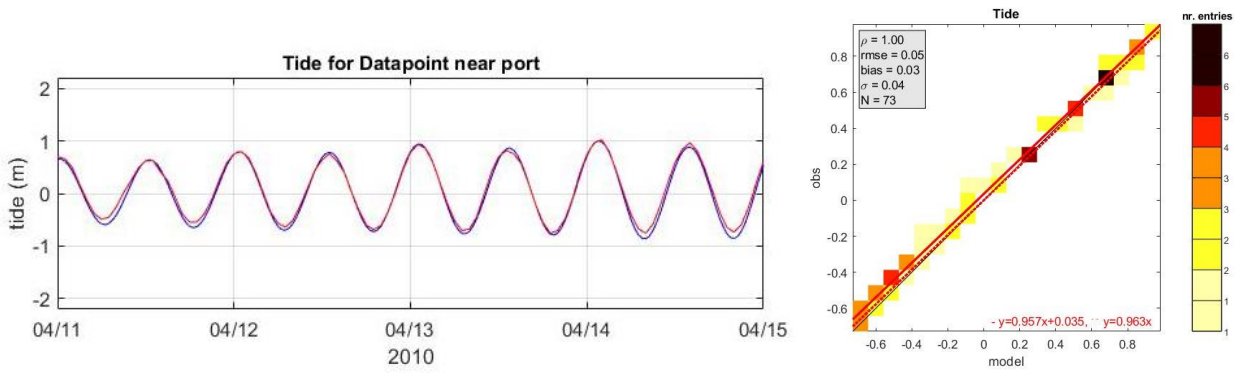

(a) **(b)**

Figure 4.1.2. (a) Typical outputs for water level at SANHO Tide Gauge. Location of SANHO Tide Gauge: 29°52'1.20"S, 31° 3'0.00"E. Blue line reflects tide from the D-Flow FM internship model and red line shows SANHO observed tide. (b) Error Statistics for tidal comparisons in (a)

4.1.1.2. Temperature for Internship model

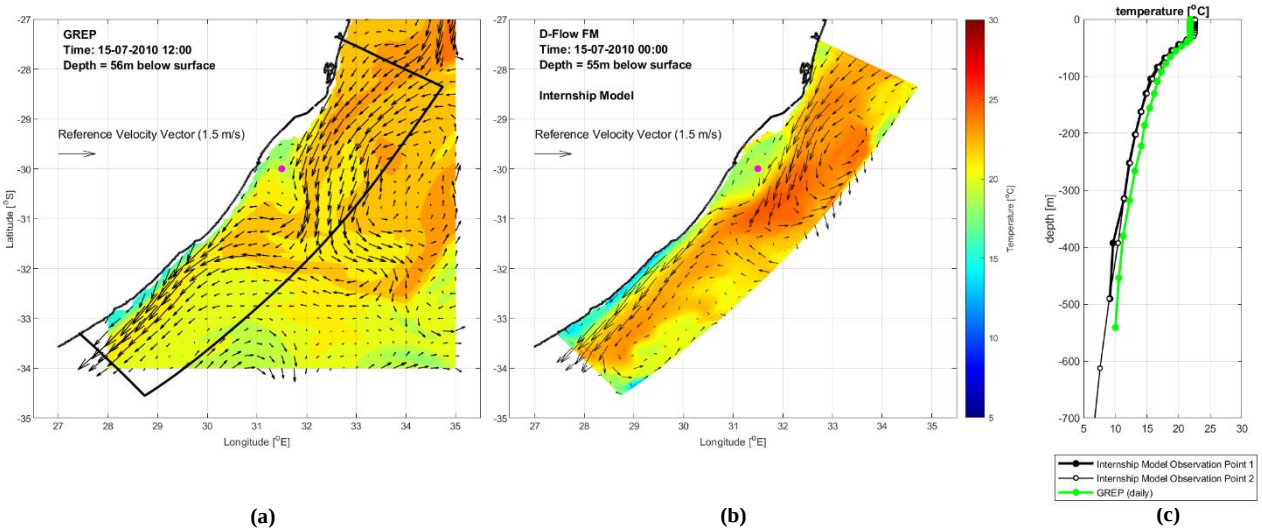

Figure 4.1.3: Typical Temperature output from the internship model simulation including velocity vectors indicating magnitude and direction of flow for 15 July 2010. (a) GREP Temperature Map Output, (b) Internship Model Temperature Map Output and (c) Temperature Profile for location (29°55'34.74"S, 31°27'38.39"E) shown with red dot on (a) and (b) and closest two observation points from the Internship Model.

In Figure 4.1.3, temperature outputs show similar attributes to temperature values that we can expect and have noticed in both literature and global model conditions (23 to 26 º C). The main current in Figure 4.1.3 shows temperatures ranging from 23 to 25 º C for this particular instance, which corresponds well with what is mentioned in section 2.2.

4.1.1.3. Salinity for Internship model

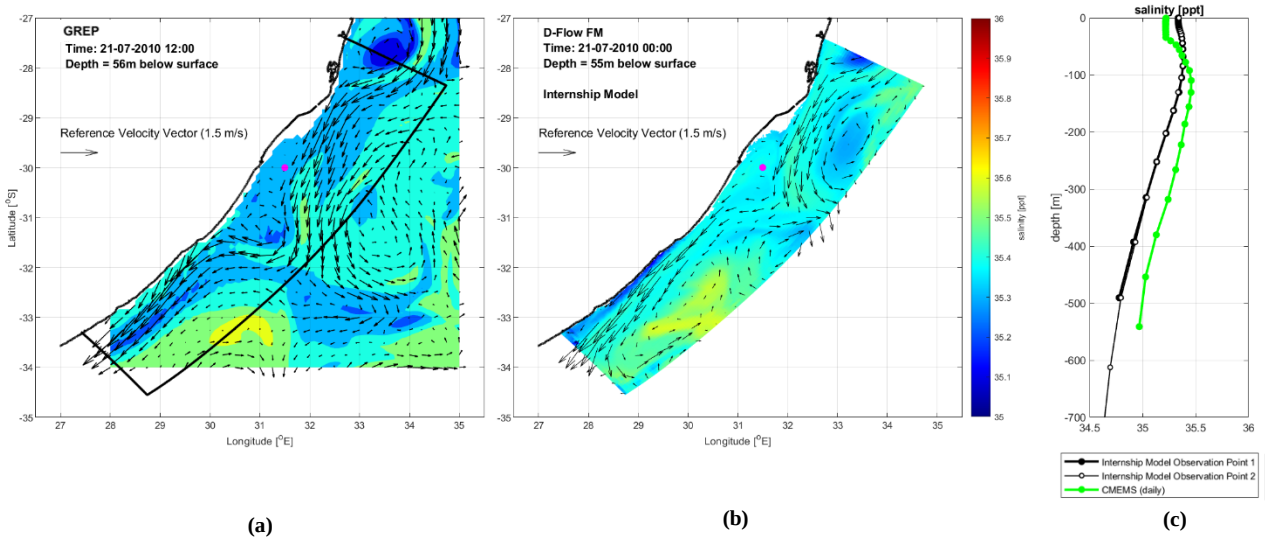

Figure 4.1.4: Typical Salinity output from the internship model simulation including velocity vectors indicating magnitude and direction of flow for 21 July 2010. (a) GREP Salinity Map Output, (b) Internship Model Salinity Map Output and (c) Salinity Profile for location (29°55'34.74"S, 31°27'38.39"E) shown with red dot on (a) and (b) and closest two observation points from the Internship Model.

Like temperature outputs, salinity results correspond to outputs that we can expect and have seen from literature and global models, with the main flow of the current showing a constant salinity measurement of 35.4 parts per thousand (as mentioned in section 2.4). Salinity values along the main current are in proximity of what has been observed and measured before.

4.1.1.4. Velocity Ux and Uy for Internship model

Figure 4.1.5 shows a strong Agulhas Current that reaches magnitudes of 2m/s. It also shows how the current meanders as it travels further south in the model. Current direction and magnitudes are also indicated by the velocity vectors on the map. This output was taken from the upper surface layers of the model, where we can expect the Agulhas Current to be strong. Velocity vectors pointing out of the model indicate outflow at the boundary whereas velocity vectors pointing into the model indicate inflow. This shows that the model is not a closed grid which allows the open boundaries to prescribe whatever is coming in and out of the model without crashing.

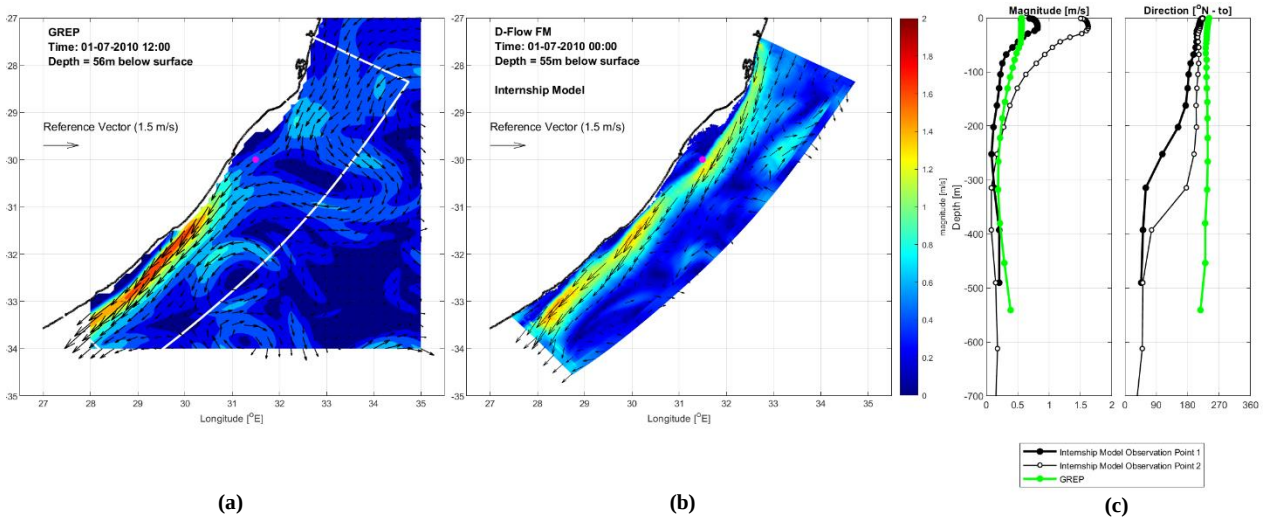

Figure 4.1.5: Typical Velocity output from the internship model simulation including velocity vectors indicating magnitude and direction of flow for 21 July 2010. (a) GREP Velocity Map Output, (b) Internship Model Velocity Map Output and (c) Velocity Profile for location (29°55'34.74"S, 31°27'38.39"E) shown with red dot on (a) and (b) and closest two observation points from the Internship Model.

4.1.2. Comparing the initial model with observed data

4.1.2.1. Offshore ADCP, GREP and Internship Model

Figure 4.1.6 shows a comparison of the model results to GREP and the Offshore ADCP at similar locations near the surface. Daily mean values were extracted from the GREP, whilst the internship model and Offshore ADCP both outputted hourly values. Although different temporal resolutions

were used for this comparison, it was acceptable for an initial time series comparison of the D-Flow FM model. From these initial results we can see that in certain instances, the model does bridge a gap between GREP and observed data. This result is promising and meets the objectives of the initial model. The Internship model time series corresponds better with the observed data at some periods (example on the 6th of July 2009), but in other instances the GREP time series corresponds better with the observed data as compared to the internship model (October 2009).

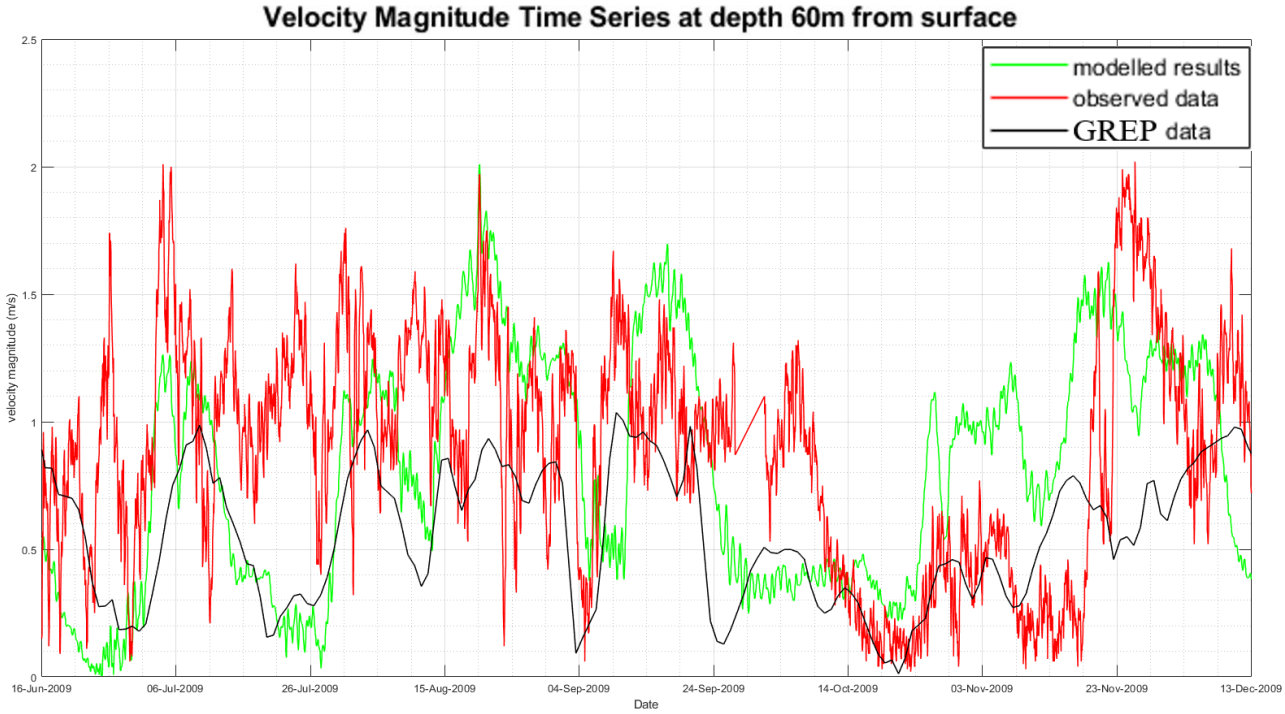

Figure 4.1.6: Time series for the year 2009 showing velocity magnitude of: GREP data (in black), Offshore ADCP (in red) and Internship model data (in green).

Some implications of not using the same sampling interval for this initial comparison include lower current values in the daily GREP data as compared to the hourly analysis from the ADCP and D-Flow FM model. This is better represented in later sections where the data is resampled to the lowest temporal resolution (daily) for comparisons including Test08.

Similar to velocity magnitude, a time series output for velocity direction was also produced. In Figure 4.1.7 below, the current direction erratically changes at certain periods, which also suggests the stochastic nature of currents in this location. The initial outputs of the model suggest instabilities from the start-up of the model. In certain instances, GREP represents the direction of velocity better than the Internship model at this location, which suggests room for improvement.

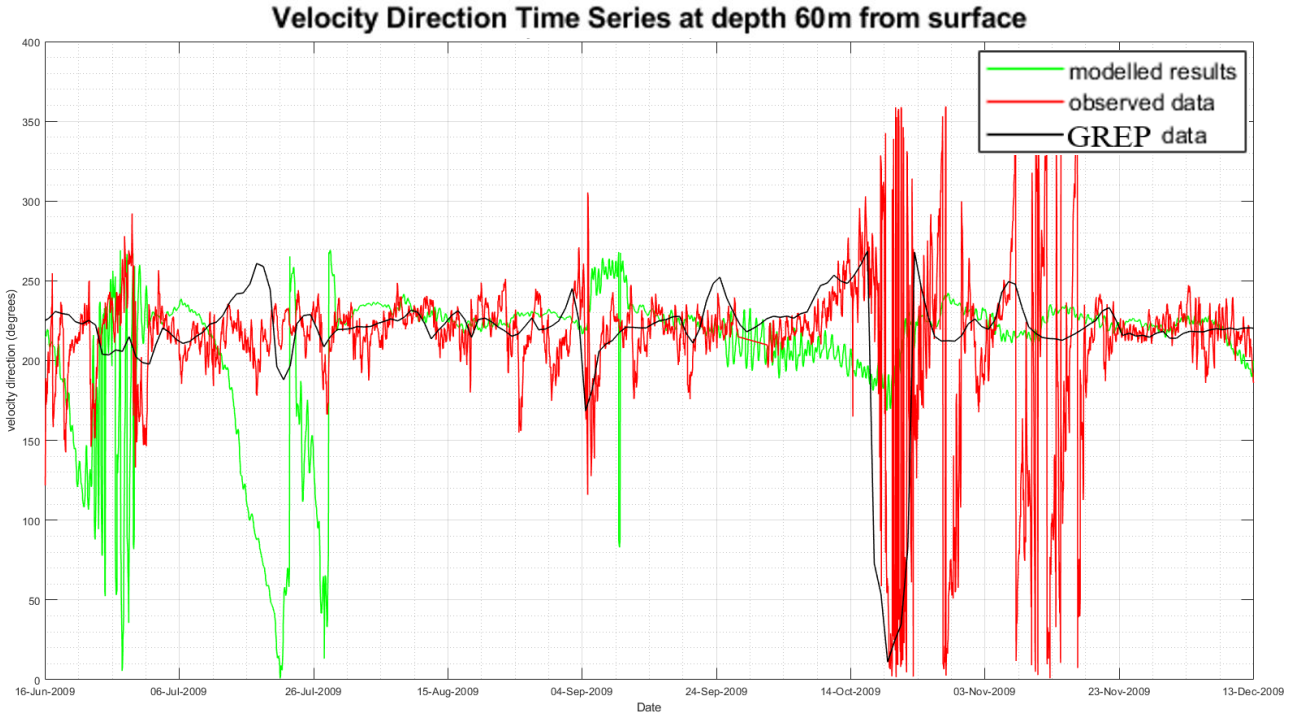

Figure 4.1.7: Time series for the year 2009 showing velocity direction of: GREP data (in black), Offshore ADCP (in red) and Internship model data (in green).

4.1.2.2. ACEP, GREP and Internship Model

Initial model results were then compared to measurements recorded in the ACEP survey. The locations described in Figure 3.5.2 are shown in Figure 4.1.8 with comparisons of both GREP and the Internship model.

From Figure 4.1.8, it is easy to visually compare model results to the observed instantaneous ACEP data. At locations A and D, there is a strong visual correlation between the velocity magnitude and direction of both values. However, at location B, this is not the case. Model inaccuracies or invalid ACEP data could both be contributing factors at location B as well as the intricate position of this location.

For initial model outputs to already compare well with observed data is a good sign of the model's validity and accuracy. Most survey points are well represented in the model already and any further development of the model should only increase the accuracy of the comparisons shown above.

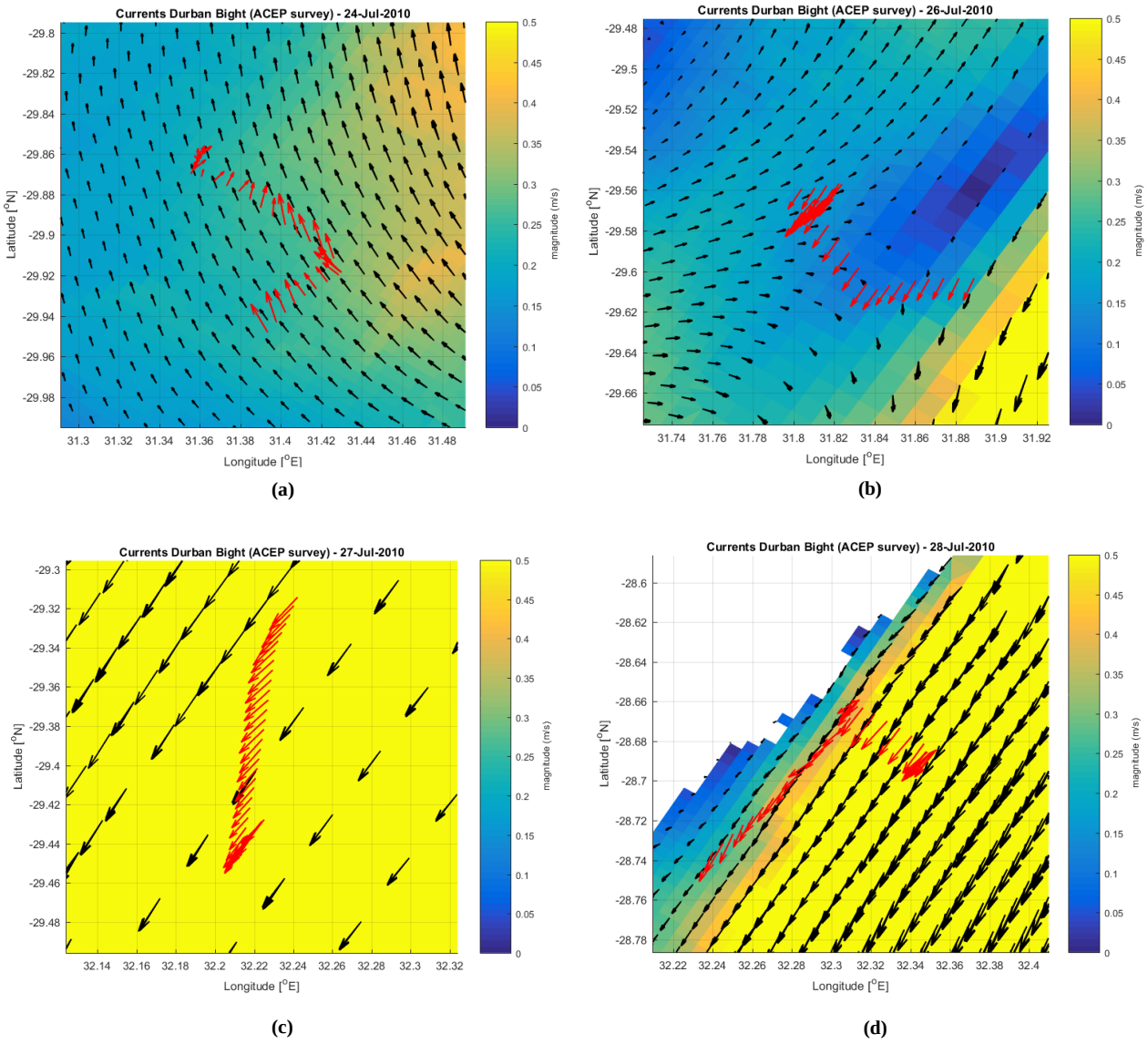

Figure 4.1.8: (a) Location A from ACEP survey, (b) Location B from ACEP survey. (c) Location C from ACEP survey, (d) Location D from ACEP survey. Red vectors show ACEP ADCP velocity magnitude and direction, while black vectors show Internship model velocity magnitude and direction

4.1.3. The Durban Eddy

As explained in chapter 2, the Durban Eddy is a phenomenon that occurs half of the year. The eddy occurs between the main Agulhas Current and the Durban shore. To accurately depict this feature, a more refined and local model was produced. Global models such as GREP's NEMO model, cannot resolve coastal scale features due to limitation in their grid resolution.

Figure 4.1.9 shows the need to downscale the GREP data, as the model output in (a) shows a lower grid resolution which cannot resolve the eddy. The D-Flow FM model in (b) shows a well-formed Durban Eddy as well as spin off currents flowing into the KZN bight, which can directly influence the adjacent coast.

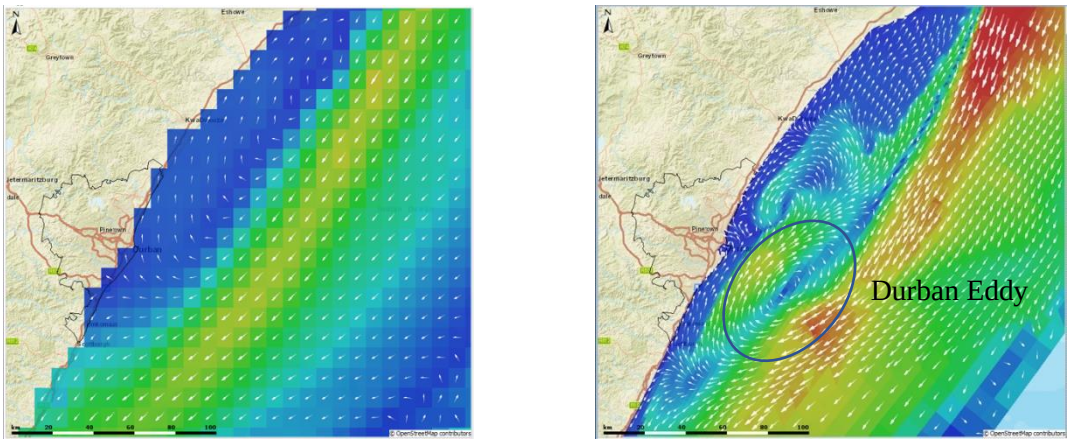

(a) **(b)**

Figure 4.1.9: (a) GREP Surface Map Output extracted from the eThekwini Municipalities FEWS, (b) D-Flow FM Model Surface Map Output extracted from the eThekwini Municipalities FEWS. Both outputs are taken on 6th September 2021at 0m depths (surface).

The Internship Model was successful in simulating a typical Durban Eddy condition. This can be seen in Figure 4.1.9 above. This not only allows us to model such a phenomenon but illustrates the success of the model in bridging the gap between ocean and coastal models.

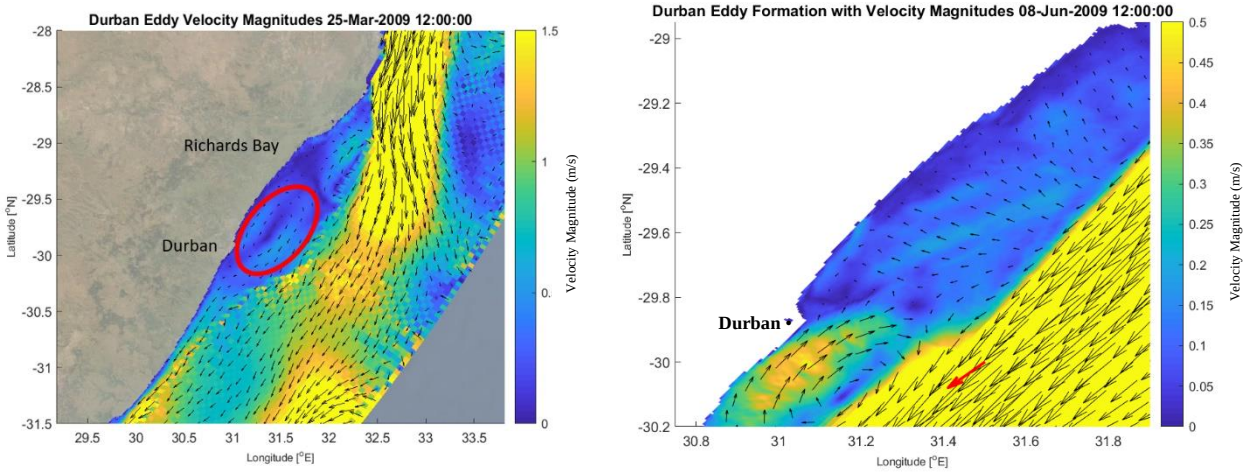

(a) **(b)**

Figure 4.1.10: (a) Map output from the Internship Model indicating simulated size and location of the Durban (red circle), (b) Zoomed in map output showing edge of the Agulhas Current and Durban Eddy from the Internship Model with the Offshore ADCP velocity magnitude and direction shown by the vector in red

Figure 4.1.10 depicts a fully formed Durban Eddy and its influences within the receding bay further north. The red vector represents the Offshore ADCP. As illustrated in Figure 4.1.10, the red vector and the black vectors (modelled results) show both similar direction and magnitude, motivating for the accuracy in the modelled results.

As illustrated in literature, the Durban Eddy is said to be half as strong as the main Agulhas Current. This is well portrayed in Figure 4.1.10 above, as the main current has a magnitude of 1.5m/s in this instance and the Durban Eddy is between 1 and 0.5m/s (±0.75). This suggests that the model agrees with velocity magnitudes delineated by literature.

Visual inspections of the Internship model outputs from 1 April 2010 to 1 July 2010 (3 months), show approximately five eddies being formed offshore Durban within this time scale. This is an average of 1.66 eddies per month. This is in close proximity with the frequency of the eddy mentioned in Table 1.

Using Figure 4.1.10, degrees were converted to kilometres to estimate the length and size of the Durban Eddy. For this particular eddy, a length of 62.79 km and a width of 40.02 km were calculated. This falls within the ranges stipulated in Table 1.

4.1.3.1. Simulations showing the formation of the Durban Eddy

The Durban Eddy has an overall duration of approximately 8 days. A typical formation of the eddy involves the upwelling of cooler water along the coast interacting with warmer waters from the main current. Figure 4.1.11 shows the formation, duration and dissipation of the eddy.

In Figure 4.1.11 (a), a high temperature is illustrated along where the main Agulhas Current can be expected. Figure 4.1.11 (b) begins to show cooler water along the coastline starting to mix with this warmer water. From Figure 4.1.11 (c) through to (j), circulation of these different temperatures occurs, forming an “eddy-like” feature. In Figure 4.1.11 (i) we notice dissipation of this circular motion which suggests the weakening of the eddy.

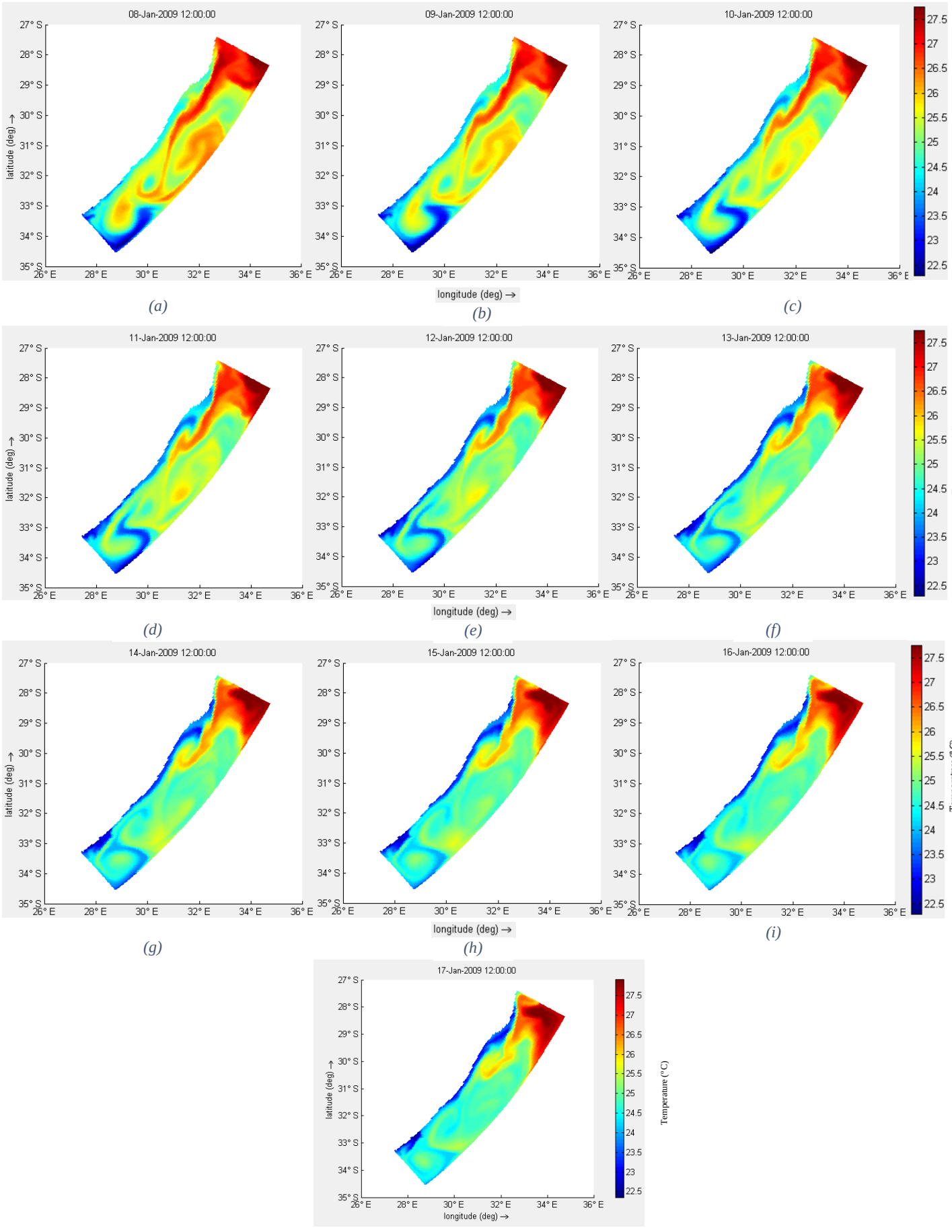

Figure 4.1.11: Temperature simulations showing the formation of the Durban Eddy from the 8th to the 17th of January 2009.

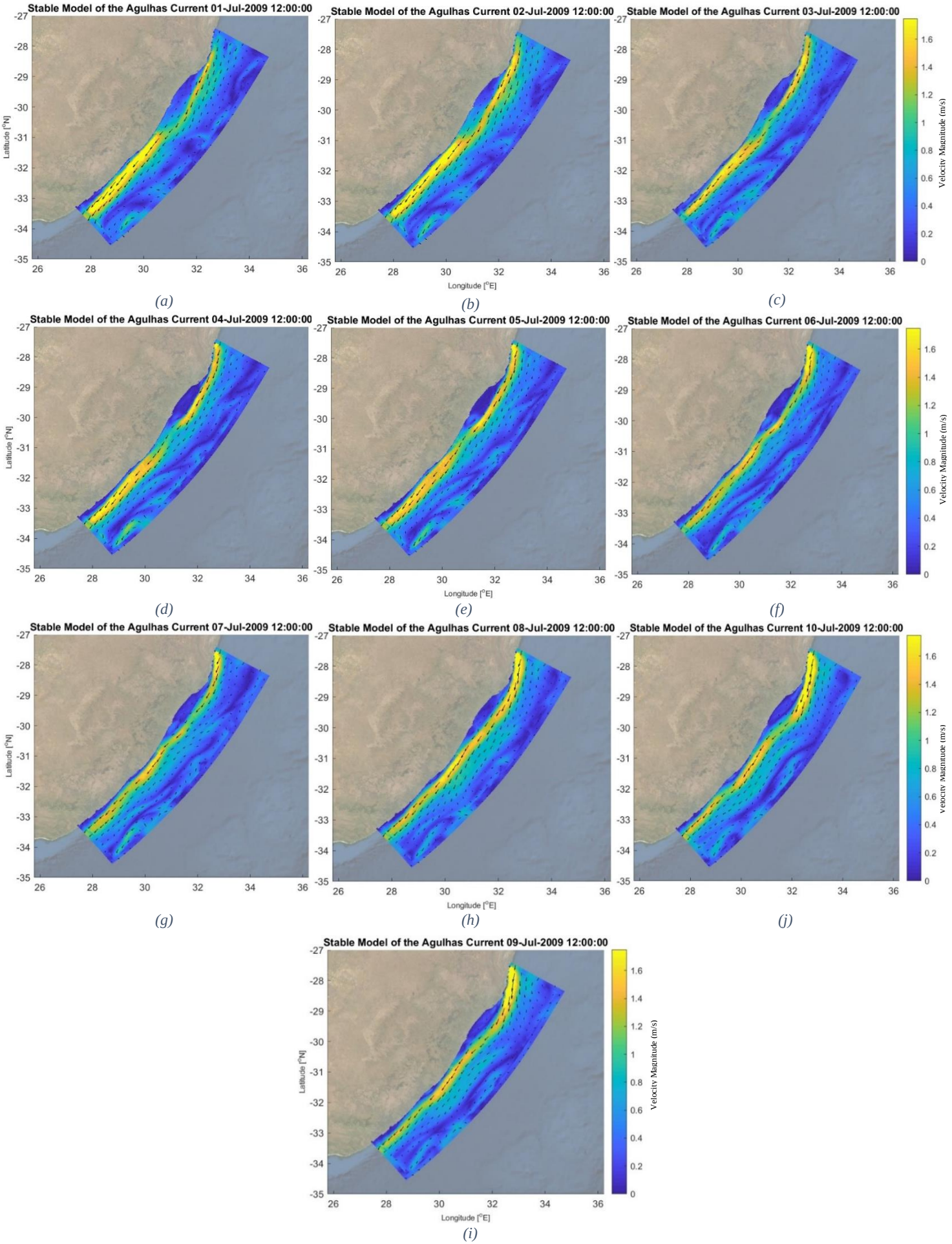

Figure 4.1.12: Velocity magnitude simulations showing the formation of the Durban Eddy from the 1st of July 2009 to the 10th of July 2009

Similarly, with advection velocities, we also notice the different stages of formation of the Durban Eddy. Although this is for a different period in time compared to the temperature simulations, the same duration and stages are depicted and identified. This also shows consistency within the model at different time intervals.

A strong Agulhas Current hugs the continental shelf in Figure 4.1.12 (a). It starts to move away from the coast in Figure 4.1.12 (b) and a weaker current is shown just south of Durban in Figure 4.1.12 (c). In Figure 4.1.12 (d) we can see a circulation starting to form. A fully-fledged eddy can be seen from Figure 4.1.12 (e) through to Figure 4.1.12 (g). In Figure 4.1.12 (h) and (i) the eddy is dissipating and Figure 4.1.12 (j) shows the main Agulhas Current back to the edge of the continental shelf with no eddy present.

4.1.3.2. Effects of the Durban Eddy on the Durban Coast

Literature suggests that the Durban Eddy is associated with and deflects the core of the main Agulhas Current further away from the coast. This is noticed on a coastal scale in Figure 4.1.10 and on larger scales in Figures 4.1.11 and 4.1.12.

Figure 4.1.13 shows model outputs zoomed in around the Durban shore. The red arrow indicates the velocity magnitude and direction of the Offshore ADCP in both instances. The edge of the Agulhas Current is much closer to the shore when there is no eddy present. The eddy deflects the current further offshore when it persists off the coast of Durban. It is also important to note that the model suggests that the presence of the Durban Eddy reverses the direction of the currents along the coastline northwards from Durban. This is an extremely important effect from the eddy and can have significant impacts on Durban's coast when modelling closer to the coast. Changes in current direction and magnitude can directly affect particle movements which in turn affect water quality and sediment transportation modelling.

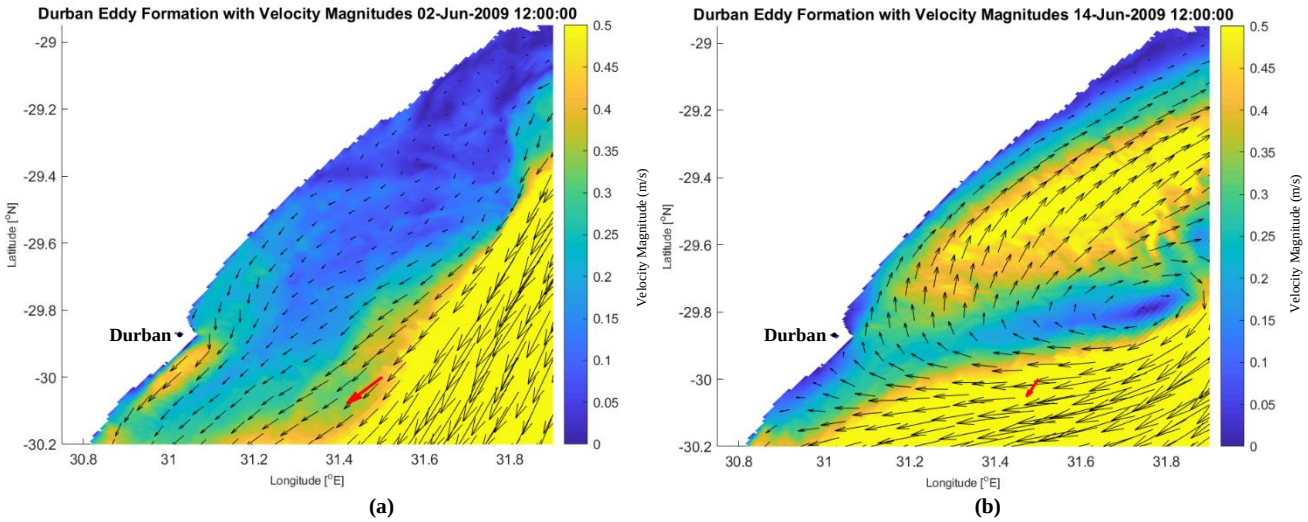

Figure 4.1.13: (a) Simulation off the Durban coast showing velocity magnitudes when there is no eddy present and (b) when the eddy is situated off Durban , with the Offshore ADCP velocity vector (red arrow)

4.2. Test08

As explained in 3.4, the Internship model was further refined and calibrated. It is important to note that the transformed model (test08) did not use internal nudging within the model but only for the initial conditions of the model (initial nudging). This was the biggest difference between the two models, apart from the grid refinement and structure.

4.2.1. Offshore ADCP

4.2.1.1. Time series

The Offshore ADCP measurements were used to compare with GREP, the Internship model and the Test08 with some results illustrated in Figure 4.2.1.

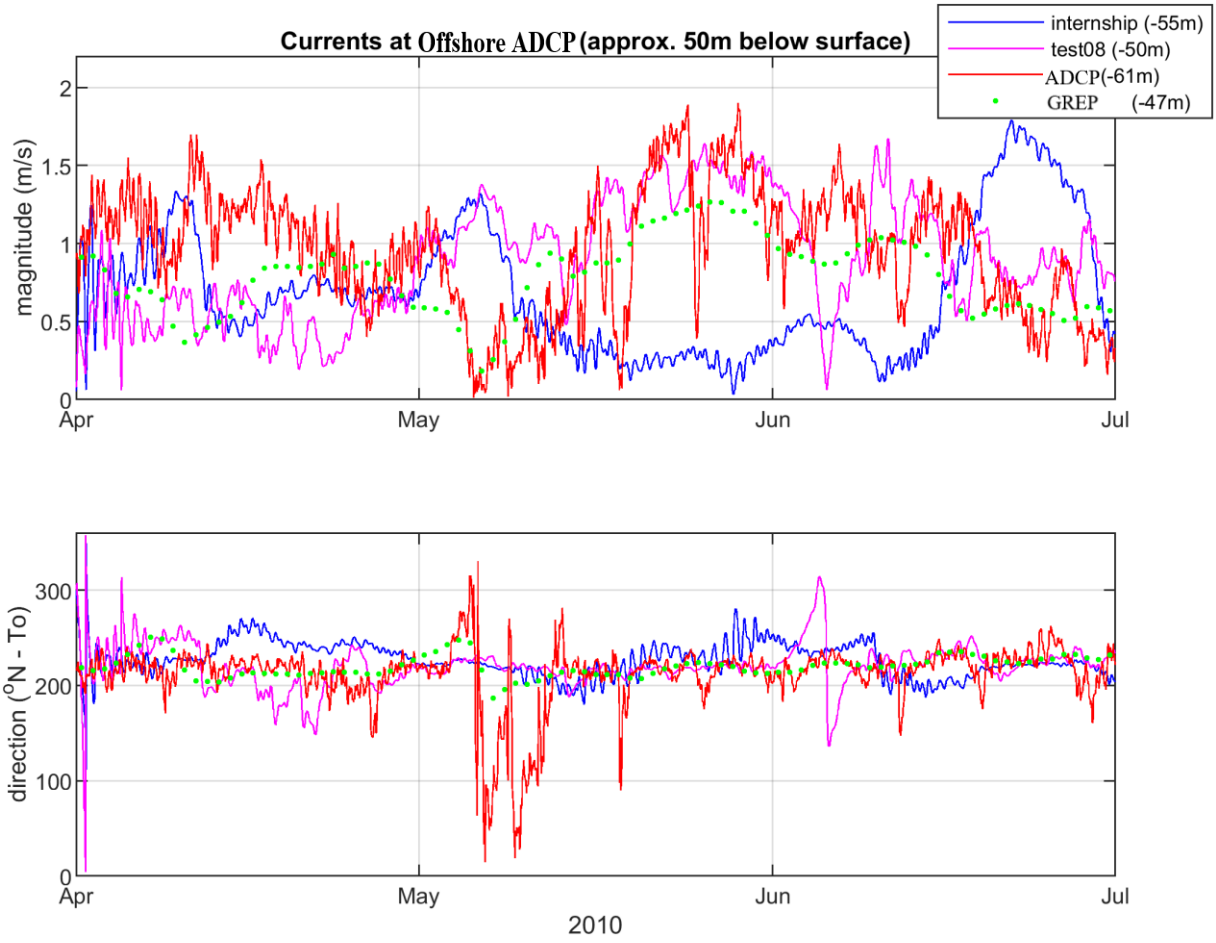

Figure 4.2.1: Time series comparing velocity magnitudes and directions for the Offshore ADCP measurements, GREP and the D-Flow FM models at similar water depths (approximately 50m) below the surface from April 2010 to July 2010

The Offshore ADCP exhibits the expected behaviour of velocity magnitudes, as analysed in Chapter 2. Speeds of close to 2m/s near the surface (in the main current) were recorded in the field, but the models seem to have slightly lower speeds. Although initially, the internship model is much closer to the observed data, as the time series continues, we see that test08 follows the observed data well.

Looking at the overall comparisons in Figure 4.2.1, it is evident that test08 performs better than the internship model. The test08 time series corresponds better with the Offshore ADCP data and in some instances, performs better than the GREP time series. The sudden drop in magnitude and drastic change in direction in June, suggests the occurrence of a Durban Eddy.

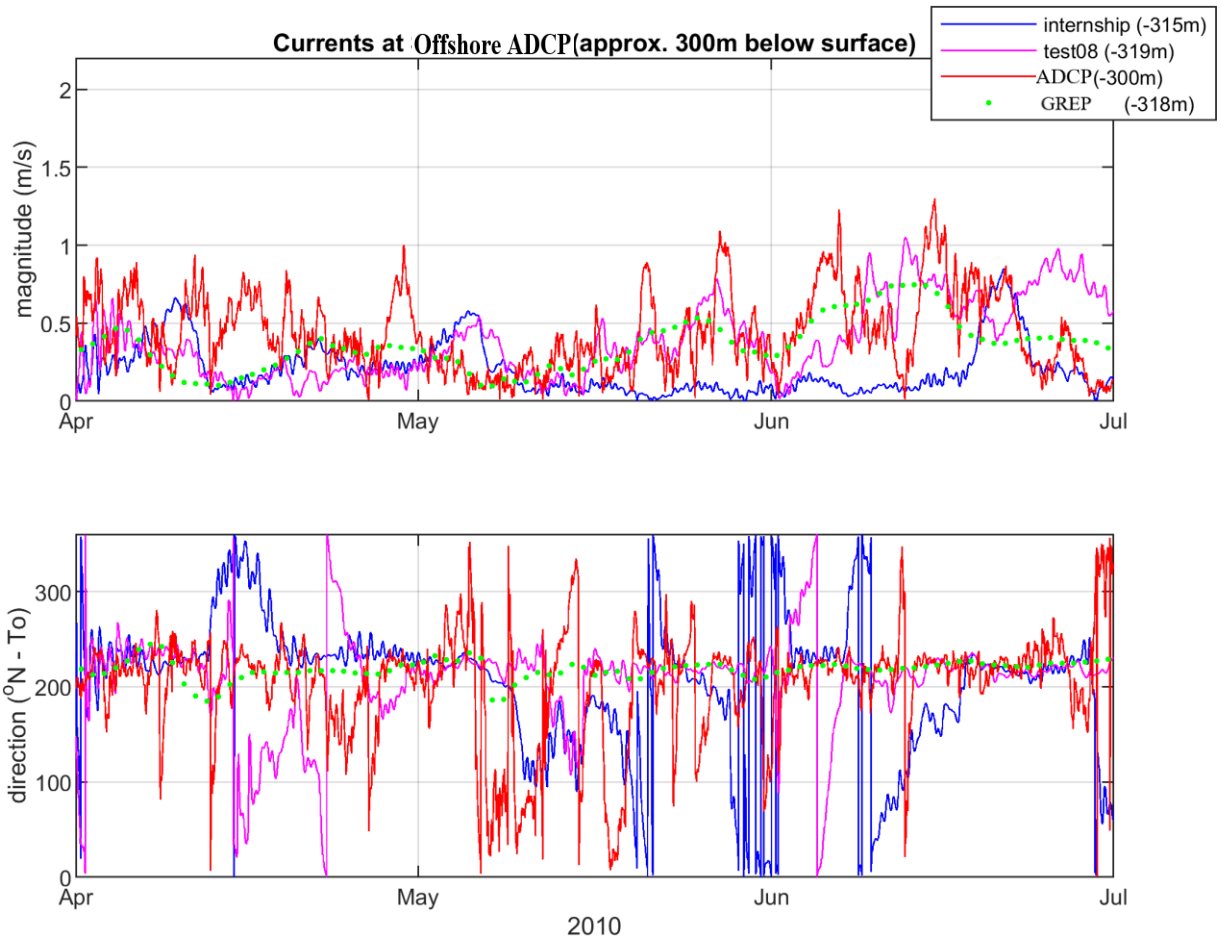

Figure 4.2.2: Time series comparing velocity magnitudes and directions for the Offshore ADCP measurements, GREP and the D-Flow FM models at similar water depths (approximately 300m) below the surface

Much lower velocities were recorded at 300m depths. This is also confirmed by literature in Chapter 2, as the main Agulhas Current is much stronger on the surface. Similarly, to Figure 4.2.1, test08 performs better than the internship model and follows the Offshore ADCP time series quite well throughout the specified duration.

4.2.1.2. Statistical Analysis

Daily Outputs:

Error Statistic Analysis was done for GREP data, the Internship model and Test08 based on the Offshore ADCP measurements for the period between April and July 2010 (same as 4.2.1 and 4.2.2) at 60m depths. Only daily outputs could be retrieved from the GREP, which gives a rough representation of the data compared to the Offshore ADCP which provides hourly recordings. The correlation coefficient (ρ), Root Mean Square Error (RMSE), Bias, and Standard Deviation (σ) are calculated from all data resampled at a daily temporal resolution.

Velocity magnitudes were compared for all three models, however, to accurately analyse how well these models perform, both x-component and y-component velocity magnitudes were investigated to include the effect of velocity direction in these error statistics.

X-Velocity Component

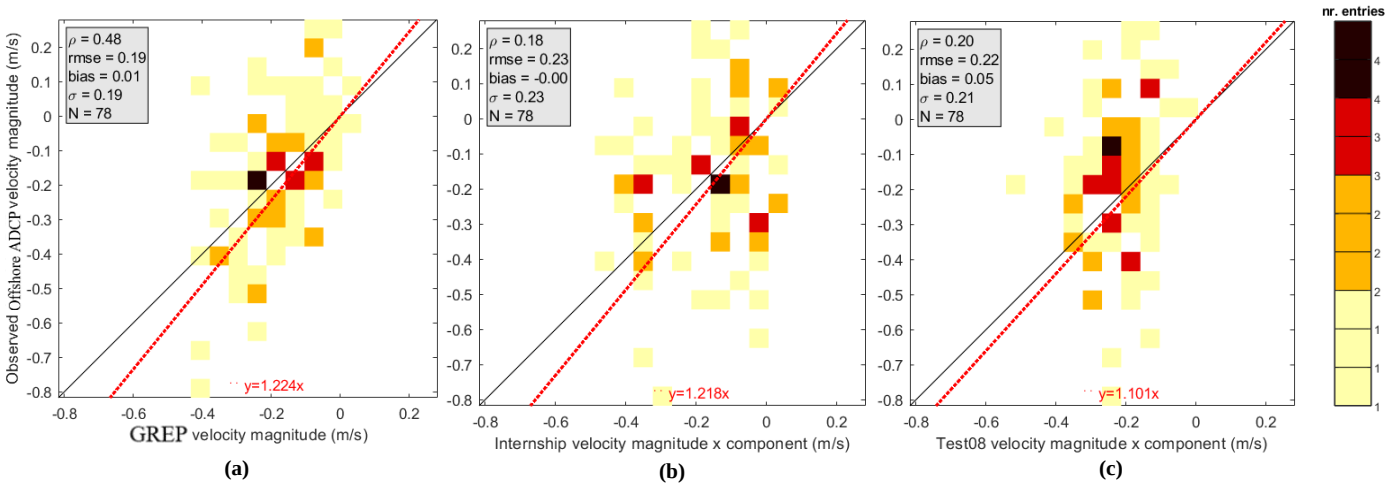

Figure 4.2.3: Error Analysis on Offshore ADCP Daily Data between April and July 2010 for x-velocity component: (a) GREP Error Analysis, (b) Internship Model Error Analysis and (c) Test08 Error Analysis

Figure 4.2.3 shows a comparative error analysis for the GREP data, Internship model and Test08 for the x-velocity component. Their correlation coefficients are 0.48, 0.18 and 0.20 respectively. Both the Internship and Test08 models correlate less to the Offshore ADCP as compared to the GREP data. All three have similar RMSE and Bias values. The GREP data has the lowest standard deviation, but it does not differ much from the D-Flow Models.

Although it is difficult to assume which model performs better with such coarse model outputs, from the correlation co-efficient for the x-velocity component, the GREP performs the best with the Offshore ADCP for this instance (could be due to the reanalysis and assimilation of observed data), but the coarse model still cannot resolve coastal scale features.

Y-Velocity Component

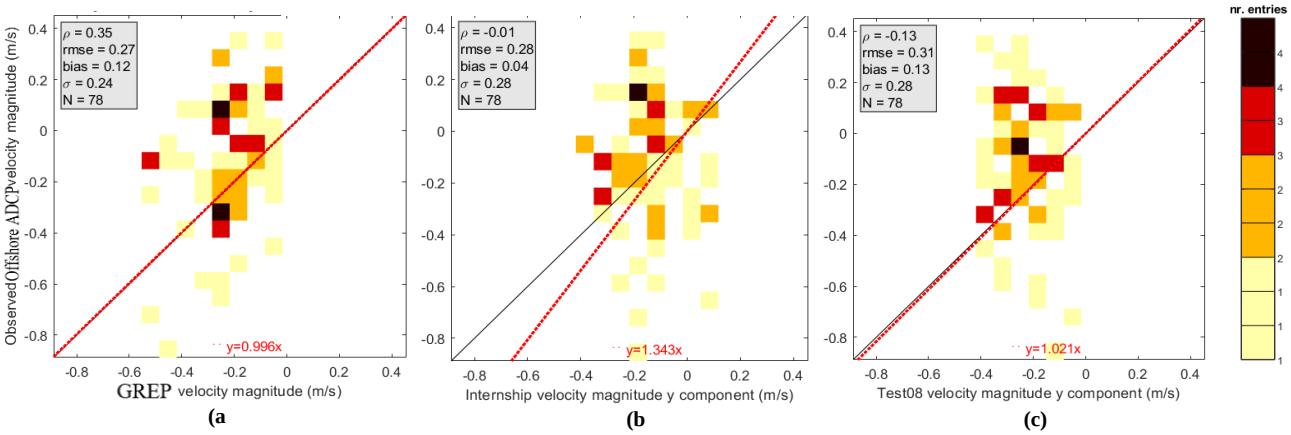

Figure 4.2.4: Error Analysis on Offshore ADCP Daily Data between April and July 2010 for y-velocity component: (a) GREP Error Analysis, (b) Internship Model Error Analysis and (c) Test08 Error Analysis

Figure 4.2.4 similarly shows that both D-Flow FM models have lower correlation coefficients than the GREP data for the y-velocity component, which implies that GREP performs better than the D-Flow FM models. RMSE are similar for all three, with the Bias of the Internship model being the lowest of the three. However, the standard deviation is lowest for the GREP data, but not by much as compared to Test08 and Internship models.

Hourly Outputs:

To analyse and compare the difference between how well the Internship and Test08 performed based on the Offshore ADCP measurements, hourly error statistics was calculated for both x and y velocity components.

X-Velocity Component

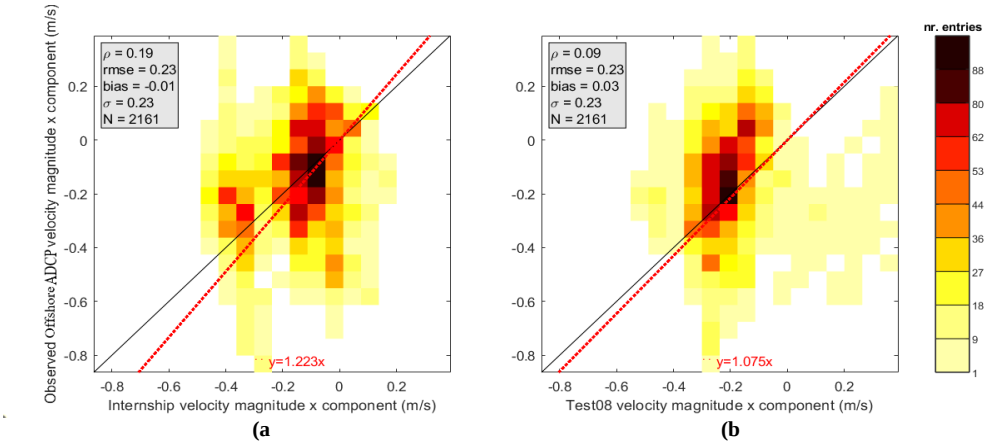

Figure 4.2.5: Error Analysis on Offshore ADCP Hourly Data between April and July 2010 for x-velocity component: (a) Internship Model Error Analysis and (b) Test08 Error Analysis

The standard deviation and RMSE are exactly the same for both the Internship and Test08 models for the x-velocity component. The Internship model has a lower Bias than the Test08 model (closer to zero) but Test08's correlation coefficient is significantly lower than the Internship model. This suggests that the Internship model performs better that the Test08 model when compared statistically with the Offshore ADCP for the x-velocity component.

Y-Velocity Component

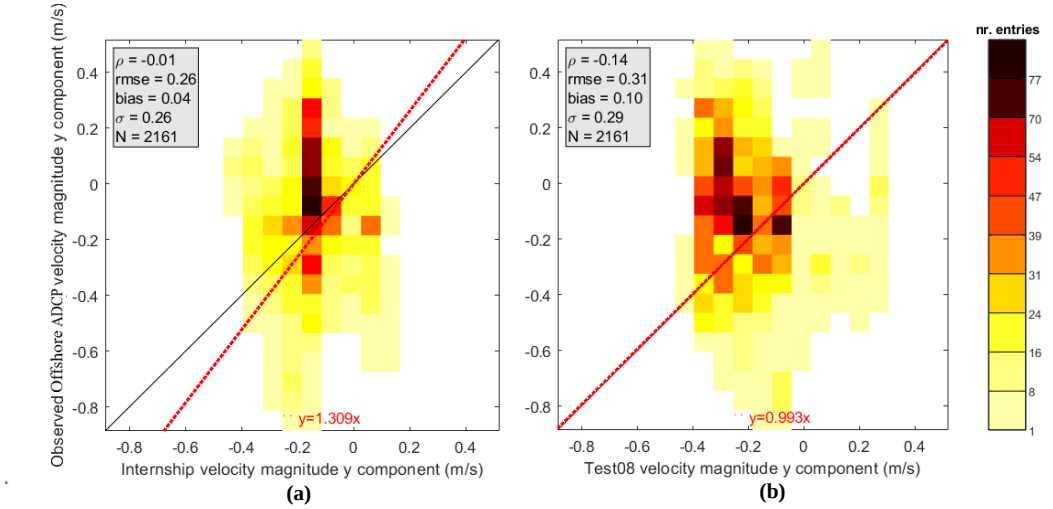

Figure 4.2.6: Error Analysis on Offshore ADCP Hourly Data between April and July 2010 for y-velocity component: (a) Internship Model Error Analysis and (b) Test08 Error Analysis

Figure 4.2.6 shows a negative or inverse correlation co-efficient for the Internship and Test08 models. Correlation coefficient, RMSE, Bias and the standard deviation are all lower for the Internship model for the y-velocity component.

However, the hourly output statistic results when compared to the daily GREP results show less correlation and error figures for the D-Flow FM models. GREP has correlation coefficients of 0.48 and 0.35 for the x- and y-velocity components respectively, whereas the Internship hourly results for ρ are 0.19 and -0.01 respectively. Test08 has hourly correlation results with 0.09 and -0.14 respectively.

Current Roses:

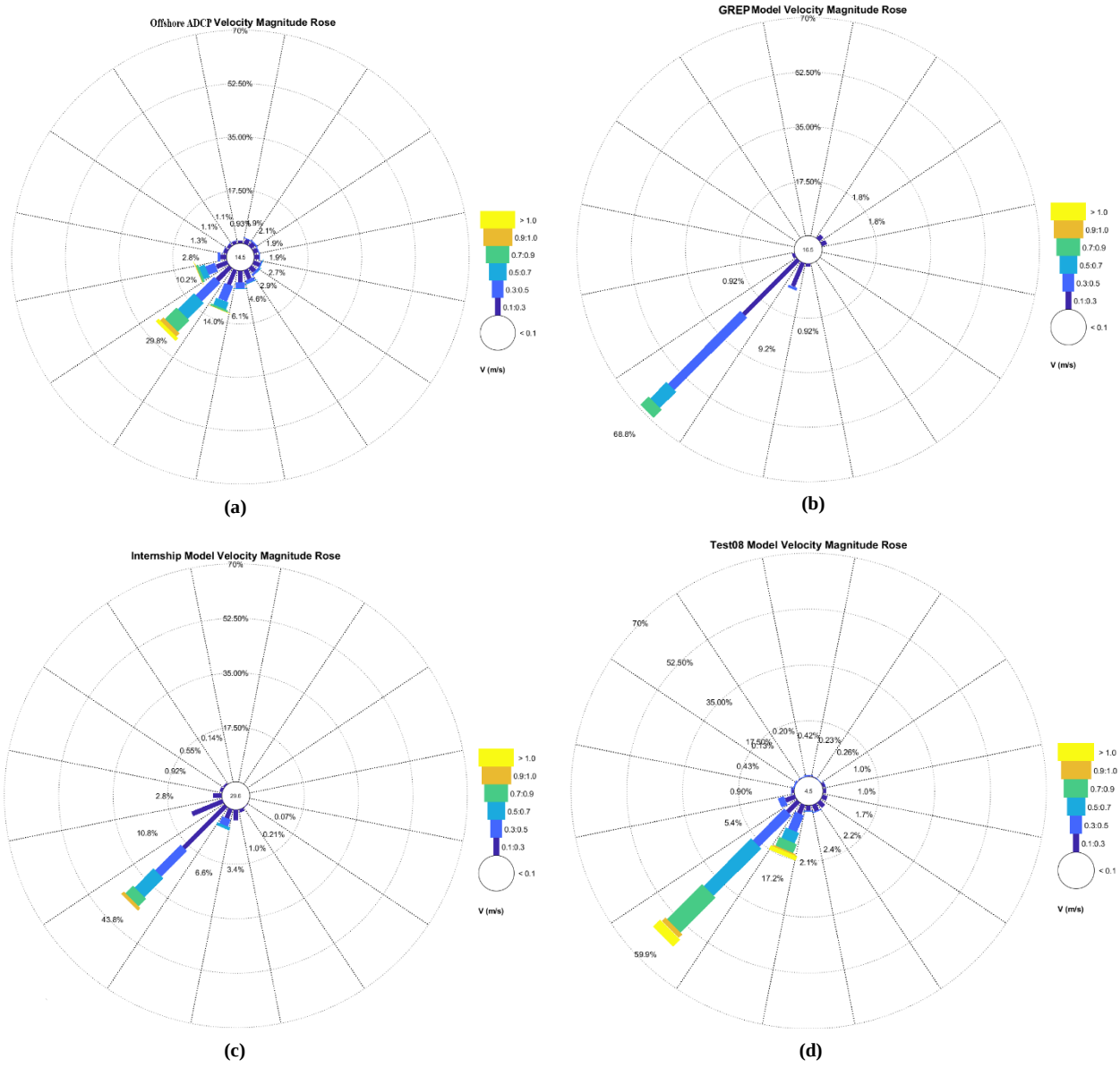

Figure 4.2.7: Current Rose showing frequency distribution of velocity magnitude and direction at depth 60m from surface: (a) Offshore ADCP Current Rose, (b) GREP Current Rose, (c) Internship Model Current Rose and (d) Test08 Current Rose

Figure 4.2.7 shows the current patterns for the period between April and July 2010. GREP, Internship and Test08 all show a similar average direction (from Southwest) to the Offshore ADCP. The Offshore ADCP results (a) are more scattered with the percentage occurrence of the currents spreading out in several directions. This could be a result of smaller scale features such as the Durban Eddy. The current roses are showing the importance of the current variability that GREP doesn't resolve.

The percentage occurrence of the southwest velocity direction bar for the Offshore ADCP is 29.8%. The next lowest percentage occurrence for this direction is 43.8% for the Internship Model (c). This suggests that the Internship model overall simulates better average velocity magnitudes and directions when compared to the Offshore ADCP for this comparison period. Test08 has a percentage occurrence of 59.9% (d) which is still better than the GREP data which has 68.8% occurrence (b). The GREP current rose is less scattered when compared to the Offshore ADCP and this could be due the coarse scale of GREP which does not allow the NEMO model to resolve the Durban Eddy.

The directionality of the currents in both Internship and Test08 models are relatively good compared to the in-situ ADCP. However, the currents are over-estimated, especially in Test08. The D-Flow FM models do not capture any northerly flow even though they are able to model the Durban Eddy. This could mean that the models might not position the eddy accurately. The Agulhas Current and the Durban Eddy could be modelled too far inshore in the D-Flow FM models.

4.2.1.3. Vertical Profiles and Velocity Maps

In Figure 4.2.8, the first thing to notice is that the Offshore ADCP is located at a rather tricky position. The slightest deviation of the main Agulhas Current can result in drastic velocity changes in both direction and magnitude. Therefore, when analysing the data, it is important to look at the map plots next to the vertical profiles so that the position of the current is identifiable. It is unrealistic to expect that any model can exactly predict phenomena such as the Durban Eddy, so to properly analyse the Offshore ADCP data, velocity magnitude maps were investigated alongside vertical profiles for available data periods.

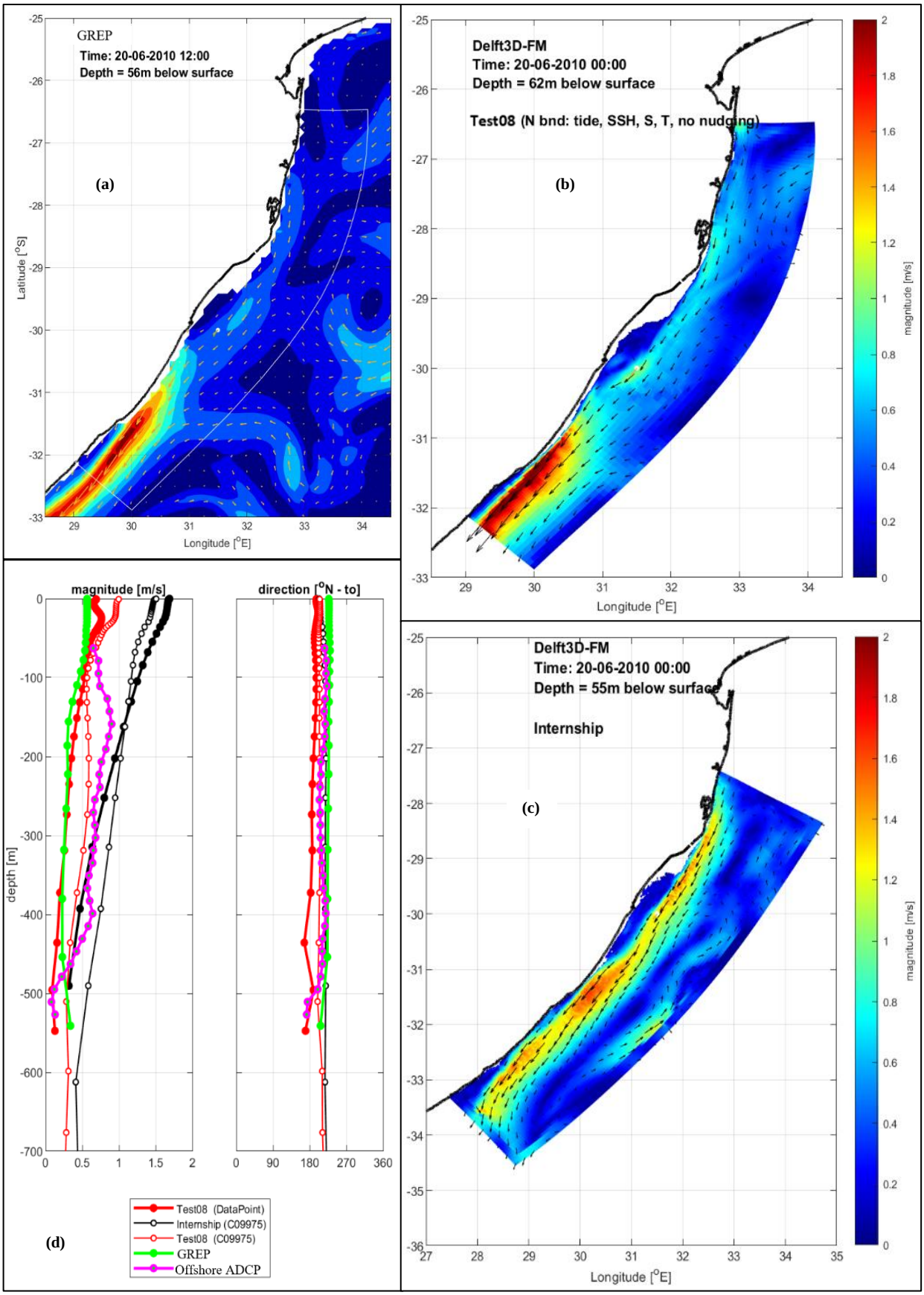

Figure 4.2.8: Offshore ADCP Data (white dot on maps) compared to GREP, Test08 and Internship Models. (a) GREP Velocity Magnitude Map, (b) Test08 Velocity Magnitude Map, (c) Internship Velocity Magnitude Map and (d) Vertical Profiles for Magnitude and Direction which include the closest 2 observation points(to the Offshore ADCP) for both the Internship and Test08 models – 20 June 2010

4.2.2. ACEP Data:

Four locations in particular (see Figure 3.5.2) were analysed from the ACEP survey over four consecutive days. The survey provided observed data recorded for these locations across several depths, but for this research, the results are shown for approximate depths of 17m, 57m and 161m below surface. Both D-Flow FM model outputs were examined (test08 and the internship models) as well as the GREP when compared to the ACEP data.

Location A:

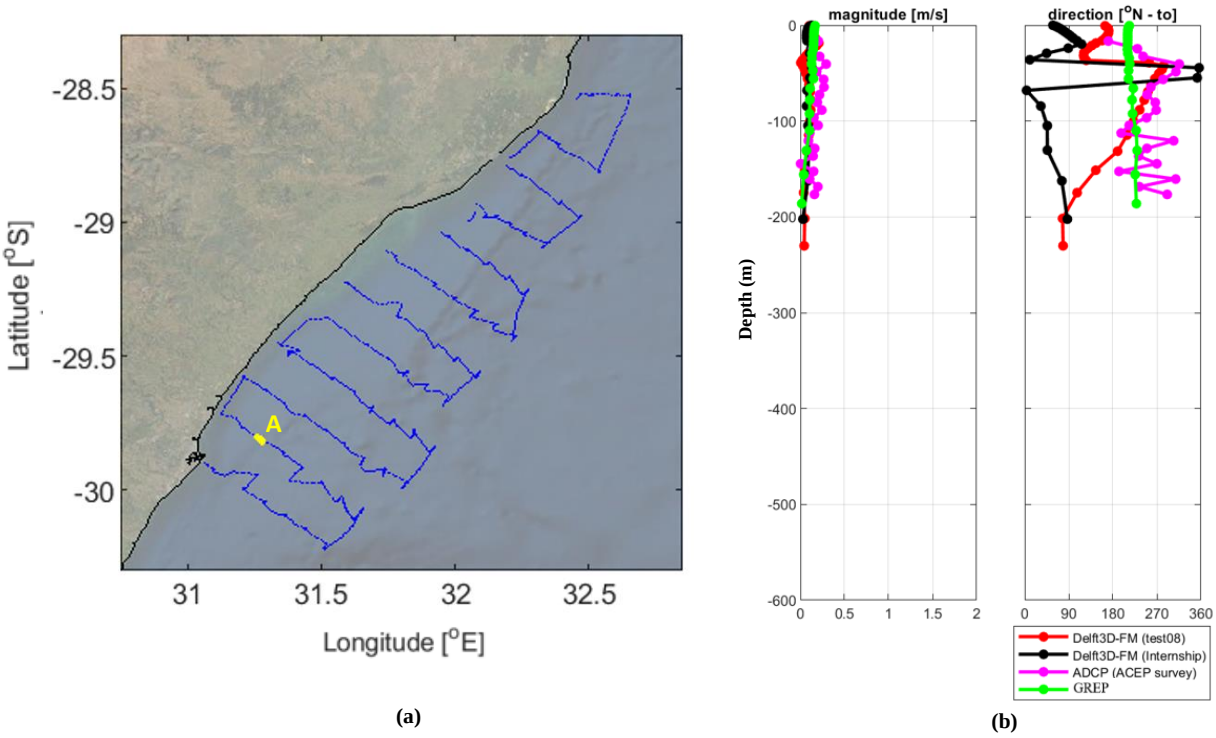

Figure 4.2.9: (a) Location A from the ACEP survey and (b) vertical average depth velocity magnitude and direction profiles of GREP, ACEP ADCP and both D-Flow FM Models, test08 and internship, for Location A on 24 July 2010

This location is closest to the Durban Bight compared to the other 3 chosen locations. Smaller currents can be expected here as this is inshore of the edge of the Agulhas Current and closer to the coast. Variations in direction can also be expected here due to the meandering nature of the main current. Current reversals and the Durban Eddy could influence this location. Looking at the vertical profiles, small currents and variable directions are noticed, which confirmed what we expected from this location. All models represent the velocity magnitude well, but the direction is best represented by test08. Test08 performs better than the Internship and GREP outputs when compared to ACEP.

(a) Depth 17m:

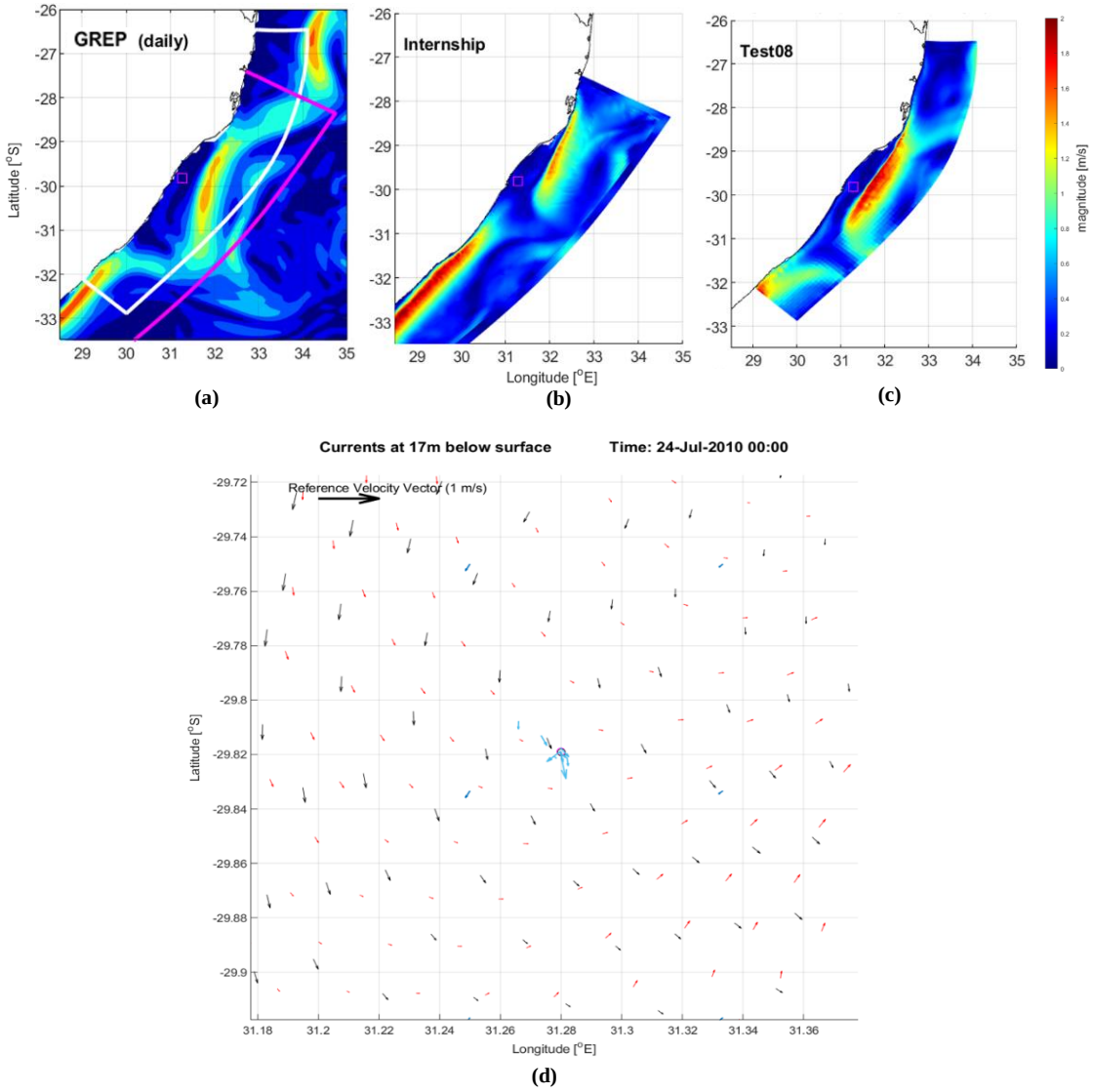

Figure 4.2.10: Velocity Map outputs for approximately 17m depths on 24 July 2010: (a) GREP Velocity Map Output with Internship (Pink) and Test08 (White) Model Domain Outlines, (b) Internship Model Velocity Map Output, (c) Test08 Model Velocity Map Output and (d) Velocity vectors indicating velocity magnitude and direction at location A: ACEP survey datapoints (light blue), GREP (dark blue), Internship (black) and Test08 (red). Size and direction of vectors correlate to velocity magnitude and direction respectively.

The shape of the current is important to note in the map outputs. GREP data and Test08 map outputs show a meandering current whereas the internship model shows the current flowing straighter and more adjacent to the coast. The bottom map shows how the ACEP velocity vectors scatter in several directions which correlates with the direction profile in Figure 4.2.9. All three models show that the main current does not flow in this location at this particular time. Low velocities (<0.25m/s) are shown in (d), with velocity direction differing for all model outputs. Vectors are scattered and vary at this location.

(b) Depth 57m:

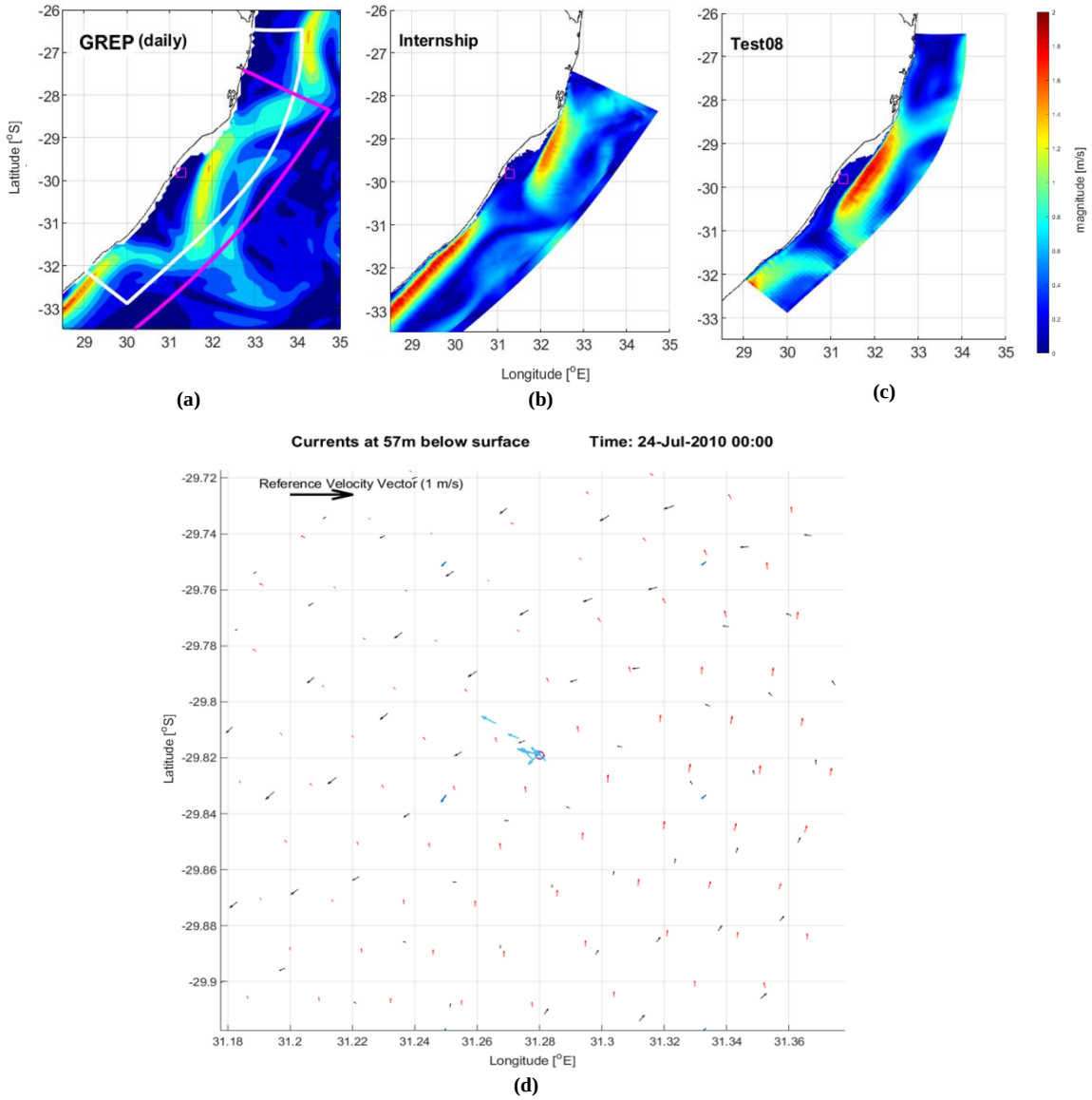

Figure 4.2.11: Velocity Map outputs for approximately 57m depths on 24 July 2010: (a) GREP Velocity Map Output with Internship (Pink) and Test08 (White) Model Domain Outlines, (b) Internship Model Velocity Map Output, (c) Test08 Model Velocity Map Output and (d) Velocity vectors indicating velocity magnitude and direction at location A: ACEP survey datapoints (light blue), GREP (dark blue), Internship (black) and Test08 (red). Size and direction of vectors correlate to velocity magnitude and direction respectively.

Similar to the depth of 17 metres, the ACEP velocity vectors divert into different directions. The direction of the velocity vectors at 57 metres contrasts the direction at 17 meters, which is also shown in the direction profile. Low velocities are still recorded at this depth, with the models showing varied directions as compared to the ACEP ADCP data. This scattered pattern can be expected with such low velocities in this region.

(c) Depth 161m:

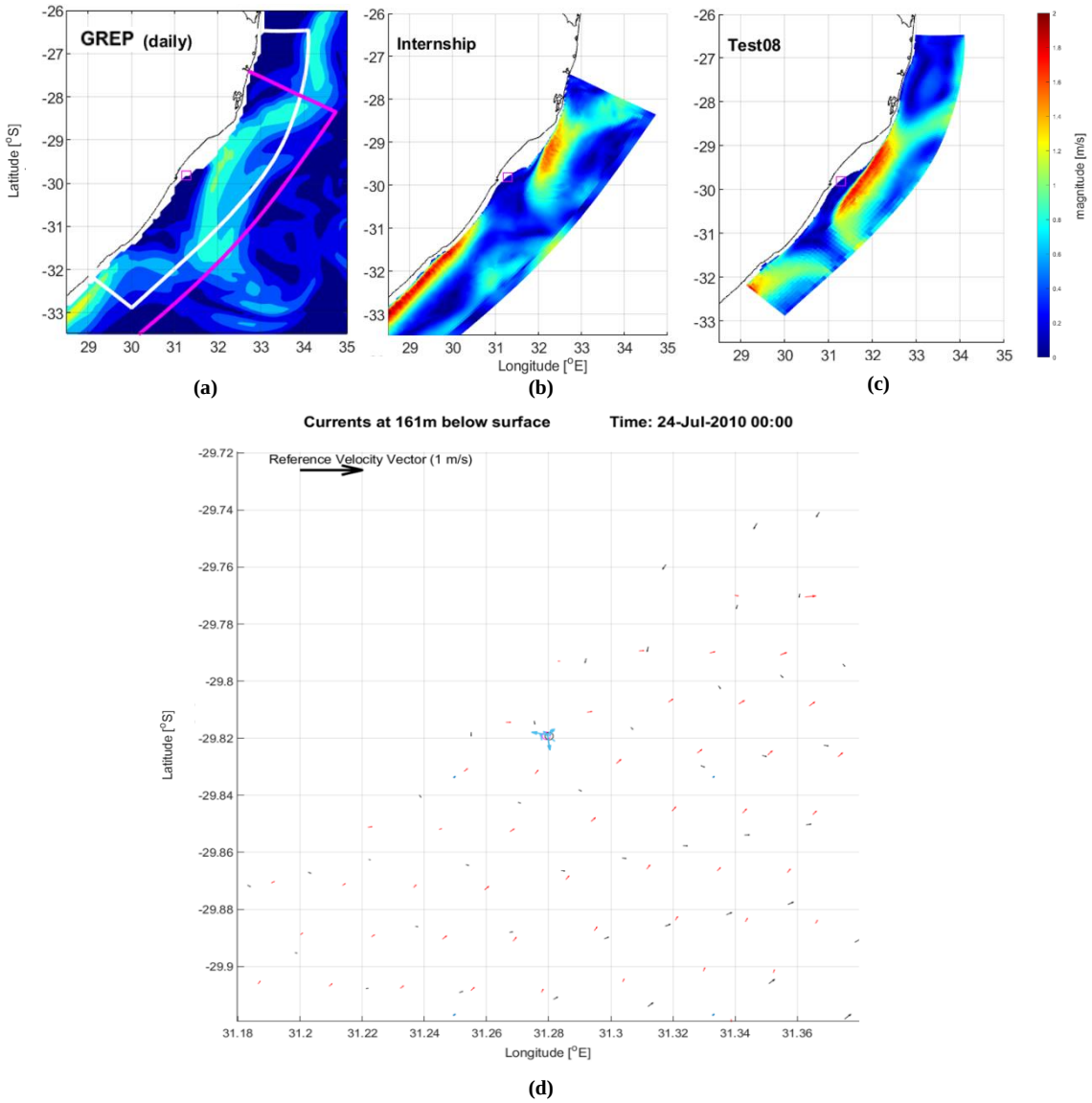

Figure 4.2.12: Velocity Map outputs for approximately 161m depths on 24 July 2010: (a) GREP Velocity Map Output with Internship (Pink) and Test08 (White) Model Domain Outlines, (b) Internship Model Velocity Map Output, (c) Test08 Model Velocity Map Output and (d) Velocity vectors indicating velocity magnitude and direction at location A: ACEP survey datapoints (light blue), GREP (dark blue), Internship (black) and Test08 (red). Size and direction of vectors correlate to velocity magnitude and direction respectively.

At a depth of 161 metres, variations in the recorded directions are still noticeable and this is confirmed in the vertical profile plot in Figure 4.2.9. The lowest velocity magnitudes are shown on these map plots, which corresponds to the decrease in magnitude shown in the vertical profile. It is important to note the white spaces between the land and the ocean which indicates that the seabed level is shallower than 161 metres in this region, therefore there is no applicable data from the models.

Location B:

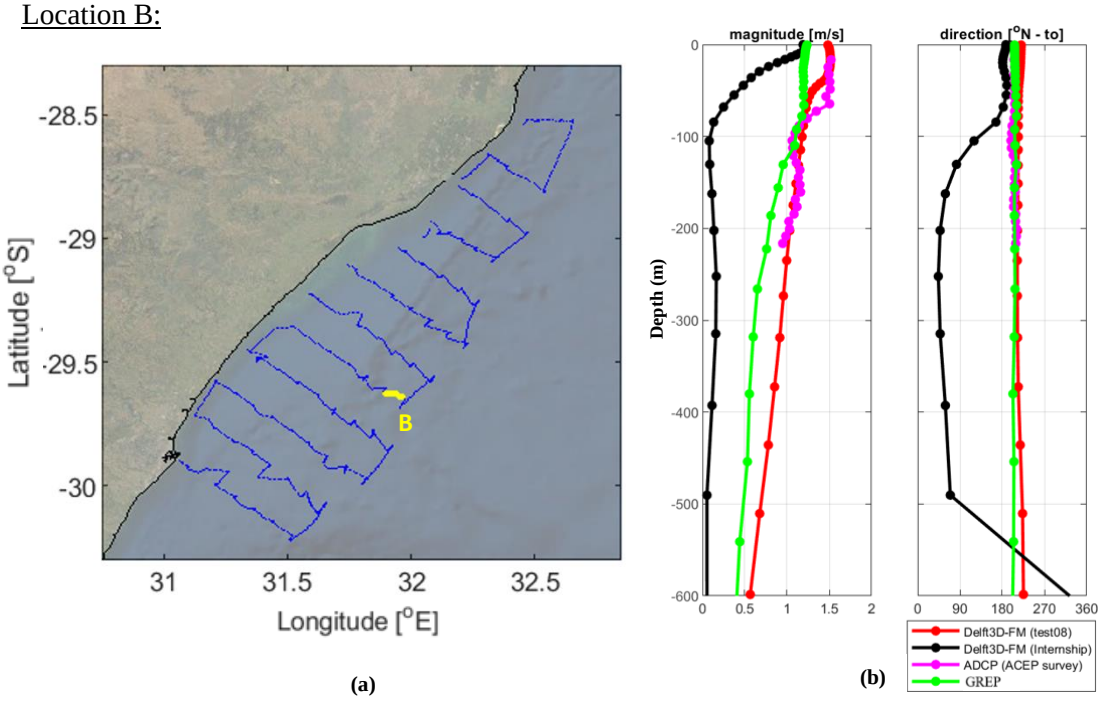

Figure 4.2.13: (a) Location B from the ACEP survey and (b) vertical average depth velocity magnitude and direction profiles of GREP, ACEP ADCP and both D-Flow FM Models, test08 and internship, for Location A on 26 July 2010

This location is positioned the furthest away from the land and is likely to show strong velocity magnitudes when the current is stable here. Location B shown in Figure 4.2.13, is situated just off the shelf and around the vicinity of the Tugela canyon. This location lies in the middle of where we can expect the Agulhas Current to flow. However, depending on the stability of the current here, variations in velocity magnitude can occur.

Much higher velocity magnitudes are shown in this location as compared to location A, which can be seen in the magnitude profile in Figure 4.2.13. Recorded velocity magnitudes of around 1.5m/s at the surface of the profile indicate that this location is situated within the centre of the Agulhas Current. A constant direction in a south-westerly direction shows a strong and stable current flow of which we can expect from literature.

From the vertical profiles in Figure 4.2.13, it is evident that the Internship model does not accurately depict the magnitude and direction of the observed velocities at this location. Test08 however, performs extremely well, almost replicating the recorded measurements exactly for both direction and magnitude. The velocity magnitude profile shows that Test08 correlates better with the ACEP survey than the GREP NEMO model.

(a) Depth 17m:

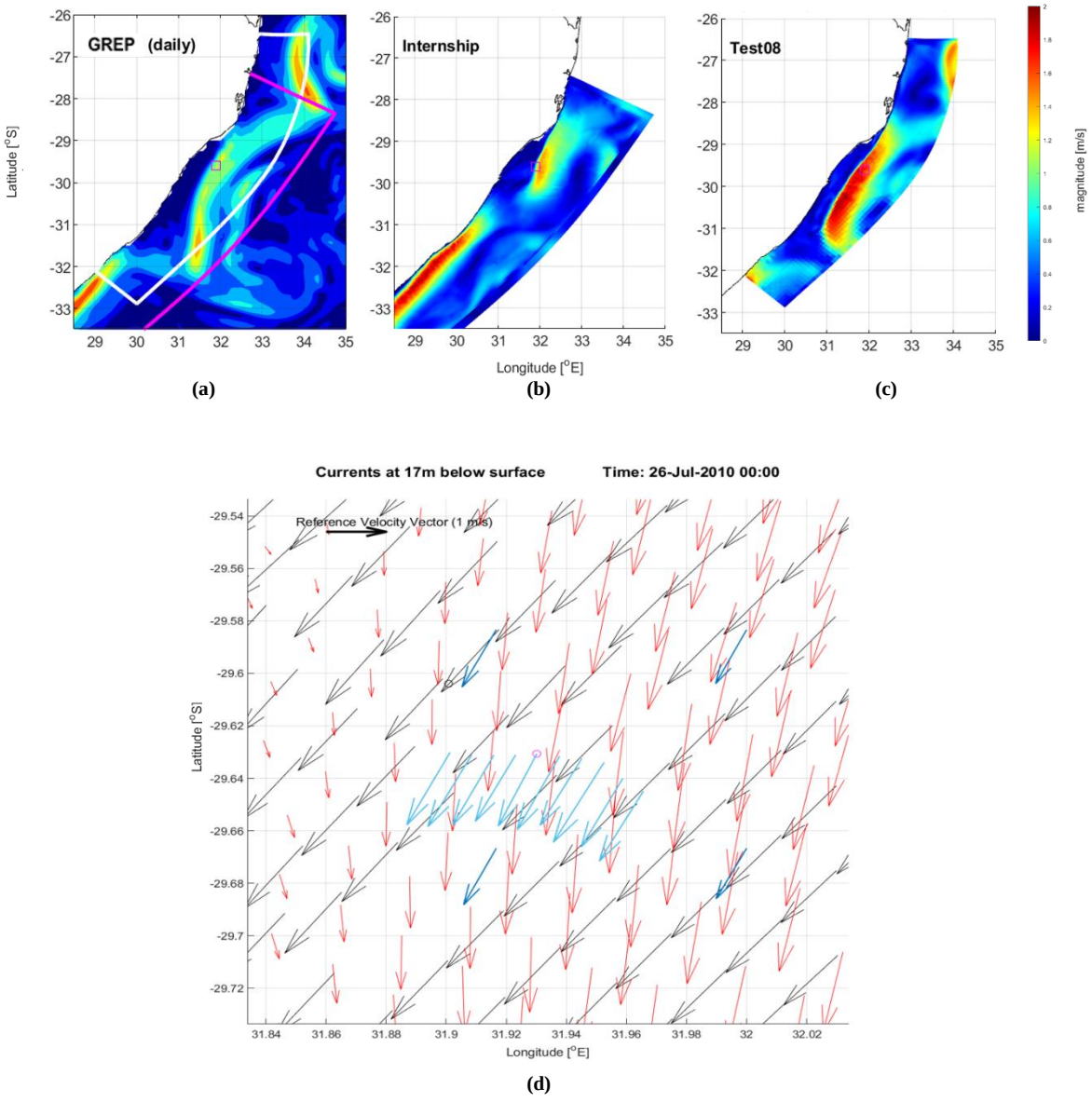

Figure 4.2.14: Velocity Map outputs for approximately 17m depths on 26 July 2010: (a) GREP Velocity Map Output with Internship (Pink) and Test08 (White) Model Domain Outlines, (b) Internship Model Velocity Map Output, (c) Test08 Model Velocity Map Output and (d) Velocity vectors indicating velocity magnitude and direction at location B: ACEP survey datapoints (light blue), GREP (dark blue), Internship (black) and Test08 (red). Size and direction of vectors correlate to velocity magnitude and direction respectively.

Figure 4.2.14 above shows that the position of the current is different in the Internship model compared to the GREP NEMO and Test08 models. This drastically influences both velocity direction and magnitudes, which is evident in the vertical profiles in Figure 4.2.13. The red velocity vectors in the bottom map are different from the light blue, black and dark blue vectors which reiterate that the internship model does not display the correct velocity directions for this location at this depth.

(b) Depth 57m:

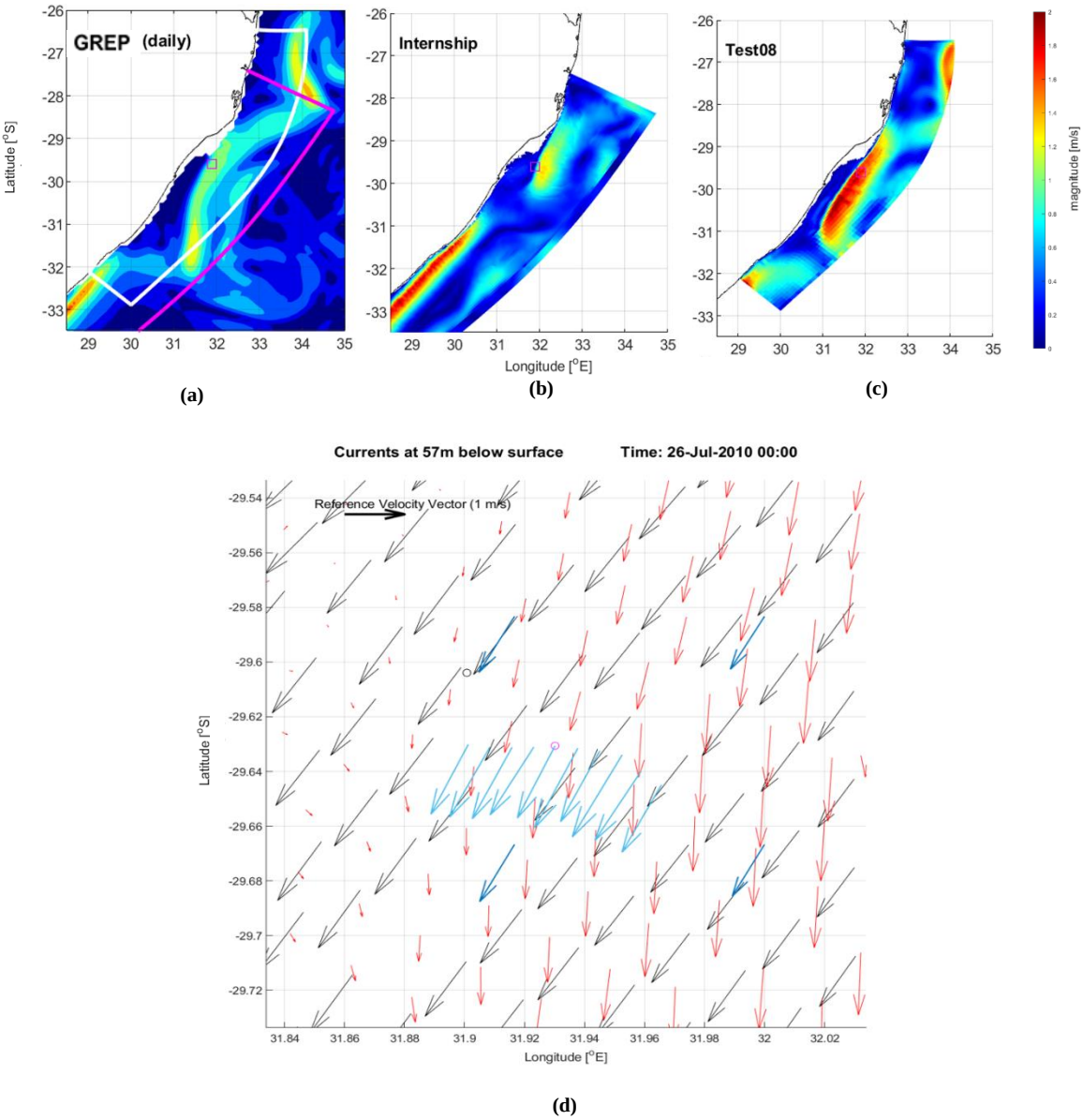

Figure 4.2.15: Velocity Map outputs for approximately 57m depths on 26 July 2010: (a) GREP Velocity Map Output with Internship (Pink) and Test08 (White) Model Domain Outlines, (b) Internship Model Velocity Map Output, (c) Test08 Model Velocity Map Output and (d) Velocity vectors indicating velocity magnitude and direction at location B: ACEP survey datapoints (light blue), GREP (dark blue), Internship (black) and Test08 (red). Size and direction of vectors correlate to velocity magnitude and direction respectively.

The Internship model indicates that this location is at the edge of the main current, as depicted in the Internship map plot (b). However, this is not the case in the GREP NEMO and Test08 models which show that this location is situated in the middle of the main current, with stronger velocities and a south-westerly flow. The ACEP survey confirms this direction (light blue vectors), which shows that in this instance the Internship model does not replicate the observed data well. GREP and Test08 vectors correspond well with the ACEP vectors.

(c) Depth 161m:

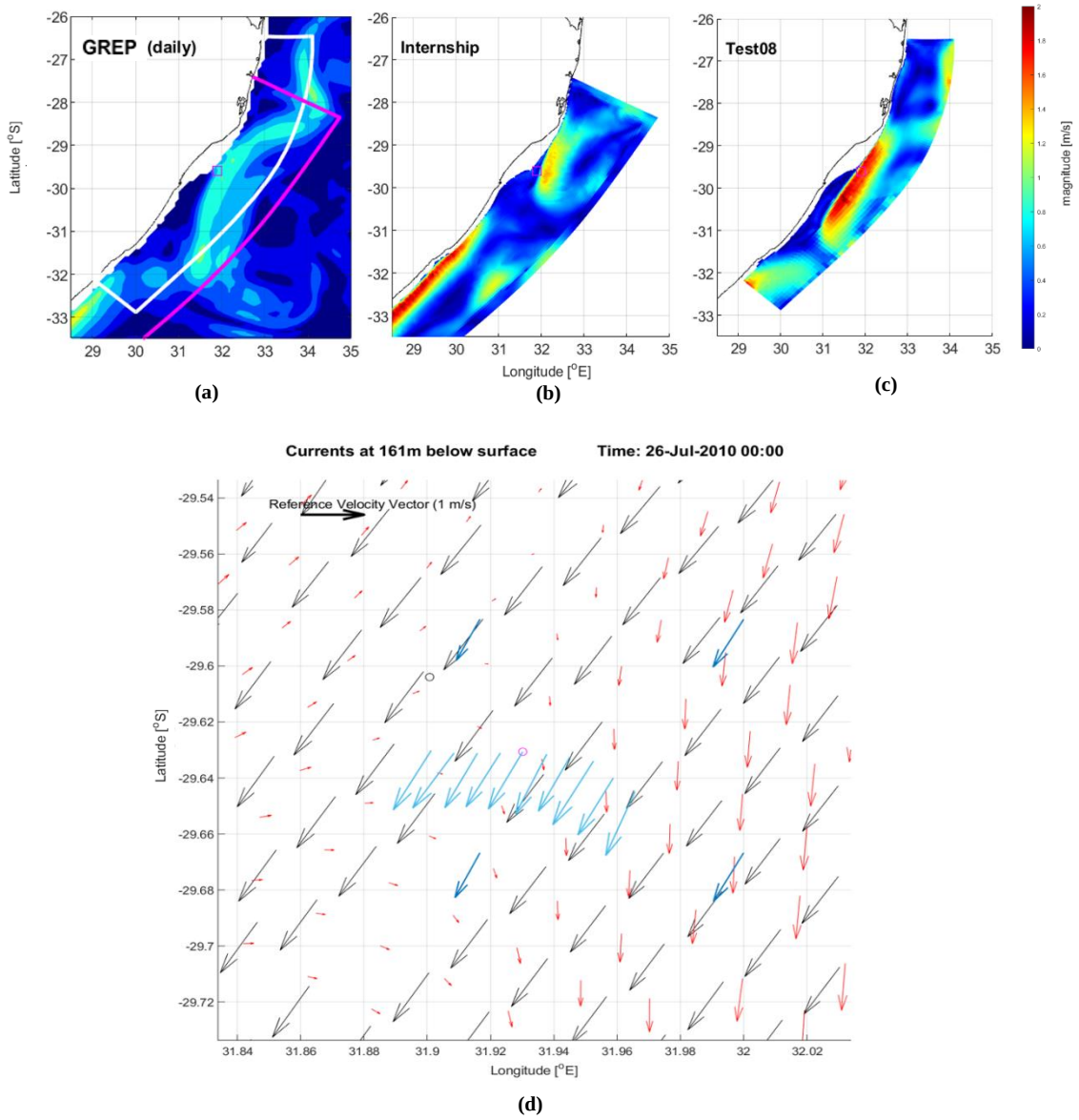

Figure 4.2.16: Velocity Map outputs for approximately 161m depths on 26 July 2010: (a) GREP Velocity Map Output with Internship (Pink) and Test08 (White) Model Domain Outlines, (b) Internship Model Velocity Map Output, (c) Test08 Model Velocity Map Output and (d) Velocity vectors indicating velocity magnitude and direction at location B: ACEP survey datapoints (light blue), GREP (dark blue), Internship (black) and Test08 (red). Size and direction of vectors correlate to velocity magnitude and direction respectively.

Similarly, for a depth of 161 meters, the internship model differs from both the GREP NEMO and Test08 models. It also does not correspond well with the ACEP survey, which is consistent with the vertical profiles for this location shown in Figure 4.2.13. The length of the ACEP vectors (light blue) which indicate current strength, is slightly longer than the GREP velocity vectors (dark blue), which indicates a higher magnitude than what GREP gives us. Test08 exhibits similar velocity strength and direction to the ACEP vectors. This is also shown in the velocity magnitude profile in Figure 4.2.13.

Location C:

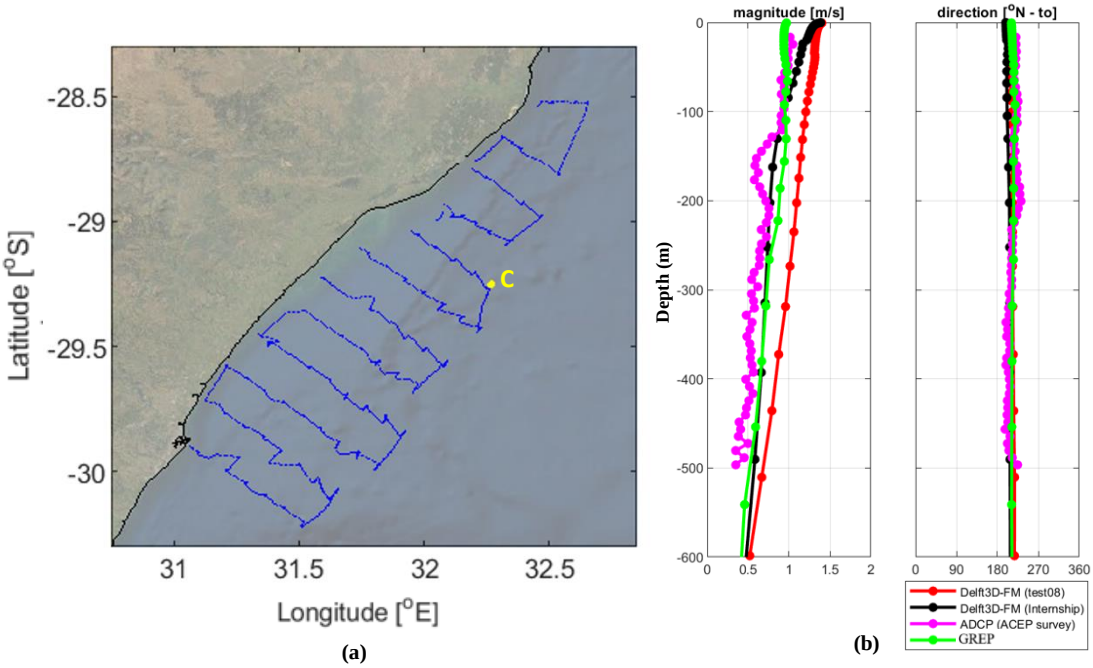

Figure 4.2.17: (a) Location C from the ACEP survey and (b) vertical average depth velocity magnitude and direction profiles of GREP, ACEP ADCP and both D-Flow FM Models, test08 and internship, for Location A on 27 July 2010

This position should also be located within the main Agulhas Current (similar to location B) and should show results of constant velocity magnitudes and direction. Location C is just north of where the current begins to meander so there should not be any drastic changes in both velocity magnitude and direction.

As can be seen from the vertical profiles shown in Figure 4.2.17, the Internship model resembles the ACEP recorded magnitudes closer to that of Test08. This is in contradiction to location B. At certain depths, the Internship model performs better than even the GREP NEMO model. The velocity magnitudes recorded at this location for this particular time are lower than those recorded at location B, which suggests that the Agulhas Current is not as strong or stable on this day. Recorded current strength only reaches 1m/s at the surface.

(a) Depth 17m:

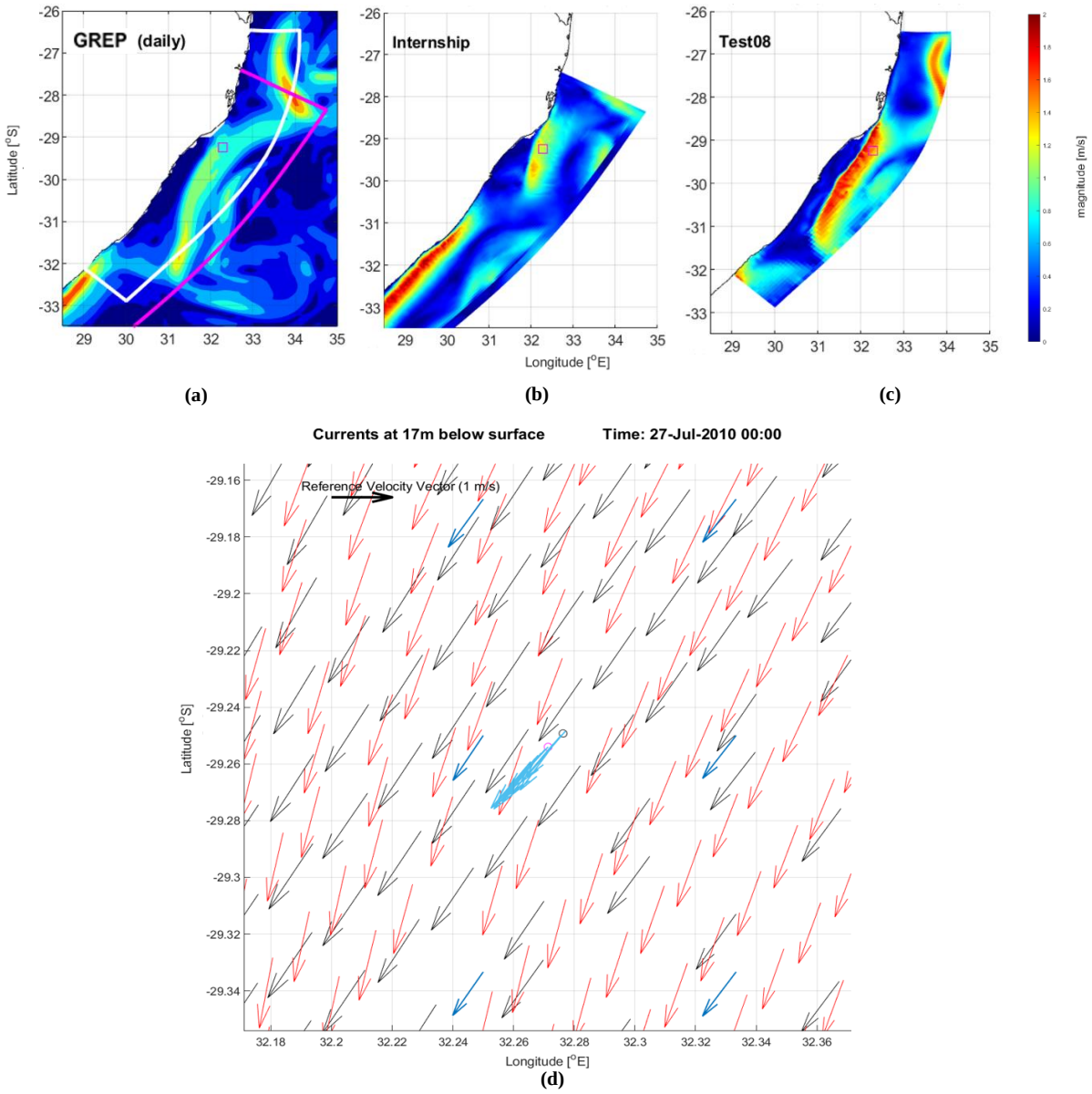

Figure 4.2.18: Velocity Map outputs for approximately 17m depths on 27 July 2010: (a) GREP Velocity Map Output with Internship (Pink) and Test08 (White) Model Domain Outlines, (b) Internship Model Velocity Map Output, (c) Test08 Model Velocity Map Output and (d) Velocity vectors indicating velocity magnitude and direction at location C: ACEP survey datapoints (light blue), GREP (dark blue), Internship (black) and Test08 (red). Size and direction of vectors correlate to velocity magnitude and direction respectively.

All three models show similar velocity direction, as can be seen by the velocity vectors in the bottom plot (d) in Figure 4.2.18. The GREP and Internship map plots show a meandering or unstable current whereas Test08 shows a strong, stable Agulhas Current. This difference in the nature of the current at this particular location and time explains the variance of velocity magnitudes as seen in Figure 4.2.17. At this location, a strong Agulhas Current is expected, which is evident from the plots in Figure 4.2.18.

(b) Depth 57m:

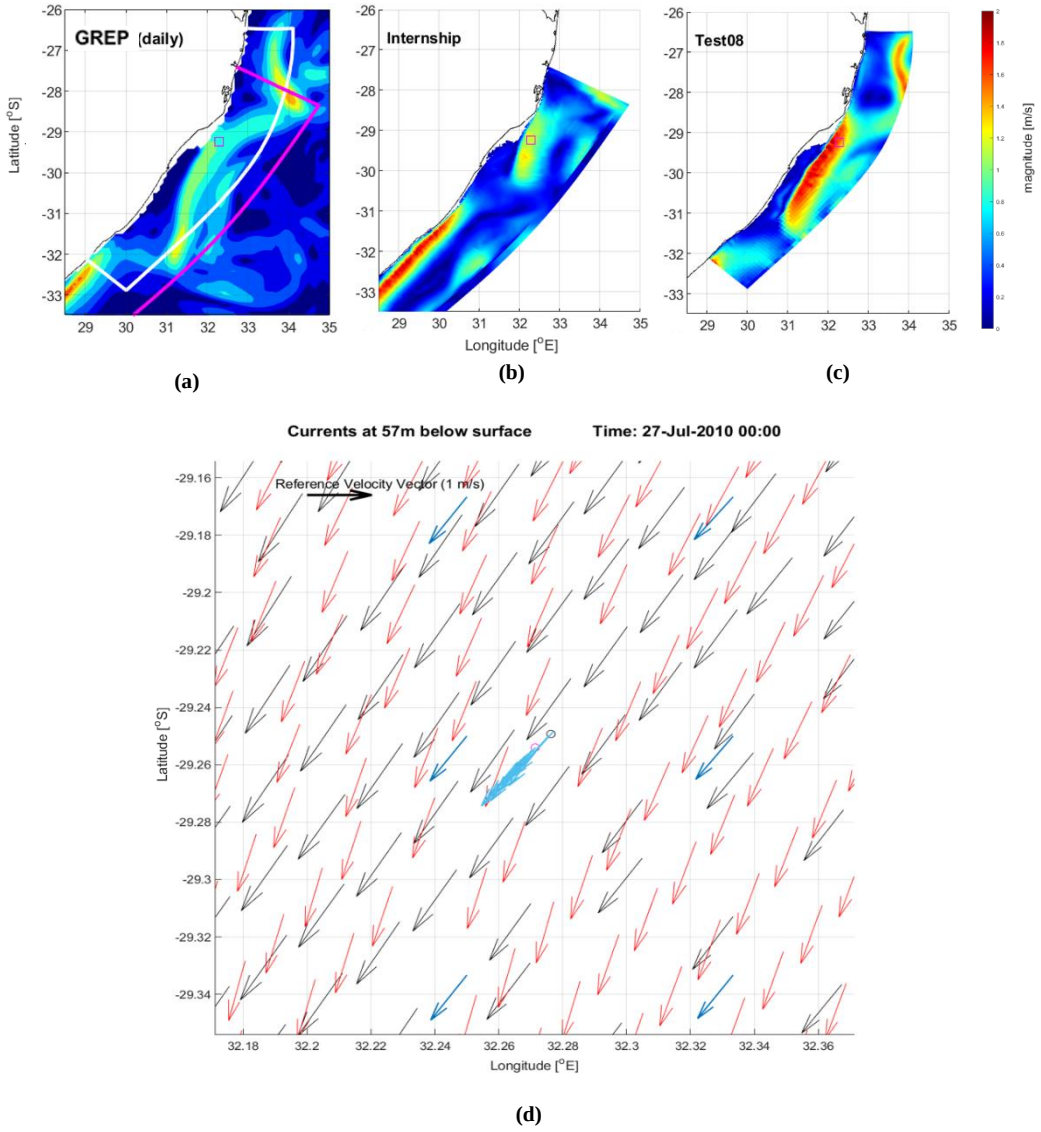

Figure 4.2.19: Velocity Map outputs for approximately 57m depths on 27 July 2010: (a) GREP Velocity Map Output with Internship (Pink) and Test08 (White) Model Domain Outlines, (b) Internship Model Velocity Map Output, (c) Test08 Model Velocity Map Output and (d) Velocity vectors indicating velocity magnitude and direction at location C: ACEP survey datapoints (light blue), GREP (dark blue), Internship (black) and Test08 (red). Size and direction of vectors correlate to velocity magnitude and direction respectively.

Similar to the outputs at 17 metres depths for location C, GREP NEMO and the Internship models show a meandering or unstable current. Test08 shows higher current magnitudes than the other two models, which corresponds with the velocity magnitude profile in Figure 4.2.17. The Internship model outputs velocity magnitudes of 1m/s at a depth of 57 meters for location C, which is slightly higher than that of the ACEP survey. However, the Internship model corresponds the closest to the ACEP survey as compared to the other models.

(c) Depth 161m:

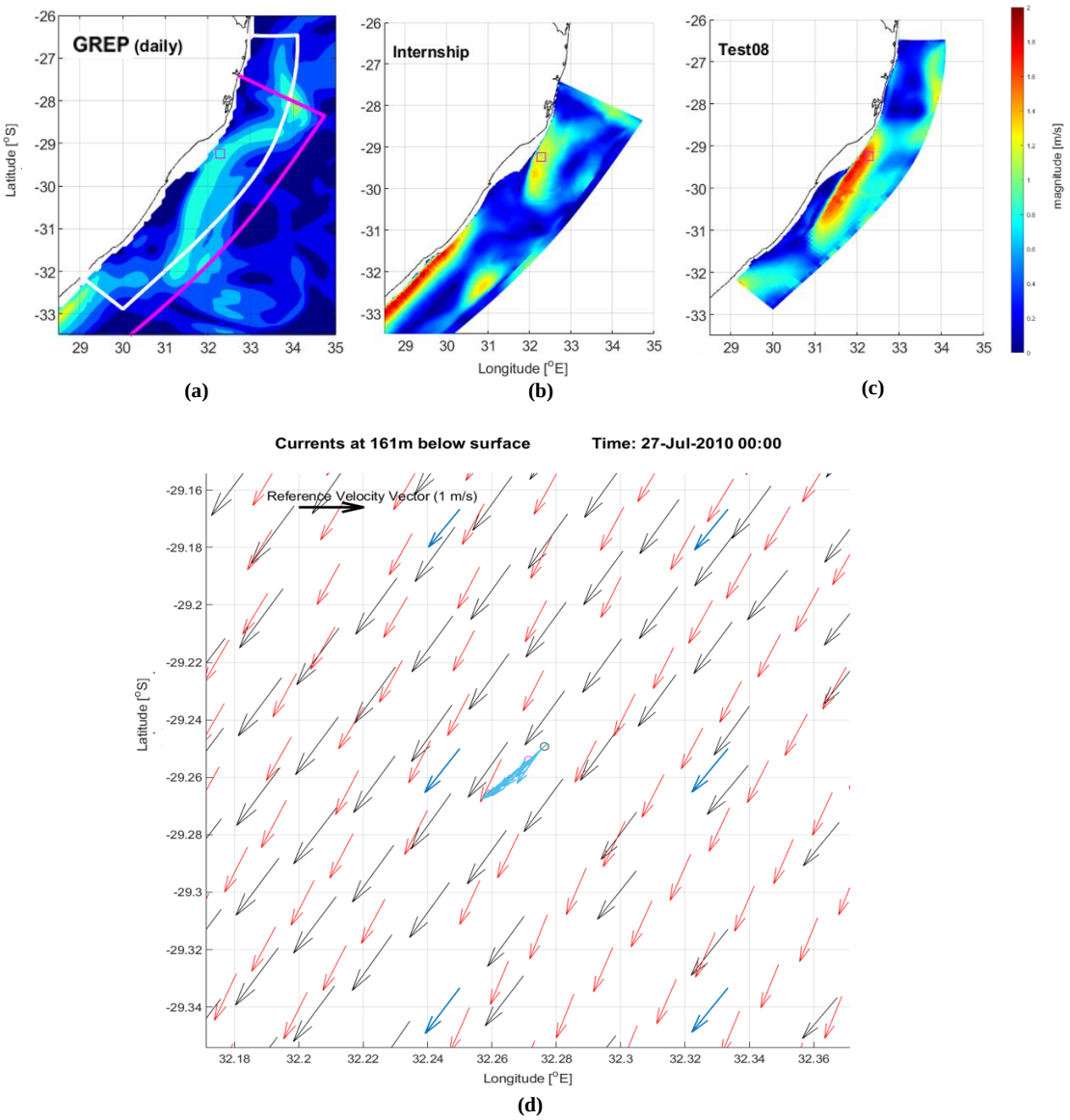

Figure 4.2.20: Velocity Map outputs for approximately 161m depths on 27 July 2010: (a) GREP Velocity Map Output with Internship (Pink) and Test08 (White) Model Domain Outlines, (b) Internship Model Velocity Map Output, (c) Test08 Model Velocity Map Output and (d) Velocity vectors indicating velocity magnitude and direction at location C: ACEP survey datapoints (light blue), GREP (dark blue), Internship (black) and Test08 (red). Size and direction of vectors correlate to velocity magnitude and direction respectively.

At a depth of 161 metres, the velocity magnitude should be lower than that of the surface. The GREP and Internship map plots indicate this, however Test8 still suggests strong velocities for this location and depth. The bottom plot shows an overall velocity of 0.8m/s, which suggests the Agulhas Current still flows at a depth of 161 metres, but not as strong as its surface flow. This is also confirmed from the velocity magnitude profile in Figure 4.2.17. All three models and the ACEP survey show similar directions, like the 17 and 57 metre outputs.

Location D:

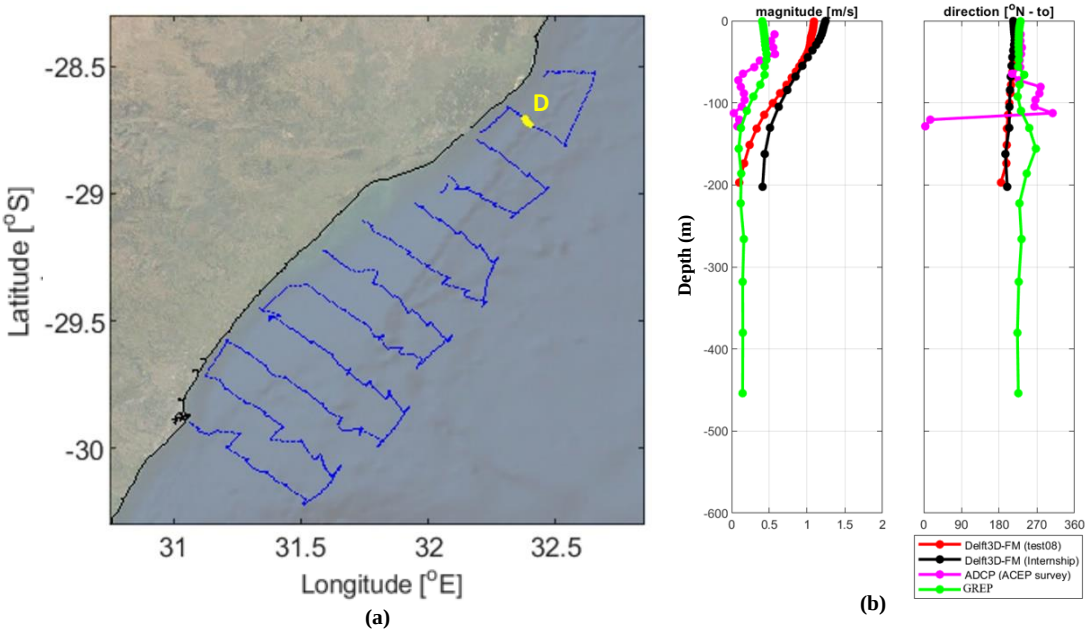

Figure 4.2.21: (a) Location D from the ACEP survey and (b) vertical average depth velocity magnitude and direction profiles of GREP, ACEP ADCP and both D-Flow FM Models, test08 and internship, for Location A on 28 July 2010

Location D should exhibit the strongest velocities as compared to the three previous locations. The main current is stable here and velocities should be consistent within this region. This location is closest to the land and is situated on the shelf edge.

However, analysing the velocity profiles, the recorded current magnitudes are small in this location for this time. Both D-Flow FM models produce results that we would expect from this location (from literature) but GREP and the ACEP velocities are much lower here. The direction profile also suggests a drastic change in direction at a depth of 120 metres, but GREP does not show this. This could be an error in the recorded data or a possible instability of the current. If the current meanders at this location and Location D is situated at the edge of the current, then the change in direction could also reflect a return current. The GREP NEMO model corresponds the closest to the observed data from the ACEP survey at this location.

(a) Depth 17m:

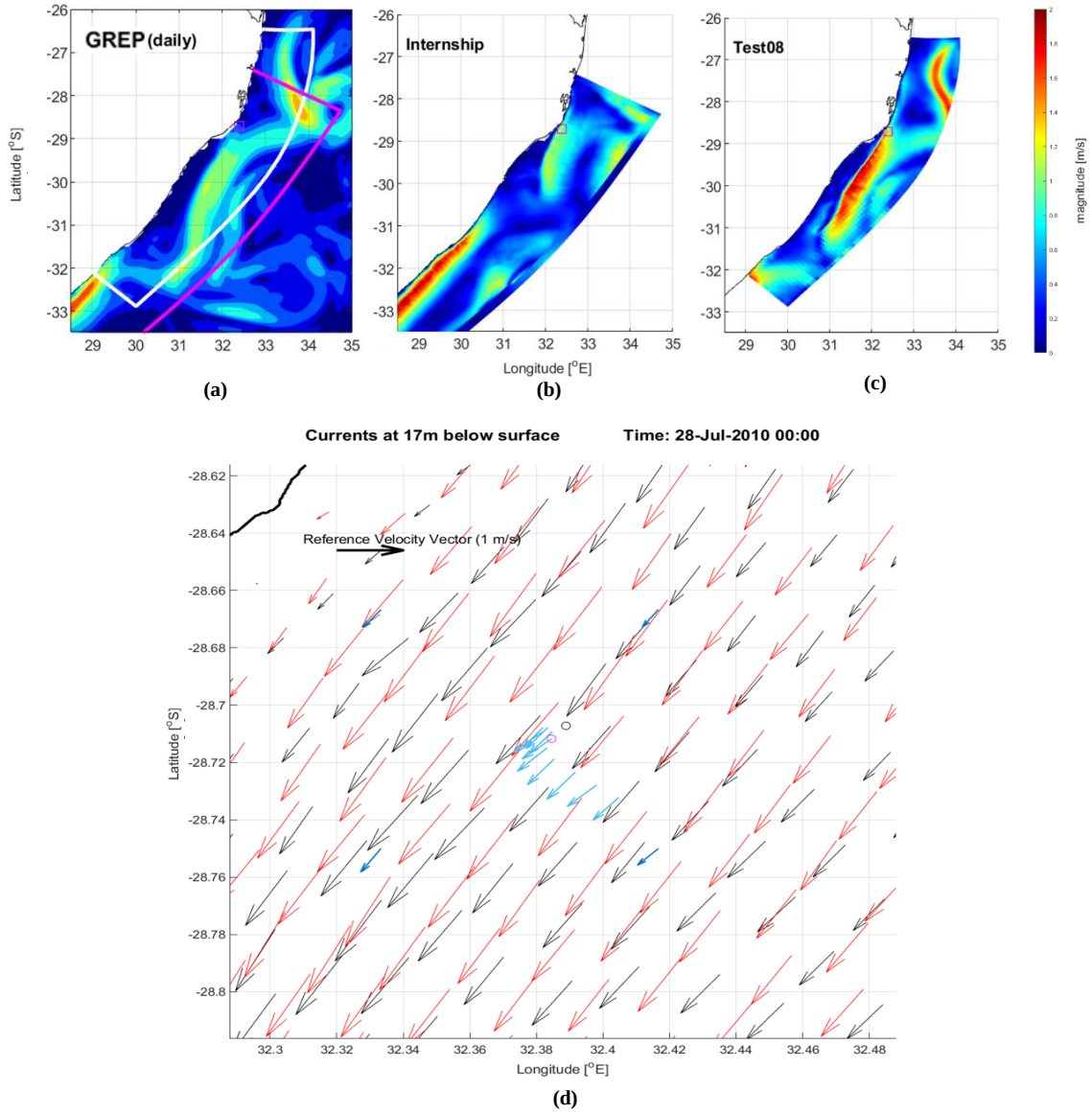

Figure 4.2.22: Velocity Map outputs for approximately 17m depths on 28 July 2010: (a) GREP Velocity Map Output with Internship (Pink) and Test08 (White) Model Domain Outlines, (b) Internship Model Velocity Map Output, (c) Test08 Model Velocity Map Output and (d) Velocity vectors indicating velocity magnitude and direction at location D: ACEP survey datapoints (light blue), GREP (dark blue), Internship (black) and Test08 (red). Size and direction of vectors correlate to velocity magnitude and direction respectively.

The models show quite different map outputs shown in Figure 4.2.22. Although the same meandering pattern is shown in both Test08 and GREP, at location D the current is much stronger in Test08 than that of GREP. The bottom plot (d) shows that the Internship model has a magnitude of 1.2m/s at the surface, which is much stronger than what the ACEP survey suggests. Although at this depth of 17 metres, the directions of the models and the survey seem to be the same, but there is a big difference in the magnitude of the velocities as the D-Flow FM models both exhibit currents almost double than that of the ACEP survey. Location D could just be inshore of the main current at this time which would explain the low recorded velocities.

(b) Depth 57m:

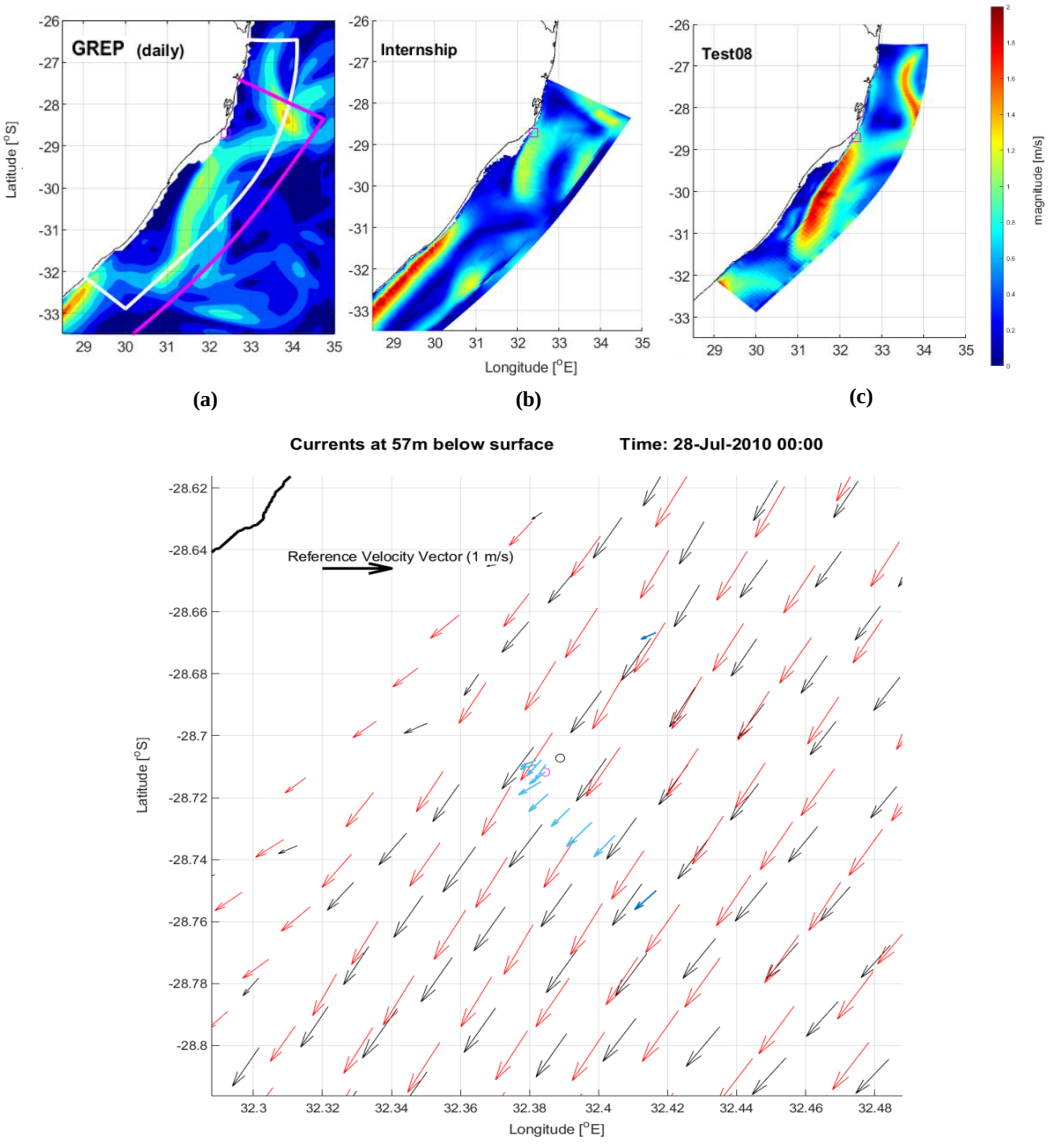

Figure 4.2.23: Velocity Map outputs for approximately 57m depths on 28 July 2010: (a) GREP Velocity Map Output with Internship (Pink) and Test08 (White) Model Domain Outlines, (b) Internship Model Velocity Map Output, (c) Test08 Model Velocity Map Output and (d) Velocity vectors indicating velocity magnitude and direction at location D: ACEP survey datapoints (light blue), GREP (dark blue), Internship (black) and Test08 (red). Size and direction of vectors correlate to velocity magnitude and direction respectively.

Similar to the 17 metre depth outputs, Test08 and the Internship models show much higher velocities than that of GREP and the ACEP survey. The bottom plot (d) shows a velocity magnitude of 1m/s for the Internship model whereas the ACEP data only reaches up to 0.6m/s as shown in the velocity magnitude profile in Figure 4.2.17. The ACEP velocity vectors are much smaller here than the vectors from both D-Flow FM models, which also suggests much lower velocities. The directions at this location, however, are rather similar for all outputs. Both models exaggerate the current magnitude in this location for this time. This could be due to the stability or positioning of the main current. GREP replicated the magnitude well at this location.

(c) Depth 161m:

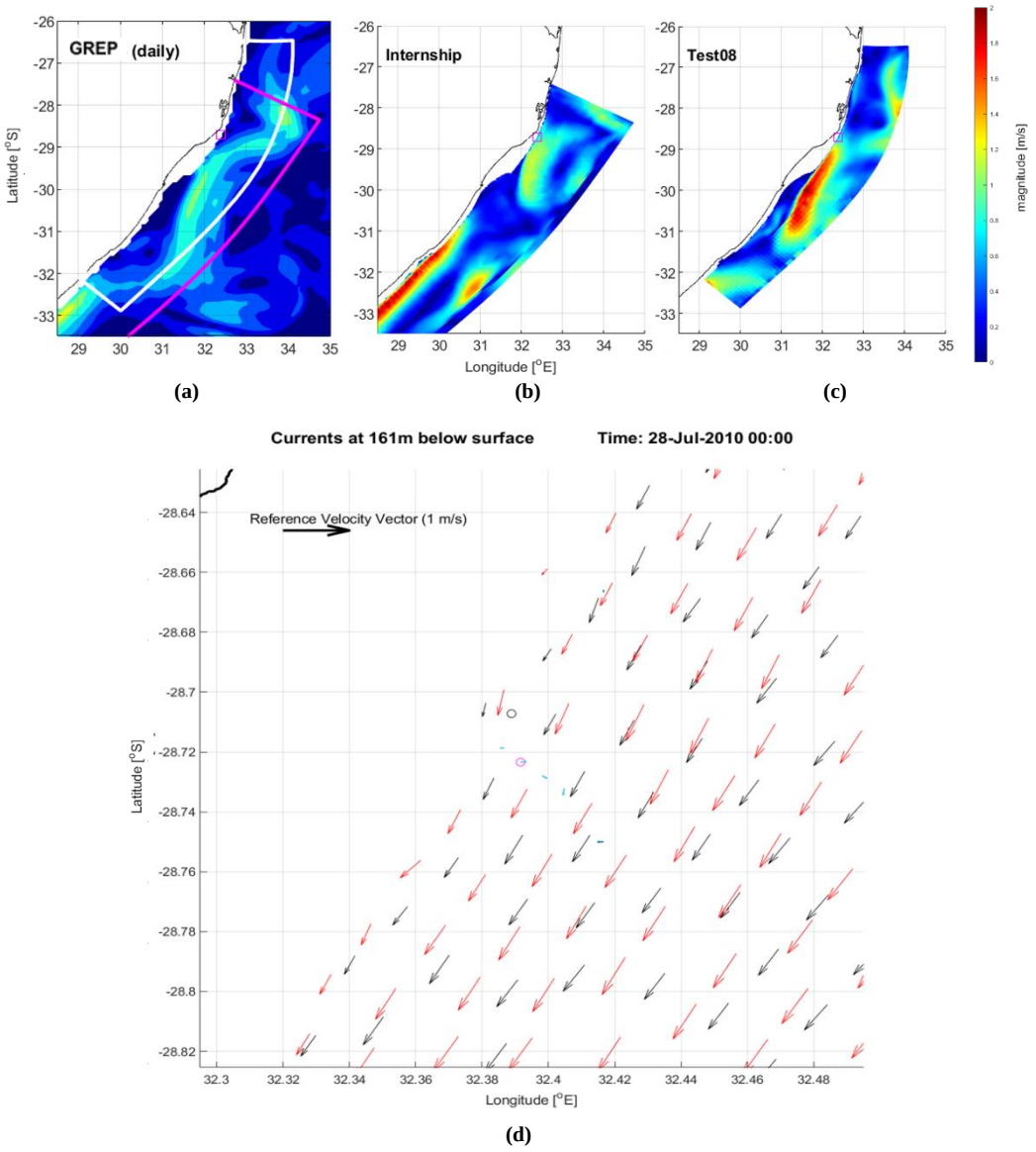

Figure 4.2.24: Velocity Map outputs for approximately 161m depths on 28 July 2010: (a) GREP Velocity Map Output with Internship (Pink) and Test08 (White) Model Domain Outlines, (b) Internship Model Velocity Map Output, (c) Test08 Model Velocity Map Output and (d) Internship Model Velocity Map Output with velocity vectors indicating velocity magnitude and direction at location D: ACEP survey datapoints (blue), GREP (green), Internship (black) and Test08 (red). Size and direction of vectors correlate to velocity magnitude and direction respectively and map background is based on Internship model velocity magnitudes.

Although lower velocities are shown in the bottom plot for a depth of 161 metres as compared to the 57 and 17 metre plots, 0.7m/s is still quite high compared to the ACEP survey recording of 0m/s at a depth of 120 metres. There is no available data from the ACEP survey for this depth but judging from the velocity profile the models still overestimate the magnitudes at this depth. Similarly, the modelled positioning and stability of the current could be inaccurate for both models at this location and time.

4.3. Operational Engineering Applications

The latest version of the D-Flow FM model (Test08) is already being used in several initiatives for the eThekwini Municipality. Validation and improvements to the model are constantly being updated and analysed. Ongoing and Future Engineering Applications of the model include the following:

4.3.1. Forecast Early Warning System (FEWS)

The D-Flow FM model developed in this study is running operationally in FEWS. It is possible to compare the CMEMS GREP and the D-Flow FM model in real-time for Water Level, Temperature, Salinity and Velocity. For example, Figure 4.3.1 shows both GREP and D-Flow FM model outputs for the 6th of September 2021. The D-Flow FM model clearly shows a higher resolution towards the coast than the GREP NEMO model, with noticeable spin-off currents along the shelf. GREP does not show these spin-off currents, which promotes the need for a coastal model. These spin-off features can drastically affect velocity magnitudes and direction within the continental shelf, which in turn can change results in other corresponding features such as water quality parameters and particle tracking.

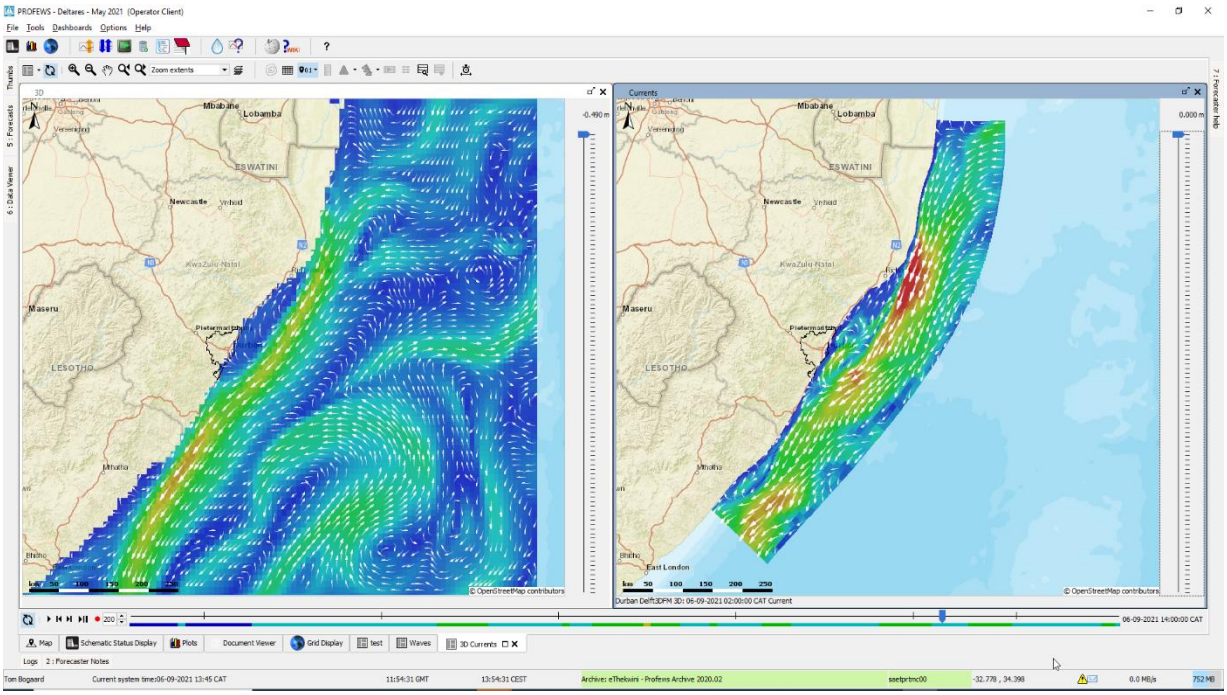

Figure 4.3.1: Screenshot taken from eThekwini Municipalities FEWS, showing CMEMS model (left) and D-Flow FM Flexible Mesh model (right). Deltares (2019b).

In addition to real-time comparisons, the D-Flow FM model is also used to forecast data.

A smooth transition between hindcast and forecast data can be seen in Figure 4.3.2, with near-perfect comparisons with measurements.

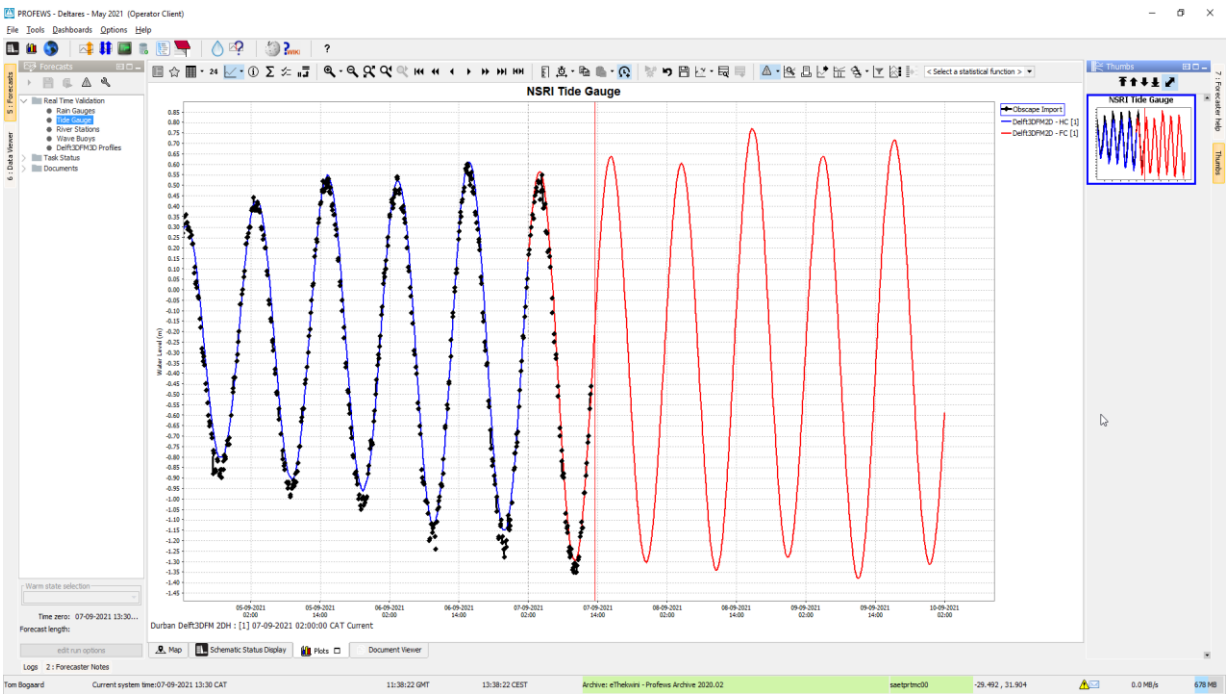

Figure 4.3.2: Water level output showing hindcast (blue) and forecast (red) data for NSRI tide gauge (black dots) and D-Flow FM model (solid lines). Deltares (2019b).

4.3.2. Coastal Inundation

The D-Flow FM model is also used for input into other models for coastal inundation. Boundary conditions for flow parameters are taken from the D-Flow FM model for Simulating Waves Nearshore (SWAN) and Super-Fast Inundation of Coasts (SFINCS) models. Figure 4.3.3 shows the SWAN model set up in FEWS.

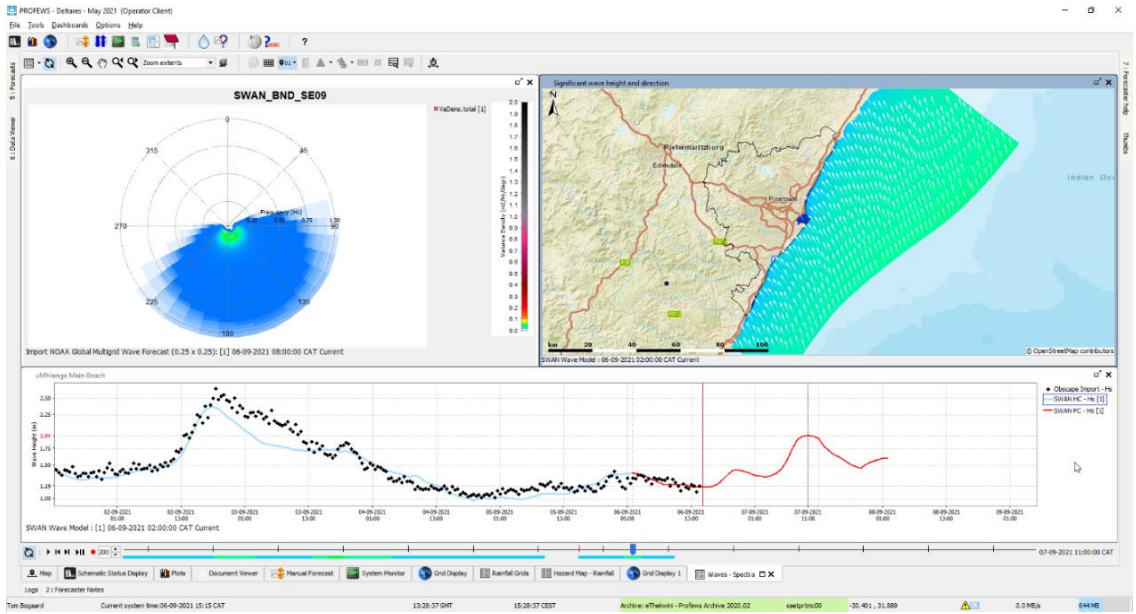

Figure 4.3.3: Typical SWAN output from FEWS for an observation point off the Umhlanga Main Beach, including wave composition (top left), SWAN model grid (top right) and hindcast and forecast data (bottom). Deltares (2019b).

The wave forecast is imported from NOAA (National Oceanic and Atmospheric Administration) and an observation point located off Umhlanga Main Beach is shown in the wave spectrum (top left). The SWAN model domain is shown on the top right. The bottom of the figure shows both forecasted and hindcast wave heights at this location, with comparable measured wave heights from eThekwini's Umhlanga wave buoy.

Figure 4.3.4 shows a SWAN simulation (left) for the 12th of March 2017 to replicate the coastal flood occurrence on Durban's Main Beachfront. SFINCS was used for the simulation output shown on the right, which shows the overtopping of the main promenade area in Durban. This corresponds with images and videos taken on the day of the event. Coastal inundation modelling for Durban is being developed by Deltares with assistance from the eThekwini FEWS Team.

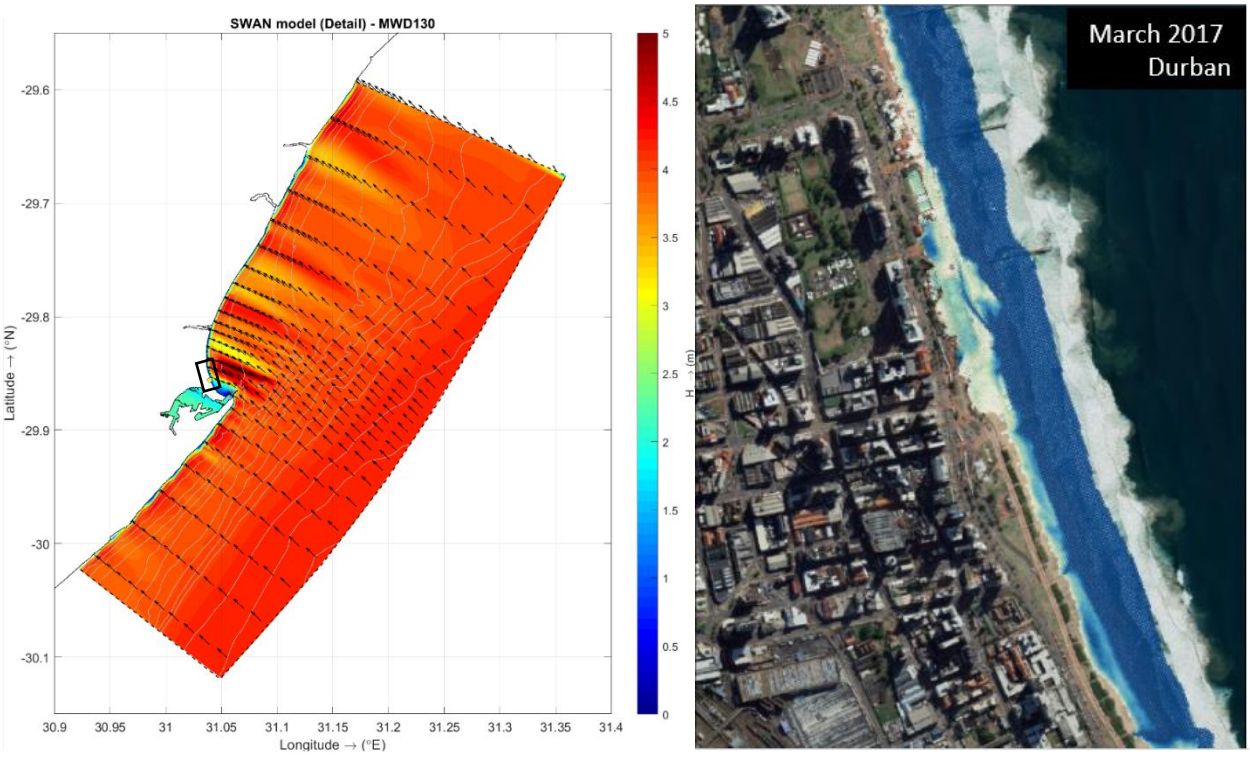

Figure 4.3.4: Model outputs for March 2017 Coastal Inundation at Durban Central Beachfront. SWAN model output (left) and SFINCS model output (right). Deltares (2019b).

This type of modelling is currently being developed and calibrated offline. After validation and calibration, it will be implemented operationally within the FEWS interface.

4.3.3 Particle Tracking

Particles can be released within the D-Flow FM model to track their movements. The current magnitude and direction within the D-Flow FM model directly influences particle tracking.

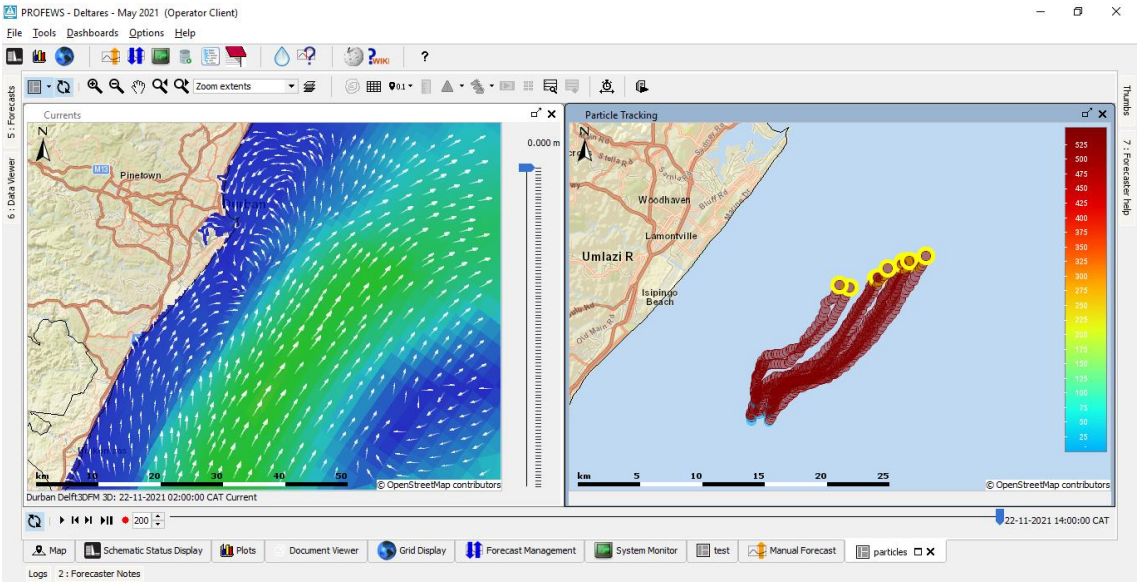

Figure 4.3.5: Typical example of Particle Tracking within FEWS with the D-Flow FM model (left) and corresponding particle migration (right).

Figure 4.3.5 shows the release of 10 particles just south of the Durban harbour. The currents that are shown in the D-Flow FM model progress northwards, which directly affects the particle migration (also in a northward direction). This simulation is a test scenario that was only run for an hour. Wind is not included yet as this type of modelling is still under development.

However, we can already see the effect and need for a coastal D-Flow FM model from inspecting these preliminary results. In Figure 4.3.6, which represents the same simulation shown in Figure 4.3.5, direct comparisons can be seen between GREP and D-Flow FM within FEWS. The D-Flow FM model shows the presence of a Durban Eddy, whereas this is not the case in GREP. The currents that are shown from the GREP output travel in a southerly direction which contradicts the currents shown and produced by the D-Flow FM model. The direction of flow significantly influences the tracking of particles, therefore accurately simulating and forecasting velocity magnitude is vital for particle tracking. The GREP NEMO model does not simulate a Durban Eddy due to its coarse-scale which reiterates the need for a coastal scale D-Flow FM model.

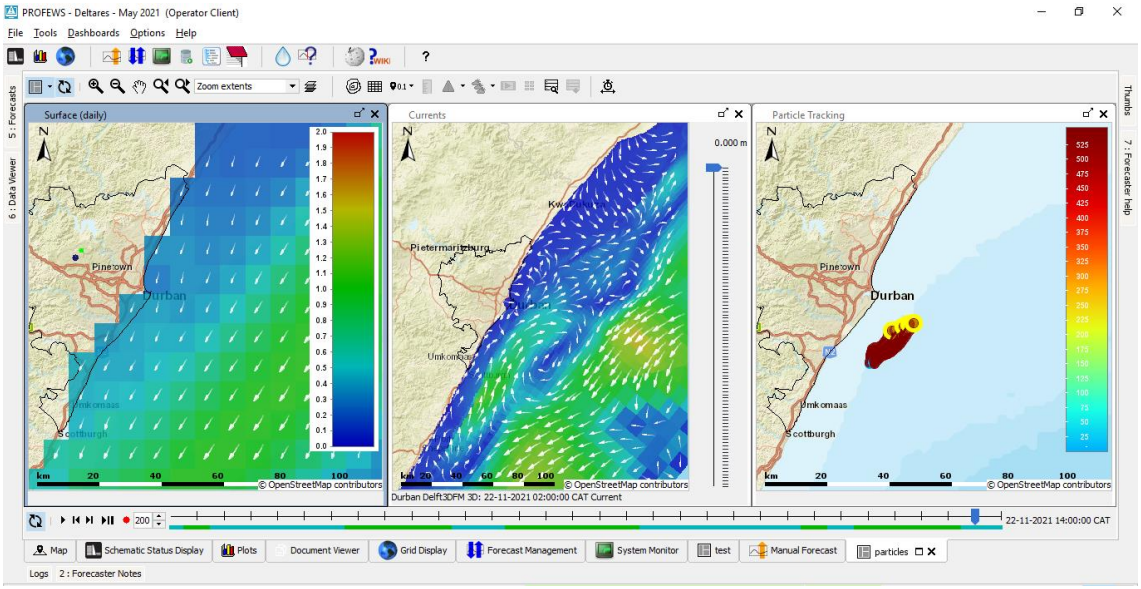

Figure 4.3.6: CMEMS velocity output (left), D-Flow FM velocity output (middle) and particle tracking simulation (left)

4.4 Limitations

4.4.1 D-Flow FM

As seen in Chapter 4, some of the model results do not correlate as accurately with the measured data as GREP does. Sometimes the model overestimates the Agulhas Current magnitudes and sometimes the models do not simulate the correct current directions. Although the current itself is unstable and observations show drastic variability in recordings (depending on the currents position), D-Flow FM should strive to successfully achieve accurate representations of flow fields. Software improvements, such as those achieved during the internship (See Appendix A), could allow for a more accurate representation of measurements.

Model resolution and extent could also be contributing factors when trying to accurately simulate the Agulhas. Model domain was important in allowing the current to develop from the northern boundary conditions. Therefore, limiting the domain to reduce computation costs could also lead to inaccurate results.

Boundary condition implementation was troublesome, with several instabilities forming for various reasons as explained in Appendix A. D-Flow FM becomes unstable if these instabilities are not resolved. Software improvements during the internship stabilised the use of boundary conditions and the model then proved to be robust when forcing it with ocean boundary conditions.

4.4.2 Bathymetry

Detailed and good quality bathymetry data is required at the shelf edge. This region is responsible for the formation of spin-off features and the meandering of the Durban Eddy. Lack of detail in the bathymetry surveys can inaccurately produce these features in a model simulation. As seen in Figure 3.4.3, some depth soundings show unrealistic depths which were smoothened out. This could be seabed characteristics that aren't detailed in the survey (such as troughs or canyons), which also influence the Agulhas. Removing these survey points or not having enough depth measurements in the shelf region can add to inaccurate model results, which would explain the low correlation values for the D-Flow FM models seen in 4.2.1.2. The sensitivity of the topography in this frontal region of the shelf could result in the Agulhas Current not being modelled in the right place.

4.4.3 Current Measurements

Although two sets of surveys were used for validation of model results, these surveys are limited. The Offshore ADCP only provides one data buoy location which is in the middle of where we expect the Durban Eddy to form. Due to its location, drastic changes in both current magnitude and direction are observed. This is a difficult dataset to compare to. The ACEP survey has a limited period of data available. Seasonal variations cannot be analysed with this dataset. The ACEP survey is also restricted to the area within the KZN Bight, so currents on the shelf north of Durban (where ethe Agulhas Current hugs the upper shelf edge) which play a vital role in the Agulhas system have limited recordings.

4.4.4 Durban Eddy

Relatively short model runs (3-month inspection) were used to analyse simulations of the Durban Eddy. Longer simulations could provide different frequency results as mentioned in 4.1.3. Longer and more detailed observations of the model are required to accurately compare with suggested literature parameters of the Durban Eddy. The number of eddies was visually inspected and recognised, whereas identifying the eddy could be an automated process (according to current direction and magnitudes) with further coding and model development.

CHAPTER 5

DISCUSSIONS AND CONCLUSIONS

This chapter finalises this research, discussing the results and comparisons from the previous chapter and relating these outputs to the research questions (as defined in section 1.3) of this dissertation. It also provides recommendations for model development and engineering applications.

5.1. Discussions

5.1.1. Modelling of the Agulhas Current

From the several outputs displayed in Chapter 4, it is clear that the D-Flow FM software is now capable of including the forcing of ocean currents, such as the complex and meandering Agulhas Current, as well as adding tide and wind driven currents within the same model (Research question 1). Although initially, it was difficult to keep this current stable along the continental shelf, after several model testing and calibration as described in the Appendix, techniques such as nudging and boundary dampening assist in stabilizing the current.

Realistic velocity magnitudes and directions across a three-dimensional spectrum (2m/s current speeds shown on surface maps and lower current magnitudes in deeper areas of main current) are produced by the D-Flow FM models, which is justified by literature where speeds can exceed 2m/s (Lutjeharms, 2006, 2007, McMonigal et al, 2022, Barlow et al., 2013, 2015) and observed data (ACEP and Offshore ADCP). The models now also allow for incoming and outgoing velocities, which is an improvement from the initial modelling software. Spin-off features such as the Durban Eddy are also realistic within the model. Statistical error analysis shows that both D-Flow FM Models do not perform better than the GREP when compared to the Offshore ADCP. However, the GREP is still too coarse in scale to resolve small scale features, which motivates for the need to downscale the GREP to a D-Flow FM model. Single point analysis does not provide a spatial structure of the flow for investigating the use of more refined models. The effect of the Agulhas Current on the nearshore hydrodynamics of the Durban coastline (Research question 3) is shown with the current direction along the coast of the KZN bight and when the Durban Eddy is present and deflects the current. The positioning of the core of the current can significantly influence the spin- off currents flowing alongside the coast, which ultimately affect the tracking of currents, particles and water quality parameters.

5.1.2. The Durban Eddy

5.1.2.1. Characteristics

As described in 4.1.3, the D-Flow FM model outputs a cyclonic circulation pattern between the main Agulhas Current and the Durban coastline. The velocity directions show this circulation or eddy-like pattern (see Figure 4.1.10) and velocity magnitudes suggest that this eddy is half the strength of the main current (±0.75m/s). The size was also calculated and the modelled length and width of the eddy in Figure 4.2.10 was calculated to be 62.79 km and 40.02 km respectively. This is similar to the average eddy length (60-90km) and width (40-50km) as shown in Table 1. These characteristics are also described in the literature review in section 2.2.4 by Guastella and Roberts (2016). Therefore, the model can confirm the characteristics of the Durban Eddy as defined in the literature.

5.1.2.2. Frequency and Duration

The duration of the Durban Eddy from formation stage to dissipation is approximately eight days long. From Table 1, the life span suggested by Guastella and Roberts (2016) is 8.6 days, which means that the model correlates with the observed duration. As mentioned in 4.1.3, over a model run of 3 months, 5 eddies were visually identified. This suggests a frequency of 1.66 eddies per month, which is approximately 2 eddies as described in Table 1.

5.1.2.3. Upwelling

As the formation of the eddy occurs, cooler waters are brought alongside the coastline. The temperatures show that the inshore side of the eddy is cooler than the side adjacent to the Agulhas Current. The process of cooler waters being brought to the coast by a cyclonic circulation shows the upwelling phenomenon described in Chapter 2. Therefore the physical aspects of the Durban Eddy are verified by the model (Research question 2).

5.1.3. The Agulhas Current and the Durban Coastline

The Agulhas Current is pushed further offshore when it reaches the KZN Bight. Both literature (Lutjeharms, 2006, Roberts et al., 2016) and the models confirm this. It meanders and is subject to flow instabilities every now and again (Natal Pulses). Spin-off features are created due to these instabilities within this current. These spin-off features interact with tide and wind-induced currents in the shallow waters of the Durban Bight, which alter the flow around Durban's nearshore environment (as seen in the comparisons between GREP NEMO and D-Flow FM

models). GREP does not include tide and the D-Flow FM models (which include tide and wind) both show variations in nearshore current fields when compared with GREP. This shows that tide, wind and ocean currents directly influence currents in the shallow waters off Durban. The meandering of the Agulhas Current also causes variations in the current direction and magnitude, which directly affects its influence on the Durban coastline. When the current flows alongside the continental shelf (no eddy is present), the models suggest that the current direction alongside the Durban Bight flows in a southerly direction. However, when the eddy is present and the Agulhas Current is deflected further offshore, the model suggests that a northerly flow persists on the coastline. This reversal of current direction is shown in Figure 4.2.13 and is a phenomenon commonly known about the Durban coastline (see section 2.1). Therefore, the model suggests that the positioning of the Agulhas Current directly affects the direction and possibly strength of the currents flowing alongside the Durban coastline. Upwelling of cooler waters is another impact from the spin-off feature of the Agulhas Current, bringing colder, nutrient-rich water to the Durban coastline.

Although the D-Flow FM models have lower correlation values than the GREP when compared to the Offshore ADCP, these models can resolve smaller scaled features unlike GREP. GREP includes assimilation of observed data which could be why this product corresponds closer to the measured records (The Offshore ADCP data could already be incorporated within GREP). It is important to understand the positioning of the simulated current when looking at the measured recordings. This is done for the ACEP survey over depths 17m, 57m and 161m for GREP, the Internship Model and Test08. Analysing the map plots, vertical profiles and instantaneous recordings provide a better understanding of why each model does/does not correspond well with the ACEP data. The D-Flow FM can be seen as overestimating the surface velocities in some instances, which could be due to inaccurate surface forcing or poorly parametrized diffusion. However, by looking at the map plots at different depth intervals in 4.2.2, the model performance in the vertical structure is seen. The positioning of the Agulhas Current directly influences the models results and therefore the model's correlation with the observed measurements. The slightest inaccuracy in the currents positioning can prevent good data correlation.

5.1.4 Summary

The model developed herein successfully reproduces the formation of Durban eddy with characteristics consistent with literature (Guastella and Roberts, 2016). A well-formed Durban eddy is identified as well as the transformation stages of the formation of the eddy. It is also evident that when the eddy is present, the Agulhas Current is deflected further offshore. The Internship model already confirms many features and characteristics specified in the literature

review in chapter 2. This suggests that the Internship model is already useful in determining such features and understanding the nearshore dynamics off the KZN Bight.

Test08 shows better results in some instances of the ACEP map outputs for overall current flow and trajectory (similar to ACEP measurements). When comparing this model with observed measurements from both Offshore and ACEP ADCP's, the model is capable of replicating observations of flow well. Looking at both GREP and observed data, in many instances, the model does bridge the gap between these two. However, there are still examples where GREP better predicts the observed measurements compared to the D-Flow FM models. The GREP is a reanalysis product which includes the assimilation of observed data. This could be the reason why in some instances the GREP data corresponds better with observed measurements.

The 2009 time-series comparisons in Figures 4.1.6 and 4.1.7 suggest that the Internship model performs better than GREP when compared to the Offshore ADCP over time. However, the comparisons with the 2010 Offshore ADCP survey suggest higher accuracy with the Test08. Statistical error analysis shows that both D-Flow FM Models do not perform better than the GREP when compared to the Offshore ADCP, with a higher correlation coefficient for GREP for daily averaged data. This could be due to the reanalysis of observed data within the GREP. However, it is difficult to conclude anything on the basis of these single-point statistics in a very complex area which is why the general trend of the currents give a better understanding of the performance of these models. This comes across in the velocity map outputs, specifically the ACEP results section.

Analysing the ACEP survey data for specific days and depths shows how well the models correlate to observed data. In some instances, the Internship model performs better than GREP and Test08, and in other instances, Test08 performs the best when compared to ACEP observations. However, at location D (on the shelf edge closer to the coast), GREP NEMO model outputs are closest to the ACEP data. This suggests that there is still room for improvement. It is unrealistic to produce a model that completely predicts or models' exact comparisons to measured data, especially for such a dynamic and complex area. However, from the available measurements, the D-Flow FM models can compare well with the general current trends.

5.2. Recommendations

Achieving accurate flow magnitudes and directions is vital for a hydrodynamic coastal model. Considering that this model will be used as a basis for a future water quality model, it is crucial to not only understand but also reproduce realistic conditions. The model plays a critical role in future development and research and the following are recommended:

- Further simulations and comparisons should be done to further validate and calibrate the D-Flow FM model.
- Improved grid resolution and delineation could improve model results.
- A more optimum domain demarcation could be possible.
- Software and model updates are ongoing, but more field measurements are required to validate if these changes are improvements to the model. Field measurements should cover longer periods to cater for seasonal variations.
- Higher resolution and/or newer bathymetry along the continental shelf could assist in maintaining or simulating features of the Agulhas Current. The slightest deviation in the bathymetry could result in contrasting results, therefore accurate bathymetry is crucial for correctly modelling the dynamics of the Agulhas Current.
- More regular bathymetry surveys can be done to provide an accurate representation of the seabed level. Surveys should also be focused along the continental shelf of KZN.
- Longer simulations should be done for the Durban Eddy to analyse its characteristics and influence on Durban's nearshore.
- A more technical or automated approach could be established to identify frequency, duration and size of the Durban Eddy.
- More measurements of where the eddy persists should be collected, over longer periods.

Results for other models could be unreliable if the incorrect flow values are fed from D-Flow FM. Therefore, the reliability of the D-Flow FM model is critical in future model developments.

5.3. Conclusion

Both D-Flow FM models (Internship and Test08) replicate the main Agulhas Current well and identify features such as the Durban Eddy.

The internship model shows promising results and gives an adequate insight into the characteristics of both the Agulhas Current and its spin-off features. It successfully reproduces the strong western boundary current as well as identifies and characterizes the Durban Eddy well. The results in this study suggest D-Flow FM can predict the occurrence of the Durban Eddy and other flow features when compared to observation.

When compared with observed measurements, the model results are validated and mostly realistic. Variability of the Agulhas Current and its spin-off features can be better simulated by the models and validated by future observed measurements. Results of the models tie into both measured data and extracts from literature. Statistical error analysis shows that both D-Flow FM Models perform better than the GREP when compared to the Offshore ADCP.

Improvements to the Internship model, by Deltares experts, progressed to develop Test08. This model, with updated software, refined resolution, better grid configuration and reviewed bathymetry, shows better results than the Internship model when compared to the available observed measurements. Therefore, Test08 will be used in FEWS operationally.

Therefore, it can be concluded that D-Flow FM can accurately simulate the overall hydrodynamics in the Durban offshore and nearshore under the combined forcing of tide, wind and ocean currents, but there is still room for improvement. This research has explored and concluded that the Agulhas Current and its spin-off features does influence the nearshore hydrodynamics of the Durban coastline.

REFERENCES

2016. Bathymetric Survey Coverage of the Durban Bight Technical Report. Durban: Environmental Mapping and Survey.

2005. *South African Navy Bathymetry Data Set*. Depth Soundings off the South African Eastern Coastline.

Anderson FP, Gründlingh ML, Stavropoulos CC. 1988. Kinematics of the southern Natal coastal circulation: some historic measurements 1962–63. *South African Journal of Science* 84: 857–860.

Ardhuin, F., Gille, S., Menemenlis, D., Rocha, C., Rascle, N., Chapron, B., Gula, J. and Molemaker, J., 2017. Small-scale open ocean currents have large effects on wind wave heights. *Journal of Geophysical Research: Oceans*, 122(6), pp.4500-4517.

Barlow, R., T. Lamont, K. Britz, and H. Sessions, 2013: Mechanisms of phytoplankton adaptation to environmental variability in a shelf ecosystem. *Estuarine Coastal Shelf Sci.*, **133**, 45–57

Beal, L., 2009: A time series of Agulhas Undercurrent transport. *J. Phys. Oceanogr.*, **39 ,** 2436–2450.

Beal, L, T. Chereskin, Y. Lenn, and S. Elipot, 2006: The sources and mixing characteristics of the Agulhas Current. J. Phys. Oceanogr., 36, 2060–2074.

Beal, L., and H. L. Bryden, 1997: Observations of an Agulhas Undercurrent. *Deep-Sea Res.*, **44**, 1715–1724.

Beal, L. M., and S. Elipot, 2016: Broadening not strengthening of the Agulhas Current since the early 1990s. *Nature*, **540**, 570–573, https://doi.org/10.1038/nature19853.

Beal, L., De Ruijter, W., Biastoch, A. and Zahn, R., 2011. On the role of the Agulhas system in ocean circulation and climate. *Nature*, 472(7344), pp.429-436.

Beal, L. M., Elipot, S., Houk, A., & Leber, G. M. (2015). Capturing the Transport Variability of a Western Boundary Jet: Results from the Agulhas Current Time-Series Experiment (ACT)*. *Journal of Physical Oceanography*, *45*(5), 1302–1324. http://doi.org/10.1175/JPO-D-14-0119.1

Biastoch, A., Beal, L., Lutjeharms, J. and Casal, T., 2009. Variability and Coherence of the Agulhas Undercurrent in a High-Resolution Ocean General Circulation Model. *Journal of Physical Oceanography*, 39(10), pp.2417-2435.

Bleck, R., 2002. An oceanic general circulation model framed in hybrid isopycnic-Cartesian coordinates. *Ocean Modelling*, 4(1), pp.55-88.

Bleck, R. and Boudra, D., 1981. Initial Testing of a Numerical Ocean Circulation Model Using a Hybrid (Quasi-Isopycnic) Vertical Coordinate. *Journal of Physical Oceanography*, 11(6), pp.755-770.

Boebel, O & Rossby, T & Lutjeharms, J & Zenk, W & Barron, C. (2002). Path and variability of the Agulhas Return Current. Deep-sea Research Part Ii-topical Studies in Oceanography - DEEP-SEA RES PT II-TOP ST OCE. 50. 35-56. 10.1016/S0967-0645(02)00377-6.

Bosboom, J., & Stive, M. J. F. (2013). Coastal Dynamics I. Delft: VSSD.

Boyd, A. J. and Oberholster, G. P. I. (1994). Currents off the West and South Coasts of South Africa. South African Shipping News and Fishing Industry Review, Sept/Oct 26-28.

Braby, L., B. C. Backeberg, I. Ansorge, M. J. Roberts, M. Krug, and C. J. C. Reason (2016), Observed eddy dissipation in the Agulhas Current, Geophys. Res. Lett., 43, 8143–8150, doi:10.1002/2016GL069480.

Bryden, H.L., Beal, L.M. & Duncan, L.M. Structure and Transport of the Agulhas Current and Its Temporal Variability. *J Oceanogr* **61,** 479–492 (2005). https://doi.org/10.1007/s10872-005-0057-8

Chassignet, E., Hurlburt, H., Smedstad, O., Halliwell, G., Wallcraft, A., Metzger, E., Blanton, B., Lozano, C., Rao, D., Hogan, P. and Srinivasan, A., 2006. Generalized Vertical Coordinates for Eddy-Resolving Global and Coastal Ocean Forecasts. *Oceanography*, 19(1), pp.118-129.

CMEMS, 2019. *Access to products.* [Online] Available at: http://marine.copernicus.eu/services-portfolio/access-to-products/?option=com_csw&view=details&product_id=GLOBAL_ANALYSIS_FORECAST_PHY_001_024 [Accessed 21 10 2019].

Corbella, S. & Stretch, Derek. (2012a). Multivariate return periods of sea storms for coastal erosion risk assessment. Natural Hazards and Earth System Sciences. 12. 2699-2708. 10.5194/nhess-12-2699-2012.

Corbella, S, & Stretch, D D. (2012b). The wave climate on the KwaZulu-Natal coast of South Africa. *Journal of the South African Institution of Civil Engineering*, *54*(2), 45-54. Retrieved October 25, 2021, from http://www.scielo.org.za/scielo.php?script=sci_arttext&pid=S1021-20192012000200005&lng=en&tlng=en.

Deltares, 2016. *Delft Dashboard (DDB).* [Online] Available at: https://publicwiki.deltares.nl/pages/viewpage.action?pageId=42401894

Deltares, 2017. *Delft-FEWS.* [Online] Available at: http://oss.deltares.nl/web/delft-fews/

Deltares, 2019a. Herman Kernkamp, lead developer of D-FLOW Flexible Mesh

Deltares, 2019b. Reimer de Graaf, Coastal and Offshore Engineer

Deltares, 2020a. *Delft3D Flow, User Manual*. Hydro-Morphodynamics. Delft: Deltares.

Deltares, 2020b. *D-Flow Flexible Mesh, User Manual*. Computational Cores and User Interface. Delft: Deltares.

Deltares, 2021. *D-Flow Flexible Mesh - Deltares*. [online] Available at: <https://www.deltares.nl/en/software/module/d-flow-flexible-mesh/> [Accessed 21 June 2021].

de Goede, Erik. (2020). Historical overview of 2D and 3D hydrodynamic modelling of shallow water flows in the Netherlands. Ocean Dynamics. 70. 10.1007/s10236-019-01336-5.

de Ruijter, W. P. M., H. Ridderinkhof, J. Lutjeharms, M. Schouten, and C. Veth, 2002: Observations of the flow in the Mozambique Channel. Geophys. Res. Lett., 29, L1502, doi:10.1029/2001GL013714.

DNV-RP-C205, 2010. Recommended Practice DNV-RP-C205: ENVIRONMENTAL CONDITIONS AND ENVIRONMENTAL LOADS. Bærum, Norway: DET NORSKE VERITAS, p.45.

dos Santos Gil, J., 2014. Application of the Delft3D System in the Modelling of Laboratory and Field Longshore Currents. Master of Science Degree in Civil Engineering. Tecnico Lisboa.

ECMWF. 2019. *ERA5*. [online] Available at: <https://www.ecmwf.int/en/forecasts/datasets/reanalysis-datasets/era5> [Accessed 24 November 2019].

Elipot S, Beal LM. 2015. Characteristics, energetics, and origins of Agulhas Current meanders and their limited influence on ring shedding. *Journal of Physical Oceanography* 45: 2294–2314.

Fennessy ST, Roberts MJ & Paterson AW (2016) A brief overview of the ACEP project: Ecosystem Processes in the KwaZulu-Natal Bight, African Journal of Marine Science, 38:sup1, S1-S6, DOI: 10.2989/1814232X.2016.1141116

Flemming BW. 1980. Sand transport and bedform patterns on the continental shelf between Durban and Port Elizabeth (southeast African continental margin). *Sedimentary Geology* 26: 179–205.

Fringer, O., Dawson, C., He, R., Ralston, D. and Zhang, Y., 2019. The future of coastal and estuarine modeling: Findings from a workshop. *Ocean Modelling*, 143, p.101458.

GEBCO. 2021. *GEBCO - The General Bathymetric Chart of the Oceans*. [online] Available at: <https://www.gebco.net/> [Accessed 3 June 2021].

Gründlingh ML, Pearce AF. 1990. Frontal features of the Agulhas Current in the Natal Bight. *South African Geographical Journal* 72: 11–14.

Guastella L. A-M. (1994) A quantitative assessment of recreational angling in Durban Harbour, South Africa, South African Journal of Marine Science, 14:1, 187-203, DOI: 10.2989/025776194784287120

Guastella LA, Roberts MJ. 2016. Dynamics and role of the Durban cyclonic eddy in the KwaZulu-Natal Bight ecosystem. In: Roberts MJ, Fennessy ST, Barlow RG (eds), *Ecosystem processes in the KwaZulu-Natal Bight*. *African Journal of Marine Science*, 38(Supplement): S23–S42.

Halo, I., Backeberg, B., Penven, P., Ansorge, I., Reason, C. and Ullgren, J., 2014. Eddy properties in the Mozambique Channel: A comparison between observations and two numerical ocean circulation models. *Deep Sea Research Part II: Topical Studies in Oceanography*, 100, pp.38-53.

Herman, Kernkamp & Dam, Arthur & Stelling, Guus & de Goede, Erik. (2011). Efficient scheme for the shallow water equations on unstructured grids with application to the Continental Shelf. Ocean Dynamics. 61. 1175-1188. 10.1007/s10236-011-0423-6.

Hutchinson, K. (2017). The Agulhas Current and its seasonality explained. *SAEON Egagasini Node*. [online] Available at: http://www.saeon.ac.za/enewsletter/archives/2017/june2017/doc10 [Accessed 5 Sep. 2019].

Isabel Iglesias, Paulo Avilez-Valente, José Luís Pinho, Ana Bio, José Manuel Vieira, Luísa Bastos and Fernando Veloso-Gomes (2019). Numerical Modeling Tools Applied to Estuarine and Coastal Hydrodynamics: A User Perspective, Coastal and Marine Environments - Physical Processes and Numerical Modelling, José Simão Antunes Do Carmo, IntechOpen, DOI: 10.5772/intechopen.85521. Available from: https://www.intechopen.com/chapters/66266

Krug, M., and Penven, P. (2011), New perspectives on Natal Pulses from satellite observations, *J. Geophys. Res.*, 116, C07013, doi:10.1029/2010JC006866.

Kruger A, 2014.Climate. Ugu Lwethu – Our Coast. A profile of coastal KwaZulu-Natal. KwaZulu-Natal Department of Agriculture and Environmental Affairs and the Oceanographic Research Institute, Cedara, 15-16.

Lakshmi H. Kantha & Carol Anne Clayson (2000). *Numerical Models of Oceans and Oceanic Processes*. Academic Press. p. 56 (Table 1.5.1). ISBN 0-12-434068-7.

Lamont, T., van den Berg, M. and Barlow, R., 2016. Agulhas Current Influence on the Shelf Dynamics of the KwaZulu-Natal Bight. *Journal of Physical Oceanography*, 46(4), pp.1323-1338.

Legg, S., Hallberg, R.W., Girton, J.B., 2006. Comparison of entrainment in overflows simulated by z-coordinate, isopycnal and non-hydrostatic models. Ocean Model. 11 (1–2), 69–97.

Lesser, G. R., Roelvink, J. A., van Kester, J. A. & Stelling, G. S., 2004. Development and validation of a three-dimensional morphological model. *Coastal Engineering*, 51(8-9), p. 883–915.

Lutjeharms, J. R. E. and Connell, A. D. (1989): The Natal Pulse and inshore counter currents off the South African east coast, S. Afr. J. Sci., 85, 533–535.

Lutjeharms J.R.E and Roberts HR. 1988. The Natal pulse: an extreme transient on the Agulhas Current. *Journal of Geophysical Research* 93: 631–645.

Lutjeharms, J.R.E. and van Ballegooyen, R. C. (1988). The retroflection of the Agulhas Current. Journal of physical Oceanography, 18 (11), 1570-1583.

Lutjeharms, J.R.E. (2006): The coastal oceans of south-eastern Africa, in: The Sea, volume 14B, edited by Robinson, A. R., Brink, K. H., pp. 783–834.

Lutjeharms, J.R.E, Catzel, R. and Valentine, HR (1989). Eddies and other boundary phenomena of the Agulhas Current. Continental Shelf Research, 9(7), 597-616

Lutjeharms J.R.E, Connell AD. 1989. The Natal Pulse and inshore counter currents off the South African east coast. South African Journal of Science 85: 533–535.

Lutjeharms, J.R.E. and de Ruijter, W. P. M. (1996). The influence of the Agulhas Current on the adjacent coastal ocean: possible impacts of climate change. Journal of Marine Systems, 7, 321-336.

Lutjeharms, J.R.E. and Ansorge, I. J. (2001). The Agulhas Return Current. Journal of Marine Systems, 30,115-138.

Lutjeharms, J.R.E., O. Boebel, P. C. F. van der Vaart, W. P. M. de Ruijter, T. H. Rossby, and H. L. Bryden, 2001: Evidence that the Natal pulse involves the Agulhas Current to its full depth. *Geophys. Res. Lett.*, **28**, 3449–3452

Lutjeharms J.R.E. 2006. *The Agulhas Current*. Berlin: Springer-Verlag.

Lutjeharms, J.R.E., (2007). Three decades of research on the greater Agulhas Current. *Ocean Science*, 3(1), pp.129-147.

Malange, M., 2018. BUILDING A MEAN-STATE OF OCEANOGRAPHIC PROPERTIES (TEMPERATURE AND SALINITY) FOR THE KWAZULU-NATAL BIGHT USING THE ROMS MODEL: A CONTRIBUTION TOWARDS MARINE PROTECTED AREAS ANALYSIS. Master of Science in Applied Ocean Sciences. University of Cape Town.

Maltrud, M. E., and J. McClean, 2005: An eddy resolving global 1/10 deg ocean simulation. Ocean Modell., 8, 31–54.

Marchesiello, P., Debreu, L. and Couvelard, X., 2009. Spurious diapycnal mixing in terrain-following coordinate models: The problem and a solution. *Ocean Modelling*, 26(3-4), pp.156-169.

Marchesiello, P., McWilliams, J. C., and Shchepetkin, A. (2001). Open boundary conditions for long-term integration of regional oceanic models. Ocean Modelling, 3(1-2):1–20.

Martyr-Koller, R., Kernkamp, H., van Dam, A., van der Wegen, M., Lucas, L., Knowles, N., Jaffe, B. and Fregoso, T., 2017. Application of an unstructured 3D finite volume numerical model to flows and salinity dynamics in the San Francisco Bay-Delta. *Estuarine, Coastal and Shelf Science*, 192, pp.86-107.

Mather, A. and Stretch, D., 2012. A Perspective on Sea Level Rise and Coastal Storm Surge from Southern and Eastern Africa: A Case Study Near Durban, South Africa. *Water*, 4(1), pp.237-259.

McMonigal, K., Gunn, K. L., Beal, L. M., Elipot, S., and Willis, J. K. (2022). Reduction in Meridional Heat Export Contributes to Recent Indian Ocean Warming. *Journal of Physical Oceanography* 52, 3, 329-345, available from: <https://doi.org/10.1175/JPO-D-21-0085.1> [Accessed 12 May 2022]

Meyer AA, Lutjeharms J.R.E., de Villiers S. 2002. The nutrient characteristics of the Natal Bight, South Africa. Journal of Marine Research 35: 1–37.

Muofhe, T., Chikoore, H., Bopape, M., Nethengwe, N., Ndarana, T. and Rambuwani, G., 2020. Forecasting Intense Cut-Off Lows in South Africa Using the 4.4 km Unified Model. *Climate*, 8(11), p.129.

Ming, Xie, 2014. "Verification and Comparison of Two Commonly Used Numerical Modeling Systems in Hydrodynamic Simulation at a Dual-Inlet System, West-Central Florida". Graduate Theses and Dissertations. https://scholarcommons.usf.edu/etd/5442

National Geographic Society. 2021. *Coriolis Effect*. [online] Available at: <https://www.nationalgeographic.org/encyclopedia/ [Accessed 30 June 2021].

Nauw, J., H. van Aken, J. Lutjeharms, W. de Ruijter, and A. Webb, 2008: Observations in the southern East Madagascar Current and Undercurrent system. J. Geophys. Res., 113, C08006, doi:10.1029/2007JC004639

Nof, D. (1999), Strange encounters of eddies with walls, J. Mar. Res., 57, 739–761.

Oliff WD. 1969. The disposal of effluents into the sea off the Natal coast. NTRPC Report No. 14. Pietermaritzburg: Natal Town and Regional Planning Commission.

Pearce AE. 1977. The shelf circulation off the east coast of South Africa. CSIR Research Report No. 361. Council for Scientific and Industrial Research, Stellenbosch.

Pearce AF, Schumann EH, Lundie GSH. 1978. Features of the shelf circulation off the Natal coast. *South African Journal of Science* 74: 328–331.

Penven, P., Debreu, L., Marchesiello, P. and McWilliams, J., 2006. Evaluation and application of the ROMS 1-way embedding procedure to the central california upwelling system. *Ocean Modelling*, 12(1-2), pp.157-187.

Penven, P., Herbette, S. and Rouault, M., 2010. Ocean Modelling of the Agulhas Current System.

Nemo-ocean.eu. 2017. *Primitive Equations*. [online] Available at: <https://www.nemo-ocean.eu/doc/node6.html> [Accessed 7 November 2021].

Rautenbach, C., Barnes, M. and de Vos, M., 2019. Tidal characteristics of South Africa. *Deep Sea Research Part I: Oceanographic Research Papers*, 150, p.103079.

Roberts, M. J., C. D. van der Lingen, C. Whittle, and M. van den Berg, 2010: Shelf currents, lee-trapped and transient eddies on the inshore boundary of the Agulhas Current, South Africa: Their relevance to the KwaZulu-Natal sardine run. *Afr. J. Mar. Sci.*, **32**, 423–447

Roberts MJ, Ternon JF, Morris T. 2014. Interaction of dipole eddies with the western continental slope of the Mozambique Channel. Deep-Sea Research II 100: 54–67.

Roberts MJ, Nieuwenhuys C. 2016. Observations and mechanisms of upwelling in the northern KwaZulu-Natal Bight, South Africa. In: Roberts MJ, Fennessy ST, Barlow RG (eds), Ecosystem processes in the KwaZulu-Natal Bight. African Journal of Marine Science 38(Supplement): S43–S63.

Roberts MJ, Nieuwenhuys C, Guastella LA. 2016. Circulation of shelf waters in the KwaZulu-Natal Bight, South Africa. In: Roberts MJ, Fennessy ST, Barlow RG (eds), Ecosystem processes in the KwaZulu-Natal Bight. African Journal of Marine Science 38(Supplement): S7–S21.

Scharler, Ursula & Ayers, Morag & M. de Lecea, Ander & Pretorius, M & Fennessy, Sean & Huggett, Jenny & MacKay, CF & Muir, D. (2016). Riverine influence determines nearshore heterogeneity of nutrient (C, N, P) content and stoichiometry in the KwaZulu-Natal Bight, South Africa. African Journal of Marine Science. 38. S193-S203. 10.2989/1814232X.2016.1150347.

Scharler UM, Ayers MJ (2019) Stoichiometric multitrophic networks reveal significance of land-sea interaction to ecosystem function in a subtropical nutrient-poor bight, South Africa. PLoS ONE 14(1): e0210295. https://doi.org/10.1371/journal.pone.0210295

Schumann EH. 1981. Low frequency fluctuations off the Natal coast. *Journal of Geophysical Research* 86: 6499–6508.

Schumann EH. 1982. Inshore circulation of the Agulhas Current off Natal. *Journal of Marine Research* 40: 43–55.

Schumann EH. 1988. Physical oceanography off Natal. In: Schumann EH (ed.), Coastal ocean studies off Natal, South Africa. Lecture Notes on Coastal and Estuarine Studies 26. Berlin: Springer-Verlag. pp 101–130.

Schumann, E. H., Lutjeharms, J. R. E., Boyd, A. J., Grundlingh, M. L. and Brundrit, G. B. (1991). Physical oceanography in South Africa: 1987 to 1990. South African Journal of Science, 87, 486-492.

Schumann, E. H., and J. A. Martin, 1991: Climatological aspects of the coastal wind field at Cape Town, Port Elizabeth and Durban. *S. Afr. Geogr. J.*, **73**, 48–51

Schumann, E. H., 1992: Interannual wind variability on the south and east coasts of South Africa. *J. Geophys. Res.*, **97**, 20 397–20 403

Shchepetkin, A. and McWilliams, J., 2005. The regional oceanic modeling system (ROMS): a split-explicit, free-surface, topography-following-coordinate oceanic model. *Ocean Modelling*, 9(4), pp.347-404.

Sjodin, B., 2016. *What's The Difference Between FEM, FDM, and FVM?*. [online] Machinedesign.com. Available at: <https://www.machinedesign.com/3d-printing-cad/fea-and-simulation/article/21832072/whats-the-difference-between-fem-fdm-and-fvm> [Accessed 25 October 2021].

Skogen, M. D., 1999: A biophysical model for the Benguela upwelling system. S. Afr. J. Mar. Sci., 21, 235–249.

Storto, A., Masina, S., Simoncelli, S., Iovino, D., Cipollone, A., Drevillon, M. and Drillet, Y. (2019) 'The added value of the multi-system spread information for ocean heat content and steric sea level investigations in the CMEMS GREP ensemble reanalysis product', *Climate Dynamics*, 53(1-2), 287+, available: https://link.gale.com/apps/doc/A589156069/AONE?u=anon~b576f5e5&sid=googleScholar&xid=104467ce

Song, Y. and Haidvogel, D., 1994. A Semi-implicit Ocean Circulation Model Using a Generalized Topography-Following Coordinate System. *Journal of Computational Physics*, 115(1), pp.228-244.

Tedesco, Pauline & Gula, Jonathan & Ménesguen, Claire & Penven, Pierrick & Krug, Marjolaine. (2019). Generation of Submesoscale Frontal Eddies in the Agulhas Current. Journal of Geophysical Research: Oceans. 124. 10.1029/2019JC015229.

Tedesco, P., Gula, J., Penven, P., & Ménesguen, C. (2022). Mesoscale Eddy Kinetic Energy Budgets and Transfers between Vertical Modes in the Agulhas Current, *Journal of Physical Oceanography*, *52*(4), 677-704. Retrieved May 12, 2022, from https://journals.ametsoc.org/view/journals/phoc/52/4/JPO-D-21-0110.1.xml

Tripp RT. 1967. An atlas of coastal surface drifts Cape Town to Durban. Cape Town: South African Oceanographic Data Centre, University of Cape Town.

Trotta, F., Federico, I., Pinardi, N., Coppini, G., Causio, S., Jansen, E., Iovino, D. and Masina, S., 2021. A Relocatable Ocean Modeling Platform for Downscaling to Shelf-Coastal Areas to Support Disaster Risk Reduction.

Tsugawa, M., and H. Hasumi (2010), Generation and growth of the Natal Pulse, J. Phys. Oceanogr., 40, 1597–1612. van Leeuwen, P. J., W. P. M. de Ruijter, and J. R. E. Lutjeharms

(2000), Natal Pulses and the formation of Agulhas rings, J. Geophys. Res., 105, 6425–6436, doi:10.1029/1999JC900196.

Ye, F., Zhang, Y., Wang, H., Friedrichs, M.A.M., Irby, I.D., Alteljevich, E., Valle-Levinson, A., Wang, Z., Huang, H., Shen, J., Du, J., 2018. A 3D unstructured-grid model for Chesapeake Bay: importance of bathymetry. Ocean Model. 127, 16–39.

Zhai, X., H. L. Johnson, and D. P. Marshall (2010), Significant sink of ocean-eddy energy near western boundaries, Nat. Geosci., 3, 608–612, doi:10.1038/NGEO943.

Zhang, Y., Baptista, A.M., 2008. SELFE: A semi-implicit Eulerian–Lagrangian finite-element model for cross-scale ocean circulation. Ocean Model. 21, 71–96.

APPENDIX A

A.1 Introduction

This appendix serves as an additional attachment that details the model attempts which are summarised in chapter 6. The several test runs provide a better understanding of the processes undertaken during the internship and breaks down the steps undergone and needed to achieve the stable model. It also displays the relationship with Deltares and the constant collaboration.

A.2 Initial Boundary Implementation:

Attempt Number: 1

Date: 16/09/2019

Test Name/s: Run1

Input Parameters: Water Level, Temperature, Salinity and UxUyAdvection Velocities

Status: Initial run works, but huge depressions start to occur as the model progresses

Analysis: Boundary condition files were constructed by downloading CMEMS data for the input parameters for the year 2009 (to match the period in literature for comparative analysis). The boundaries were then run with the initial model setup. This model did not run. Further inspection is required.

Attempt Number: 2

Date: 17/09/2019

Test Name/s: Run2 to Run4

Input Parameters: Water Level, Temperature, Salinity and UxUyAdvection Velocities

Status: Model crashes, error file suggests “segmentation fault”

Analysis: UxUy boundaries were not being read and were being ignored by the model. When the advection velocity was finally being read, the model crashed. Core and error files were produced, which meant that there was something very wrong with the model. Changes were made to all the input files and rewording or re-labelling of the parameters were done to match a previously

successful run. Boundary conditions were still not being successfully read. The same error message kept occurring in the error file and a huge memory usage was noticed during the run. A laptop with higher memory capacity was then used, yet the model still crashed with the same errors.

Individual boundary conditions were then implemented and tested. First test of the boundary conditions was the Water Level Boundary to identify if depressions were being caused by this boundary condition.

Attempt Number: 3

Date: 20/09/2019

Test Name/s: Run5

Input Parameters: Water Level

Status: Water Level Boundary successfully implemented

Analysis: No depressions were identified in this run. The model is stable.

Now that we know the Water Level Boundary is implemented successfully, we need to check the other boundary conditions. We know that the Temperature and Salinity Boundaries are being read by the model, but we still need to see if the velocity boundaries are being implemented.

Attempt Number: 4

Date: 21/09/2019

Test Name/s: Run6

Input Parameters: Water Level, Advection Velocities

Status: Run 6 crashes.

Analysis: Water Level Boundary is required to run the advection velocities within the model. However, this run still do not show any indication of the velocity boundaries being successfully implemented.

Attempt Number: 5

Date: 23/09/2019

Test Name/s: New Boundaries: Run1

Input Parameters: Water Level, Temperature, Salinity and UxUyAdv n ection Velocities

Status: Model crashes. Velocity boundaries are still not working.

Analysis: We had suspected that the Master Definition file was not correct or not the latest version. We tried using a different one from a previous successful model. We also used new boundary data that was collected from a previous model for this region for March 2009. These processes still did not work. We also tried switching from Z-layers to σ-layers to see if the velocity boundaries worked in this type of vertical specification. The velocity boundaries were still not being implemented correctly in the model.

Attempt Number: 6

Date: 24/09/2019

Test Name/s: New Boundaries: Run2

Input Parameters: Water Level, Temperature and Salinity

Status: Initial values of Temperature and Salinity are displayed only

Analysis: Only the initial conditions for temperature and salinity are being prescribed as per the specified values in the master definition file. This means that the boundary conditions are not being implemented in the model.

Attempt Number: 7

Date: 25/09/2019

Test Name/s: New Boundaries: Run3

Input Parameters: Temperature and Salinity

Status: Model runs

Analysis: Another model was used to test previous complications. This model's master definition file was then edited to suit the Durban model inputs. This model was a σ-layer model and ran both parameters successfully.

Attempt Number: 8

Date: 25/09/2019

Test Name/s: New Boundaries: Run4

Input Parameters: Temperature and Salinity

Status: Model runs, invalid output

Analysis: The previous model run was then adapted for a Z-layer model. This model runs, however patches in the data for the first layer (surface layer) were noticed.

Attempt Number: 9

Date: 25/09/2019

Test Name/s: New Boundaries: Run5

Input Parameters: Water Level, Temperature and Salinity

Status: Model runs

Analysis: A previous coarse model for the same region was then used with the boundaries that were already successfully implemented. This model was successful.

Attempt Number: 10

Date: 25/09/2019

Test Name/s: New Boundaries: Run6

Input Parameters: Water Levlel, Temperature, Salinity and Advection Velocities

Status: Model runs

Analysis: Model inputs from “New Boundaries: Run 6” was combined with the master definition file from “New Boundaries: Run3”. This model runs with these conditions from other model inputs.

Attempt Number: 11

Date: 25/09/2019

Test Name/s: New Boundaries: Run7

Input Parameters: Water Level, Temperature, Salinity and Advection Velocities

Status: Model crashes

Analysis: Model inputs from the initial boundary files was then combined with the master definition file from “New Boundaries: Run6” above. This model crashes and advection velocities still do not work.

Attempt Number: 12

Date: 26/09/2019

Test Name/s: Jan2012: Run1

Input Parameters: Water Level

Status: Model is stable

Analysis: The model was then tested for a different time period (January 2012). The boundary files were then changed with the data re-downloaded from CMEMS for the new period. The first boundary condition that was tested was water level only. The water level outputs looked quite constant and acceptable.

Attempt Number: 13

Date: 26/09/2019

Test Name/s: Jan2012: Run2

Input Parameters: Water Level, Temperature

Status: Depression start to occur within the model again

Analysis: Temperature was then added to the previous run, "Jan2012: Run1". Depressions were starting to occur again, and noticeable patches appeared in the temperature outputs.

Unfortunately, after all these attempts, Temperature and Salinity boundary conditions could not be successfully implemented within the model. We then had to retreat, go back to the D-Flow FM developers and ask them for assistance. They noticed that the software could only read specific formats of the boundary condition files and we had to manipulate our input files accordingly for Temperature and Salinity. They also noticed that there were some complications in the mathematical equations required to correctly interpolate the advection velocity calculations from only implementing these two boundary conditions. Before even considering the velocity boundary implementations, we first needed to apply the Temperature and Salinity boundaries successfully.

After several days of collaboration and testing, the software development team produced a new version of the D-Flow FM software which has improved capabilities to alleviate the challenges mentioned above. Water Level, Temperature and Salinity Boundary Conditions were finally successfully applied, and a stable model was achieved. The next challenge was to implement the velocity boundaries, but this was done in conjunction with analysing and applying the nudging technique.

A.3 Testing the Nudging Technique:

Several runs were done to explore the nudging technique, different forms of nudging, boundary conditions with nudging and different input parameters. New data was downloaded for the period between the year 2009 and 2011 for a smaller, more refined grid (shown in Figure 3.3.2) as compared to the coarse grid used in the previous runs.

Attempt Number: 14

Date: 27/09/2019

Test Name/s: Nudging: Multiple Runs

Input Parameters: Water Level, Temperature, Salinity, Advection Velocities, Nudging files, refined grid

Status: Model is stable but need to determine if boundaries are doing what they are supposed to. Disturbances noticed at boundaries.

Analysis and Procedures:

- The model cannot run without Water Level boundaries
- Nudging was attempted to replicate CMEMS data. A nudging file was created and implantation in the master definition file was done (IniwithNudge = 1, nudge completely, =2, initial conditions only)
- Nudging only replicated values of CMEMS for salinity and temperature however abnormal values were experienced at the boundary
- Tides only worked well (as before)
- 2D tides (no depth layers) worked well
- Creating a thicker top layer eliminated the patches in quickplot which meant that the actual top layer of the model could be used to plot maps
- Complete nudging with all boundary conditions showed excessive upwelling on the eastern boundary (extreme velocities due to colder waters coming up onto the surface)
- Nudging was then attempted with multiple cores but the same disturbances on the eastern boundary remained
- Vertical Spatial nudging was used for depths below -500m from MSL for every 7 days – run showed first sign of Durban eddy formation – however this is without any boundary conditions and for a coarse, small grid
- The small grid was then refined for both 1000m and 500m isobaths (each refinement of scale factor 2)
- The new grid was run for a period of a year
- Incorrect data outputs were noticed as the nudging file was incorrectly created
- Horizontal Spatial Nudging was then attempted to manipulate the intensity of the nudging (7 days is more intense than 15 days)
- 15 days showed promising results, better than 3 days intensity (which suggests that too much nudging in shallow waters with coarse input data does not cover such resolution – nudging intensity should match input data periods)
- Tested all boundary conditions (including velocity boundaries) > still experience disturbances at boundary, but at least the model runs and reads the velocity boundary conditions

A.4 Model Boundary Testing with Nudging:

Attempt Number: 15

Date: 03/10/2019 – 15/10/2019

Test Name/s: **BC_ST_IniNudge** (Boundary Conditions with Salinity and Temperature boundaries and initial nudging only)

Input Parameters: Water Level, Temperature, Salinity, Initial nudging

Analysis:

Water Level:

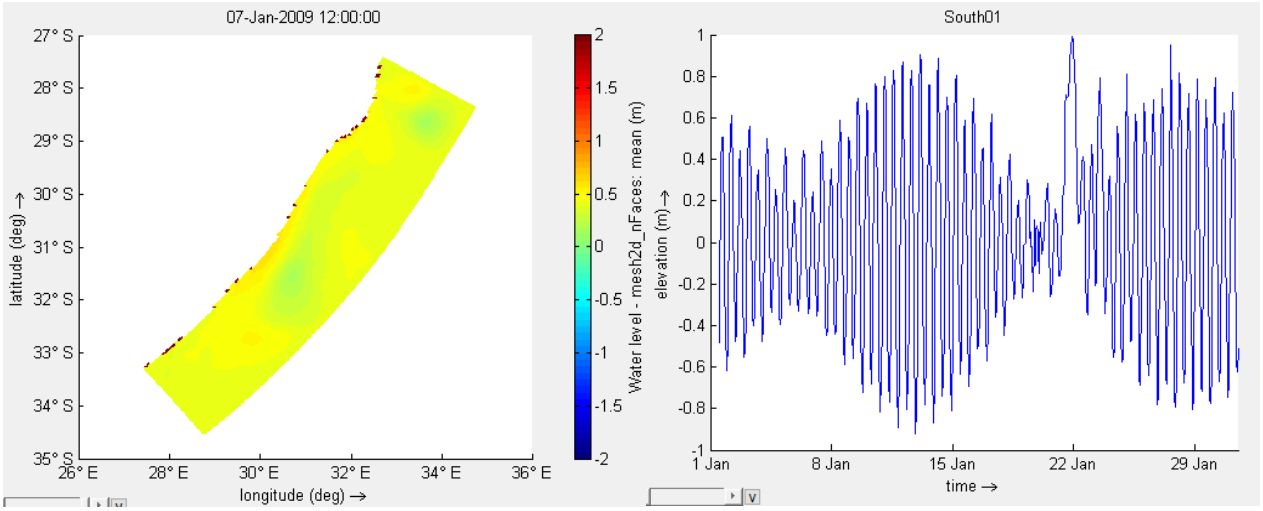

Figure A1: BC_ST_IniNudge - Water Level Outputs for surface layer of the model (left) and vertical profile from MSL (right)

These outputs exhibit expected behaviour with a range from (-1m to 1m). Coastline disturbances could be due to coarse land boundary cells or "dry points" at these locations and not due to disturbances from the model. These can be ignored.

Temperature:

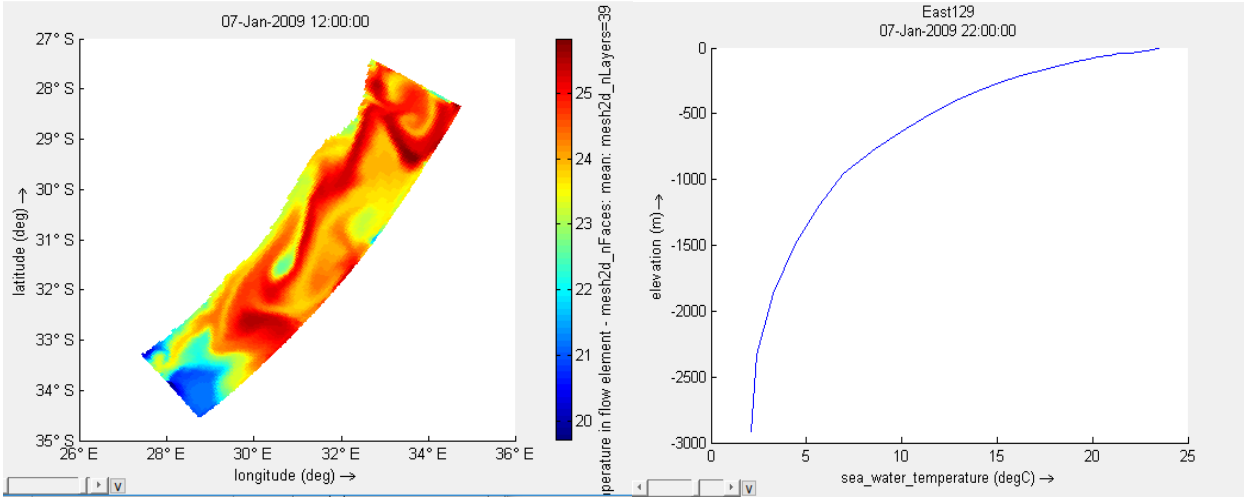

Figure A2: BC_ST_IniNudge - Temperature Outputs for surface layer of the model (left) and temperature vertical profile (right)

Surface layer outputs are similar to that of CMEMS temperature images, with refined outputs closer to the coast. Smooth boundary conditions are achieved, and the vertical temperature profile suggests successful results.

Salinity:

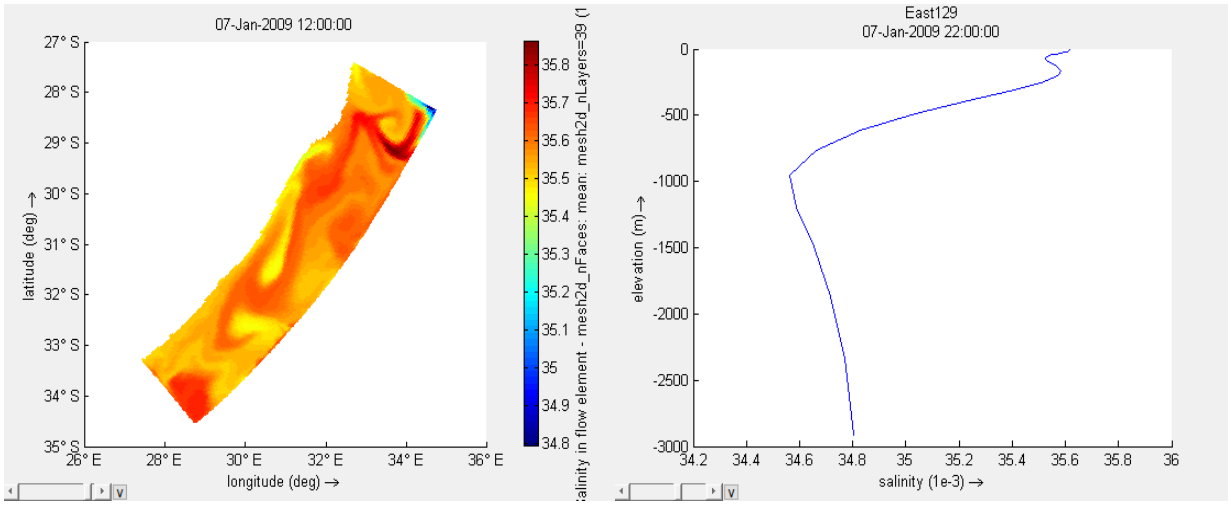

Figure A3: BC_ST_IniNudge - Salinity Outputs for surface layer of the model (left) and salinity vertical profile (right)

Surface layer outputs are similar to that of CMEMS salinity images, with refined outputs closer to the coast. Smooth boundary conditions are achieved, and the vertical salinity profile suggests successful results.

Velocity:

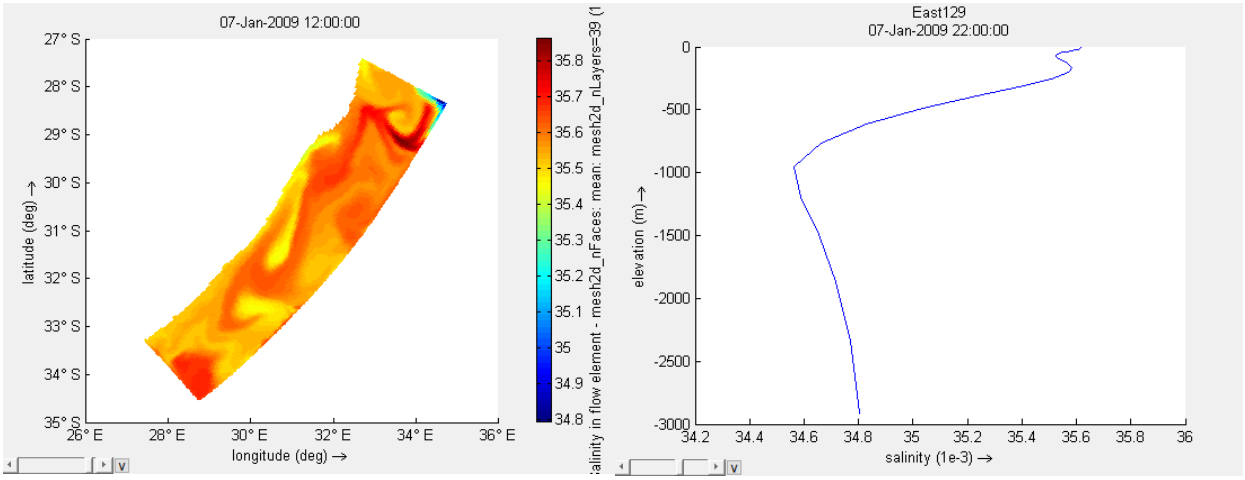

Figure A4: BC_ST_IniNudge - Initial Velocity Outputs for surface layer of the model (left) and initial velocity vertical profile (right)

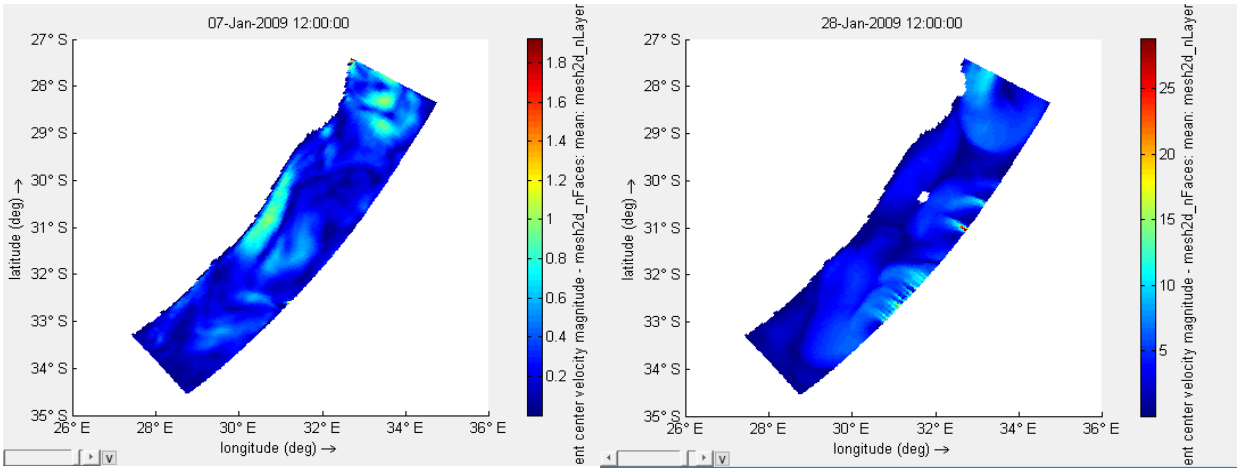

Figure A5: BC_ST_IniNudge - Velocity Outputs for surface layers of the model as the model progresses

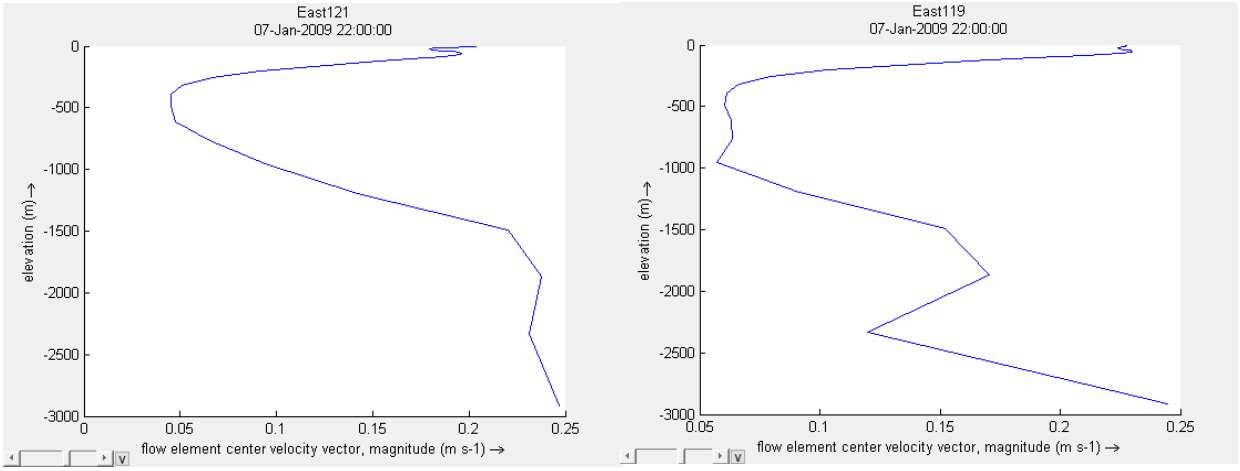

Figure A6: BC_ST_IniNudge - Velocity Vertical Profiles of the model as the model progresses

Figure A4 shows the initial velocities in the model. This suggest that the model has successfully implemented the boundary conditions and velocities are being calculated within the model. However, as the model progresses, disturbances (especially on the eastern boundary) and voids appear as can be seen in Figure A5. This means that there is something wrong with the velocity interpolations. The vertical profiles shown in Figure A6 also shows unrealistic results as the bottom velocity magnitudes are higher than the upper surface velocities. This seems quite unlikely and suggests that there is something wrong with the model. The model is therefore unstable.

Test Name/s: <u>BC_ST_noIniNudge</u> (Boundary Conditions with Salinity and Temperature boundaries and NO initial nudging)

Input Parameters: Water Level, Temperature, Salinity

Analysis:

Water Level:

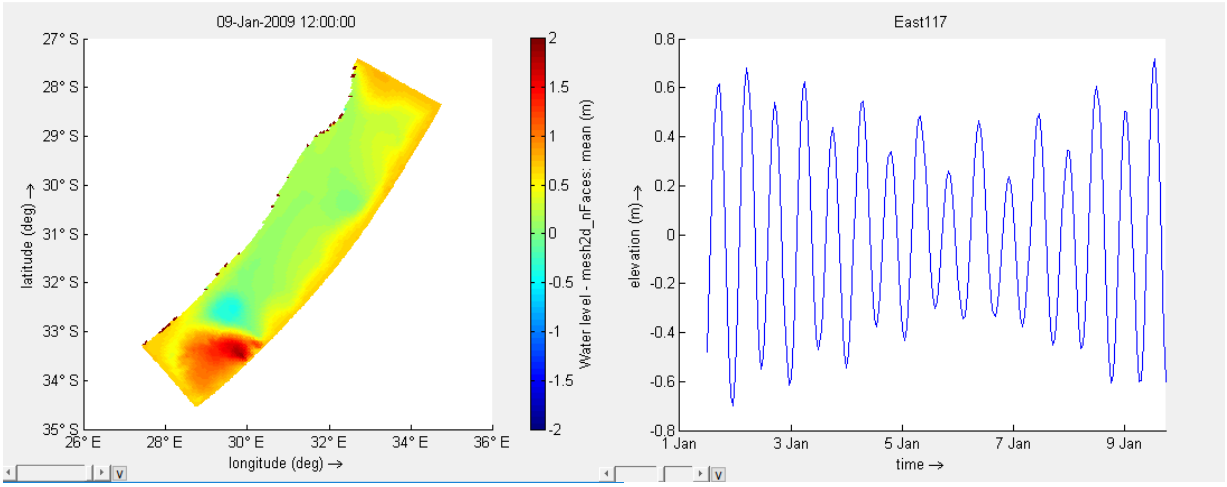

Figure A7: BC_ST_noIniNudge - Water Level Outputs for surface layer of the model (left) and vertical profile from MSL (right)

These outputs exhibit expected behaviour with a range from (-0.8m to 0.8m). However, it takes time to prescribe the water level within the model.

Temperature:

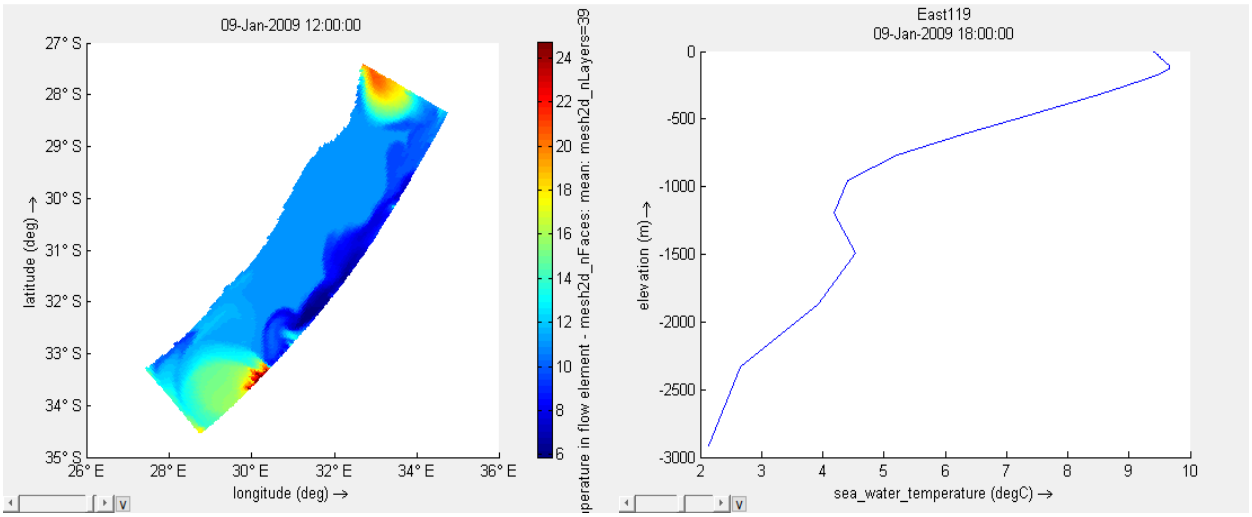

Figure A8: BC_ST_noIniNudge – Temperature Outputs for surface layer of the model (left) and temperature vertical profile (right)

Without any nudging and just inputting the temperature boundaries, we can see in Figure A8 that huge disturbances begin to occur from the boundaries. The model starts up from a cold start and this could be the reason for these disturbances.

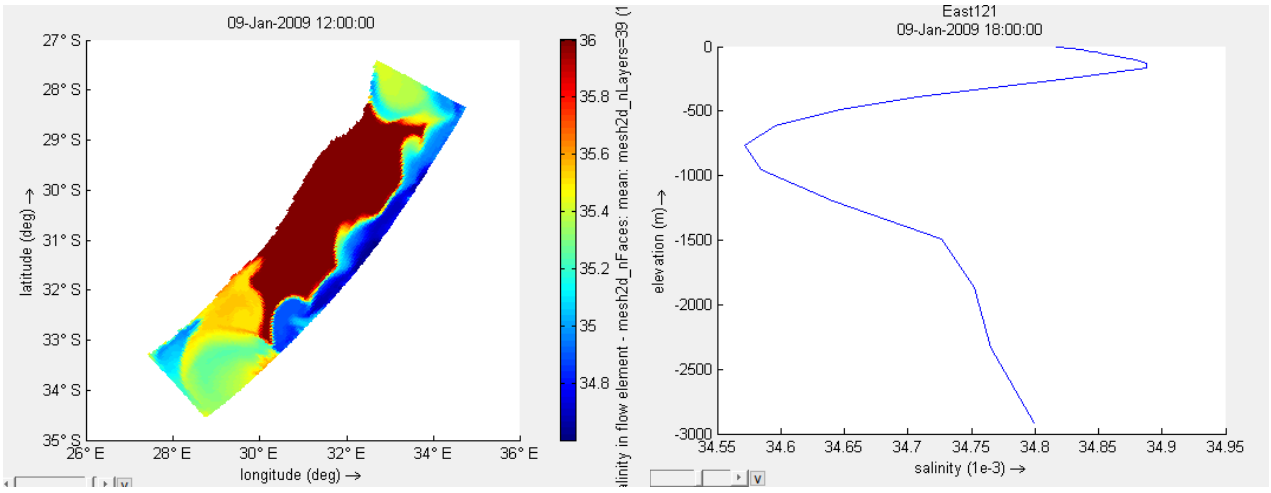

Figure A9: BC_ST_noIniNudge – Salinity Outputs for surface layer of the model (left) and Salinity vertical profile (right)

Similar to temperature, salinity outputs also show huge disturbances at the boundaries and exhibit unrealistic behaviours (Figure A9). The suggests that the model is in fact unstable.

Velocity:

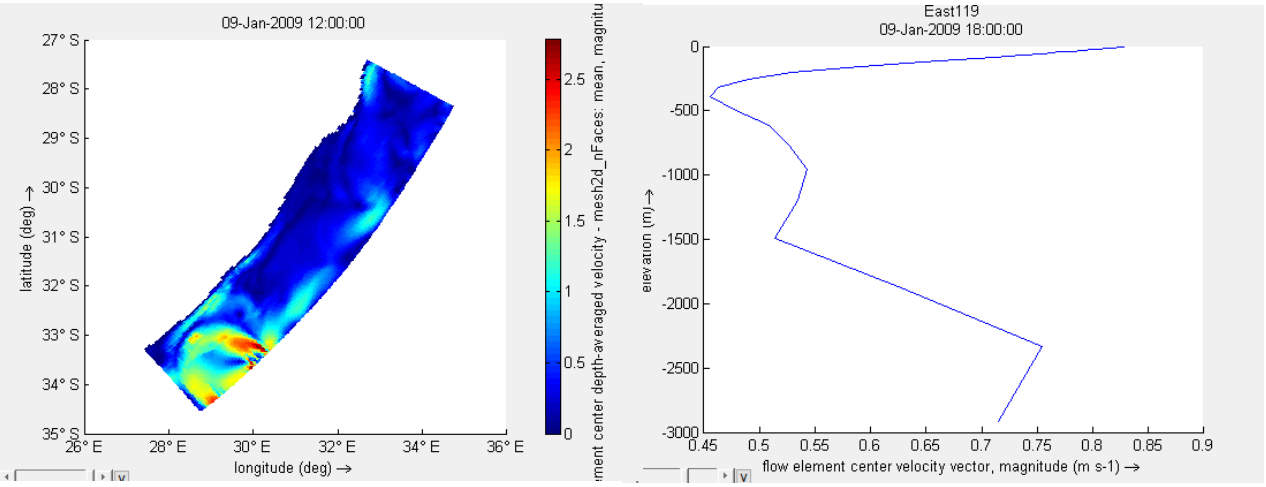

Figure A10: BC_ST_noIniNudge – Velocity Outputs for surface layer of the model (left) and Velocity vertical profile (right)

In Figure A10, the south-east boundary experiences higher velocities. This is an indication of the model not working correctly. The vertical velocity profile also shows some strange results. It does not make sense to have high velocities at the bottom of the profile.

Test Name/s: <u>BC_ST_Nudge</u> (Boundary Conditions with Salinity and Temperature boundaries and complete nudging throughout the model)

Input Parameters: Water Level, Temperature, Salinity, Internal Complete Nudging

Analysis:

Water Level:

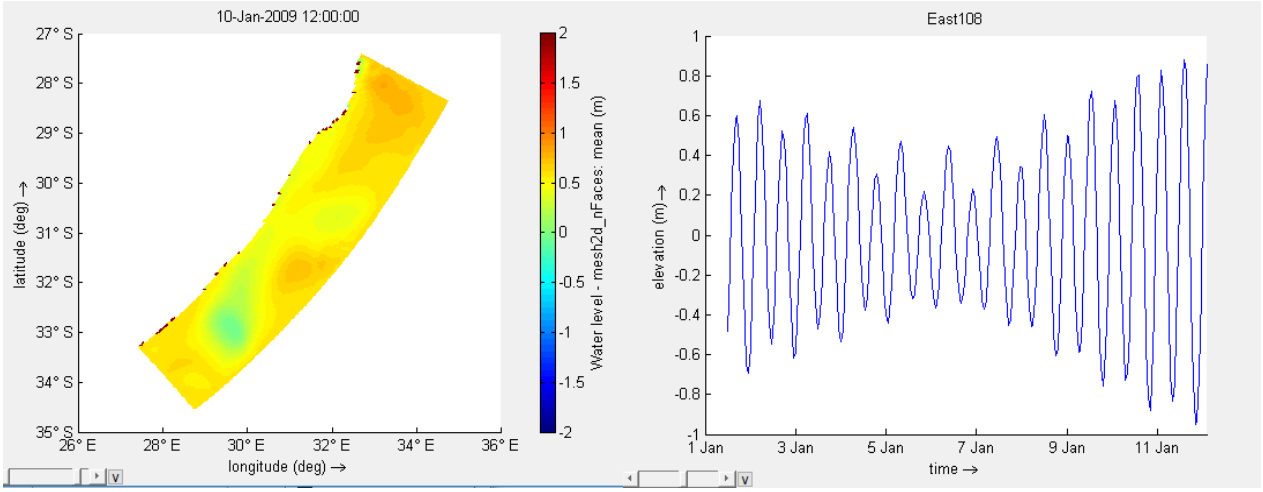

Figure A11: BC_ST_Nudge - Water Level Outputs for surface layer of the model (left) and vertical profile from MSL (right)

These outputs exhibit expected behaviour with a range from (-1m to 1m). Coastline disturbances could be due to coarse land boundary cells or “dry points” at these locations and not due to disturbances from the model. These can be ignored.

Temperature:

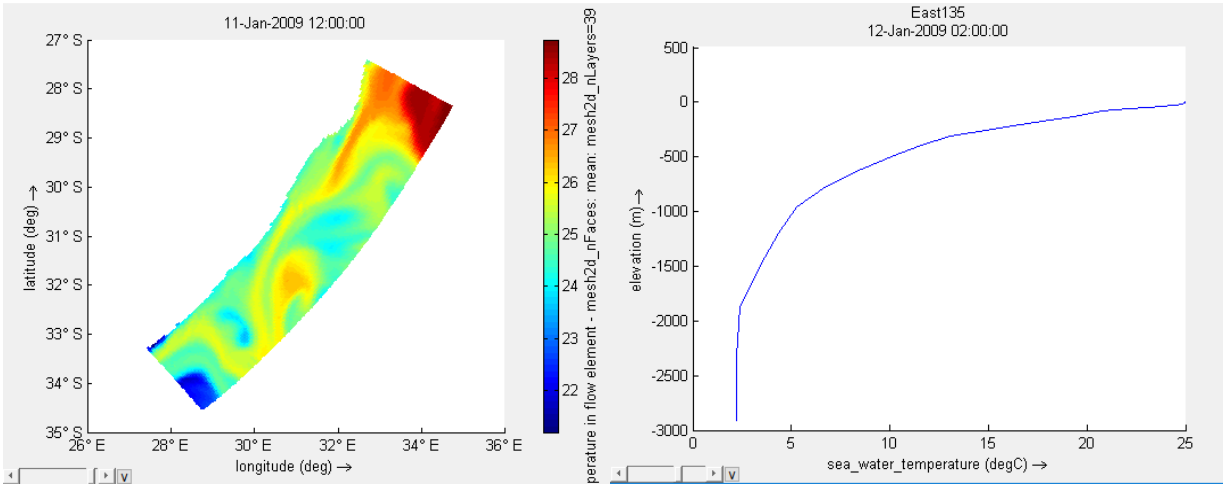

Figure A12: BC_ST_Nudge – Temperature Outputs for surface layer of the model (left) and temperature vertical profile (right)

Completely nudging within the model, we see that the initial temperature outputs are as can be expected. These outputs in FigureA12 show a close correlation to that of CMEMS data for this time and date.

Salinity:

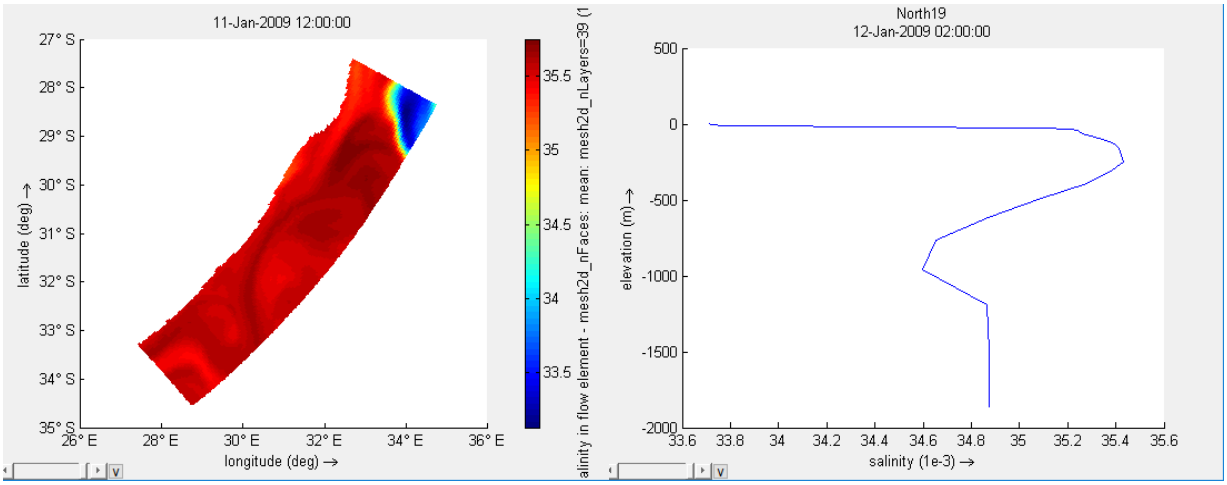

Figure A13: BC_ST_Nudge – Salinity Outputs for surface layer of the model (left) and salinity vertical profile (right)

Similarly, with Salinity outputs, the initial results replicate CMEMS values and this can be expected.

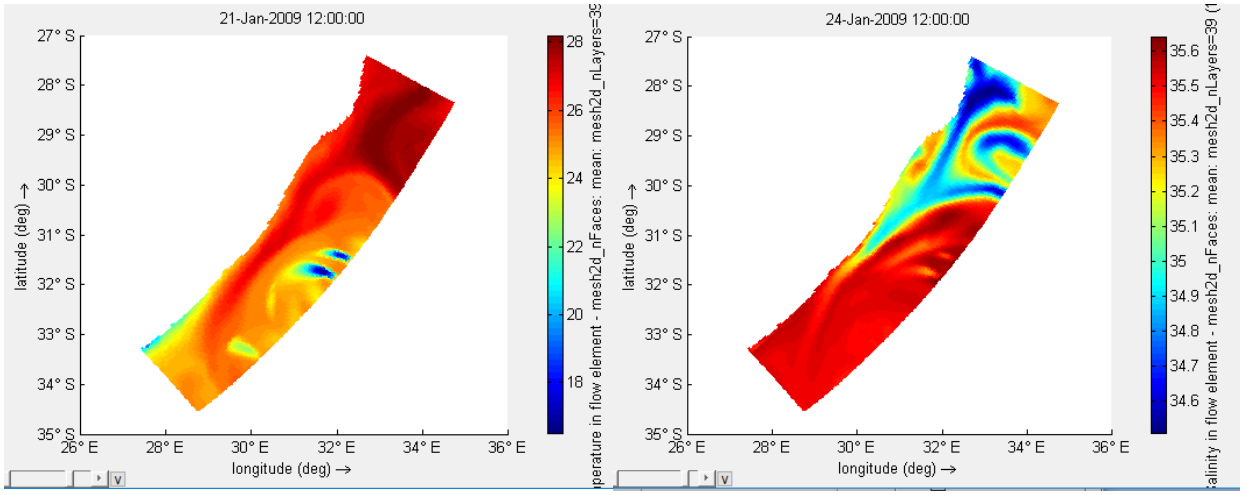

Figure A14: BC_ST_Nudge – Temperature Outputs for surface layer of the model (left) Salinity Outputs for surface layer of the model (right)

However, if we look at the outputs as the model progresses, we notice disturbances at the eastern boundary in both temperature and salinity surface displays (Figure A15). This suggests that over time, the boundary conditions are clashing with the internal model values, which means there is a clash between complete internal nudging within the model and temperature and salinity boundary conditions. This does not make sense as theoretically they are supposed to be the same values as they both come from CMEMS input files. This needs to be investigated further.

Velocity:

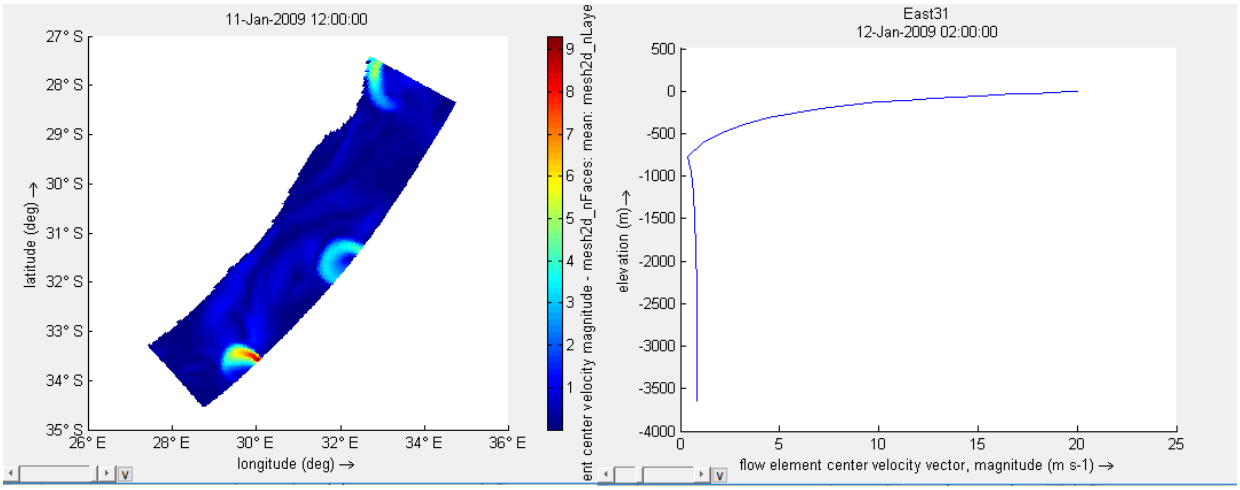

Figure A15: BC_ST_Nudge – Velocity Outputs for surface layer of the model (left) and velocity vertical profile (right)

These disturbances can also be noticed in the velocity surface outputs as the model progresses. Disturbances are evident in both the north and eastern boundaries. This suggests further instabilities within the model.

Test Name/s: **<u>BC_STV_IniNudge</u>** (Boundary Conditions with Velocity, Salinity and Temperature boundaries and initial nudging within the model)

Input Parameters: Water Level, Temperature, Salinity, Velocity, Initial Nudging

Analysis:

Water Level:

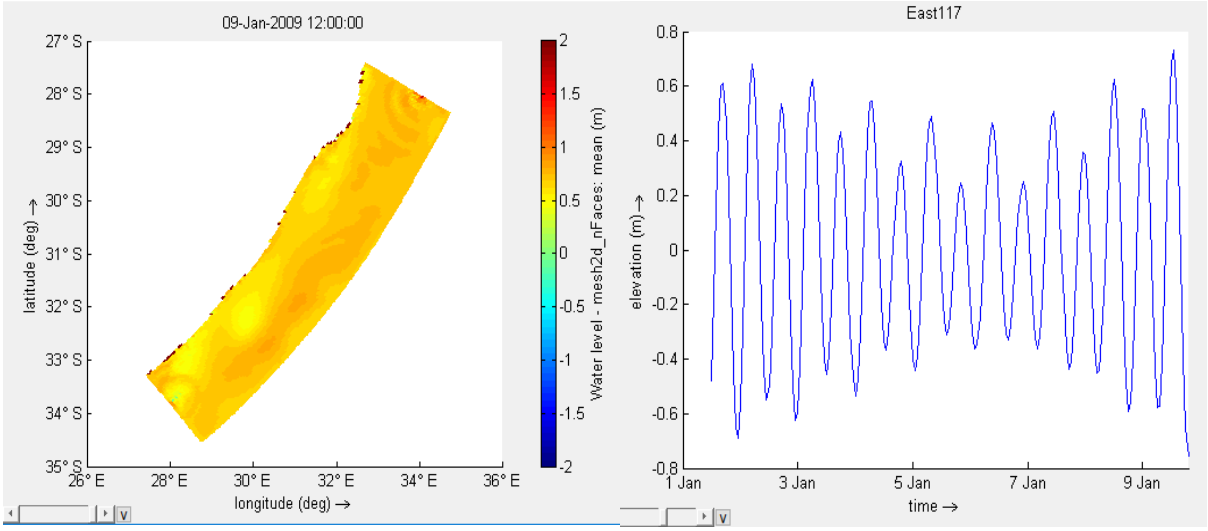

Figure A16: BC_STV_IniNudge – Water Level Outputs for surface layer of the model (left) and vertical profile from MSL (right)

These outputs exhibit expected behaviour with a range from (-0.8m to 0.8m). Coastline disturbances could be due to coarse land boundary cells or "dry points" at these locations and not due to disturbances from the model. These can be ignored.

Temperature:

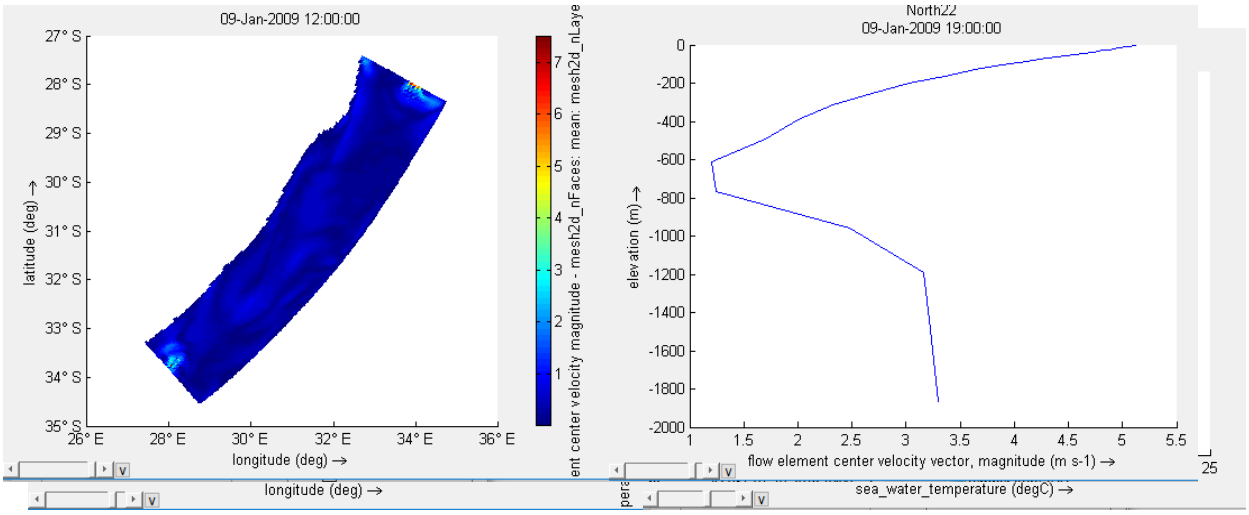

Figure A17: BC_STV_Nudge – Velocity Outputs for surface layer of the model (left) and velocity vertical profile (right)

Initially nudging within the model, we see that the temperature outputs are as can be expected. The outputs in Figure A18 show a close correlation to that of CMEMS data for this time and date.

Salinity:

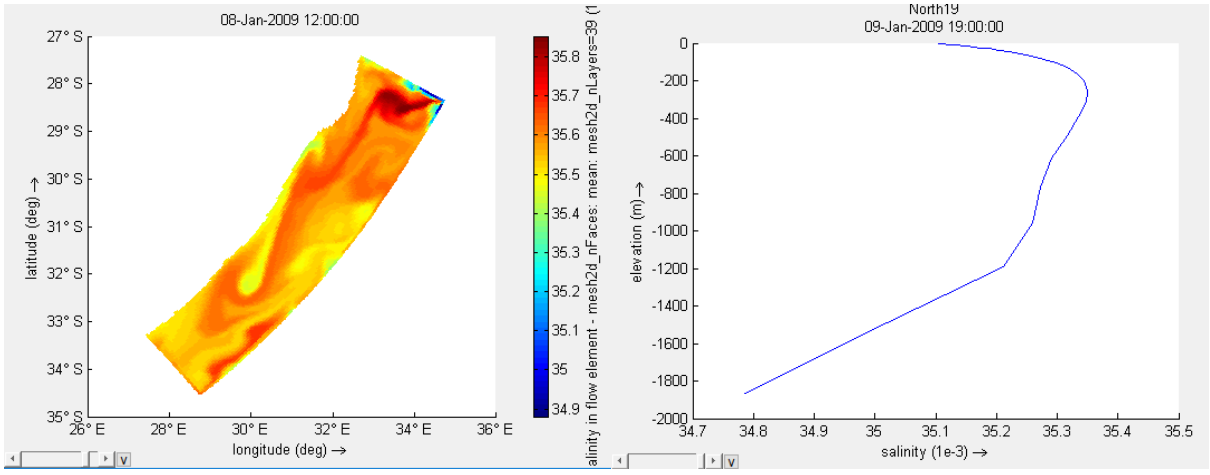

Figure A18: BC_STV_Nudge – Salinity Outputs for surface layer of the model (left) and salinity vertical profile (right)

Similarly, with Salinity outputs, the initial results replicate CMEMS values, and this can be expected.

Velocity:

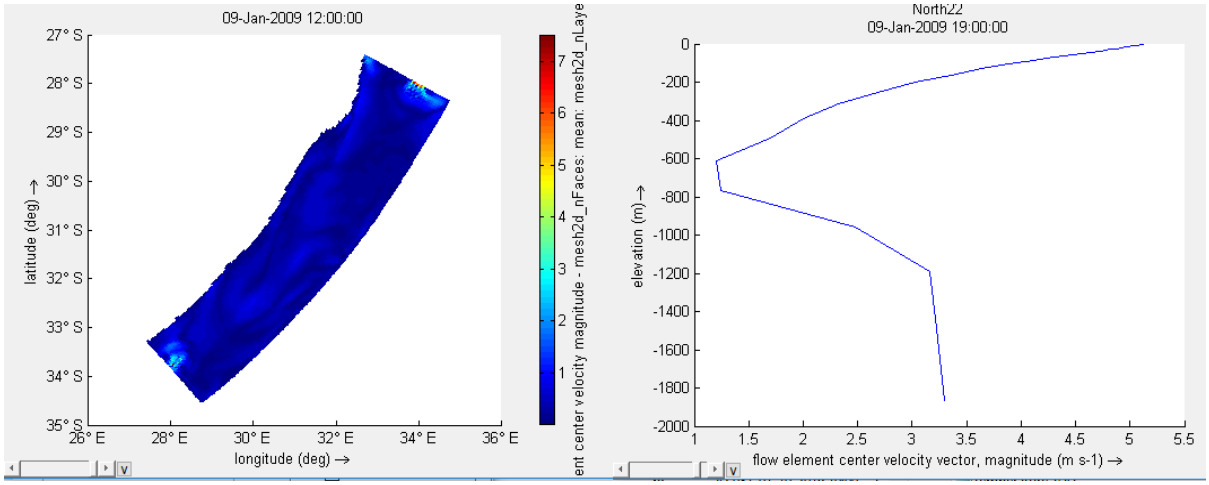

Figure A19: BC_STV_Nudge – Velocity Outputs for surface layer of the model (left) and velocity vertical profile (right)

The velocity outputs, however, show disturbances in both the north and south boundaries. This means that the model is unstable and is not interpolating the velocity boundaries correctly.

Test Name/s: <u>BC_STV_NoIniNudge</u> (Only Boundary Conditions with Velocity, Salinity and Temperature boundaries and no nudging throughout the model)

Input Parameters: Water Level, Temperature, Salinity, Velocity

Analysis:

Water Level:

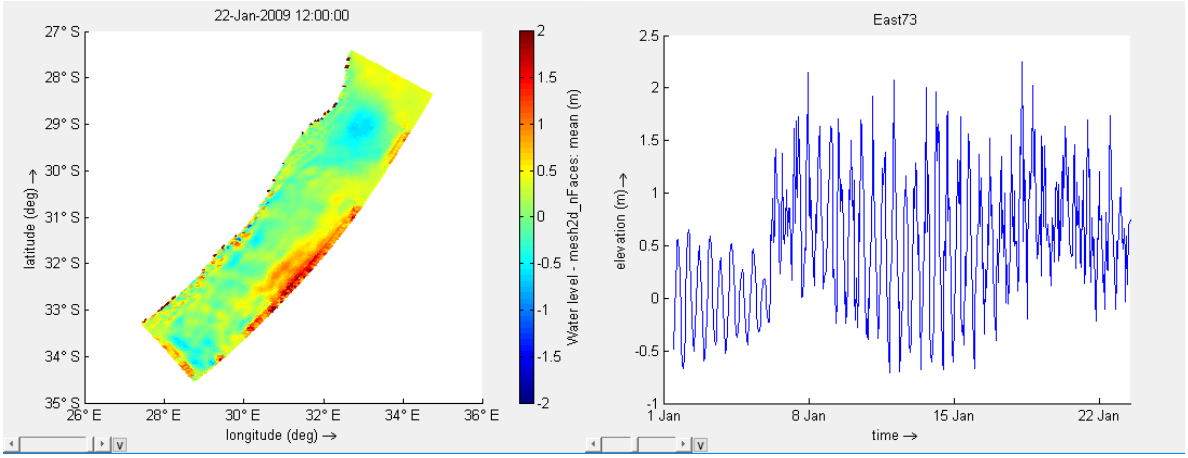

Figure A20: BC_STV_NoIniNudge – Water Level Outputs for surface layer of the model (left) and vertical profile from MSL (right)

After the model runs over a certain period, disturbances at the boundaries are noticeable in the water level outputs. This is mainly evident on the eastern boundary (Figure A22). This suggests that the model is unstable.

Temperature:

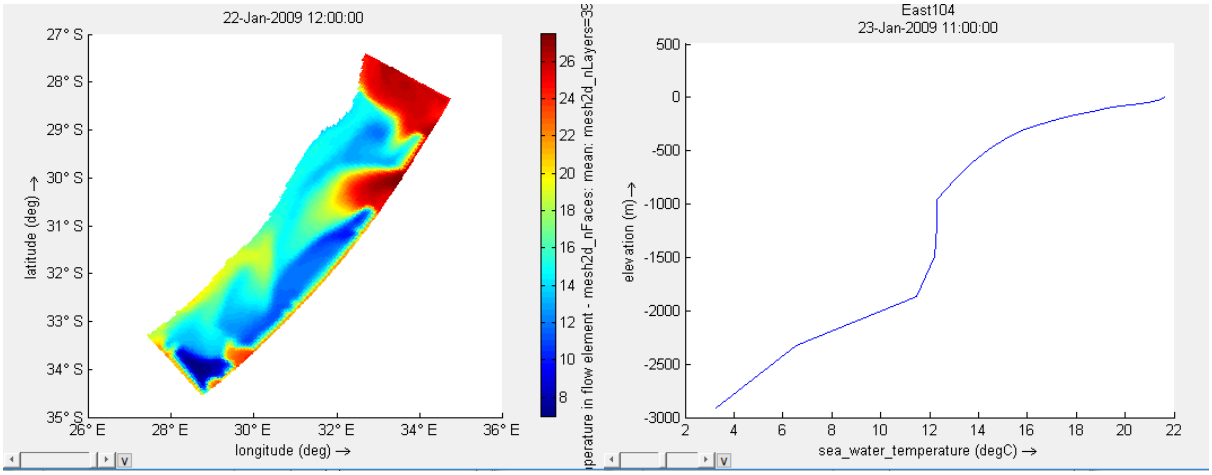

Figure A21: BC_STV_NoIniNudge – Temperature Outputs for surface layer of the model (left) and temperature vertical profile (right)

Velocity outputs also show similar disturbances to that of the water level outputs on the eastern boundary. The vertical profile also shows unrealistic values for temperature on the eastern boundary. Similarly, this can be seen for salinity in Figure A23 below.

Salinity:

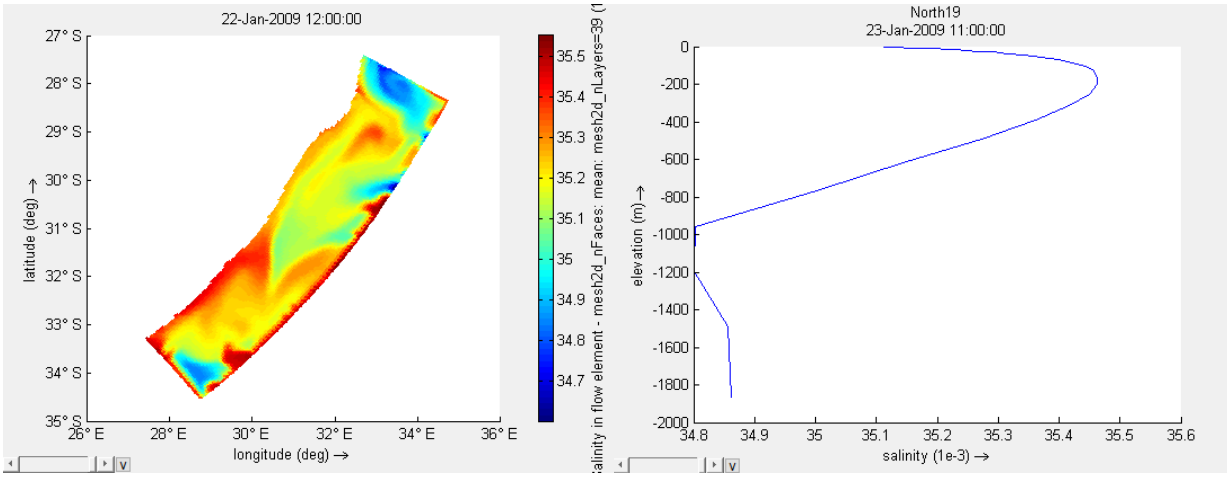

Figure A22: BC_STV_NoIniNudge – Salinity Outputs for surface layer of the model (left) and salinity vertical profile (right)

Velocity:

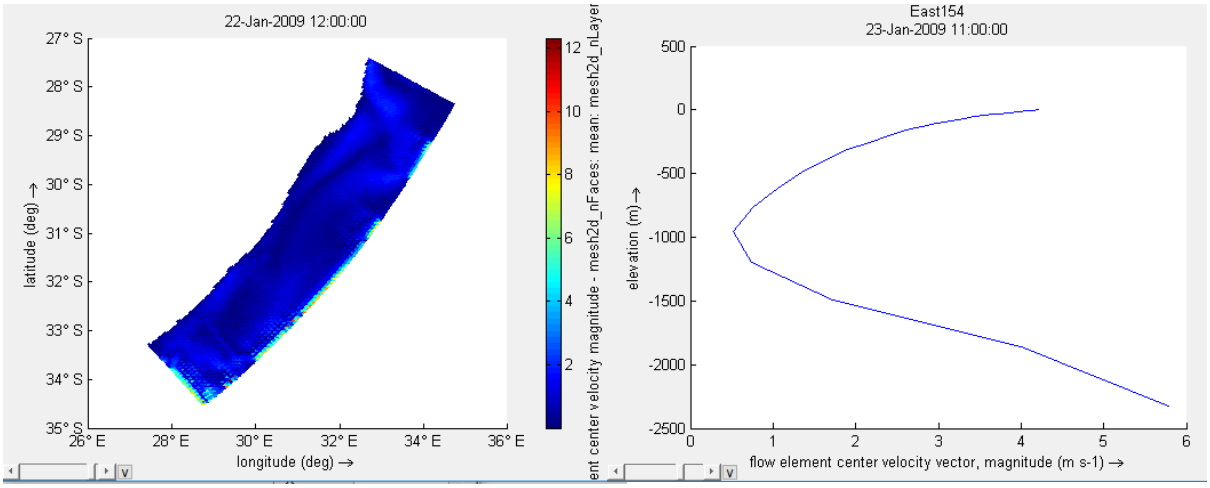

Figure A23: BC_STV_NoIniNudge – Velocity Outputs for surface layer of the model (left) and velocity vertical profile (right)

The velocity outputs in Figure A24 also exhibit strange disturbances similar to temperature and salinity outputs. Instabilities can also be seen on the eastern boundary and the velocity profile shows unlikely current speeds at the seabed floor.

Test Name/s: <u>BC_STV_Nudge</u> (Boundary Conditions with Velocity, Salinity and Temperature boundaries and internal nudging throughout the model)

Input Parameters: Water Level, Temperature, Salinity, Velocity, Internal nudging

Analysis:

Water Level:

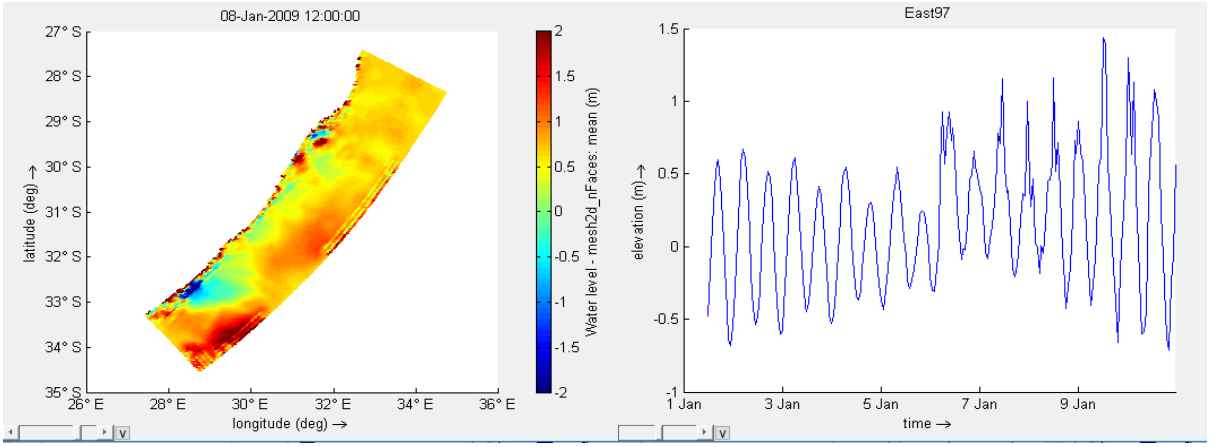

Figure A24: BC_STV_Nudge – Water Level Outputs for surface layer of the model (left) and vertical profile from MSL (right)

The water level outputs for this model run shows erratic and unlikely behaviour. There are many disturbances within this simulation which causes the model to eventually crash.

Temperature:

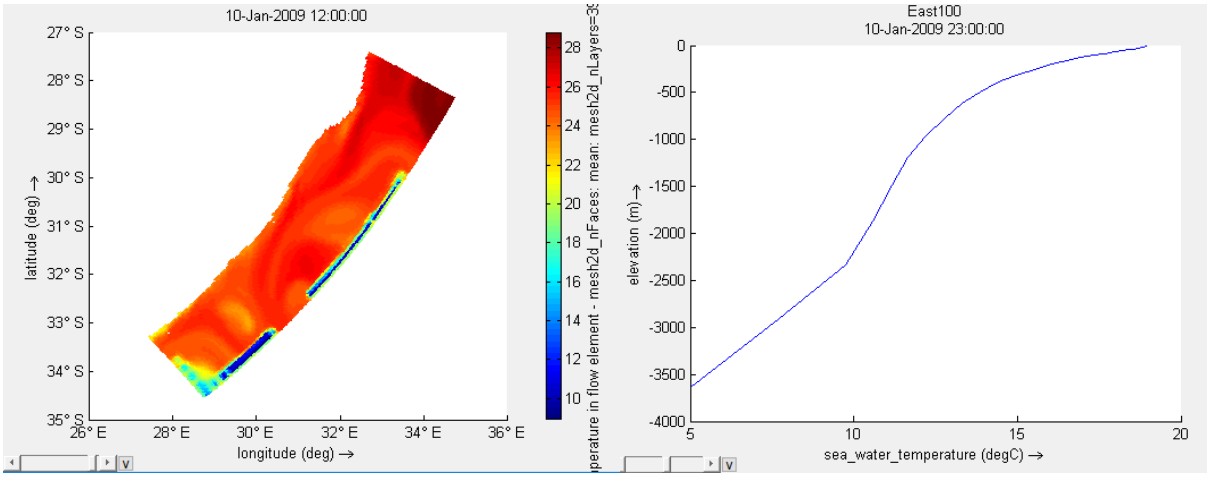

Figure A25: BC_STV_Nudge – Temperature Outputs for surface layer of the model (left) and temperature vertical profile (right)

The temperature outputs in Figure A26 show much colder water on the eastern boundary which is not usual for this region. This also suggests instabilities within the model for complete nudging and temperature, salinity and velocity boundary conditions.

Salinity:

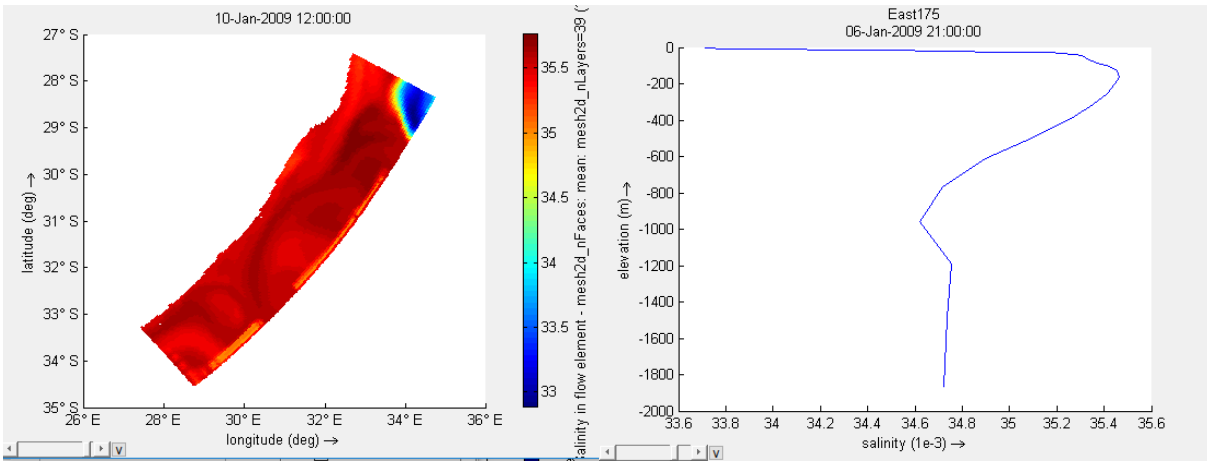

Figure A26: BC_STV_Nudge – Salinity Outputs for surface layer of the model (left) and salinity vertical profile (right)

Comparable to water level and temperature outputs, salinity outputs also demonstrate disturbances at the eastern boundary. This is more evident at the surface of the vertical profile in Figure A27.

Velocity:

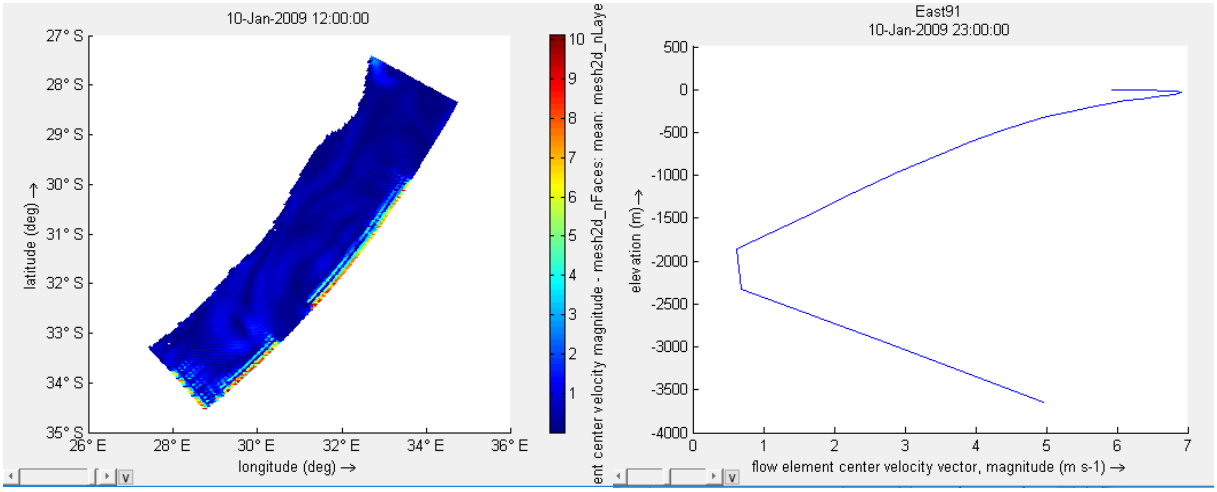

Figure A27: BC_STV_Nudge – Velocity Outputs for surface layer of the model (left) and velocity vertical profile (right)

The velocity outputs in Figure A28 also correspond with the previous output for the BC_STV_Nudge run. Instabilities on the eastern boundary are clearly noticeable and the vertical profile indicates unrealistically high velocities on the eastern boundary. This reiterates the instability of the model.

Test Name/s: <u>BC_V_Nudge</u> (Boundary Conditions with Velocity boundary only and internal nudging throughout the model)

Input Parameters: Water Level, Velocity, Internal nudging

Analysis:

Water Level:

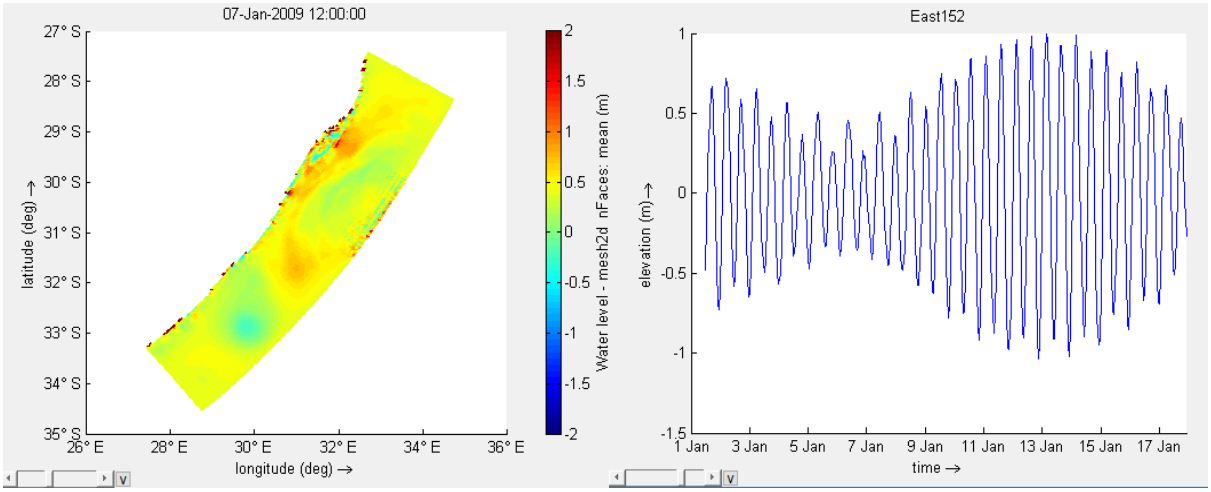

Figure A28: BC_V_Nudge – Water Level Outputs for surface layer of the model (left) and vertical profile from MSL (right)

Although the vertical profile in Figure A29 suggests expected water level outputs (ranges from -1m to 1m), the water level outputs for the surface layer clearly shows instabilities within the model. The eastern boundary is still experiencing some disturbances which suggests velocity boundaries are still an issue.

Temperature:

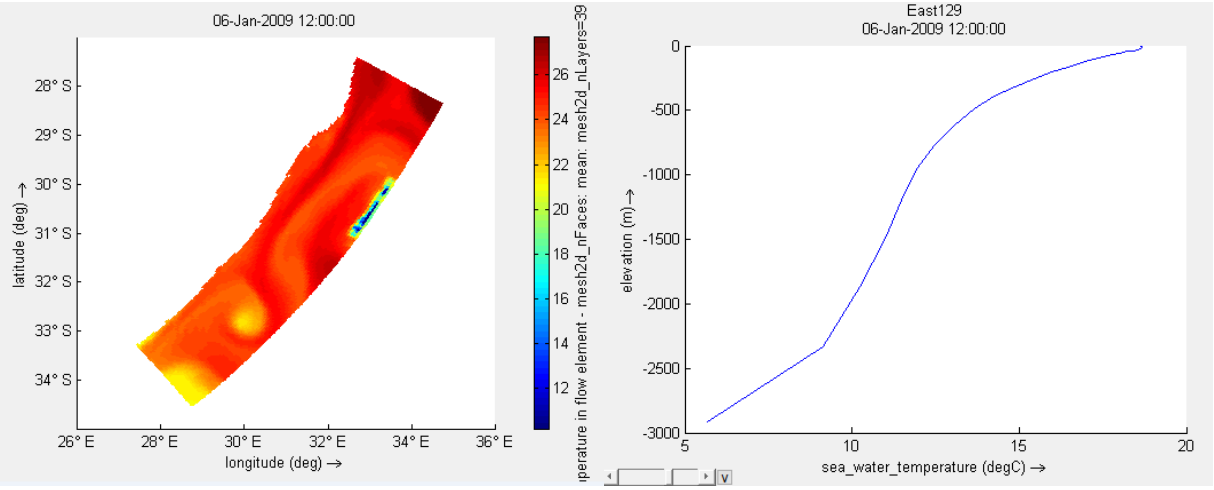

Figure A29: BC_V_Nudge – Temperature Outputs for surface layer of the model (left) and temperature vertical profile (right)

The eastern boundary sees cold surface temperatures, which only expands further along the boundary as the model progresses. This can be seen in Figure A30.

Salinity:

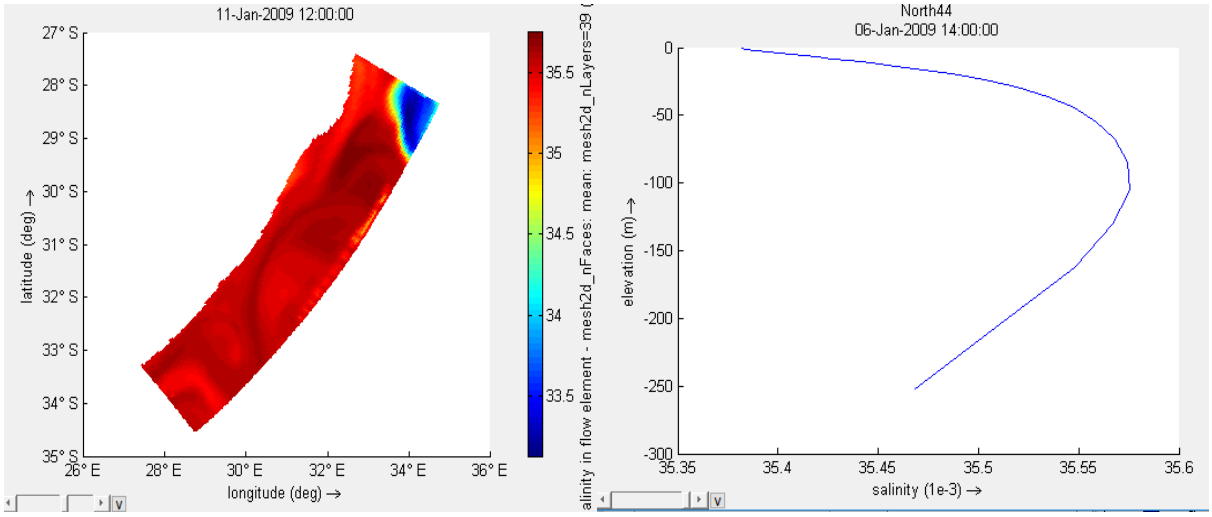

Figure A30: BC_V_Nudge – Salinity Outputs for surface layer of the model (left) and salinity vertical profile (right)

Similar disturbances are also noticed for salinity outputs. Figure A31 shows this same disturbance occurring on the eastern boundary. Less saline water is also noticed to be coming in from the north east corner.

Velocity:

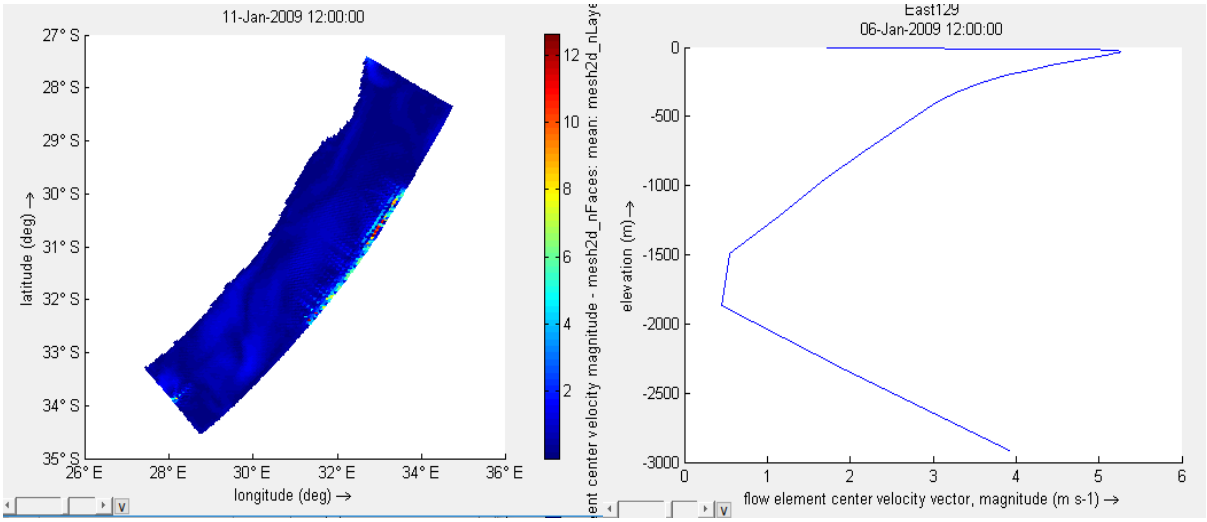

Figure A31: BC_V_Nudge – Velocity Outputs for surface layer of the model (left) and velocity vertical profile (right)

Velocity outputs for just the velocity boundary condition and internal nudging shown in Figure A32 also indicates the same eastern boundary disturbances as seen with temperature and salinity outputs. Unusually high velocities are experienced at the eastern boundary as suggested in the vertical profile.

Test Name	Water Level	Temperature BC	Salinity BC	Velocity BC	Initial Nudging	Complete Nudging	Stable Model
BC_ST_IniNudge	👍	👍	👍		👍		👍
BC_ST_noIniNudge	👍	👍	👍				👍 - long start up
BC_ST_Nudge	👍	👍	👍			👍	👍
BC_STV_IniNudge	👍	👍	👍	👍	👍		
BC_STV_noIniNudge	👍	👍	👍	👍			
BC_STV_Nudge	👍	👍	👍	👍		👍	
BC_V_Nudge	👍			👍		👍	

Table A-1: Summary of Testing Boundary Conditions and Nudging Results

From Table A1 above, it is evident that whenever velocity boundaries are inputted within the model, the model crashes or becomes unstable. This suggests that there is still something wrong with the implementation of ux/uy velocity boundary conditions.

A.5 Larger Model development and testing:

Due to the instability of advection velocity inputs within the smaller grid, a larger grid encompassing the entire Agulhas system was then created. This model hoped to reduce the instabilities caused by inputting advection velocities and allowed for temperature and salinity boundary conditions to drive the Agulhas density driven current.

Attempt Number: 16

Date: 17/10/2019 – 28/10/2019

Test Name/s: Large Grid

Input Parameters: Water Level, Temperature, Salinity, Nudging files, large, unrefined grid

Analysis: Model is stable but need to determine if boundaries are doing what they are supposed to. Disturbances noticed at boundaries.

Figure A33 below shows a well-established, large-scaled Agulhas Ocean Current which successfully mimics the characteristics that can be expected from this current, i.e., meandering, retroflection, return current, etc.

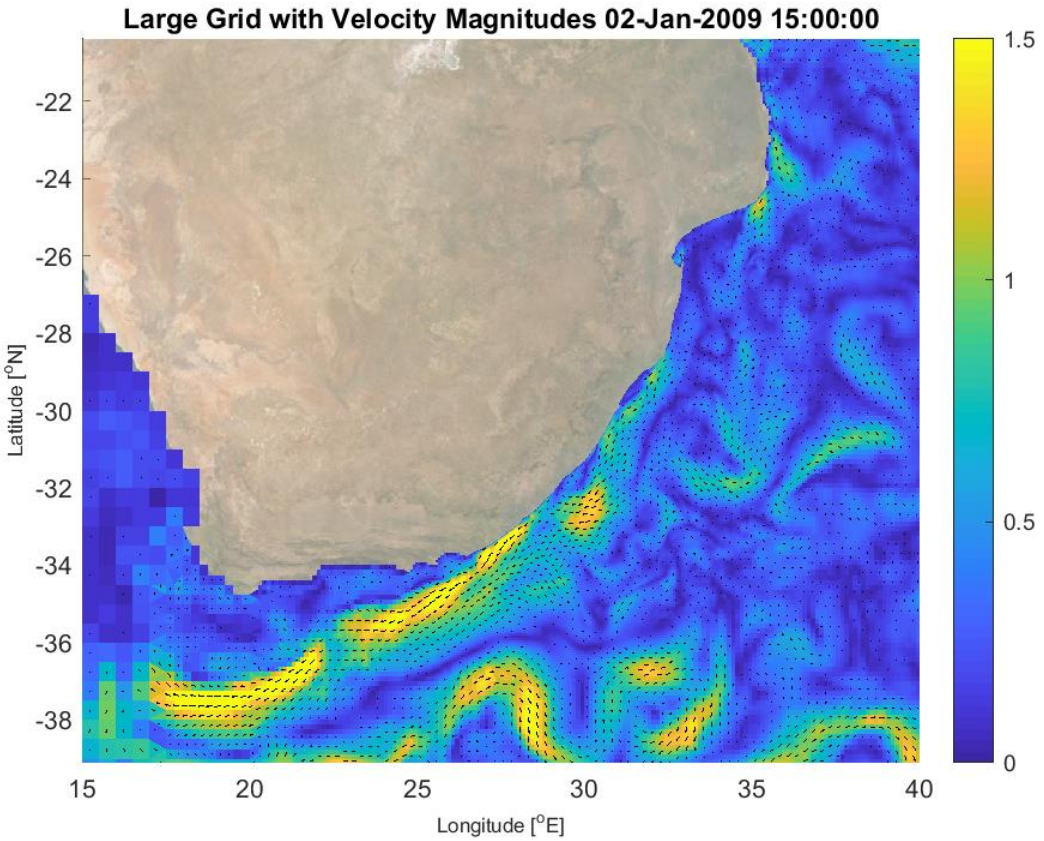

Figure A32: Velocity Magnitude Map Output from large flexible mesh grid

However, this model is far beyond our area of interest and demands massive computational capacity if further refined towards the coast. Although it was satisfactory to replicate the current on a larger scale, for operational use, it is not ideal to have such a large-scale model. The smaller model was then reverted to and used for modelling results.

A.6 Stable, Refined, Rectangular model:

A new version of DFM was then created by the software developers at Deltares to try and alleviate some of the issues experienced in the previous runs. New settings and parameters were introduced into the model to also adapt the software for deep water ocean currents. Advection velocity boundary conditions were successfully implemented within the model, with a stable model achieved. Wind and heatflux was also included.

Attempt Number: 17

Date: 28/10/2019 – 28/11/2019

Test Name/s: Refined Small Grid

Input Parameters: Water Level, Temperature, Salinity, initial nudging, restart files, refined, small grid, Advection velocities, Viscosity, Wind, Heat Flux

Analysis: Model is stable and to be used for comparative analysis

Checkerboarding occurs when refinement is done at the boundaries. To avoid this, refinement was done within the model only, avoiding interference with the boundary conditions. The model only uses Z-layer vertical stratification and restart files were experimented with to prevent a "cold start-up" of the model. The restart files were eventually replaced with initial nudging, where CMEMS values for temperature and salinity were used for initial conditions throughout the model.

The Agulhas Current has an undercurrent where in deeper layers the current reverses and flows in the opposite direction to the main current on the surface (Beal and Bryden ,1997). Upon further inspections of the model, it was noticed that the model became a "closed model" where currents were not flowing outwards and rather circulating within the model boundaries. Looking closer into the dynamics of the inputs, only the inflow of velocities was being prescribed by the velocity boundary conditions. This meant that if the velocity had a negative value within the input file, these values were being ignored. The repercussions of this meant that at the south boundary, the outflow values of the main current were not flowing out of the model and only the inflow values of the undercurrent were being prescribed.

The original default for DFM components is zero (refer to Table 2). This issue was resolved by changing the default of the lower limit for flow velocity to allow for negative values.

Heat flux was implemented for the first time within the model. This meant that temperatures would be calculated by the model and temperature would not just be transported or prescribed but also modelled. It was advised by the developers that this would help prevent mixing of temperature in the upper layers and keep stratification.

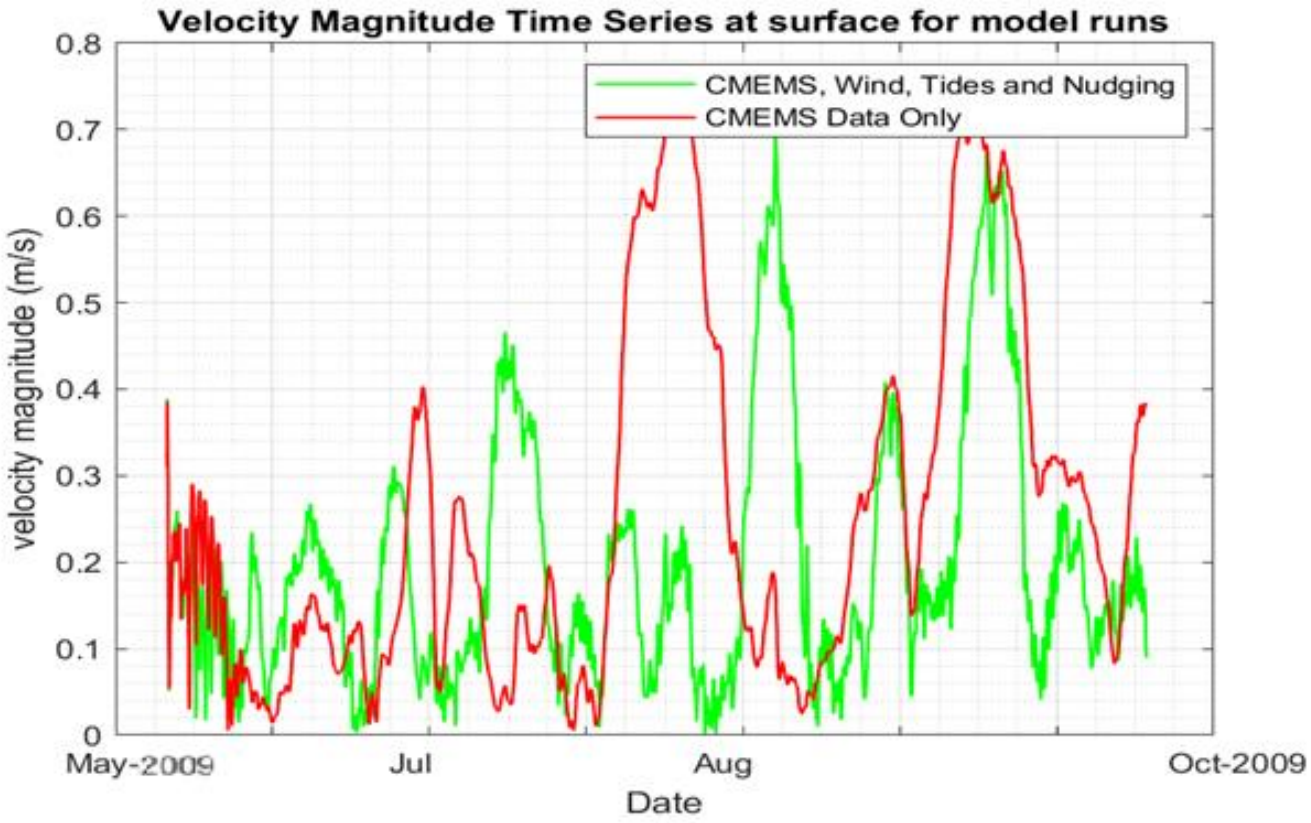

Figure A33: Time series showing the comparison between CMEMS data and the Stable, refined, rectangular model with wind, tide, and nudging inputs

Figure A34 shows the difference in the model results compared to that of CMEMS values. This indicates the variation in having a more refined, downscaled model to that of a global ocean model. This also validates the need for a more refined, local model, as if there were no differences between these two results, there would not be a need for the DFM model. Inputs could be taken directly from the CMEMS model if this were the case. The refined DFM model suggests higher accuracy which is better described when comparing with observed data.

This initial model was then used to compare model results with CMEMS values as well as observed results. After my internship, the model was developed further. These developments were done by Deltares experts and will be compared to my initial model outputs. These results can be found in chapter 7.

A.7 Summary

This appendix serves as an additional attachment to better breakdown and describe the internship process and achievements. In adjacent to chapter 3, this appendix provides a more detailed analysis of how the stable D-Flow FM model was achieved.